Faculty of Pharmacy

Chair of Pharmaceutical Chemistry

Department of Physicochemical Drug Analysis

Doctoral dissertation

Novel dual inhibitors of GSK-3β and IKK-β kinases – – synthesis and structure-activity relationship studies

Izabella Góral

Supervisor: dr hab. Anna Więckowska, prof. UJ

Co-supervisor: dr Dawid Panek

Kraków 2025

Rozprawę tę dedykuję moim świętej pamięci Rodzicom.

Moje serdeczne podziękowania składam Wszystkim, bez których ta praca nie powstałaby.

Przede wszystkim dziękuję mojej promotor, dr hab. Annie Więckowskiej, prof. UJ, której osoba zainspirowała mnie do wejścia na ścieżkę rozwoju naukowego. Dziękuję za nieustanne wsparcie i opiekę merytoryczną w trakcie studiów, wiarę we mnie I motywowanie mnie od początku do końca.

Moje podziękowania kieruję również do dr. inż. Dawida Panka, mojego promotora pomocniczego, za nieocenioną pomoc w pracy laboratoryjnej oraz wielokrotne podnoszenie mnie na duchu.

Dziękuję pracownikom i doktorantom Zakładu Fizykochemicznej Analizy Leku, a przede wszystkim: dr. Tomaszowi Wichurowi za wykonanie syntezy części związków przedstawionych w pracy, dr Justynie Godyń za wprowadzenie mnie w tajniki badań *in vitro*, liczne dyskusje w trakcie ich przeprowadzania oraz za wykonanie badań kinetyki i przenikalności w teście PAMPA. Dr Natalii Szałaj i dr Pauli Zarębie dziękuję za wyniki badań analitycznych przestawione w niniejszej pracy. Mgr Emilii Sługockiej za przeprowadzenie badań modelowania komputerowego, a mgr. Jędrzejowi Kukułowiczowi za to, że zawsze mogłam na niego liczyć.

Moim kolegom z pokoju – dr Beacie Gryzło, dr. Krzysztofowi Więckowskiemu – za miłą atmosferę we wspólnie dzielonym biurze.

Dr Annie Pasiece za przetarcie włoskich szlaków i podzielenie się inspiracjami podczas mojego stażu naukowego na Uniwersytecie Bolońskim.

Jestem również ogromnie wdzięczna za możliwość poznania wspaniałych osób, które towarzyszyły mi podczas studiów: Agnieszki Wiesner-Kiełczewskiej, Aleksandry Ciochoń, Olhi Shuklinovej, Jakuba Jurczyka. Dziękuję za wszystkie wspólnie przeżyte chwile i mam nadzieję, że to dopiero początek.

Founding sources

The research described in this thesis was founded by:

1. The National Science Center of Poland, Sonata Bis 9 Grant No. 2019/34/E/NZ7/00090 “Multitarget approach to break the vicious circle of tau pathology and neuroinflammation in Alzheimer’s disease: development of dual inhibitors of GSK-3β and IKK-β kinases”. Principal investigator: dr hab. Anna Więckowska. Date of project implementation: 04.2020 – 04.2025.
2. Excellence Initiative at the Jagiellonian University in the Research Support Module Grant No. U1C/W42/NO/28.05 “Synteza par enancjomerów pochodnych tetrahydropirymidyn-4(1*H*)-onu oraz 1,3-oksazynan-4-onu jako nowych fragmentów farmakoforowych o aktywności hamującej wobec kinazy IKK-β” Principal investigator: Izabella Góral, M.Sc. Date of the project implementation: 06.2022 – 06.2023.

Contents

Streszczenie

Choroba Alzheimera jest najczęstszą postacią demencji i jedną z wiodących przyczyn śmierci według Światowej Organizacji Zdrowia. Choroba ma złożoną etiopatogenezę, w której szczególną rolę odgrywają agregaty peptydu β-amyloidu i białka tau oraz przewlekły proces zapalny w obrębie tkanki nerwowej, prowadzące do neurodegeneracji. Z uwagi na rosnącą liczbę chorych oraz brak skutecznej metody leczenia, schorzenie to jest istotnym wyzwaniem społecznym, medycznym i ekonomicznym. W niniejszej rozprawie doktorskiej przedstawiono badania dotyczące nowej grupy związków o wielokierunkowym mechanizmie działania, eksplorujące nowy obszar terapeutyczny w leczeniu przyczynowym choroby Alzheimera.

We wstępie przestawiono charakterystykę choroby Alzheimera, koncentrując się na szczególnej roli jaką odgrywają w jej rozwoju enzymy z rodziny kinaz: kinaza syntazy glikogenu-3 beta (GSK-3β) oraz kinaza wchodząca w skład kompleksu inhibitorowego białka IκB, podjednostka beta (IKK-β). Oprócz funkcji wymienionych enzymów, szczegółowo opisano poszczególne grupy związków hamujących ich aktywność, wraz z analizą zależności struktura-aktywność. Przedstawiono także inhibitory wspomnianych kinaz, które jako kandydaci na leki dotarły do badań klinicznych. Omówiono również budowę kinaz serynowo-treoninowych, strategie projektowania inhibitorów kinaz oraz założenia otrzymywania związków o wielokierunkowym mechanizmie działania – ligandów wielofunkcyjnych.

Celem badań przeprowadzonych w ramach realizacji pracy doktorskiej była synteza oraz ocena aktywności biologicznej nowych inhibitorów kinaz o charakterze ligandów wielofunkcyjnych, oddziałujących jednocześnie z GSK-3β oraz IKK-β. Takie związki mogą odgrywać kluczową rolę w procesach związanych z rozwojem choroby Alzheimera, w tym nieprawidłowej agregacji białek (szczególnie białka tau) oraz procesach neurozapalnych, co mogłyby potencjalnie modyfikować przebieg schorzenia. Aby osiągnąć zamierzony cel, na podstawie literaturowych danych dotyczących selektywnych inhibitorów wybranych enzymów, zaprojektowano i zsyntezowano cztery serie nowych pochodnych o potencjalnej dualnej aktywności. Tożsamość każdego związku potwierdzano wynikami analiz spektralnych (NMR) oraz chromatograficznych (LC-MS). Następnie przeprowadzono ocenę aktywności hamującej kinazy GSK-3β i IKK-β w badaniach *in vitro*. Uzyskane wyniki umożliwiły sformułowanie wniosków dotyczących zależności struktura – aktywność oraz na wyselekcjonowanie najbardziej obiecujących kandydatów do dalszych badań *in cellulo* i wstępnej oceny właściwości ADME w badaniach *in vitro*. Ponadto, w celu poszerzenia wiedzy na temat oddziaływania związków w centrum aktywnym kinaz GSK-3β oraz IKK-β przeprowadzono badania modelowania molekularnego. Dodatkowo, dla wszystkich nowych związków finalnych przeprowadzono analizę parametrów fizykochemicznych *in silico* co pozwoliło na uzupełnienie oceny lekopodobności badanych związków.

Najważniejszym osiągnięciem niniejszej pracy jest wyłonienie spośród otrzymanych pochodnych, inhibitorów o dualnej aktywności hamującej względem kinaz GSK-3β i IKK-β. Na szczególną uwagę zasługują związki **40** i **60**, wykazujące silniejszą inhibicję wobec GSK-3β niż IKK-β (odpowiednio dla **40**: GSK-3β IC_{50} = 10 nM, IKK-β IC_{50} = 4.380 μM oraz dla **60**: GSK-3β IC_{50} = 10 nM, IKK-β IC_{50} = 7.351 μM) oraz związek **70** o najwyższej zbalansowanej aktywności hamującej (GSK-3β IC_{50} = 267 nM, IKK-β IC_{50} = 366 nM). Dodatkowo, w ramach badań wyselekcjonowano grupę selektywnych inhibitorów kinazy GSK-3β o wysokiej aktywności, wśród których najbardziej obiecującym okazał się związek **62** (IC_{50} = 8 nM oraz K_i = 2 nM). Badania *in cellulo* potwierdziły działanie neuroprotekcyjne tych związków w teście hiperfosforylacji indukowanej kwasem okadaikowym na linii komórkowej HT-22. Związki te wykazały również aktywność w modelu zapalenia indukowanego lipopolisacharydem, na linii komórkowej BV-2, zmniejszając wydzielanie markerów stanu zapalnego, takich jak tlenek azotu (NO), interleukina-6 (IL-6) oraz czynnik martwicy nowotworów α (TNF-α).

Podsumowując, w niniejszej pracy zaprezentowano selektywne inhibitory kinazy GSK-3β oraz pierwsze dualne ligandy GSK-3β/IKK-β o założonym, wielokierunkowym mechanizmie działania. To unikalne połączenie stanowi nowatorski kierunek w poszukiwaniu terapii modyfikującej przebieg choroby Alzheimera. Zaprezentowane wyniki stanowią solidny punkt wyjściowy do dalszej optymalizacji tej grupy inhibitorów.

Abstract

Alzheimer's disease is the most common form of dementia and one of the leading causes of death according to the World Health Organization. The disease's etiopathogenesis is elusive, indicating the aggregates of β-amyloid peptide and tau protein, along with a chronic inflammatory process within nervous tissue as pivotal in driving neurodegeneration. Given the increasing prevalence of Alzheimer's disease and the limited therapeutic efficacy of currently available drugs, AD arises as a significant social, medical, and economic challenge. This doctoral dissertation presents research on a novel class of multifunctional compounds, focused on the search for causal treatment of Alzheimer's disease.

The introduction provides an overview of Alzheimer's disease, focusing on the pivotal roles of kinases: glycogen synthase kinase-3 beta (GSK-3β) and the IκB kinase complex subunit beta (IKK-β) in its pathogenesis. In addition to a detailed discussion of the functions of these enzymes, the respective classes of compounds that inhibit their activity are described in detail, along with structure-activity relationship analysis. Furthermore, GSK-3β and IKK-β kinase inhibitors that have reached clinical trials as drug candidates are highlighted. The design section discusses the structural features of serine/threonine kinases, the types of kinase inhibitors, and the principles of the multifunctional ligand strategy.

The aim of the research presented in this doctoral dissertation was the synthesis and biological evaluation of novel kinase inhibitors characterized as multifunctional ligands, targeting both GSK-3β and IKK-β simultaneously. Such compounds may significantly impact processes associated with Alzheimer's disease development, including abnormal protein aggregation (especially tau protein) and neuroinflammatory processes, thereby potentially modifying disease progression. To achieve the stated objective, four series of novel compounds with potential dual activity were designed and subsequently synthesized. Their structure and purity, were confirmed through spectroscopic (NMR) and chromatographic (LC-MS) methods. Subsequently, all compounds were evaluated for their inhibitory activity against GSK-3β and IKK-β kinases *in vitro*. The results allowed for initial conclusions to be drawn regarding structure-activity relationships and the selection of the most promising candidates for further *in cellulo* studies and preliminary ADME profile assessment *in vitro*. To expand knowledge about the interaction of compounds within the active site of GSK-3β and IKK-β kinases, molecular modeling studies were conducted. Additionally, all final compounds were subjected to *in silico* analysis of the physicochemical parameters, supplementing the drug-likeness evaluation.

The most significant achievement presented in the dissertation is the identification of dual inhibitors of GSK-3β and IKK-β kinases among the synthesized derivatives. Special attention should be given to compounds **40** and **60**, which exhibit stronger inhibition of GSK-3β than IKK-β (for **40**: GSK-3β IC_{50} = 10 nM, IKK-β IC_{50} = 4.380 μM; for **60**: GSK-3β IC_{50} = 10 nM, IKK-β IC_{50} = 7.351 μM),

as well as to compound **70**, which demonstrates the highest balanced inhibitory activity (GSK-3β IC_{50} = 267 nM, IKK-β IC_{50} = 366 nM). Additionally, the research identified a group of selective GSK-3β inhibitors with high inhibitory potency, among which compound **62** proved to be the most promising (IC_{50} = 8 nM and K_i = 2 nM). *In cellulo* studies confirmed their neuroprotective properties in the okadaic acid-induced hyperphosphorylation assay in the HT-22 cell line. These compounds also exhibited significant activity in a lipopolysaccharide-induced inflammation model in the BV-2 cell line, reducing the secretion of inflammatory markers such as nitric oxide (NO), interleukin-6 (IL-6), and tumor necrosis factor-alpha (TNF-α).

In summary, the described research presents selective GSK-3β kinase inhibitors and the first dual GSK-3β/IKK-β ligands with a desired multitarget activity. This unique combination represents an innovative direction in the search for disease-modifying therapies for Alzheimer's disease. Moreover, the presented results provide a solid foundation for further optimization of this group of inhibitors.

List of publications

Covered by the doctoral dissertation:

1. Góral, I.; Wichur, T.; Sługocka, E.; Godyń, J.; Szałaj, N.; Zaręba, P.; Głuch-Lutwin, M.; Mordyl, B.; Panek, D.; Więckowska, A. Connecting GSK-3β Inhibitory Activity with IKK-β or ROCK-1 Inhibition to Target Tau Aggregation and Neuroinflammation in Alzheimer's Disease—Discovery, In Vitro and In Cellulo Activity of Thiazole-Based Inhibitors. *Molecules* **2024**, *29*, 2616, doi:10.3390/molecules29112616.
2. Góral, I.; Wichur, T.; Sługocka, E.; Grygier, P.; Głuch-Lutwin, M.; Mordyl, B.; Honkisz-Orzechowska, E.; Szałaj, N.; Godyń, J.; Panek, D.; Zaręba, P.; Sarka, A.; Żmudzki, P.; Latacz, G.; Pustelny, K.; Bucki, A.; Czarna, A.; Menezes, F.; Więckowska, A. Exploring Novel GSK-3β Inhibitors for Anti-Neuroinflammatory and Neuroprotective Effects: Synthesis, Crystallography, Computational Analysis, and Biological Evaluation. *ACS Chem Neurosci.* **2024**, *15*, 3181–3201, doi:10.1021/acschemneuro.4c00365.

Other scientific publications:

1. Wei, W.; Jing, L.; Tian, Y.; Więckowska, A.; Kang, D.; Meng, B.; Panek, D.; Godyń, J.; Góral, I.; Song, Y.; Liu, X.; Zhan, P. Multifunctional Agents Against Alzheimer's Disease Based on Oxidative Stress: Polysubstituted Pyrazine Derivatives Synthesized by Multicomponent Reactions. *Bioorg. Med. Chem.* **2023**, *96*, 117535, doi:10.1016/j.bmc.2023.117535.
2. Więckowski, K.; Szałaj, N.; Gryzło, B.; Wichur, T.; Góral, I.; Sługocka, E.; Śniecikowska, J.; Latacz, G.; Siwek, A.; Godyń, J.; Bucki, A.; Kołaczkowski, M.; Więckowska, A. Serotonin 5-HT_6 Receptor Ligands and Butyrylcholinesterase Inhibitors Displaying Antioxidant Activity—Design, Synthesis and Biological Evaluation of Multifunctional Agents against Alzheimer's Disease. *Int. J. Mol. Sci.* **2022**, *23*, 9443, doi:10.3390/ijms23169443.
3. Stary, D.; Kukułowicz, J.; Góral, I.; Baltrukevich, H.; Barbasevich, M.; Godyń, J.; Bajda, M. Multilevel Virtual Screening Approach for Discovery of Thymidine Phosphorylase Inhibitors as Potential Anticancer Agents. *J. Mol. Struct.* **2022**, *1249*, 131648, doi:10.1016/j.molstruc.2021.131648.
4. Wichur, T.; Godyń, J.; Góral, I.; Latacz, G.; Bucki, A.; Siwek, A.; Głuch-Lutwin, M.; Mordyl, B.; Śniecikowska, J.; Walczak, M.; Knez, D.; Jukic, M.; Sałat, K.; Gobec, S.; Kołaczkowski, M.; Malawska, B.; Brazzolotto, X.; Więckowska, A. Development and Crystallography-Aided SAR Studies of Multifunctional BuChE Inhibitors and 5-HT_6R Antagonists with β-amyloid Anti-Aggregation Properties. *Eur. J. Med. Chem.* **2021**, *225*, 113792, doi:10.1016/j.ejmech.2021.113792.
5. Wichur, T.; Pasieka, A.; Godyń, J.; Panek, D.; Góral, I.; Latacz, G.; Honkisz-Orzechowska, E.; Bucki, A.; Siwek, A.; Głuch-Lutwin, M.; Knez, D.; Brazzolotto, X.; Gobec, S.; Kołaczkowski, M.; Sabate, R.; Malawska, B.; Więckowska, A.

Discovery of 1-(Phenylsulfonyl)-1*H*-indole-Based Multifunctional Ligands Targeting Cholinesterases and 5-HT_6 Receptor with Anti-Aggregation Properties against Amyloid-Beta and Tau. *Eur. J. Med. Chem.* **2021**, *225*, 113783, doi:10.1016/j.ejmech.2021.113783.

6. Więckowska, A.; Szałaj, N.; Góral, I.; Bucki, A.; Latacz, G.; Kieć-Kononowicz, K.; Bautista-Aguilera, Ò. M.; Romero, A.; Ramos, E.; Egea, J.; Farré-Alíns, V.; González-Rodríguez, Á.; López-Muñoz, F.; Chioua, M.; Marco-Contelles, J. In Vitro and In Silico ADME-Tox Profiling and Safety Significance of Multifunctional Monoamine Oxidase Inhibitors Targeting Neurodegenerative Diseases. *ACS Chem. Neurosci*. **2020**, *11*, 3793—3801, doi:10.1021/acschemneuro.0c00489.
7. Góral, I.; Łątka, K.; Bajda, M. Structure Modeling of the Norepinephrine Transporter. *Biomolecules.* **2020**, *10*, 102, doi:10.3390/biom10010102.

Contribution to scientific conferences and seminars

1. XXVIII EFMC International Symposium on Medicinal Chemistry (EFMC-ISMC 2024), September 1st–5th, 2024, Rome, Italy.
   Poster presentation: "The first-in-class dual inhibitor targeting GSK-3β and IKK-β kinases to address tauopathy and neuroinflammation in Alzheimer's disease". I. Góral, T. Wichur, J. Godyń, N. Szałaj, P. Zaręba, E. Sługocka, M. Głuch-Lutwin, B. Mordyl, A. Pasieka, A. Bucki, D. Panek, A. Więckowska.
2. European School of Medicinal Chemistry ESMEC – 43rd Advanced Course of Medicinal Chemistry and Seminar for PhD students, June 30th–July 4th, Urbino, Italy.
   Poster presentation: "GSK-3β inhibition as a tool against tauopathy and neuroinflammation in Alzheimer's disease". I. Góral.
3. The 4th edition of nationwide conference for medical students – Medical Knowledge Fair, December 1st–2nd, Krakow, Poland.
   Oral presentation: "Nowe inhibitory kinazy syntazy glikogenu 3β przeciwko tauopatii i neurozapaleniu w chorobie Alzheimera". I. Góral.
4. IX EFMC International Symposium on Advances in Synthetic and Medicinal Chemistry (EFMC-ASMC 2023), September 3rd–7th, Zagreb, Croatia.
   Poster presentation: "GSK-3β and ROCK-1 kinases under the magnifying glass – identification of dual inhibitors against tauopathy and neuroinflammation in Alzheimer's disease". I. Góral, T. Wichur, D. Panek, J. Godyń, M. Głuch-Lutwin, B. Mordyl, E. Sługocka, A. Bucki, A. Więckowska.
5. 17th EFMC Short Course on Medicinal Chemistry – "Small Molecule Protein Degraders: A New Opportunity for Drug Design and Development". April 23rd–26th, 2023, Oegstgeest, Netherlands.
   Participation in scientific seminar without presenting own research results.
6. 30th Young Research Fellows Meeting (YRFM 2023), February 1st–3rd, 2023, Paris, France.
   Poster presentation: "Discovery of novel Glycogen Synthase Kinase 3β inhibitors to combat tauopathy and neuroinflammation in Alzheimer's disease". I. Góral, T. Wichur, D. Panek, J. Godyń, M. Głuch-Lutwin, B. Mordyl, E. Sługocka, A. Bucki, A. Więckowska.
7. Interdisciplinary Conference on Drug Sciences ACCORD 2022, May 26th –28th, 2022, Warsaw, Poland.
   Poster presentation: "Structure-activity relationship in a series of glycogen synthase kinase 3β inhibitors based on *N*-(pyridin-2-yl)carboxamide scaffold". I. Góral, N. Szałaj, D. Panek, T. Wichur, J. Godyń, A. Więckowska.
8. 2nd International Conference on Neuroprotection by Drugs, Nutraceuticals, and Physical Activity, December 9th–10th, 2022, virtual event.
   Poster presentation: "Targeting Glycogen Synthase Kinase 3β to combat tauopathy in Alzheimer's disease – structure-activity relationship of novel GSK-3β inhibitors". I. Góral, T. Wichur, D. Panek, J. Godyń, A. Więckowska.

9. 8th EFMC Young Medicinal Chemists' Symposium (EFMC-YMCS 2021), September 9th–10th, 2021, virtual event.

   Poster presentation: "5-HT_6 receptor antagonists and cholinesterase inhibitors with antioxidant properties as new multifunctional anti-Alzheimer's ligands". I. Góral, N. Szałaj, B. Gryzło, A. Siwek, J. Śniecikowska, T. Wichur, K. Więckowski, M. Kołaczkowski, A. Więckowska.

10. 10th Medicinal Chemistry Seminar, September 3rd–5th, 2021, Lublin, Poland.

    Poster presentation: "Donepezil derivatives as new multifunctional anti-Alzheimer's ligands combining 5-HT_6R antagonism, cholinesterase inhibition with antioxidant and chelating properties". I. Góral, K. Więckowski, B. Gryzło, N. Szałaj, T. Wichur, J. Śniecikowska, A. Siwek, M. Kołaczkowski, A. Więckowska.

List of abbreviations and acronyms

AD	Alzheimer's disease
ADMET	absorption-distribution-metabolism-excretion-toxicity
ADP	adenosine diphosphate
A-loop	activation loop
APE	alanine–propline–glutamic acid
APP	amyloid precursor protein
ATP	adenosine triphosphate
Aβ	amyloid β
BACE1	β-secretase
BBB	brain-blood barrier
Boc	*tert*-butoxycarbonyl
BPSD	behavioral and psychological symptoms of dementia
CDK	cyclin-dependent kinases
CK1	casein kinase 1
CNS	central nervous system
CNS MPO	central nervous system multiparameter optimization
COX-2	cyclooxygenase-2
DAN	2,3-diaminonaphthalene
DCM	dichloromethane
DIEA	*N*,*N*-diisopropylethylamine
DFG	aspartic acid–phenylalanine–glycine
DIAD	diisopropyl azodicarboxylate
DMAP	4-dimethylaminopyridine
DMEDA	*N*,*N*'-dimethylethylenediamine
DMF	*N*,*N*-dimethylformamide
DMSO	dimethylsulfoxide
DPBS	Dulbecco’s phosphate-buffered saline
DYRK	dual-specificity tyrosine-regulated kinase
EDC	1-ethyl-3-(3-dimethylaminopropyl)carbodiimide
EtOAc	ethyl acetate
EtOH	ethanol
FDA	Food and Drug Administration
G-loop	glycine-rich loop
GSK-3	Glycogen Synthase Kinase 3
HATU	hexafluorophosphate azabenzotriazole tetramethyl uronium
HBA	hydrogen bond acceptor

HBD	hydrogen bond donor
HIV-1	human immunodeficiency virus type 1
HLM	human liver microsomes
IFN-γ	interferon gamma
IKK-β	IκB kinase complex subunit β
IL-10	interleukin-10
IL-12	interleukin-12
IL-1β	interleukin-1β
IL-6	interleukin-6
iNOS	inducible nitric oxide synthase
i-PrOH	isopropanol
IκB	inhibitor of kappa B
JNK	C-Jun *N*-terminal kinase
KE	ketoconazole
K_i	inhibition constant
KOs	knockouts
LogD	distribution coefficient
LogP	octanol-water partition coefficient
LPS	lipopolysaccharide
LTD	long-term depression
LTP	long-term potentiation
MAPK	mitogen-activated protein kinase
MeOH	methanol
MLM	mouse liver microsomes
MTBE	methyl *tert*-butyl ether
MTDLs	multitarget-directed ligands
MW	molecular weight
NBS	*N*-bromosuccinimide
NFTs	neurofibrillary tangles
NF-κB	nuclear factor kappa-light-chain-enhancer of activated B cells
NMDA	*N*-methyl-D-aspartate
NO	nitric oxide
OA	okadaic acid
PAMPA	parallel artificial membrane permeability assay
$Pd(dppf)Cl_2$	1,1′-bis(diphenylphosphino)ferrocene]dichloropalladium(II)
$Pd(PPh_3)_4$	tetrakis(triphenylphosphine)palladium(0)
Pd/C	palladium on carbon

Pe	permeability coefficient
P-gp	P-glycoprotein
PPh_3	triphenylphosphine
p-TSA	*para*-toluenesulfonic acid
QD	quinidine
ROCK1	Rho-associated coiled-coil protein kinase 1
ROS	reactive oxygen species
rt	room temperature
SAPK	stress-activated protein kinase
SAR	structure-activity relationship
SD	standard deviation
SE	sulfaphenazole
SEM	standard error of the mean
T_3P	propanephosphonic acid anhydride
TBAF	tetra-*n*-butylammonium fluoride
TBDMS	*tert*-butyldimethylsilyl
TBK	tank-binding kinase
t-BuOK	potassium *tert*-butoxide
TEA	triethylamine
TFA	trifluoroacetic acid
THF	tetrahydrofuran
TLRs	Toll-like receptors
TNF-α	tumor necrosis factor-α
TPSA	topological polar surface area
XPhos Pd G2	chloro(2-dicyclohexylphosphino-2′,4′,6′-triisopropyl-1,1′-biphenyl)[2-(2′-amino-1,1′-biphenyl)]palladium(II)
Xphos	2-dicyclohexylphosphino-2′,4′,6′-triisopropylbiphenyl

1. Introduction

1.1. Overview of Alzheimer's Disease

Dementia is a pathological condition associated with a progressive decline in cognitive functions due to neurodegenerative changes and resulting loss of neurons. Among the various types of dementia, Alzheimer's disease (AD) is the most common cause and its prevalence increases as the global population ages. According to the World Health Organization, the disease is ranked as the fifth leading cause of death, imposing a vast burden on the global economy [1]. Aside from disrupted memory patterns, AD frequently manifests with behavioral and psychological symptoms of dementia (BPSD), such as hallucinations, apathy, anxiety, or depression [2].

Neurodegenerative changes in AD primarily affect the cerebral cortex and hippocampus, driven by tau protein aggregates known as neurofibrillary tangles (NFTs) and amyloid β (Aβ) plaques, which are hallmarks of AD [3]. The phenomenon of protein aggregation underlays AD pathophysiology, however, the molecular mechanisms driving plaque formation remain elusive. The tau hypothesis suggests that excessive phosphorylation of the microtubule-associated protein tau leads to its detachment from microtubule and subsequent disassembly of the microtubule structure. Hyperphosphorylated tau in its unbound form begins to accumulate into insoluble paired helical filaments, eventually leading to the formation of intracellular NFTs. This process is attributed to the disrupted equilibrium between the activities of phosphorylation state-controlling enzymes – kinases and phosphatases [4,5]. The amyloid hypothesis posits that the accumulation and aggregation of the Aβ peptide arise from an imbalance between its production and clearance [6]. Aβ peptide is produced from amyloid precursor protein (APP) that is cleaved by the enzyme β-secretase (BACE1) via amyloidogenic pathway [7]. Once formed, Aβ aggregates into higher-order protein assemblies in the form of highly toxic oligomers, protofibrils and senile plaques, which drive a cascade of events leading to neuronal degeneration. Sustained elevation of Aβ levels promotes massive calcium influx, mitochondrial dysfunction, and among others, changes in the kinase/phosphatase system [8]. Moreover, Aβ deposits trigger an innate immune response by binding to microglial pattern recognition receptors, such as Toll-like receptors (TLRs), which activate their prominent intracellular regulator – the NF-κB signaling pathway. [9]. This in turn, leads to the maturation and release of pro-inflammatory mediators: interleukin-1β (IL-1β), interleukin-6 (IL-6), tumor necrosis factor-α (TNF-α), nitric oxide (NO), and reactive oxygen species (ROS), resulting in neuroinflammation. Evidence from clinical studies demonstrates that about 20% of AD patients exhibit chronic inflammation of the nervous tissue [10,11]. These events further increase tau phosphorylation, disrupt the oxidative and metabolic balance, induce synaptic dysfunction, and correlate with disease progression [12,13].

Given the complexity of Alzheimer's disease, the development of novel, innovative therapeutic solutions remains a significant challenge. Currently, accessible

pharmacological interventions, such as cholinesterase inhibitors (donepezil, galantamine, and rivastigmine) and the *N*-methyl-D-aspartate (NMDA) receptor antagonist memantine, focus on providing temporary cognitive and functional improvement and slightly delay symptom progression, but do not target the underlying neurodegenerative process [14,15]. In 2021, the Food and Drug Administration (FDA) granted accelerated approval to the anti-amyloid monoclonal antibody aducanumab, marking a landmark milestone in AD treatment. The primary objective was to enhance the clearance of Aβ deposits in patients with mild cognitive impairment. However, in 2024, the manufacturer discontinued aducanumab to reallocate resources toward another anti-AD antibody, lecanemab [16]. Despite the clinical potential, both drugs are associated with severe side effects and considerable treatment costs [17–19]. Additionally, a third antibody, donanemab, has shown efficacy in slowing cognitive decline by only 4–7 months. These therapeutic interventions are currently restricted to addressing early symptomatic stages of AD [20]. The search for disease-modifying therapies remains a major priority, as evidenced by ongoing clinical trials. Small-molecule compounds continue to dominate the field, with the primary areas of focus on targeting inflammatory processes and enhancing synaptic plasticity and neurogenesis. Among the disease-modifying biologics, the development primarily includes anti-Aβ and anti-tau antibodies, as well as antibodies with anti-inflammatory properties [21]. Validation of the hypothesis regarding their effectiveness will be pivotal in shaping future therapeutic strategies for AD.

1.2. GSK-β kinase and its functions

Glycogen Synthase Kinase 3 (GSK-3) is a protein kinase, initially recognized for its critical role in the regulation of glycogen metabolism [22]. In mammals, there are two highly homologous isoforms of GSK-3: GSK-3α and GSK-3β. Although the two kinases share a high degree of similarity, genetic studies have demonstrated functional differences between them. GSK-3β is essential for embryonic development, with knockouts (KOs) being lethal, whereas GSK-3α KO mice survive, albeit with significant consequences [23]. GSK-3α plays a key role in metabolic regulation by influencing glucose and insulin sensitivity. Conversely, GSK-3β is crucial for processes like TNF-α-induced NF-kappaB activation in hepatocytes [24].

Besides its influence on glycogen synthase regulation, the GSK-3β isoform is highly expressed in the central nervous system (CNS), and its levels increase with age [25]. Therefore, GSK-3β has attracted more attention as a target, especially for the regulation of neurological functions.

GSK-3β is implicated in the onset and progression of Alzheimer's disease through its involvement in the formation of Aβ plaques and neurofibrillary tangles. Primarily, GSK-3β regulates BACE1 gene expression, thereby exacerbating amyloidogenic APP processing. Studies on SH-SY5Y cells showed that disrupting GSK-3β activity in two independent approaches – either through GSK-3β knockout or by treatment with its selective inhibitor – decreased BACE1 mRNA levels. The molecular mechanism depends on NF-κB signalling, as disruption of NF-κB expression correlated with blocked GSK-3β-induced BACE1 transcription [26]. Consequently, inhibition of GSK-3β activity attenuates APP cleavage and improves memory deficits in several AD animal models [26–28]. Additionally, direct phosphorylation of APP by GSK-3β affects its trafficking to the plasma membrane, leading to neuronal accumulation, disrupted calcium homeostasis, and altered neuronal excitability in rat cortical neurons [29]. The deposition of Aβ aggregates enhances the activity of GSK-3β, initiating a vicious cycle leading to increased levels of tau oligomerization, cellular uptake, accumulation, and toxicity [4]. Therefore, GSK-3β inhibition reduces NFTs formation and restores cognitive deficits both *in vitro* and *in vivo* [30,31].

GSK-3β, as a pleiotropic enzyme, also has an impact on the modulation of the immune response within the CNS [32]. Studies using lipopolysaccharide-induced (LPS) inflammation in BV-2 microglial cells and genetic mutants of NF-κB regulators have proven that GSK-3β participates in NF-κB signalling through several mechanisms:

- Transactivation of the p65 subunit, a member of NF-κB family, by controlling its acetylation state, which is required for its transcriptional activity [33].
- Affecting signaling cascades, such as the MLK3/JNK pathway, which influence NF-κB-mediated gene expression [34].
- Phosphorylation of directly controlling components, such as the IKK-γ kinase subunit [35].

Moreover, GSK-3β regulates the release of pro- and anti-inflammatory mediators induced by TLR agonists – a model of Aβ-triggered neuroinflammation [36]. Inactivation of GSK-3β decreases pro-inflammatory IL-1β, IL-6, TNF-α, interleukin-12 (IL-12), interferon gamma (IFN-γ) and NO levels while increasing anti-inflammatory interleukin-10 (IL-10) levels *in vivo* [34,37,38].

The cognitive decline associated with AD may be alleviated by the indirect modulation of learning and memory consolidation through alternative mechanisms by GSK-3β. GSK-3β is known to regulate neurogenesis, and its inhibition in neuronal stem cells facilitates neurite development and axon-dendrite polarization [39,40]. Furthermore, GSK-3β plays a crucial role in synaptic plasticity. Long-term potentiation (LTP) is a long-lasting enhancement in signal transmission between two neurons resulting from their simultaneous activation, induced by NMDA receptors. During the LTP state, GSK-3β undergoes inhibitory phosphorylation, which is essential for maintaining synaptic strength. Conversely, the activation of GSK-3β promotes a switch to long-term depression (LTD), reducing synaptic efficacy [41,42]. These findings are supported by results from *in vivo* studies on transgenic Tet/GSK-3β mice, which lack aberrant tau deposits, have shown that overexpression of GSK-3β activity impairs spatial learning in the Morris Water Maze [43]. This evidence suggests a strong correlation between GSK-3β and alterations in intracellular signalling pathways. The modulation of the aforementioned processes, along with the influence on Aβ and tau protein aggregation and neuroinflammation, underscores the potential therapeutic significance of targeting GSK-3β in the treatment of AD.

.

1.3. GSK-3β inhibitors

GSK-3β modulates different signalling cascades, and its inhibition has been explored in addressing diabetes [44], cancers [45], inflammation [46], cerebral ischemia [47], and various neuropsychiatric disorders with neurodegenerative backgrounds [48]. However, the development of GSK-3β inhibitors has reached a golden era of advancement, particularly in the context of designing future treatments for AD treatment [49–52]. In the following subsection, I highlighted selected chemical groups based on the dominant scaffold and the adenosine triphosphate (ATP)-competitive binding mechanism that have been investigated in AD-animal models, along with a brief summary of the drug candidates from clinical trials.

Maleimides

Among the earliest synthetic inhibitors of GSK-3β are the maleimide derivatives **SB-216763** and **SB-415286** (Figure 1), developed by GlaxoSmithKline, which inhibited nonselectively GSK-3α and GSK-3β with similar potency (IC_{50} of 34 nM and 78 nM, respectively) [53]. Both compounds exhibited neuroprotective effects by preventing neuronal cell death in response to potassium deprivation and inhibited phosphorylation of tau protein both in HEK293 cells [54] and *in vivo* [55]. From a molecular perspective, the maleimide core serves as a scaffold that interacts with the amino acid residues of the kinase hinge region, specifically binding to the Asp133 carbonyl oxygen and the backbone nitrogen of Val135 in GSK-3β. The hinge region possesses highly conserved amino acids within the protein kinase family, potentially leading to a lack of selectivity for compounds targeting this site. However, both compounds exhibited a high selectivity profile at the panel of 24 kinases. Given their potent activity, selectivity, and *in vivo* performance in neurodegenerative models, maleimides have garnered significant interest, leading to the synthesis of numerous derivatives [56]. Among this class, compound **1** containing pyrazolo[1,5-*a*]pyridinyl moiety, exhibited outstanding GSK-3β inhibitory potency (IC_{50} = 0.7 nM) and blocked tau phosphorylation in SH-SY5Y neuroblastoma cells [57], while compound **2** with macrocyclic structure (IC_{50} = 3 nM), demonstrated improved selectivity over 100 other kinases due to its pyridine-containing linker [58].

A structurally related natural compound is **staurosporine**, an alkaloid isolated from the bacterium *Streptomyces staurosporeus*. **Staurosporine** acts as a nonselective inhibitor of protein kinases and exhibits potent inhibitory activity against GSK-3β as well (IC_{50} = 15 nM) [59]. It demonstrates a broad spectrum of activities, including antifungal and hypotensive effects. However, due to its strong cytotoxicity against cancer cells, staurosporine is primarily used as an inducer of apoptosis [60].

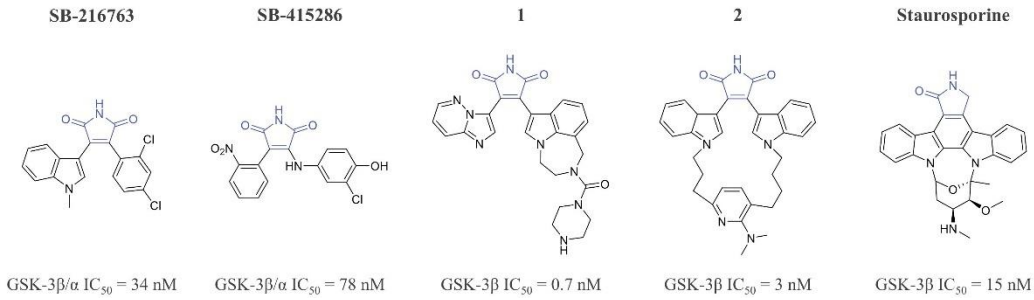

Figure 1. GSK-3β inhibitors based on maleimide core: **SB-216763** and **SB-415286** reported by Coghlan et al. [53], **1** published by Engler [57], **2** developed by Johnson & Johnson [58], and **staurosporine**.

Aminopyridines & -pyrimidines

In 2015, Sivaprakasam et al. proposed a model for constructing high-affinity ATP-competitive GSK-3β inhibitors. This inhibitor model combines structural elements that target the kinase hinge region and interact with a lysine residue crucial for ATP catalysis. These elements are connected by a central heterocyclic spacer, ensuring their optimal spatial arrangement. Analysis of ligand/GSK-3β X-ray complexes from the Protein Data Bank, combined with screening of the in-house library, led to the identification of a novel pyrrolopyridinone chemotype (Figure 2), with an aminopyridine core as a fixed, hinge binding fragment. Based on these findings several compounds were synthesized and evaluated for their biological activity. Compound **3**, with a phenyl spacer, was classified as a potent inhibitor with an IC_{50} of 2.4 nM. Exchanging the cyclic amide with a second benzene ring to form naphthalene derivative **4** dramatically reduced inhibitory potency due to the lack of a group with the hydrogen bond acceptor functionality. Structural diversification to thiazole derivative **5** resulted in activity against GSK-3β with the IC_{50} of 30 nM, while modifying the substitution pattern of the amide and methoxy substituent, as seen in the last compound (which serves as a reference in the research project presented within this doctoral dissertation, referred to as compound **I**), further increased inhibitory potency to 1.1 nM. Then, compound **5** and compound **I** were subjected to selectivity screening, revealing the superiority of compound **5** over compound **I**. However, due to its outstanding inhibitory potency, compound **I**, along with compound **3**, were evaluated in an Alzheimer's disease model using 3xTg-C57BL6 mice with elevated levels of hyperphosphorylated tau protein. Compound **I** exhibited a significant reduction in phosphorylated tau levels, whereas compound **3** did not show an effect compared to the vehicle. Therefore, despite a poor selectivity profile, thiazole derivative compound **I** was considered a lead candidate for further development.

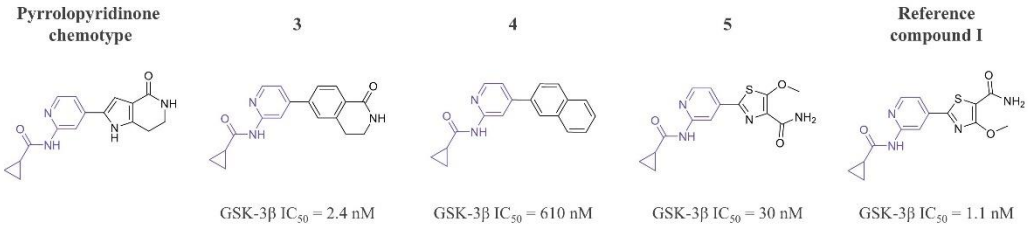

Figure 2. GSK-3β inhibitors reported by Sivaprakasam et al. based on aminopyridine core [61].

Luo et al. published a series of GSK-3β inhibitors designed based on the Sivaprakasam paradigm (Figure 3), utilizing an isonicotinamide derivative. The molecules consist of an aminopyridine core to interact with the hinge region and a second pyridine moiety acting as a hydrogen bond acceptor to target the catalytic lysine, both of which are linked by an amide group. Additionally, various substituents were introduced at the 4-position of the pyridine (**6**–**7**) to target the hydrophobic pocket that adopts ribose of ATP, optimizing potency and selectivity. The novel inhibitors demonstrated high inhibitory potency and selectivity against a panel of 400 kinases, except for GSK-3α, which they inhibited with similar potency to the β isoform. The most promising compounds, such as **6** and **7**, were investigated *in vivo* for their effects on tau phosphorylation levels in a triple transgenic AD mouse model. In metabolic stability studies, the compounds underwent high clearance in rodent liver microsomes, due to the hydrolysis of the pyridyl-2-aminocarboxamide and pyridyl *N*-oxidation. Nonetheless, they demonstrated significant *in vivo* activity following oral administration at a dosage of 30 mg/kg [62]. Consequently, the Luo group designed a novel series of isonicotinamides, exploring alternative substituents and their patterns at the 3- 4- and 5-position of the pyridine ring targeting the catalytic lysine. While the compounds showed improved inhibitory potency, their microsomal stability remained poor. The most promising candidate, **8**, a close 3-substituted analogue of **7** exhibiting high metabolic stability, did not demonstrate any oral activity in an AD mouse model when administered at the same dosage of 30 mg/kg [63].

The isonitcotinamide derivatives were also explored in research published by Shi [64]. The compound structure incorporates an additional amino group attached to the 3-pyridine ring, resulting in substituted 2,3-diaminopyridines that facilitate metal chelation ability in coordination with nitrogen from amide bond or imine nitrogen. The dyshomeostasis of heavy metal ions such as Cu^{2+} or Zn^{2+} and their accumulation are known to exacerbate the Aβ aggregation and toxicity, while also promoting the generation of ROS due to their redox activity [65]. Therefore, compounds that act as a metal chelators are endowed with antioxidant properties and are considered as potential anti-AD therapeutics [66]. The series of amide derivatives, represented by compound **9**, exhibited moderate inhibitory potency (IC_{50} = 148 nM) and weak chelating ability due to the electron-withdrawing nature of carbonyl oxygen, which decreases electron density and reduces metal-chelating potency. Changing the amide bond to an imine,

as in compound **10**, resulted in stronger GSK-3β inhibition (IC_{50} = 49 nM), which similarly led to the inhibition of Cu^{2+}-induced Aβ aggregation and ROS formation *in vitro*. Furthermore, compound **10** inhibited Aβ-induced tau protein phosphorylation in SH-SY5Y cells, demonstrating ist multidirectional activity.

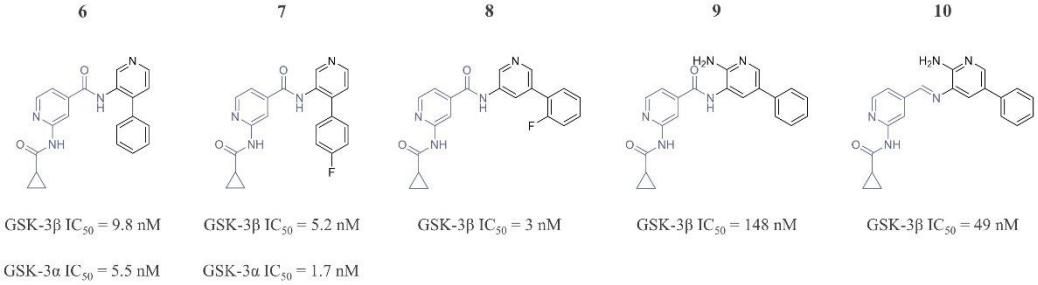

Figure 3. Isonicotinamides as GSK-3β inhibitors: **6**, **7** [62] and **8** [63] published by Luo et al., **9** and imine derivative **10** reported by Shi et al. [64].

A structurally related class of GSK-3β inhibitors are recently reported aminopyrimidines (Figure 4) [67]. The design of these compounds was based on inhibitor **11**, isonicotinamide derivative published by Luo et al. [62]. However, due to the high clearance ratio, the fragment of pyridyl-2-aminocarboxamide, which underwent hydrolysis, required optimization. The optimization resulted in compound **12**, which incorporates a pyridin-2-yl-amino group, with the pyridine nitrogen acting analogously to the carbonyl oxygen as a hydrogen bond acceptor, achieving subnanomolar inhibitory activity against GSK-3β (IC_{50} = 0.89 nM). The general structure of the inhibitors underwent several modification strategies: (1) replacing the pyridine heterocycle with a pyrimidine; (2) structure-activity relationship (SAR) studies of the substituent at the 2-position of the pyrimidine; and (3) varying the substituents and their patterns on the 3-pyridinyl ring. These modifications led to the development of inhibitor **13** (IC_{50} = 0.20 nM), which incorporates a phenyl ring in the hinge binding motif, facilitating hydrophobic interactions, and a 4,4-difluoropiperidin-1-yl substituent at the 3-pyridine position, targeting the kinase's sugar pocket. The latter modification significantly influenced metabolic stability *in vitro*, resulting in a high clearance rate. Replacing this group with a 4-fluorophenyl substituent resulted in the development of the lead compound **14**. In addition to its high potency against GSK-3β (IC_{50} = 0.35 nM), compound **14** exhibited high metabolic stability *in vitro* and high oral bioavailability *in vivo*, significantly lowering tau phosphorylation in a triple-transgenic mouse model.

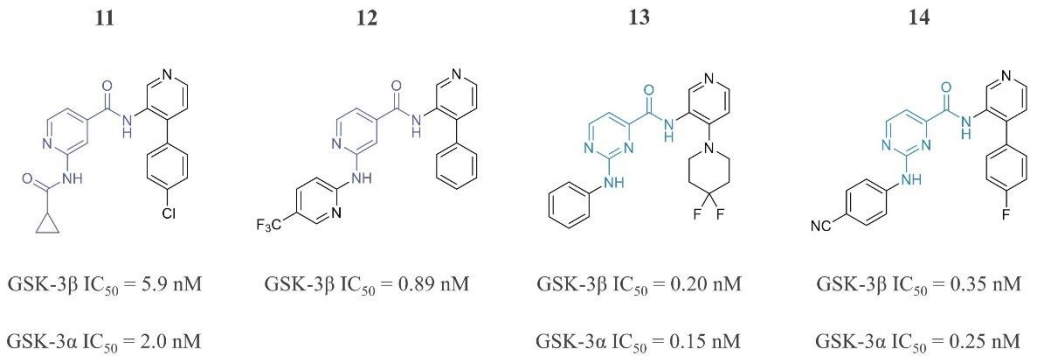

Figure 4. GSK-3β inhibitors containing aminopyridine: compounds **11** [62] and **12** [67], and aminopyrimidine scaffold: **13** and **14** [67].

Supported by promising results from *in vivo* experiments, several compounds advanced to clinical trials (Figure 5). However, only two – **tideglusib** (**NP-031112**) and **AZD1080** – were developed for the treatment of AD. **Tideglusib** is a thiadiazolidinone derivative with potent inhibitory activity (IC_{50} = 62 nM), exhibiting a non-ATP competitive binding mode [68]. In APP/tau double transgenic mice, **tideglusib** effectively reduced tau phosphorylation and decreased Aβ deposition, thereby restoring spatial memory deficits [69,70]. Moreover, it decreases the expression of TNF-α and (cyclooxygenase-2) COX-2, activated during the inflammatory response, and exerts a potent neuroprotective effect in glutamate-induced toxicity in rat astrocytes and microglia [71]. The results obtained in Phase I also confirmed its safety and tolerability along with improved cognitive functions compared to placebo [72]. Nevertheless, the study was terminated after Phase II due to a lack of significant efficacy in an expanded cohort of patients with mild to moderate AD [73]. Apart from trials for AD treatment, **tideglusib** has been or is currently being investigated for the treatment of other neurodegenerative disorders, such as progressive supranuclear palsy and amyotrophic lateral sclerosis, as well as myotonic dystrophy, autism, and arrhythmogenic cardiomyopathy [74]. The second potential drug candidate, ATP-competitive indole derivative **AZD1080**, inhibited tau protein phosphorylation *in cellulo* and restored the LTP state after blockade by an NMDA receptor antagonist [75]. However, after preliminary classification into Phase I, the trials were eventually abandoned due to severe side effects observed in dogs at clinically relevant doses [76]. Other compounds that progressed to clinical trials are ATP-competitive GSK-3β inhibitors and were evaluated for the treatment of several types of tumors: maleimide derivatives **LY2090314** and **elraglusib** (**9-ING-41**), as well as **TWS119** with a pyrrolopyrimidine core [77]. Both maleimide derivatives were investigated in combination with standard chemotherapy to achieve synergistic anti-tumor efficacy [78–80]. Moreover, **elraglusib** was effective in inhibiting myofibroblast differentiation and therefore attenuated the progression of pulmonary fibrosis [81], while **TWS119** proved its effectiveness in alleviating brain damage after ischemic stroke in rats [82]. This year, the FDA granted orphan drug designation to **elraglusib** for the treatment

of patients with soft tissue sarcoma, marking it as the first approved GSK-3β inhibitor available on the market [83].

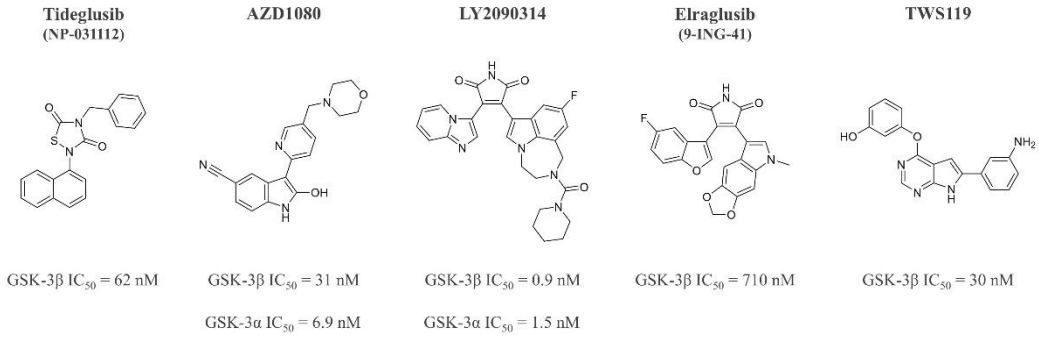

Figure 5. GSK-3β inhibitors that reached clinical trials with **elraglusib** that is the first GSK-3β inhibitor approved for soft tissue sarcoma.

1.4. IKK-β kinase and its functions

A regulatory network activated in response to Aβ deposits involves signal transduction mediated by the NF-κB (Nuclear Factor kappa-light-chain-enhancer of activated B cells) [84]. The NF-κB is a family that consists of five transcription factors: p105/p50 (NF-κB1), p100/52 (NF-κB2), p65 (RelA), RelB, and c-Rel, which under physiological conditions form inactive complexes with the IκB inhibitory protein (inhibitor of kappa B) in the cytoplasm. Upon pro-inflammatory stimulation, IκB is phosphorylated, triggering its ubiquitination and proteasomal degradation, which in turn results in the release of NF-κB from the dimer and its translocation to the nucleus. In the nucleus, NF-κB triggers the expression of target genes, including inflammatory cytokines, chemokines and other transcription factors [85]. A major pathway leading to the NF-κB activation is controlled by the IκB protein kinase complex (IKK), that contains two catalytic subunits (IKK-α and IKK-β) and a regulatory subunit (IKK-γ). Although IKK-α and IKK-β consist of similar structural domains with highly conserved amino acid sequences, they serve different functions. IKK-β activity is more critical in the regulation of the inflammatory NF-κB pathway and predominates under pathological stimuli [86]. In contrast, IKK-α is pivotal in epidermal keratinocyte differentiation and controls the morphogenesis of mesodermally derived skeletal structures [87]. Therefore, as a novel direction in the treatment of neuroinflammation, the inhibition of IKK-β isoform has gained significant attention [88]. The hypothesis already has demonstrated its plausibility based on results from animal models of AD. Neuronal deletion of IKK-β in APP-transgenic mice significantly decreases microglial activation and the transcription of TNF-α, IL-1β, and inducible nitric oxide synthase (iNOS) inflammatory genes, which correlated with improved cognitive functions and attenuated synaptic impairments [89]. Further studies revealed that IKK-β deficiency in myeloid cells enhances microglial recruitment toward Aβ deposits and facilitates their clearance [90]. Moreover, the improvement in cognitive functions is supported by the induction of LTP, which underlies synaptic plasticity [91]. Targeting the overexpressed IKK-β in another neurodegenerative condition with inflammatory pathogenesis, Parkinson's disease, similarly prevents microglial activation, attenuates neuron loss, and thereby alleviates its symptoms [92]. Apart from regulating the inflammatory response, NF-kB signalling facilitates BACE1 gene expression and thereby APP processing via the amyloidogenic pathway, which exacerbates AD progression through different molecular mechanisms [93].

Modulation of aberrant activation of the NF-κB cascade through IKK-β inhibition plays a role in addressing distinct pathological conditions, revealing a multifaceted function of the kinase:

- Induction of cancer cell death through antiproliferative mechanisms, including the inhibition of cell division and promotion of apoptosis [94–96]. When combined with chemotherapeutic agents, inhibitors enhance sensitivity to cytotoxic effects [97,98].

- Attenuation of joint tissue destruction in rheumatoid arthritis and inhibition of fibrotic reaction – a pathological state causing organ dysfunction. In both conditions the mechanism relied on the prevention of the release of cytokines followed by activation and recruitment of macrophages [99–102].
- Suppression of human immunodeficiency virus type 1 (HIV-1) replication, resulting from the downregulation of viral gene expression controlled by cytokines or T-cell activators [103–105].
- Alleviation of pro-inflammatory myeloid cell activation and infiltration characteristic after spinal cord injury, thereby reducing neuronal loss and motor activity deficits [106,107].
- Enhancement of bone formation by promoting osteoblast differentiation while inhibiting osteoclast maturation and bone resorption – processes impaired in osteoporosis [108,109].
- Reduction of insulin resistance, body weight gain and lipid abnormalities which has an impact on metabolic diseases such as diabetes, obesity or atherosclerosis [110,111].

1.5. IKK-β inhibitors

Dysregulation of IKK-β kinase activity holds a fundamental role in the pathogenesis of many diseases with an inflammatory, autoimmune, and oncological background; therefore, the search for its inhibitors has been of special interest for more than two decades [112–115]. However, its crystal structure was not available until 2011, hence the inhibitors' discovery was often indicative and primarily based on the high-throughput screening, supported by further elucidation using constructed homology models of the kinase. Nevertheless, to date, numerous compounds targeting IKK-β have been developed with few that have progressed to clinical trials. These serve as pivotal probes for modulating diseases with disordered NF-κB activation.

The novel inhibitors presented within this dissertation aim to target the ATP-binding site. Therefore, in the following subsection, I focused on presenting selected compounds with the same mechanism of action and divided them into groups based on the heterocyclic core that they consist of. Their activity was confirmed in functional cellular assays and for some representatives also in animal models. In addition, I summarized the advances in clinical trials of compounds inhibiting IKK-β kinase.

Aminopyrimidines

The precursor of all synthetic small molecule IKK inhibitors is **SPC839** (also known as **AS602868**) reported in 2001 by Celgene Corporation. It selectively targets isoform β with the IC_{50} of 62 nM (Figure 6). The compound was developed for the treatment of rheumatoid arthritis and was effective in paw oedema [116] and acute myeloid leukemia animal models [117]. Three years later, Bingham et al. designed a novel group of inhibitors based on the aminopyrimidine core found in **SPC839**. However, the initial hit compound **15** lacked selectivity and inhibited both IKK-β and the α isoform with similar nanomolar potency [118]. The analysis of the structure-activity relationship of the multitude of electron-donating (as methyl, methyl ether) and electron-withdrawing (nitro group, nitrile, trifluoromethyl) substituents indicated that the latter are in favor of IKK-β selectivity. The lead compound **16** with improved selectivity was found to be effective in suppressing pro-inflammatory gene transcription in E-selectin reporter cell assay [119]. Subsequent redesign published by Shin et al. led to compound **17** (IC_{50} = 41 nM) with a sulfanilamide group that formed additional interactions in the solvent exposed region of the kinase and present potent anti-inflammatory activity in LPS-mediated inflammation *in cellulo* significantly reducing pro-inflammatory cytokine levels (IL-1α, IL-6, and TNF-α). Further research indicated that the anti-inflammatory effect was induced by the inhibition by inhibition of NF-κB translocation from cytosol to nucleus [120].

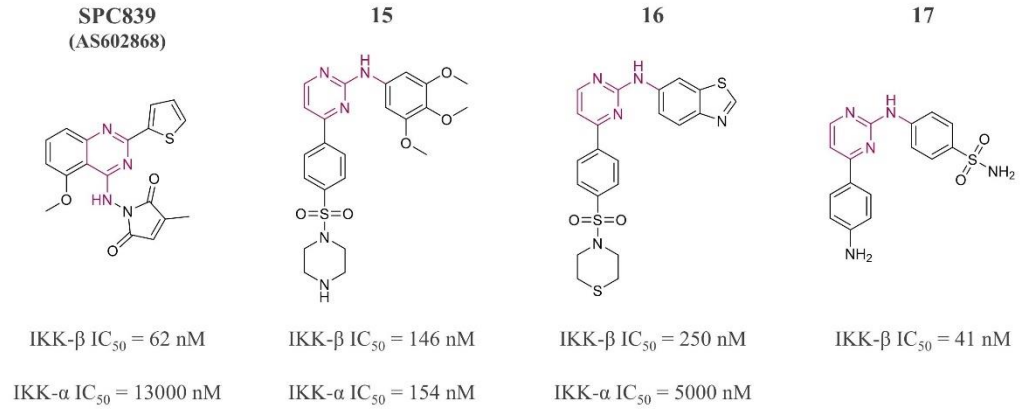

Figure 6. IKK-β inhibitors based on aminopyrimidine core reported by Palanki et al. (**SPC839**) [116], Bingham et al. (**15**) [118] and (**16**) [119] and Shin et al. (**17**) [120].

Independently Waelchli et al. designed a series of novel series of IKK-β inhibitors developed from the hit compounds (**18** and **19**) with micromolar activity, selected based on screening of Novartis archive (Figure 7A) [121]. The lead molecule **IKK16** with nanomolar activity (IC_{50} = 40 nM) and good oral bioavailability displayed potent pre-clinical therapeutic efficacy due to its anti-inflammatory and endothelial protective properties in LPS-induced acute model of cytokine release *in vivo*: hemorrhagic shock [122], sepsis [123], as well as in ventilation-induced lung injury [124], and acute kidney injury [125]. While another IKK-β inhibitor based on the aminopyridine scaffold **LY2409881** (IC_{50} = 30 nM) effectively inhibited the growth and survival of lymphoma both *in vitro* and *in vivo* by blocking antiapoptotic NF-κB signal activation (Figure 7B) [126].

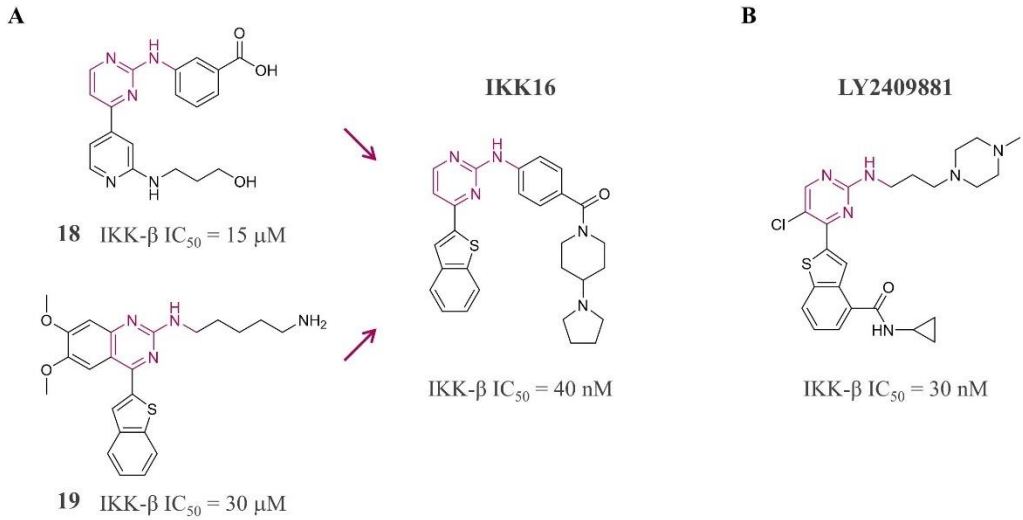

Figure 7. IKK-β inhibitors based on aminopyrimidine core: (**A**) hits from the screening of Novartis archive (**18** and **19**) with the lead compound **IKK16** [121], (**B**) **LY2409881** [126].

Pyridines

In 2003, Murata et al. introduced the novel class of potent pyridine analogues, derived from a scaffold identified through the screening of the Bayer library (Figure 8). The hit compound **20**, effectively inhibited IKK-β with an IC_{50} of 1.5 μM and exhibited activity in cellular assays (IC_{50} = 8 μM). These included inhibition of NF-κB-dependent reporter gene expression, as well as suppression of chemokines, cytokines, and IgE production. Structural optimization led to compound **21** in which the oxotetrahydrofurane moiety was replaced by basic piperidine in a 2-carbon linker, resulting in nanomolar activity against IKK-β (IC_{50} = 600 nM). Subsequently, both compounds were examined for LPS-induced TNF-α production in mice. Despite the promising efficacy after intraperitoneal administration, compound **20** lacks oral activity due to low bioavailability, while compound **21**, displayed anti-inflammatory effect after both oral and intraperitoneal administration [127]. Further optimization focused on enhancing cellular activity, which resulted in compound **22**. Compound **22** was derived by simplifying the structure of compound **21** through the removal of the pyridylpropanamide moiety and the replacement of the phenyl with a piperidine ring. These modifications resulted in increased inhibitory potency (IC_{50} = 25 nM), while retaining selectivity toward other kinases. Subsequent SAR studies on the piperidine ring confirmed that the unsubstituted NH group significantly influences the activity [128]. However, chemical instability of the compound in buffer solution led to the formation of a cyclized byproduct, resulting from a nucleophilic attack of the piperidine nitrogen onto the nitrile substituent. This, in turn caused the bioavailability of the **22** to fall below the threshold required to exert an *in vivo* effect. The applied structural rearrangement of the 4-piperidin-3-ylpyridine moiety into 4-piperidin-4-ylpyridine led to the development of **ACHP**, an analogue of **22**, with an additional alkoxy moiety. Optimization of the structure resulted in a robust *in vitro* profile (IKK-β IC_{50} = 8.5 nM, cell IC_{50} = 60 nM) and efficacy in *in vivo* anti-inflammatory assays (arachidonic acid-induced ear oedema model in mice), with favourable bioavailability due to the low clearance [129]. Since its development, **ACHP** demonstrated its activity in multiple oncological and inflammatory models such as: multiple myeloma [95], T-cell leukemia [96], LPS-induced acute lung injury [130], fibrosis [131] as well as in HIV-1 replication [105].

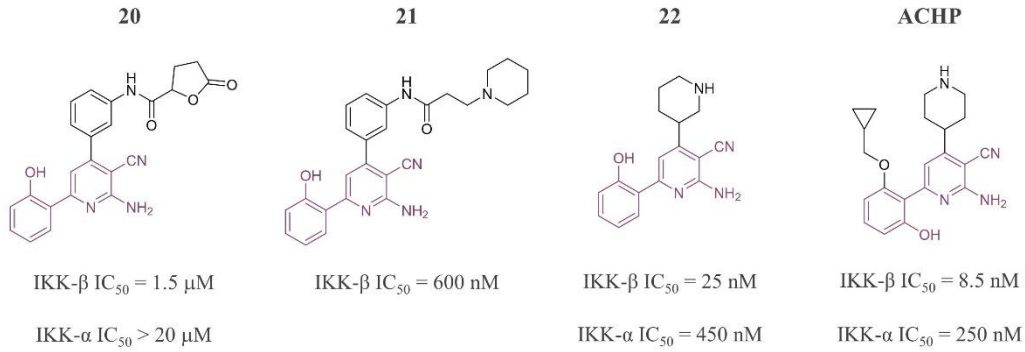

Figure 8. IKK-β inhibitors based on pyridine core reported by Murata et al. – **20** and **21** [127], **22** [128], **ACHP** [129].

Thiophene-based inhibitors

One of the most widely used frameworks among IKK-β inhibitors is thiophecarboxamide scaffold (Figure 9). The first compound bearing this structure was **SC-514** reported by Kishore et al. Despite its moderate, micromolar activity (IC_{50} = 3–12 μM), **SC-514** significantly inhibits transcription of NF-κB-dependent genes in rheumatoid arthritis-derived synovial fibroblast cells as well as was effective in LPS-induced TNF-α model of acute inflammation *in vivo* [132]. Subsequently, the scientists from Astra Zeneca proposed compounds based on the same core structure with incorporated urea moiety. As predicted by docking to the homologous model of IKK-β, the additional hydrogen bonding donor and acceptor were responsible for anchoring the inhibitor within the hinge binding region. Indeed, compound **23** has improved inhibitory activity (IC_{50} = 63 nM) compared with **SC-514**. However, 3-thienyl substituent was identified as a potentially metabolic labile moiety and was replaced with phenyl as in compound **24**. This change further increased the inhibitory potency (IC_{50} = 25 nM), but resulted in a decrease in selectivity toward IKK-α. The *para*-fluorinated analogue (which serves as a reference in the research project presented within this doctoral dissertation, referred to as compound **II**) retained activity at the nanomolar level with 100-fold selectivity over IKK-α. Assessment of compound **II** in cell-based assays proved that the compound inhibited TNF-α production, while its *in vivo* pharmacokinetic profile showed good oral bioavailability, however with limited solubility that may affect future lead development [133]. At last, **TPCA-1** synthesized at GlaxoSmithKline, is an isomer of compound **II** with an IC_{50} of 18 nM with confirmed efficacy in numerous animal models such as airway inflammation and asthma [134], arthritis [135] and non-small cell lung cancer [136].

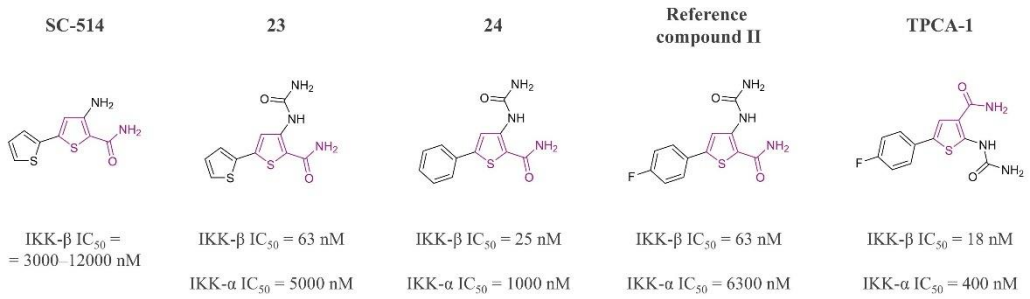

Figure 9. IKK-β inhibitors with thiophenecarboxamide scaffold: (**A**) **SC-514** reported by Kishore et al. [132] and **23**, **24** and compound **II** published by Baxter et al. [133], (**B**) structure of inhibitor **TPCA-1** [135].

Indoles

The 7-azaindole scaffold as a hinge binding functionality was proposed by Liddle et al. (Figure 10A). The first hit was compound **25**, identified during a kinase cross-screening assay, which demonstrated potent IKK-β inhibitory activity (IC_{50} = 40 nM). However, it was not selective toward alpha isoform (~6-fold), as well as for the panel of other kinases. Docking studies of compound **25** to the IKK-β homology model and performing SAR studies led to two key findings. First, the incorporation of a small substituent in the 2nd position of the indole should improve selectivity toward other kinases while maintaining the adjustment of the compound into the IKK-β binding pocket. Second, the ethylamine fragment with a sulfonamide group enhances the inhibitor's potency by interacting with the catalytic lysine. Additionally, the substitution of the sulfonamide's nitrogen tunes selectivity toward IKK-α. Consequently, the optimized structure was modified by introducing a methyl group at the 2nd position of indole, substituting the sulfonamide nitrogen with a methyl group, and replacing the terminal amine with a hydroxyl group. This hit optimization led to compound **26**, which demonstrated an improvement in selectivity toward IKK-α to 79-fold and toward other kinases while retaining inhibitory potency against IKK-β. Moreover, compound **26** was effectively inhibiting TNF-α-induced NF-κB receptor activation in cells [137].

Miller et al. proposed an indole-based scaffold with a primary amide substituted at the 7th position (compounds **27**–**29**, Figure 10B), discovered using pharmacophore-directed screening and **TPCA-1** as a reference inhibitor. The carboxamide formed hydrogen bonds not only with the hinge region of the kinase but also intramolecularly with the indole nitrogen; thus, compound **27** inhibited IKK-β in the micromolar range (IC_{50} = 1.6 μM). The subsequent introduction of the 3-piperidinyl ring at the 3rd position offered a possibility for additional hydrogen bond interaction and led to improvement in the inhibitory potency to 158 nM (compound **28**). According to the docking studies, the scientists further modified the compound structure by shifting the piperidine nitrogen atom to the 4th position and introducing a sulfonamide bond in compound **29**. This

enabled interaction with two additional amino acid residues, lysine and aspartic acid, resulting in inhibitory activity of 13 nM. Both compounds **28** and **29** were effective in cell-based assays by inhibiting LPS-induced TNF-α production. Furthermore, compound **29** prevented nuclear NF-κB translocation in TNF-α-treated cells and therefore represented a candidate with a good anti-inflammatory profile [138].

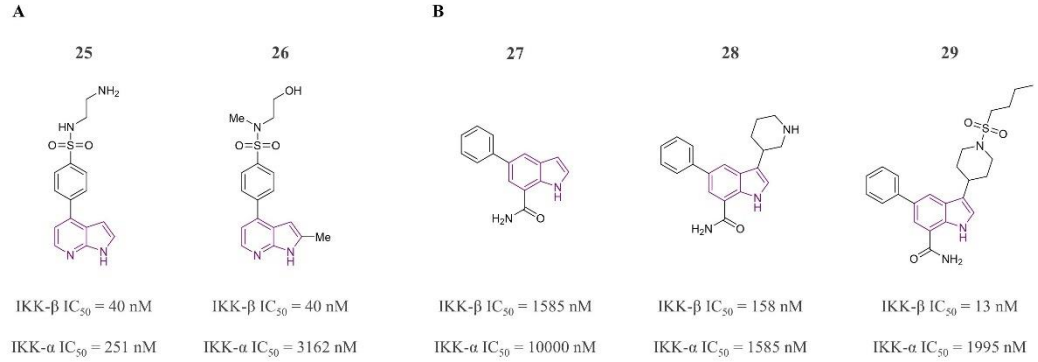

Figure 10. IKK-β inhibitors constructed with: (**A**) a 7-azaindole scaffold, reported by Liddle et al. [137] and (**B**) an indole-7-carboxamide core, published by Miller et al. [138].

Extensive efforts in the development of IKK-β inhibitors resulted in the advancement of several compounds to clinical trials (Figure 11). The forerunner was **MLN-0415** from Millennium Pharmaceuticals which in 2006 progressed to Phase I human trials for inflammatory disorders. However, the investigation was discontinued due to an unfavourable safety profile after multiple dose-escalating administrations [139]. The benzamide derivatives **IMD-0560** [140] and **IMD-0354** [102] were candidates reported by the Institute of Medicinal Molecular Design Inc., that underwent clinical trials for the treatment of rheumatoid arthritis, rheumatic osteoporosis and osteoarthritis (as a pro-drug of **IMD-0560** – **IMD-2560**) and atopic dermatitis (**IMD-0354**). Moreover, the **IMD-0354** pro-drug (with symbol **IMD-1041**) was evaluated in the proof-of-concept study for chronic obstructive pulmonary disease, however, the trial has an unknown status [141], similar to the other **IMD** compounds. The aminopyrimidine derivative **SPC-839** (described above – please refer to page 36) was qualified for Phase I for the treatment of hematological malignancies; nevertheless, due to the portfolio repositioning reasons was never tested in humans [139]. The Phase I studies of another candidate – the cyanoguanidine derivative **CHS-828** from LEO Pharma [142] – were also terminated due to no response after two courses of solid malignant tumor therapy [143]. The last compound that entered the clinical trial stage was **SAR-113945** (structure not disclosed) developed by Sanofi-Aventis for the treatment of knee osteoarthritis. The compound was a promising drug candidate due to its potent IKK-β inhibition (IC_{50} = 18 nM), high selectivity, and confirmed *in vivo* activity in animal models. Its pharmacokinetic assessments indicated sustained release and high exposure in the knee joint. Consequently, **SAR-113945** confirmed its safety and tolerability and successfully

progressed through Phase I. However, the candidate did not display significant efficacy in an expanded patient cohort and failed during phase II [144].

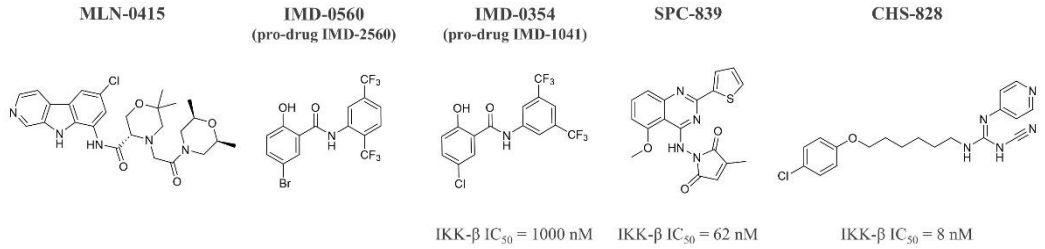

Figure 11. IKK-β inhibitors that reached clinical trials.

To date, none of the proposed inhibitors have fully succeeded in clinical trials, primarily due to unforeseen adverse effects or lack of efficacy. The absence of agents directly modulating IKK-β in the market leaves space for the rational development of novel drug candidates.

2. Aim of the presented research

The aim of the research conducted during my PhD program was to design, synthesize, evaluate in terms of biological activity, and study the structure-activity relationship of novel compounds that simultaneously inhibit GSK-3β and IKK-β kinases. This innovative approach, aimed to address the underlying mechanism of Alzheimer's disease. The foundation of this research was rooted in compelling evidence from scientific literature highlighting the role of these biological targets in Alzheimer's pathology:

- Protein aggregation: enhanced activity of GSK-3β, a key phosphorylating kinase, has been implicated in the pathological aggregation of proteins, particularly tau protein, leading to the formation of neurofibrillary tangles.
- Neuroinflammation: inflammation in nervous tissue is mediated by the NF-κB complex, whose activity is regulated by IκB kinases, with the IKK-β subunit playing a pivotal role in controlling the expression of nuclear pro-inflammatory genes.

The overall approach to achieve the stated objectives included:

1. Design of novel multifunctional compounds targeting GSK-3β and IKK-β kinases, based on the structures of known inhibitors published in the scientific literature, using knowledge-based methods and molecular modeling techniques.
2. Development of a synthetic approach and synthesis of the designed compounds using organic chemistry methods, with analytical characteristics of the obtained derivatives, including confirmation of their structure and purity through spectroscopic methods.
3. Computer-aided evaluation of selected physicochemical parameters of the novel compounds.
4. *In vitro* biological evaluation of inhibitory activity against GSK-3β and IKK-β kinases.
5. Structure-activity relationship analysis based on the results of *in vitro* and docking studies.
6. Comprehensive *in vitro* evaluation of the most promising candidates, including toxicity assessment, determination of anti-inflammatory activity and neuroprotective properties, and preliminary ADME profiling.

3. Results and discussion

3.1. Design of compounds

The doctoral dissertation presents four series of final compounds with potential multidirectional activity against GSK-3β and IKK-β kinases, following the paradigm of multitarget-directed ligands (MTDLs). The concept of multi-target-directed ligands emerged as a response to the limitations of the traditional "one-target, one-disease" approach in drug discovery. In the treatment of complex diseases such as neurodegenerative disorders [145], cardiovascular diseases [146], and cancer [147], single-target-acting drugs have often proved insufficient, as these conditions typically involve multiple factors contributing to their pathogenesis. Traditional strategies to overcome these limitations include providing a combination of several different drugs that modulate distinct therapeutic mechanisms or using a single pill that contains multiple drugs in one formulation. However, these methods may pose challenges for patients with compliance issues, such as individuals diagnosed with AD, and can be associated with side effects due to variations in the bioavailability, pharmacokinetics, and metabolism profiles of each drug. Therefore, the rationale behind MTDLs lies in their potential to enhance therapeutic efficacy by simultaneously modulating several molecular pathways; reducing the likelihood of adverse side effects by minimizing the influence of multiple drugs on ADME; and mitigating the emergence of drug resistance by addressing the multifactorial nature of a given disease [148]. The strategy aims to create hybrid molecules through a pharmacophore-based approach, which involves combining fragments selected from compounds that exhibit single pharmacological activities [149]. MTDLs have fundamentally transformed the field of medicinal chemistry in the pursuit of Alzheimer's disease therapies [150–152]. This approach has also influenced the development of GSK-3β inhibitors in combination with other targets implicated in the pathogenesis of AD [153–155].

Kinases are a superfamily of enzymes that regulate cellular signalling by transferring phosphate groups from ATP to specific substrates, a process known as phosphorylation. Both GSK-3β and IKK-β are serine/threonine protein kinases, therefore they phosphorylate the serine or threonine amino acid residue of the substrate protein [156]. The structural features are essential for their function and regulation. Kinases share a bilobal architecture, with a smaller *N*-terminal lobe containing five antiparallel β-sheet strands and a regulatory αC helix, and a C-terminal lobe comprising mostly α-helices. Both domains are connected by the hinge region, which anchors the adenine ring of ATP, and along with the deep cleft between them, they form the catalytic site. Every protein kinase sequence contains highly conserved motifs. The first is GxGxxG motif, known as glycine-rich loop (G-loop), which is located between the β1 and β2 strands of the *N*-terminal lobe. The G-loop is a highly flexible region that plays a crucial role in coordinating α and β phosphate groups of ATP. Adjacent to the glycine-rich segment in the β3 strand is the (V)AxK key motif, which contains a conserved lysine. The lysine residue binds the γ-phosphate group of ATP and catalyzes its transfer to the substrate.

The surface of the catalytic site depends on the kinase state and is regulated by the spatial arrangement of the αC helix and the activation loop (A-loop). The αC helix contains a conserved glutamic acid that, together with the catalytic lysine, constitutes (V)AxK motif. During the active state, the lysine forms a salt bridge with the glutamic acid, and their proximity helps stabilize the conformation of the kinase. This conformation is further supported by the interaction with the conserved tripeptide DFG (aspartic acid–phenylalanine–glycine) located at the *N*-terminus of the A-loop. When ATP is bound within the catalytic pocket, the triplet adopts the DFG-in conformation, characterized by an extended phenylalanine that stabilizes the complex, and aspartic acid that coordinates the Mg^{2+} ion required for catalysis. During the inactive state of the kinase, the DFG motif dislodged to the "out" position, sterically blocking ATP binding and leading to the unstructurisation of the A-loop. Within the activation loop are phosphorylation sites that regulate kinase activation through either autophosphorylation or transphosphorylation and it ends with the conserved tripeptide APE (alanine–proline–glutamic acid) [157–159].

The inhibition of kinases can be achieved through several strategies, including ATP-competitive inhibition, allosteric site inhibition, and inhibition by thiol-reactive compounds that covalently bind to key cysteine residues (Figure 12). Compounds that compete with ATP for binding to the kinase can be distinguished into two types: inhibitors that interact with the kinase in its active state (Figure 12A), and those that bind when the kinase is inactive (Figure 12B). In the active conformation, both the αC and the DFG motif are in their "in" positions, bending toward the binding pocket and thereby limiting its surface. Therefore, these types of inhibitors mainly interact with the hinge region residues, mimicking the binding of the adenine moiety of ATP. The inactive state of the kinase is characterized by the "out" conformation of the DFG motif, which, through outward movement, creates access to the back hydrophobic pocket. Inhibitors that bind to the inactive state interact both with the hinge region residues and with an adjacent hydrophobic pocket, stabilizing the kinase's conformation [160]. Type III inhibitors are compounds that target specific pockets of each kinase other than the ATP-binding site (Figure 12C). This strategy includes modulation of binding sites adjacent to the ATP-binding pocket or clefts localized distantly outside the catalytic domain. Allosteric inhibition offers a different mode of kinase activity regulation, which is highly specific and reduces the likelihood of resistance [161]. The fourth type, covalent inhibitors, are compounds with electrophilic warheads that react with nucleophilic residues, such as the thiol group in cysteine, forming covalent bonds (Figure 12D). These compounds are highly selective and offer a prolonged duration of residence due to the formation of stable connections [162]. By substituting the alpha position of the warhead with an electron-withdrawing group, it is possible to obtain reversible covalent inhibitors [163].

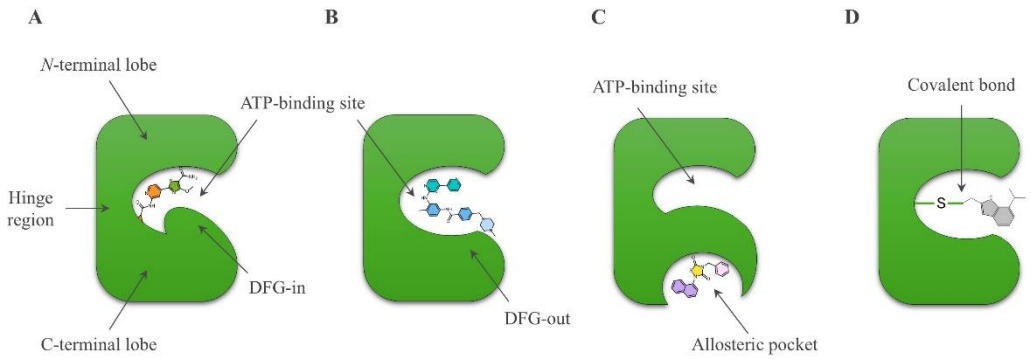

Figure 12. Representation of types of kinase inhibitors (prepared based on [157]): ATP-competitive (**A**) DFG-in and (**B**) DFG-out, (**C**) type III allosteric (binding site distant to the ATP), (**D**) type IV covalent.

In this work, the starting point for the design was ATP-competitive inhibitors reported in the literature – compounds **I and III** targeting GSK-3β [61,64] and compounds **II and IV** targeting IKK-β [133,164] (Figure 13–16). The proposed novel inhibitors consist of three structural elements – the hinge binding group, predominantly the *N*-(pyridin-2-yl)cyclopropanecarboxamide fragment, the spacer group, and the hydrogen bond acceptor (HBA) compatibile with catalytic Lys85 in GSK-3β and/or Lys44 in IKK-β – which contribute to efficient binding to the active site of the kinase.

3.1.1. Series I

In this series of compounds merging the *N*-(pyridin-2-yl)cyclopropanecarboxamide fragment of compound **I** with 3-ureidothiophene-2-carboxamide fragment of compound **II** led to **series IA** (Figure 13).

The *N*-(pyridin-2-yl)cyclopropanecarboxamide fragment contains a hydrogen bond acceptor-donor-acceptor motif, which is typically applied in GSK-3β ligands and provides interactions with Asp133–Val135 of the hinge region. To explore this chemical space and understand its impact on the potency of kinase inhibition in **series IA** and **IB** we replaced the pyridine ring with either 4-fluorobenzene, utilizing fluorine as a weak HBA [165], or benzene, which lacks this functionality. Additionally, we exchanged the carboxamide moiety at position 2 of the aromatic ring with a sulfonamide, followed by the introduction of various alkyl, cycloalkyl, and aromatic substituents. In **series IC**, the acceptor–donor system has been incorporated into the heterocycles, such as 7-azaindole (with hydrogen bond donor (HBD) group) and furo[3,2-*d*]pyrimidine (without HBD). These structures, also found in IKK-β ligands, were designed to interact with the hinge amino acid residues Cys99 and Gln100 [137]. The high similarity of this motif to the GSK-3β pharmacophore fragment suggests maintaining an affinity for both biological targets.

In parallel, 3-ureidothiophene-2-carboxamide fragment was intensively studied and modified. In **series IA**, we maintained the arrangement of the urea and carboxamide substituents unchanged to establish potential contacts with the catalytic Lys44 located inside the IKK-β binding pocket. Furthermore, the amide carbonyl group can create interactions with the analogous Lys85 residue in the GSK-3β active site. In the **series IB** and **IC** structure modifications led to ring closure to the tetrahydropyrimidone moieties. The aim was to maintain the potential binding pattern while optimizing the physicochemical parameters by reducing HBD and HBA and rigidifying the structure by lowering the number of rotatable bonds. To further explore the binding area in **series IB**, we introduced spirocyclic systems – cyclopentyl or tetrahydrofuryl, alongside the dimethyl group also found in **series IC**. In all **IA**, **IB**, and **IC series**, the thiophene ring serves as a fixed spacer group.

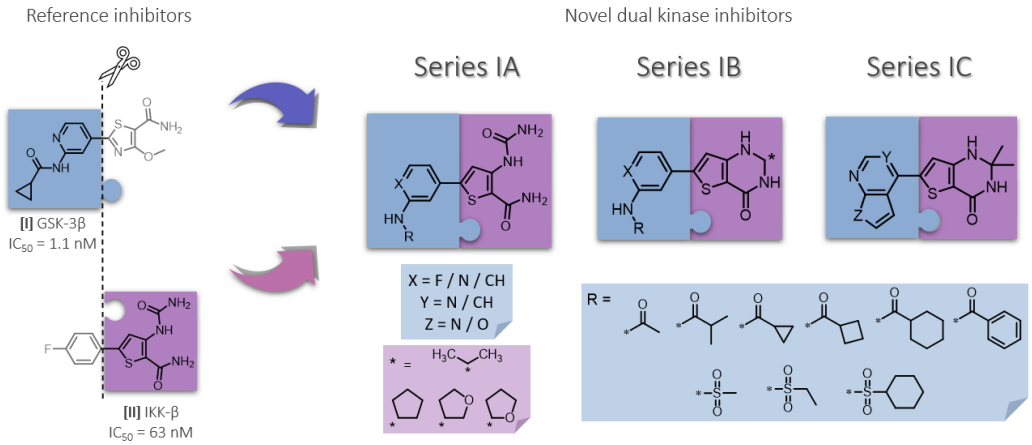

Figure 13. Design of compounds from **series I**.

3.1.2. Series II

The compounds in **series II** were designed based on the structures of GSK-3β inhibitor **III** (IC_{50} = 127 nM) [62] and the IKK-β inhibitor **IV** ("IMD-0354", IC_{50} = 1 μM) [164]. These compounds share a common structural feature of two aromatic fragments connected by an amide bond (Figure 14), which provides an opportunity to design merged-type derivatives. Additionally to their confirmed activity in both *in vitro* and *in vivo* models of tauopathy and inflammatory processes, both compounds are characterized by good drug-like properties due to their small size and potential ability to penetrate the blood-brain barrier. Therefore, we designed the novel inhibitors by retaining the *N*-(pyridin-2-yl)cyclopropanecarboxamide as a hinge-binding scaffold and connecting it via an amide spacer to a 3,5-bis(trifluoromethyl)benzene ring derived from the salicylanilide **IV** inhibitor. Subsequently, we explored the impact of benzene substitution and exchanged the 3,5-bis(trifluoromethyl) group with various types of substituents selected according to the Topliss scheme in *ortho*, *meta*, and *para*

positions: activating (methyl, methyl ether, hydroxyl), deactivating (nitro group, trifluoromethyl) and halogens (fluorine and chlorine). Apart from the benzene ring, we also utilized heterocyclic systems such as pyrrole, indole, and thiophene.

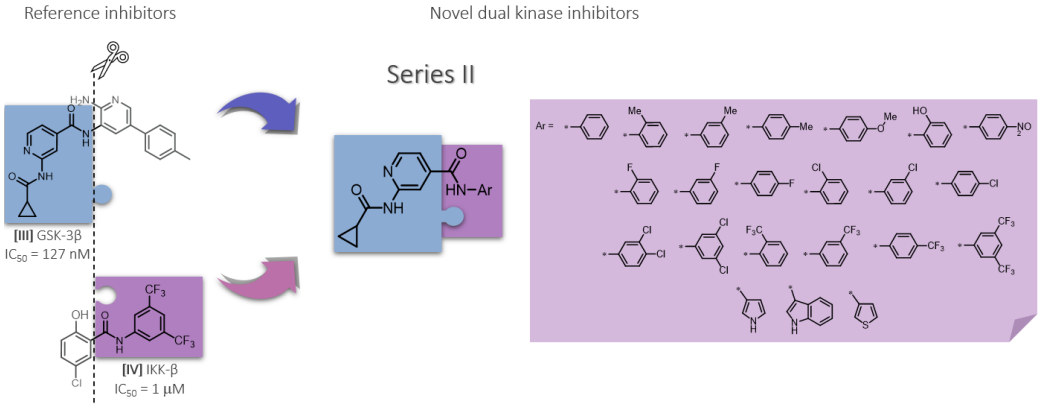

Figure 14. Design of compounds from **series II**.

3.1.3. Series III

The **third series** of inhibitors includes compounds wherein the *N*-(pyridin-2-yl)cyclopropanecarboxamide fragment is connected to a heterocyclic 2,5-dihydro-1*H*-pyrrole spacer. We exploited the secondary amino group of pyrrole to attach various HBA substituents: reversed short-chain amide, alkyl/cycloalkyl sulfonamides, or a urea derivative to steric substituents with 2-methylpyrrolidine and 2-carbonylpyrrolidine, as well as primary aliphatic amines on 2-/3-carbon chain linked by an amide or sulfonamide bond (Figure 15).

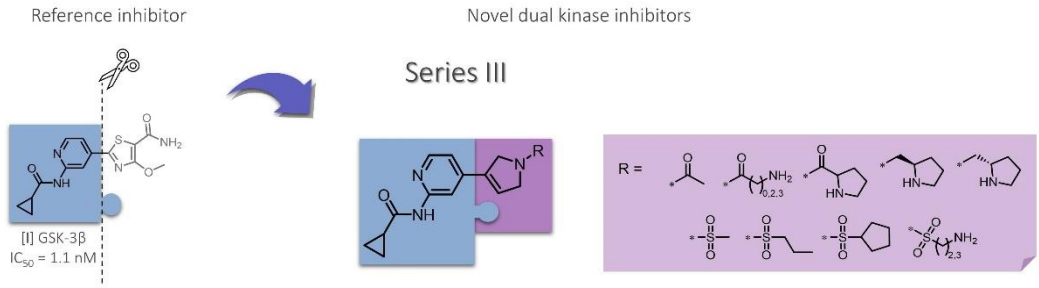

Figure 15. Design of compounds from **series III**.

3.1.4. Series IV

In designing **series IV** we used a dual GSK-3β/IKK-β inhibitor (reference compound **V**) obtained at the Department of Physicochemical Drug Analysis (Figure 16). Compound **V** is an analogue of the **IB series** compounds, featuring a tetrahydropyrimidone scaffold with one amino group removed, resulting

in the formation of a pyridinone fragment. Compounds in the **IVA series** also contain this pyridinone fragment with the cyclic amide substituted with a methyl group or alkyl groups bearing terminal amine or hydroxyl functionalities. In **series IVB**, the cyclic amide was replaced with a cyclic sulfonamide to investigate its effect on the inhibition of IKK-β kinase, along with the introduction of an additional secondary hydroxyl group. Following the strategy as in the **IVA series**, the sulfonamide nitrogen was methylated or substituted with alkyl moieties containing terminal amino or hydroxyl groups. Additionally, we evaluated the compound with a condensed tricyclic system obtained unexpectedly as a by-product in the synthesis.

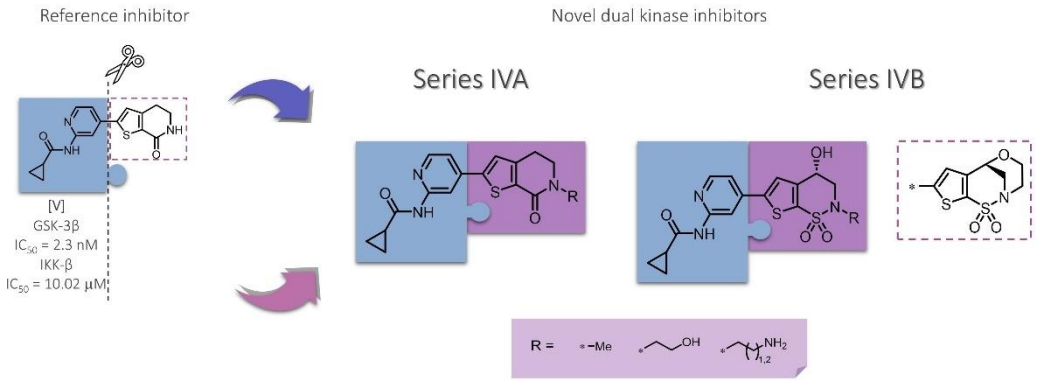

Figure 16. Design of compounds from **series IV**.

3.2. Chemistry

3.2.1. Series I

To obtain the compounds from **series IA** and **IB** we applied separate routes for the six-membered aromatic ring derivatives (pyridine/phenyl/fluorophenyl) and for thiophene building blocks and then combined them in the last step (Scheme 1)[1]. Thiophene derivatives with urea and tetrahydropyrimidone moieties were obtained from the commercially available methyl 3-amino-5-bromothiophene-2-carboxylate. In the first step, the primary amino group was protected with Boc anhydride to compound **1**, followed by the hydrolysis of an ester with an aqueous KOH solution. The resulting carboxylic group in compound **2** was then converted to primary amide **3** via condensation with NH_4HCO_3 using HATU coupling agent and DIEA as the base. Deprotection of the free amino group with TFA led to compound **4**, which subsequently underwent distinct reactions depending on the moiety introduced into the thiophene ring. Compound **5** bearing a urea moiety was obtained by acylation of the amine with trichloroacetyl isocyanate and further rearrangement of isocyanate to urea with 4 M ammonia solution in MeOH. In turn, compounds **6**–**9** with cyclic tetrahydropyrimidone were obtained via condensation with appropriate ketones or γ-butyrolactone.
For pyridine/phenyl/fluorophenyl-based compounds, the first step was sulphonylation, acylation, or alkylation of the amino group followed by Miyaura cross-coupling between bromine at the 4- or 5-position with bis(pinacolato)diboron in the presence of $Pd(dppf)Cl_2$ catalyst. Pinacol ester **37** with an inverted sulfonamide bond was prepared by sulfonylation of piperidine with 3-bromobenzenesulfonyl chloride followed by Miyaura borylation. Final compounds **38**–**62** were obtained in the Suzuki–Miyaura cross-coupling between pinacol esters and thiophene-based bromides under anhydrous conditions with potassium carbonate and $Pd(dppf)Cl_2$ catalyst in DMF. The final compound **65** prepared from 5-aryl boronic acid pinacol ester **64** and **6** was synthesized by applying different conditions. In this case, the Suzuki-Miyaura coupling reaction was performed in the presence of a 2 M aqueous solution of sodium carbonate and a $Pd(PPh_3)_4$ catalyst in dioxane.

[1] Compounds 14, 22, 23, 33, 34, 36, 37, 39, 46, 47, 51–53 and 56 were obtained by Tomasz Wichur, PhD from the Department of Physicochemical Drug Analysis.

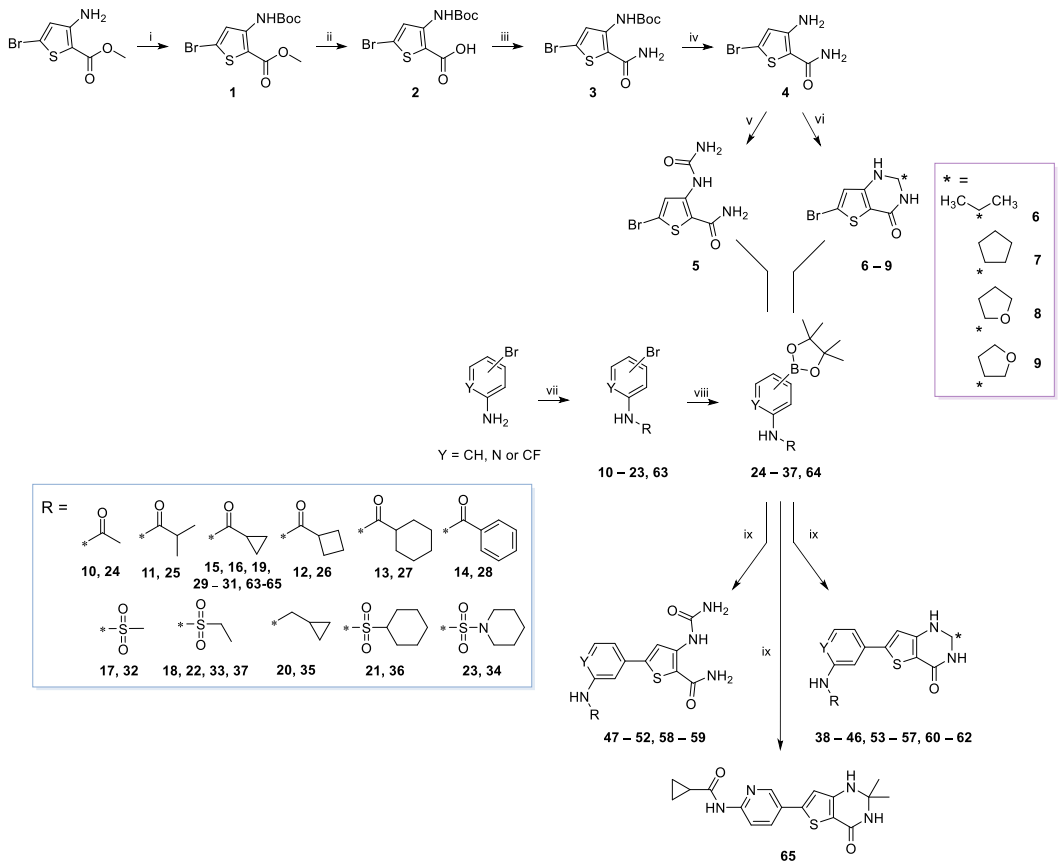

Scheme 1. Regents and conditions: (i) $(Boc)_2O$, DMAP, pyridine$_{(anh.)}$, 0 °C–rt, overnight; (ii) 10% $KOH_{(aq)}$, MeOH, reflux, 1 h; (iii) NH_4HCO_3, HATU, DIEA, DMF, rt, overnight; (iv) TFA, DCM, rt, 1 h; (v) trichloroacetyl isocyanate, THF$_{(anh.)}$, rt, 1.5 h, 4 M NH_3 sol. in MeOH, rt, 1.5 h; (vi) *p*-TSA, acetone, CH_3COOH, 80 °C, overnight or *p*-TSA, appropriate ketone / γ-butyrolactone, toluene$_{(anh.)}$, reflux, overnight; (vii) appropriate acid chloride, pyridine or TEA, DCM, 0 °C–rt, overnight / appropriate sulfonyl chloride, pyridine$_{(anh.)}$, rt, 3 h / appropriate cycloalkyl acid, pyridine$_{(anh.)}$, 50% T_3P sol. in EtOAc, DCM$_{(anh.)}$, rt, 1 h / NaH (60% in oil), DMF$_{(anh.)}$, 50 °C, 1 h, (bromomethyl)cyclopropane, 100 °C, overnight; (viii) bis(pinacolato)diboron, CH_3COOK, Pd(dppf)Cl_2, dioxane$_{(anh.)}$ or DMF$_{(anh.)}$, 80 °C or 100 °C, overnight; (ix) K_2CO_3, Pd(dppf)Cl_2, DMF$_{(anh.)}$, 80 °C, overnight / 2 M Na_2CO_3, Pd$(PPh_3)_4$, dioxane$_{(anh.)}$, 100 °C (for **65**); * substituent.

We developed two distinct approaches to prepare the compounds with heterocyclic moieties from **series IC** (Scheme 2). For the azaindole-based compound (**70**), the initial step involved protection of the NH group with Boc anhydride in commercially available 4-bromo-7-azaindole to avoid potential further complexation of coupling catalysts [166]. The obtained compound **66** underwent coupling reactions, primarily in the Miyaura borylation reaction with bis(pinacolato)diborone in the presence of a Pd(dppf)Cl_2 catalyst to yield **67**. Subsequently, the Suzuki-Miyaura cross-coupling reaction was performed with the previously obtained compound **3**, using a second-generation palladium precatalyst and an Xphos phosphine ligand, resulting in the formation of **68**. Then, the synthesis of the tetrahydropyrimidone fragment was carried out similarly

as for the compounds from the **series IB**: the Boc moieties were hydrolyzed with TFA, and the tetrahydropyrimidone ring in the final compound **70** was obtained by condensation of **69** with acetone. The preparation of the final compound **72** with a furopyrmidine core involved two steps, beginning with Miyaura borylation of previously prepared compound **6** at the 6-position. The obtained pinacol ester **71** was then directly used in the Suzuki-Miyaura cross-coupling reaction with commercially available 4-chlorofuro[3,2-*d*]pyrimidine in the presence of XPhos and the Pd_2dba_3 precatalyst as a source of active palladium species.

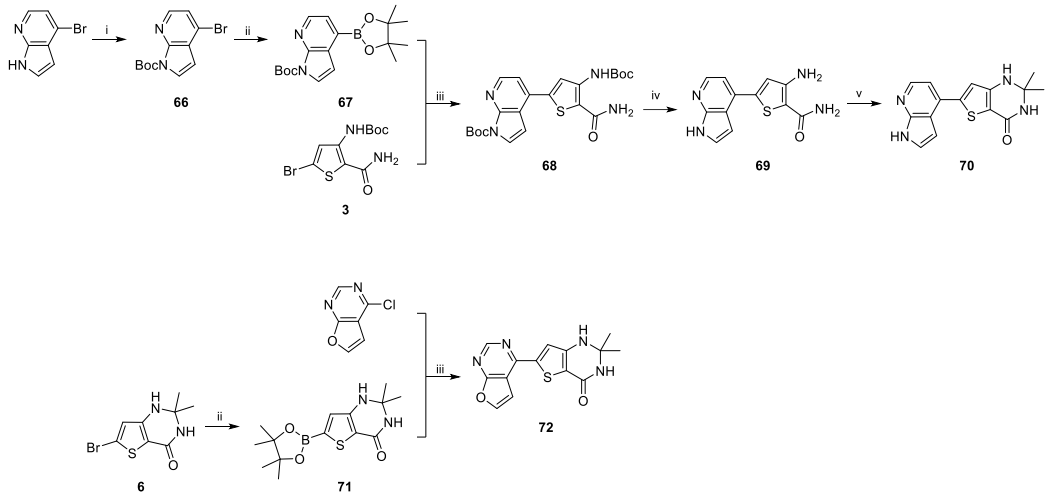

Scheme 2. Reagents and conditions: (i) $(Boc)_2O$, TEA, DMAP, $DCM_{(anh.)}$, 0 °C–rt, 2 h; (ii) bis(pinacolato)diboron, CH_3COOK, $Pd(dppf)Cl_2$, $dioxane_{(anh.)}$, 90 °C, overnight; (iii) K_3PO_4, XPhos, XPhos Pd G2 (for **68**) or Pd_2dba_3 (for **72**), $dioxane_{(anh.)}$:H_2O, 60 °C, 3 h; (iv) TFA, DCM, rt, 1 h; (v) *p*-TSA, acetone, CH_3COOH, 80 °C, overnight.

3.2.2. Series II

The final compounds from **series II** were obtained in the amide coupling. The necessary carboxylic acid (**74**) and aromatic amines were prepared using appropriate procedures. Isonicotinic acid derivative **74** was obtained in a two-step synthesis using commercially available methyl 2-aminopyridine-4-carboxylate as the starting compound. First, the amino group at the second position of an aromatic ring was acylated with cyclopropanecarbonyl chloride to **73**. The 4-methyl ester was then hydrolyzed under basic conditions with potassium carbonate to the carboxylic acid derivative in **74**. The synthetic routes applied for the preparation of heterocyclic aromatic amines varied according to the starting compound. 3-Aminopyrrole **75** was obtained directly by reducing 3-nitropyrrole with hydrogen in the presence of 10% palladium on activated carbon as a catalyst. Due to the instability of the unprotected 3-aminoindoles, compound **77** was prepared starting with the reduction of 3-nitroindole under mild conditions using zinc in the presence of a saturated aqueous NH_4Cl solution followed by Boc-protection of the amino group in the one-pot reaction. The intermediate **76** was ultimately

deprotected with a 37% hydrochloric acid solution in MeOH under reflux to obtain **77**. 2-Aminothophene **79** was prepared by amidation of 3-bromothiophene with *tert*-butyl carbamate in the presence of a CuI catalyst and DMEDA as a copper chelating agent, leading to **78**, followed by deprotection under anhydrous conditions with a 4 M HCl solution in dioxane at 90 °C. Finally, isonicotinic acid derivative **74** and primary aromatic amines were coupled using HATU or T_3P activating agent and DIEA or pyridine, respectively, as the base.

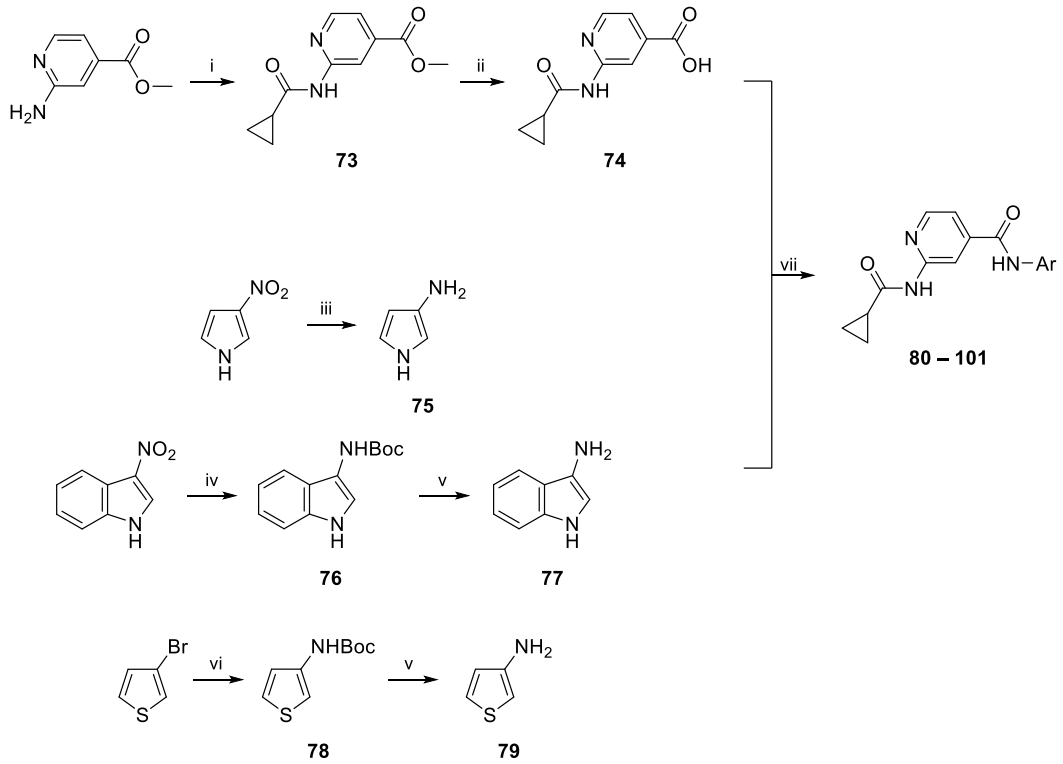

Scheme 2. Reagents and conditions: (i) cyclopropanecarbonyl chloride, pyridine, DCM, 0 °C–rt, overnight; (ii) K_2CO_3, MeOH, reflux, overnight; (iii) 10% Pd/C, $H_{2(g)}$, EtOH, rt, 4 h; (iv) $NH_4Cl_{(sat.)}$ sol. in H_2O, Zn, $(Boc)_2O$, MeOH, 0°C–rt, 1 h; (v) 37% HCl, MeOH, reflux, 1 h (for **77**) / 4 M HCl sol. in dioxane, $EtOH_{(anh.)}$, 90 °C, 2 h (for **79**); (vi) *tert*-butyl carbamate, CuI, K_2CO_3, DMEDA, $dioxane_{(anh.)}$, reflux, 24 h; (vii) appropriate aromatic amine, HATU, DIEA, $DMF_{(anh.)}$, rt, overnight / appropriate aromatic amine, $pyridine_{(anh.)}$, 50% T_3P sol. in EtOAc, $DCM_{(anh.)}$, rt, 1–3 h.

3.2.3. Series III

The general idea for the synthesis of the final compounds of **series III** was to obtain the key intermediate **104**, which was later used for structure diversification (Scheme 4). The initial step involved acylation of commercially available 4-bromopyridin-2-amine by cyclopropanecarbonyl chloride in the presence of pyridine to yield compound **102**, which was then reacted with *tert*-butyl-2,5-dihydro-1*H*-pyrrole-1-carboxylate-3-pinacol ester in the Suzuki-Miyaura cross-coupling to get compound **103**. Then **103** underwent Boc deprotection with HCl to give amine **104**, which subsequently was transformed

into the final compounds. A short-chain amide **111** was obtained by acylation with acetyl chloride under basic conditions with pyridine in DCM and urea derivative **112** by condensation with (trimethylsilyl)isocyanate under argon in THF. Sulfonamides were prepared by sulfonylation with the appropriate sulfonyl chlorides in the presence of TEA or DIPEA. The reaction resulted in the final compounds **117**–**119** or the intermediates **109** and **110**. Subsequent hydrazinolysis of **109** and **110** yielded primary aliphatic amines **120** and **121**. Amide derivatives **105**, **106** and **107** were obtained by condensation with 3-phthalimidopropionic acid, Boc-protected γ-aminobutyric acid and (*tert*-butoxycarbonyl)proline respectively, using EDC as an activating agent. Deprotection with hydrazine monohydrate (for **105**) or HCl (for **106** and **107**) afforded compounds with free amine groups **113**–**115**. Compounds with (*S*)- and (*R*)-pyrrolidine **(*S*)-108** and **(*R*)-108** were synthesized by reductive amination of the corresponding enantiomerically pure aldehydes in the presence of $NaCNBH_3$ and further Boc-deprotection to yield the final compounds **(*S*)-116** and **(*R*)-116**.

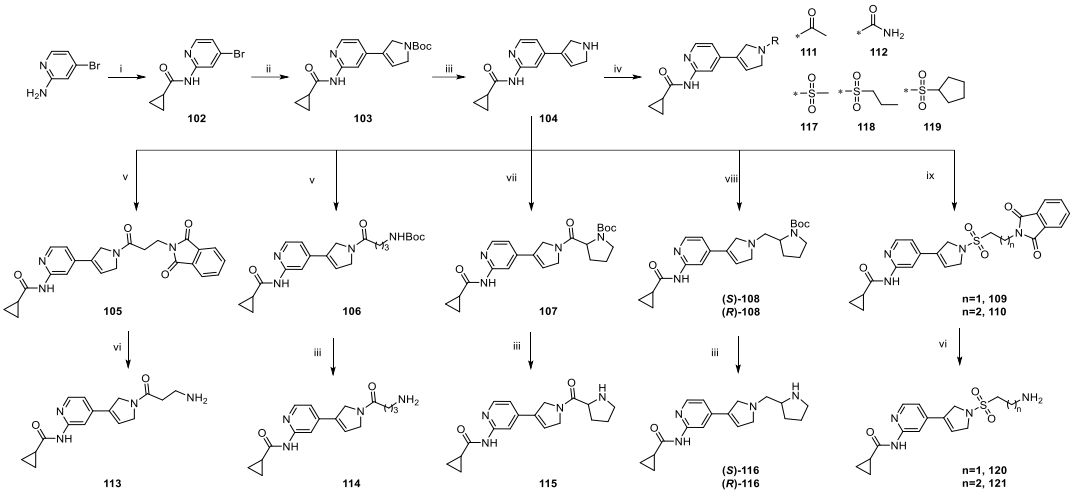

Scheme 4. Reagents and conditions: (i) cyclopropanecarbonyl chloride, pyridine, DCM, 0 °C–rt, overnight; (ii) *tert*-butyl 3-(4,4,5,5-tetramethyl-1,3,2-dioxaborolan-2-yl)-2,5-dihydro-1*H*-pyrrole-1-carboxylate, Cs_2CO_3, $Pd(dppf)Cl_2$, $dioxane_{(anh.)}$, 90 °C, 3 h; (iii) 37% HCl, EtOAc or MeOH, rt or reflux, 1 h; (iv) acetyl chloride (for **111**), pyridine, DCM, 0 °C–rt, overnight / (trimethylsilyl)isocyanate (for **112**), TEA, $THF_{(anh.)}$, rt, 8 h / appropriate sulfonyl chloride, TEA, DCM, 0 °C–rt, 1 h; (v) 3-phthalimidopropionic acid (for **105**) or 4-((*tert*-butoxycarbonyl)amino)butanoic acid (for **106**), EDC hydrochloride, DMAP, $DCM_{(anh.)}$, rt, overnight; (vi) $NH_2NH_2 \cdot H_2O$, EtOH, 78 °C, 2 h; (vii) (*tert*-butoxycarbonyl)proline, EDC hydrochloride, DMAP, DIEA, $DCM_{(anh.)}$, rt, overnight; (viii) (*S*)-*tert*-butyl 2-formylpyrrolidine-1-carboxylate (for **(*S*)-108**) or (*R*)-*tert*-butyl 2-formylpyrrolidine-1-carboxylate (for **(*R*)-108**), CH_3COOH, $NaCNBH_3$, MeOH, 0 °C–rt, overnight; (ix) 2-(1,3-dioxoisoindolin-2-yl)ethane-1-sulfonyl chloride (for **109**) or 3-(1,3-dioxoisoindolin-2-yl)propane-1-sulfonyl chloride (for **110**), DIPEA, $DCM_{(anh.)}$, rt, overnight.

3.2.4. Series IV

The key compound **124** for the synthesis of cyclic amide derivatives from the **series IVA** was obtained in three steps starting from commercially available 2-(thiophen-3-yl)ethan-1-amine (Scheme 5). The initial step involved the protection of the aliphatic amino group with Boc anhydride to **122**, which subsequently underwent a Friedel-Crafts-type intramolecular cyclisation via an isocyanate intermediate to yield a pyridinone scaffold (**123**). Finally, it was brominated at the 2-position with bromine in a glacial acetic acid medium to **124**.

Depending on the type of alkyl chain attached to the nitrogen atom of the cyclic amide moiety, distinct synthetic strategies were applied. **126** with a methyl group was obtained by *N*-alkylation with methyl iodide under basic NaH conditions to **125**, followed by a Suzuki-Miyaura cross-coupling reaction with the previously reported compound **26** from **series IB** using Pd(dppf)Cl_2 catalyst. Compound **136** with a terminal amine on a three-carbon spacer was prepared in three steps. Initially, **124** was *N*-alkylated with *N*-(3-bromopropyl)phthalimide using K_2CO_3 base and KI as a nucleophilic catalyst to afford **127**. **127** was then coupled with **26** in a Suzuki-Miyaura reaction to **128**, which finally underwent hydrazinolysis to **136** with the primary amino group. Hydroxyl and amine derivatives on a two-carbon aliphatic chain (**133** and **135**) were synthesized starting from the alkylation of **124** with ethyl bromoacetate in the presence of potassium *tert*-butoxide. Then the ester moiety in **129** was directly reduced to alcohol **130** by $NaBH_4$ in the presence of Na_2SO_4 as a hygroscopic agent. Subsequently, the hydroxyl group was protected with *tert*-butyldimethylsilyl group in **131**, following the Suzuki-Miyaura reaction under standard conditions with **26**. To obtain the final compound **133**, silyl ether in **132** was cleaved using 1 M TBAF solution in THF. The conversion of hydroxyl group into amine was accomplished by introducing phthalimide via the Mitsunobu reaction to produce **134** and subsequent hydrolysis with hydrazine monohydrate to obtain **135**.

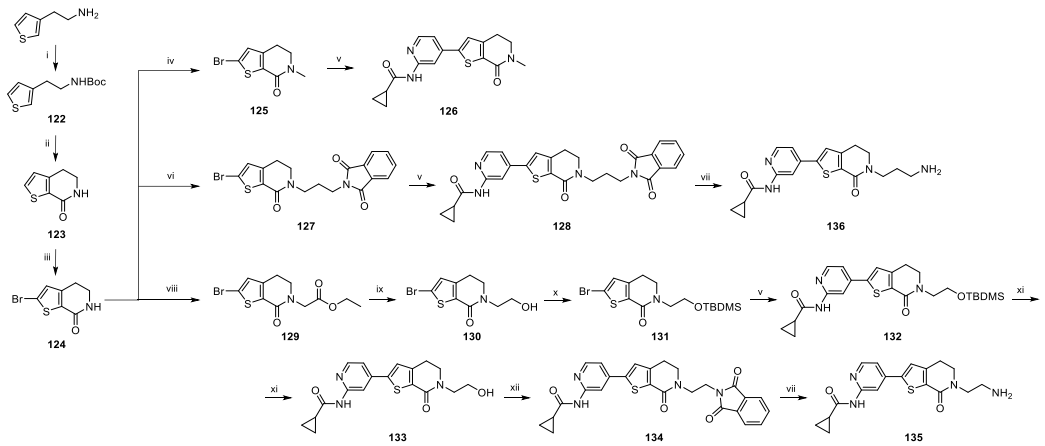

Scheme 5. Reagents and conditions: (i) di-*tert*-butyldicarbonate, K_2CO_3, THF/H_2O, 0 °C–rt, 6h; (ii) 2-chloropyridine, triflic anhydride, $BF_3 \cdot Et_2O$, DCM, -78 °C–rt, 2 h; (iii) Br_2, CH_3COOH/H_2O, 0 °C, 1 h; (iv) methyl iodide, NaH (60% in oil), $DMF_{(anh.)}$, 0 °C–rt, 3 h; (v) **26**, K_2CO_3,

$Pd(dppf)Cl_2$, $DMF_{(anh.)}$, 80 °C, overnight; (vi) NaH (60% in oil), $THF_{(anh.)}$, rt, 1 h; *N*-(3-bromopropyl)phthalimide, K_2CO_3, KI, DMF, 80 °C, overnight; (vii) $NH_2NH_2 \cdot H_2O$, EtOH, 78 °C, 2 h; (viii) ethyl bromoacetate, *t*-BuOK, $THF_{(anh.)}$, 0 °C–rt, 1 h; (ix) $NaBH_4$, Na_2SO_4, $EtOH_{(anh.)}$, 0 °C–rt, 2 h; (x) *tert*-butyl(chloro)dimethylsilane, imidazole, DCM, rt, overnight; (xi) 1 M TBAF sol. in THF, $THF_{(anh.)}$, 0 °C, 2 h; (xii) Phthalimide, PPh_3, DIAD, $Toluene_{(anh.)}$:$THF_{(anh.)}$, rt, 1 h.

The synthetic approach for the compounds of **series IVB** required the preparation of the key intermediate **141**, followed by diversification of the substituent on cyclic sulfonamide nitrogen (Scheme 6). In the initial step, commercially available 3-acetylthiophene was dibrominated with *N*-bromosuccinimide in DMF (**137**). Subsequently, compound **137** was transformed to the benzylthioether derivative **138** under basic conditions in a reaction with mercaptide generated *in situ* from thiourea and benzyl chloride. Next, the thioether moiety in the **138** was converted to a sulfonamide (**139**) in an oxidative chlorination reaction by bubbling chlorine gas through a solution of the compound in a mixture of water and ethyl acetate to form a sulfonyl chloride derivative, which was subsequently treated with an ammonium hydroxide solution. **139** was used in the alkyl chain bromination reaction with dibromantin reagent and sulfuric acid as a catalyst to yield **140**. Finally, the carbonyl group in **140** was enantioselectively reduced with (+)-β-chlorodiisopinocamphenyl-borane to (*S*)-hydroxyl derivative, which underwent intramolecular *N*-alkylation in sodium hydroxide solution to yield compound **141**.

The first derivative of **141** was **153** – a molecule with a tricyclic ring system ((6*S*)-3,4-dihydro-6*H*-2,6-methanothieno[2,3-*f*][1,5,4]oxathiazocine 1,1-dioxide). Primarily **141** underwent *N*-alkylation with 1,2-dibromoethane to **142**, followed by the Suzuki cross-coupling reaction with compound **26** previously reported in **series IB**. The formation of **153** was a result of simultaneous intramolecular *O*-alkylation with bromoethyl chain, which occurred spontaneously under basic Suzuki conditions. To avoid potential side reactions for the other derivatives, the secondary (*S*)-hydroxyl group was converted to silyl ether using *tert*-butyldimethylsilyl chloride (**143**), which was further used as a precursor for *N*-alkylated derivatives. The final compound with unsubstituted sulfonamide **149** was synthesized directly from **143** in the Suzuki reaction with **26**, along with spontaneous cleavage of the silyl ether under basic K_2CO_3 conditions. The methylated analogue **150** was obtained by *N*-alkylation with methyl iodide under basic NaH conditions to **144**, followed by a Suzuki cross-coupling with **26** as previously described and a similar pattern of secondary hydroxyl group deprotection. The synthesis of a compound bearing a hydroxyl group on a two-carbon atom linker (**151**), started with *N*-alkylation with protected bromoethanol using K_2CO_3 base and KI nucleophilic catalyst to yield **145**, which subsequently underwent Suzuki reaction with **26** and a double cleavage of the silyl ethers using 1 M TBAF solution in THF to **147**. The compound with terminal amine moiety (**152**) on the three-carbon atom linker was prepared by *N*-alkylation of **143** with *N*-(3-bromopropyl)phthalimide under basic conditions using K_2CO_3 and KI catalyst. During the Suzuki cross-coupling reaction

between compound **146** and **26** the deprotection of silyl ether proceeded in a similar manner. In the last step, compound **148** underwent hydrazinolysis with hydrazine monohydrate to obtain **152**.

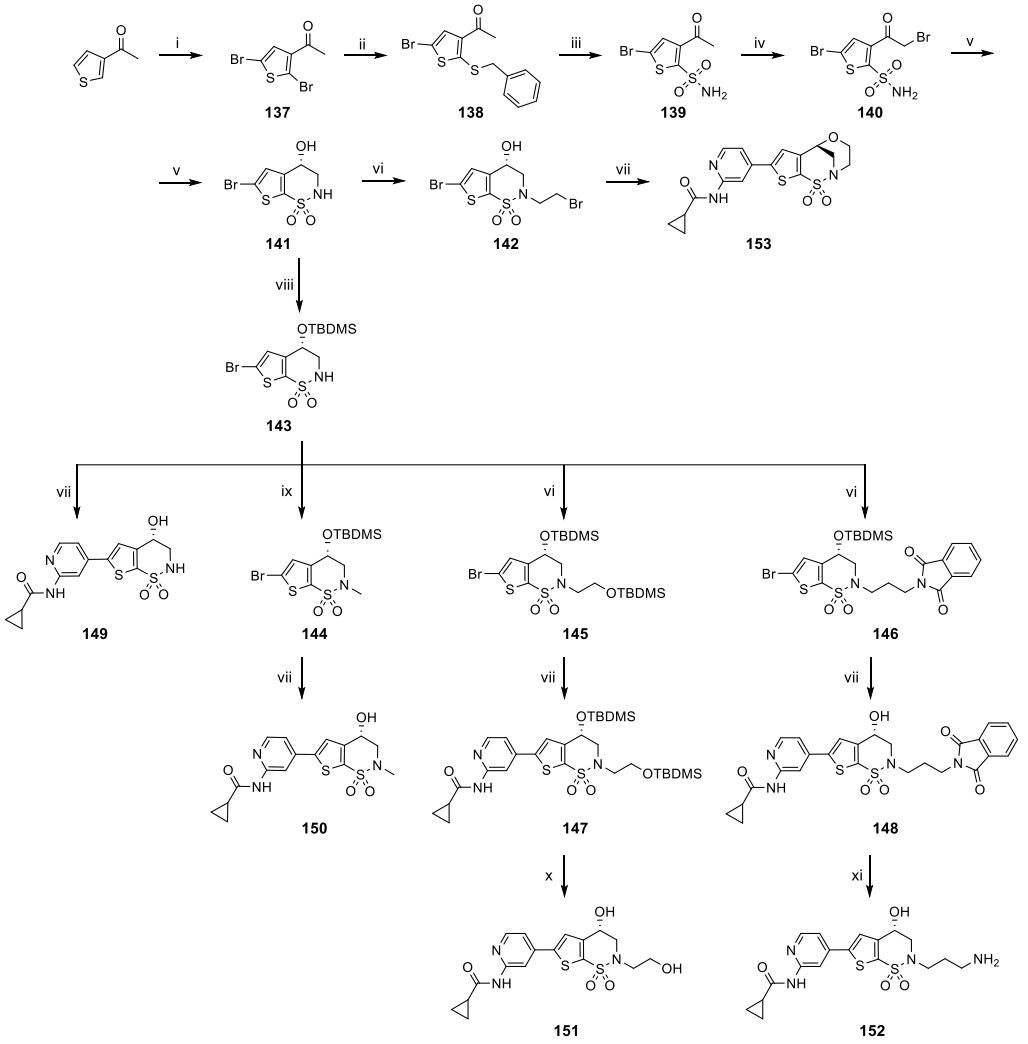

Scheme 6. Reagents and conditions: (i) NBS, DMF, rt, overnight; (ii) thiourea, benzyl chloride, *i*-PrOH:H_2O, 85 °C, 2 h; 4 M $NaOH_{(aq.)}$, 85 °C, 3 h; 2,25% NaClO, rt, 0.5 h; (iii) $Cl_{2(g)}$, EtOAc:H_2O, 0 °C, 0.5 h; ammonium $hydroxide_{(sol.)}$, 0 °C, 0.5 h; (iv) 1,3-dibromo-5,5-dimethylhydantoin, $H_2SO_{4(conc.)}$, EtOAc, 0 °C–rt, overnight; (v) 58% (+)-β-chlorodiisopinocamphenyl-borane sol. in hexane, MTBE, -30 °C – -20 °C, 1.5 h; 1 M $NaOH_{(aq.)}$, rt, 2 h; (vi) NaH (60% in oil), $THF_{(anh.)}$, rt, 1 h; 1,2-dibromoethane / *N*-(3-bromopropyl)phthalimide / (2-bromoethoxy)(*tert*-butyl)dimethylsilane, K_2CO_3, KI, DMF, 80 °C, overnight; (vii) **26**, K_2CO_3, $Pd(dppf)Cl_2$, $DMF_{(anh.)}$, 80 °C, overnight; (viii) *tert*-butyl(chloro)dimethylsilane, imidazole, DCM, rt, overnight; (ix) methyl iodide, NaH (60% in oil), $DMF_{(anh.)}$, 0 °C–rt, 3 h; (x) 1 M TBAF sol. in THF, $THF_{(anh.)}$, 0 °C, 2 h; (xi) $NH_2NH_2 \cdot H_2O$, EtOH, 78 °C, 2 h.

Within the described 4 series, I obtained 64 final compounds. The structure and molecular weight of each derivative were confirmed by ^{1}H and ^{13}C nuclear magnetic resonance spectroscopy and LC-MS mass spectrometry respectively. The compounds had a purity of over 95%, which is suitable for *in vitro* assays.

3.3. Physicochemical parameters assessment

The assessment of drug-like properties is an integral part of medicinal chemistry projects and crucial in the early stages of the drug discovery process. These properties of a compound are determined by its molecular structure and are closely related to physicochemical features such as solubility, permeability, and chemical stability. Together, these properties impact the absorption, distribution, metabolism, excretion, and toxicity (ADMET) profile *in vivo*. Therefore, their prediction is crucial for selecting the most promising candidates, ultimately increasing the likelihood of clinical success.

The pioneer who investigated how structural properties influence drugs' solubility and permeability was Chris Lipinski. Lipinski selected and set the cut-off limits for the key physicochemical descriptors and defined them as the "Rule of Five" [167]. This set of rules was established based on a library of Pfizer compounds, whose properties were correlated with favorable solubility and permeability. For high absorption or permeation, and thus a potentially greater chance of reaching the therapeutic target, the compound should meet the following limits:

- molecular weight (MW) <500;
- the count of hydrogen bond donors (as the sum of all OHs and NHs) <5;
- the count of hydrogen bond acceptors (as the sum of all OHs and NHs) <10;
- octanol-water partition coefficient (logP) <5.

The rules are based on solid physicochemical foundations. Firstly, molecular weight is linked with the size of the molecule and thus is a limiting factor for gastrointestinal absorption. Its increase not only hinders passive diffusion through the tight junctions of the aliphatic side chains in the bilayer membrane but also impairs solubility as a larger cavity needs to be formed to solubilize the compound. The number of groups with the ability to form hydrogen bonds also affects the water solubility and permeation. Effective partitioning of the compound between the aqueous environment and the lipid bilayer requires the disruption of formed hydrogen bonds. Therefore, an increased number of hydrogen bonding groups in the molecule enhances its solubility but simultaneously hinders permeation by passive diffusion. Finally, an increase in LogP correlates with a decrease in aqueous solubility, subsequently reducing absorption. However, an increase in LogP value correlates with increased affinity for the lipophilic environment, leading to better penetration into cells. This holds particular significance for compounds whose therapeutic target is expressed within the CNS [168].

Veber et al. proposed other criteria that can complement the stated above and positively correlate with high oral bioavailability in rats [169]:

- ≤10 rotatable bonds;
- ≤140 $Å^2$ topological polar surface area (TPSA), or ≤12 total hydrogen bonds (as the sum of donors and acceptors).

Moreover, compounds' absorption may be modulated by membrane transporters through the mechanisms of active uptake or efflux. One of the most important examples, which, among others, leads to resistance to chemotherapy in cancer cells, is the widely distributed P-glycoprotein (P-gp) that is also found on the surface of brain-blood barrier (BBB) endothelial cells. To reduce the probability of becoming a P-gp substrate, the compounds should stay below the following limits [170]:

- the count of N+O atoms ≤4, with a more limiting HBD than HBA group count;
- molecular weight <400;
- basic character with pK_a <8.

In the exploration of physicochemical parameters, Lovering et al. highlight the carbon bond saturation also defined as the Csp^3 fraction [171]. The descriptor combines the complexity of the molecule and the presence of chiral centres in the structure that directly correlates with solubility. The Csp^3 fraction is calculated by dividing the number of sp^3 hybridized carbon atoms by the total carbon count in the molecule. Moreover, the authors suggest that designing more complex spatial structures and introducing out-of-plane substituents into the molecules greatly impacts complementarity with the biological target, without significantly increasing the molecular weight. The average Csp^3 for compounds that successfully finished clinical trials was 0.47 or higher.

In addition to optimal bioavailability, the drug candidates targeting CNS diseases should be characterized with properties that allow them to cross the BBB via transcellular passive diffusion. A convenient tool for assessing the potential permeability and prioritizing compounds with beneficial properties for CNS activity was developed by Wager et al. as the Central Nervous System Multiparameter Optimization (CNS MPO) algorithm [172]. The algorithm evaluates six parameters simultaneously, assigning each a specific weight and combining it with a single score on a scale from 0.00 to 6.00. These parameters include MW, logP, distribution coefficient at pH 7.4 (logD), TPSA, number of HBD groups, and the strongest basic pK_a of the molecule. Compounds rated with a score of 4.00 or higher, are generally considered with a greater likelihood of CNS activity.

To assess the drug-likeness of all the obtained compounds from **series I–IV**, I calculated their selected physicochemical descriptors using Chemicalize [173], an online platform developed by ChemAxon and applying the CNS MPO algorithm [172]. In particular, I considered the following physicochemical parameters and applied cut-off values identified as optimal, to prioritize the compounds with favorable properties to absorb well from a gastrointestinal track with a high probability of penetrating the BBB:

- MW <450 g/mol [174];
- 1< LogP <4 and 0< LogD <3 [174];
- the count of HBD ≤3 and HBA ≤7 [174];

- TPSA <90 $Å^2$ [174];
- number of rotatable bonds <8 [174];
- strongest basic pK_a <10 [174];
- fraction Csp^3 >0.47 [171];
- CNS MPO score ≥4.0 [172].

3.3.1. Series I

The values of individual molecular descriptors in **series I** vary significantly as a result of applied structural modifications (Tables 1–3). 3-Ureidothiophene-2-carboxamide derivatives from **series IA** are characterized by high TPSA values (127.31–140.20 $Å^2$), and the number of HBD groups of 4 due to the presence of the urea and two amide groups. On the other hand, all compounds have a molecular weight below 400, an acceptable amount of HBA groups, and no more than 5 rotatable bonds. Moreover, the LogP and LogD values were above 1 for all compounds, except for **47** (calculated at 0.55). The strongest basic pK_a was within the desired limits for pyridine derivatives (**47**–**52**) in the range of 1.76–3.11, while for compounds with phenyl ring (**58** and **59**), it was negative and amounted to -0.53. However, the calculated TPSA values in the range of 127.31 $Å^2$ for phenyl **58** and **59** derivatives to 140.20 $Å^2$ for pyridine **47**–**52** derivatives notably exceed the accepted limit of 90 $Å^2$. The calculated fraction Csp^3 was relatively low, from 0.00 for phenyl derivative **52** rich in sp^2 hybridized carbon atoms to the most favourable 0.33 for cyclohexyl analogue **51**. Despite deviations from the desired limits, all compounds except **51** and **52** scored 4.00 or above according to the CNS MPO algorithm.

The structural modifications in **subseries IB** led to ring closure and formation of the tetrahydropyrimidone moiety and significantly improved the drug-like profile of the compounds (Table 2). These modifications helped maintain an optimal molecular weight (with the highest 419.56 calculated for derivative **56**) while reducing the number of HBD groups to 3 and decreasing the number of rotatable bonds by rigidifying the structure. Most importantly, the TPSA value was significantly improved, ranging from 66.05 $Å^2$ for compound **46** (without one carbonyl group) to 100.19 $Å^2$ for compounds **44** and **45** with a sulfonamide moiety. Additionally, LogP and LogD values were within the desired ranges for the majority of derivatives, except for compound **44** (0.89 and 0.69 calculated LogP and LogD, respectively). Notably, LogD exceeded 3 for 7 out of 18 compounds. The pK_a values fell within a range of 0.00 to 5.63. The fraction Csp^3 was also within the range of 0.15 to 0.45, indicating an improvement in the structural complexity of the compounds. This optimization resulted in higher ratings according to the CNS MPO algorithm, with compound **38** achieving the highest score of 5.17. However, compounds **42**, **43**, and **56** did not meet the criteria, most likely due to elevated logP and logD values.

Subsequent modifications resulted in compounds from **series IC** featuring two heterocyclic rings, which exhibited the most favourable properties according to the CNS MPO algorithm, with scores of 4.97 for **70** and 5.44 for **72** (Table 3). TPSA values were further reduced to 69.81 $Å^2$ and 80.05 $Å^2$ for **70** and **72** respectively, while the number of rotatable bonds was lowered to 1. Additionally, the molecular weight was slightly decreased, while maintaining LogP and LogD values within optimal ranges from 2.13 to 2.39.

Table 1. Calculated physicochemical properties of compounds **47**–**52** and **58**–**59** from **series IA**.

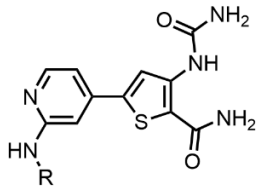

Cmpd.	R	MW	LogP	LogD	HBD	HBA	TPSA	Rotatable Bonds	Strongest basic pK_a	Fraction Csp^3	CNS MPO
47	–CO–CH_3	319.34	0.55	0.55	4	4	140.20	4	3.11	0.08	4.00
48	–CO–$CH(CH_3)_2$	347.39	1.79	1.79	4	4	140.20	5	3.10	0.20	4.00
49	–CO– 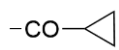	345.38	1.33	1.33	4	4	140.20	5	3.10	0.20	4.00
50	–CO– 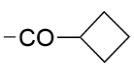	359.40	1.77	1.77	4	4	140.20	5	3.10	0.25	4.00
51	–CO– 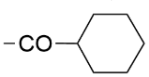	387.46	2.66	2.66	4	4	140.20	5	3.10	0.33	3.47
52	–CO– 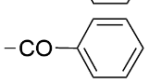	381.41	2.40	2.40	4	4	140.20	5	1.76	0.00	3.65

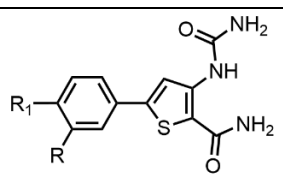

Cmpd.	R	R_1	MW	LogP	LogD	HBD	HBA	TPSA	Rotatable Bonds	Strongest basic pK_a	Fraction Csp^3	CNS MPO
58	–NHCO– 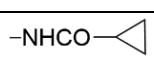	H	344.39	1.95	1.95	4	3	127.31	5	-0.53	0.19	4.00
59	–NHCO– 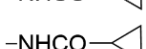	F	362.38	2.10	2.10	3	4	127.31	5	-0.53	0.19	4.10

Table 2. Calculated physicochemical properties of compounds **38**–**46**, **53**–**57**, **60**–**62** and **65** from **series IB**.

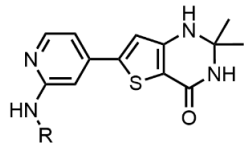

Cmpd.	R	MW	LogP	LogD	HBD	HBA	TPSA	Rotatable Bonds	Strongest basic pK_a	Fraction Csp^3	CNS MPO
38	$-CO-CH_3$	316.38	1.76	1.76	3	4	83.12	2	3.12	0.27	5.17
39	$-CO-CH(CH_3)_2$	344.43	3.00	3.00	3	4	83.12	3	3.11	0.35	4.67
40	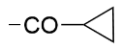	342.42	2.54	2.54	3	4	83.12	3	3.11	0.35	4.90
41	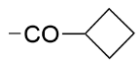	356.44	2.98	2.98	3	4	83.12	3	3.11	0.39	4.68
42	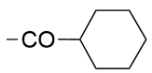	384.50	3.87	3.87	3	4	83.12	3	3.11	0.45	3.62
43	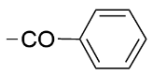	378.45	3.61	3.61	3	4	83.12	3	1.77	0.15	3.92
44	$-SO_2-CH_3$	352.43	0.89	0.69	3	5	100.19	2	0.00	0.29	4.83
45	$-SO_2-CH_2CH_3$	366.45	1.40	1.26	3	5	100.19	3	0.00	0.33	4.78
46	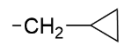	328.43	2.77	2.77	3	4	66.05	4	5.63	0.41	4.78

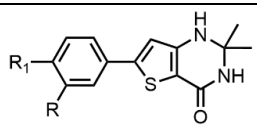

Cmpd.	R	R_1	MW	LogP	LogD	HBD	HBA	TPSA	Rotatable Bonds	Strongest basic pK_a	Fraction Csp^3	CNS MPO
53	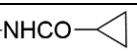	H	341.43	3.16	3.16	3	3	70.23	3	0.00	0.33	4.51

54		F	359.42	3.30	3.30	3	3	70.23	3	0.00	0.33	4.37
55	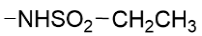	H	365.47	2.03	2.01	3	4	87.30	3	0.00	0.31	5.12
56	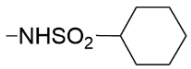	H	419.56	3.62	3.60	3	4	87.30	3	0.00	0.45	3.63
57	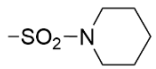	H	405.53	3.05	3.05	2	4	78.51	2	0.00	0.42	4.62

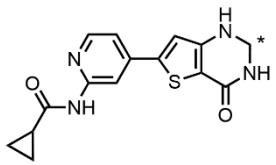

Cmpd.	R	MW	LogP	LogD	HBD	HBA	TPSA	Rotatable Bonds	Strongest basic pK_a	Fraction Csp^3	CNS MPO
60		368.46	3.35	3.35	3	4	83.12	3	3.11	0.42	4.26
61		370.43	2.93	2.92	3	5	92.35	3	3.11	0.39	4.55
62		370.43	2.56	2.56	3	5	92.35	3	3.11	0.39	4.73
65	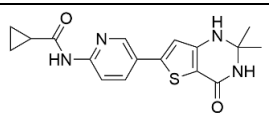	342.42	2.54	2.54	3	4	83.12	3	3.28	0.35	4.90
Cmpd. I	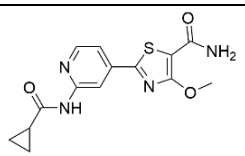	318.35	1.47	1.47	2	5	107.20	5	2.20	0.29	4.93

Cmpd. II	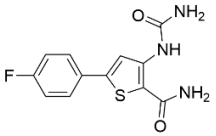	279.29	2.08	2.08	3	2	98.21	3	-0.53	0.00	4.85

Table 3. Calculated physicochemical properties of compounds **70** and **72** from **series IC**.

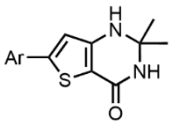

Cmpd.	R	MW	LogP	LogD	HBD	HBA	TPSA	Rotatable Bonds	Strongest basic pK_a	Fraction Csp^3	CNS MPO
70		298.36	2.39	2.39	3	3	69.81	1	3.56	0.20	4.97
72		300.34	2.13	2.13	2	4	80.05	1	3.31	0.21	5.44

3.3.2. Series II

Almost all compounds from **series II** met the desired limits (Table 4). Based on the CNS MPO algorithm, most compounds were classified with a high probability of BBB permeation, except the 3,5-bis trifluoromethyl derivative **92** (calculated CNS MPO of 3.66). This exception is primarily due to **92**'s high lipophilicity (calculated LogP and LogD of 4.22), as well as its molecular weight (417.31) and number of rotatable bonds (6) approaching the upper cut-off values. The highest CNS MPO score of 5.38 was calculated for the thiophene derivative **99**, which can be attributed to a molecular weight below 300, balanced LogP and LogD values of 2.24, an HBD count of 2, and a TPSA of 71.09 $Å^2$. Further analysis revealed that chlorinated derivatives **81–83** and **90**–**91** and trifluoromethyl analogues **84**–**86** exhibited increased lipophilicity in ranges of 3.06–3.67. In contrast, nitro **97** and hydroxyl **98** and derivatives displayed elevated TPSA values of 114.23 $Å^2$ and 91.32 $Å^2$, respectively. Moreover, all the compounds are small molecules consisting of two aromatic fragments, which lowered the values of the Csp^3 fraction to approximately half of the desired 0.47. Nevertheless, the physicochemical parameters of novel amide derivatives were significantly optimized compared to those calculated for reference compounds **III** and **IV**, with a type of substitution playing a critical role in determining drug-likeness within the group.

Table 4. Calculated physicochemical properties of compounds **80**–**101** from **series II**.

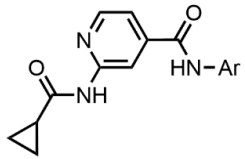

Cmpd.	R	MW	LogP	LogD	HBD	HBA	TPSA	Rotatable Bonds	Strongest basic pK_a	Fraction Csp^3	CNS MPO
80		281.31	2.46	2.46	2	3	71.09	4	1.28	0.19	5.27
81	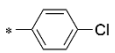	315.76	3.06	3.06	2	3	71.09	4	1.28	0.19	4.94
82		315.76	3.06	3.06	2	3	71.09	4	1.27	0.19	4.94
83		315.76	3.06	3.06	2	3	71.09	4	1.28	0.19	4.94
84	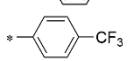	349.31	3.34	3.34	2	3	71.09	5	1.28	0.24	4.66
85		349.31	3.34	3.34	2	3	71.09	5	1.27	0.24	4.66
86	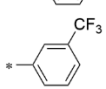	349.31	3.34	3.34	2	3	71.09	5	1.28	0.24	4.66
87	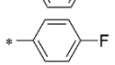	299.31	2.60	2.60	2	3	71.09	4	1.28	0.19	5.20
88		299.31	2.60	2.60	2	3	71.09	4	1.27	0.19	5.20
89		299.31	2.60	2.60	2	3	71.09	4	1.28	0.19	5.20

90	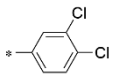	350.20	3.67	3.67	2	3	71.09	4	1.28	0.19	4.33
91	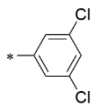	350.20	3.67	3.67	2	3	71.09	4	1.28	0.19	4.33
92		417.31	4.22	4.22	2	3	71.09	6	1.28	0.28	3.48
93	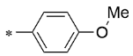	311.34	2.30	2.30	2	4	80.32	5	1.28	0.24	5.35
94	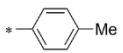	295.34	2.97	2.97	2	3	71.09	4	1.28	0.24	5.02
95		295.34	2.97	2.97	2	3	71.09	4	1.28	0.24	5.02
96	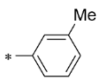	295.34	2.97	2.97	2	3	71.09	4	1.28	0.24	5.02
97	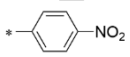	326.31	2.40	2.40	2	5	114.23	5	1.28	0.19	4.49
98		297.31	2.14	2.14	3	4	91.32	4	1.27	0.19	5.05
99		287.34	2.24	2.24	2	3	71.09	4	1.27	0.21	5.38
100		320.35	2.56	2.56	3	3	86.88	4	1.27	0.17	4.89
101	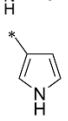	270.29	1.54	1.54	3	3	86.88	4	1.27	0.21	5.17

Cmpd.		MW	LogP	LogD	HBD	HBA	TPSA	Rotatable Bonds	Strongest basic pK_a	Fraction Csp^3	CNS MPO
Cmpd. III	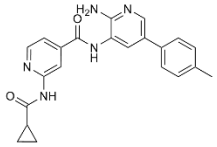	387.44	3.17	3.16	3	5	110.00	5	5.63	0.18	4.10
Cmpd. IV	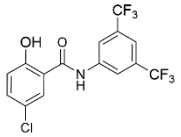	383.67	5.12	4.82	2	2	49.33	4	N/A	0.13	3.33

N/A – not applicable

3.3.3. Series III

All compounds from **series III** exhibit promising drug-like properties according to the calculated CNS MPO algorithm, with scores ranging from 4.11 to .83 (Table 5). The 2,5-dihydro-1*H*-pyrrole derivatives are characterized by molecular weight in ranges from 271.32 to 361.46, optimized TPSA values (57.26–88.32 $Å^2$), with the exception of **120** and **121**, which have TPSA values of 105.39 $Å^2$. Additionally, these compounds show improved structural complexity, as reflected in their Csp^3 fraction, which ranges from 0.36 to 0.56.

Considering all molecular descriptors together, compounds **118** and **119** stand out due to their balanced lipophilicity, with LogP and LogD values of 1.21 and 1.81, respectively, solely 1 HBD group, TPSA of 79.37 $Å^2$ and Csp^3 fraction above 0.5. However, the majority of compounds, particularly those containing an aliphatic amine moiety (**113-114** and **120-121**), exhibit excessive hydrophilicity. This is indicated by LogP values below 1, negative LogD values, and a tendency to ionize in physiological pH due to pKa oscillating between 8.45 and 9.99. In addition to hindering passive diffusion, the excessively basic nature of the compounds may also increase affinity for the P-gp, and this issue should be addressed in future optimization efforts.

Table 5. Calculated physicochemical properties of compounds **111**–**121** from **series III**.

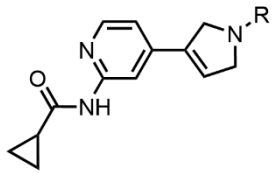

Cmpd.	R	MW	LogP	LogD	HBD	HBA	TPSA	Rotatable Bonds	Strongest basic pK_a	Fraction Csp^3	CNS MPO
111		271.32	0.68	0.68	1	3	62.30	3	4.09	0.40	5.83
112		272.31	0.35	0.35	2	3	88.32	3	4.09	0.36	5.50
113	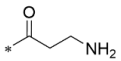	300.36	0.00	-1.72	2	4	88.32	5	9.12	0.44	4.94
114	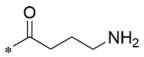	314.39	0.28	-2.17	2	4	88.32	6	9.99	0.47	4.51
115		326.40	0.81	-0.62	2	4	74.33	4	8.82	0.50	5.09
(*R*)-116		312.42	1.56	-0.89	2	4	57.26	5	9.92	0.56	4.54
(*S*)-116		312.42	1.56	-0.89	2	4	57.26	5	9.92	0.56	4.54
117		307.37	0.18	0.18	1	4	79.37	3	4.08	0.43	5.83
118		335.42	1.21	1.21	1	4	79.37	5	4.08	0.50	5.83
119		361.46	1.84	1.84	1	4	79.37	4	4.08	0.56	5.82

120	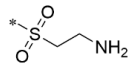	336.41	-0.47	-1.55	2	5	105.39	5	8.45	0.47	4.76
121	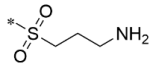	350.44	-0.41	-2.69	2	5	105.39	6	9.76	0.50	4.11
Cmpd. I	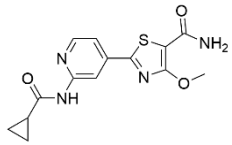	318.35	1.47	1.47	2	5	107.20	5	2.20	0.29	4.93

3.3.4. Series IV

The compounds in **series IV** are based on pyridinone core, derived from tetrahydropyrimidone fragment in **series IB**. These modifications were aimed, among others, at optimization of the physicochemical parameters. Notably, the removal of the amino group in the tetrahydropyrimidone led to the development of compound **V** with a reduced number of HBD groups (2) and a TPSA of 71.09 $Å^2$, significantly enhancing the CNS MPO score from 4.90 (as calculated for analogue **40**) to 5.48 (Table 6).

However, the positive evaluation of physicochemical descriptors varies across the series, depending on the substituent attached to the nitrogen atom of the cyclic amide or sulfonamide group. Overall, cyclic amide derivatives generally perform better than cyclic sulfonamides. For instance, **149**, the sulfonamide counterpart of compound **V** has an increased number of HBD and HBA groups, which significantly influences its TPSA (108.39 $Å^2$) and shifts the molecule toward a more hydrophilic character, with LogP of 0.91 and LogD of 0.89. The methylated amide derivative **126** has the highest CNS MPO score in the series (5.70), due to a further reduction of HBD groups to 1 and an increase in lipophilicity. According to the algorithm, compounds **133**, **150** and **153** also scored above 5, conforming to the accepted limits, except for **150**, which exceeded TPSA limit. The presence of a basic ionising group such as terminal aliphatic amine in compounds **135**, **136** and **152** with a pKa near cut-off limits (9.15–9.76), significantly affected lipophilicity, leading to a marked drop in the LogD values (negative 0.28–1.89), an increase in TPSA (88.32–125.62 $Å^2$). Nevertheless, the aliphatic amine derivatives from **subseries IVA** still exhibit good drug-like properties, according to the CNS MPO scores over 4.

Table 6. Calculated physicochemical properties of compounds **126**, **133**, **135**–**136** and **149-153** from **series IV**.

SERIES IVA

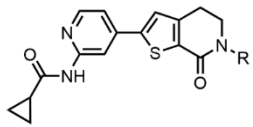

Cmpd.	R	MW	LogP	LogD	HBD	HBA	TPSA	Rotatable Bonds	Strongest basic pK_a	Fraction Csp^3	CNS MPO
Cmpd. V	H	313.38	2.04	2.04	2	3	71.09	3	3.14	0.31	5.48
126	*–Me	327.40	2.26	2.26	1	3	62.30	3	3.14	0.35	5.70
133	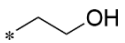	357.43	1.57	1.57	2	4	82.53	5	3.14	0.39	5.50
135	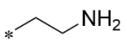	356.44	1.47	-0.28	2	4	88.32	5	9.15	0.39	4.93
136	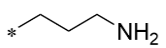	370.47	1.53	-0.76	2	4	88.32	6	9.76	0.42	4.55

SERIES IVB

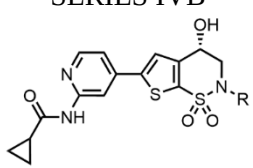

149	H	365.42	0.91	0.89	3	5	108.39	3	3.02	0.33	4.51
150	*–Me	379.45	1.13	1.13	2	5	99.60	3	3.02	0.37	5.04
151	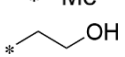	409.48	0.44	0.44	3	6	119.83	5	3.02	0.41	3.82
152	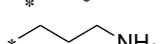	422.52	0.40	-1.89	3	6	125.62	6	9.76	0.44	2.84
153	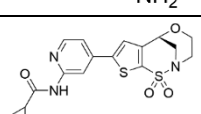	391.46	1.60	1.60	1	5	88.60	3	3.02	0.41	5.61

3.4. Biological evaluation

The following stage involved the evaluation of the obtained compounds to determine their biological activity, safety, and key pharmacokinetic and toxicological properties in biological assays (Figure 17).

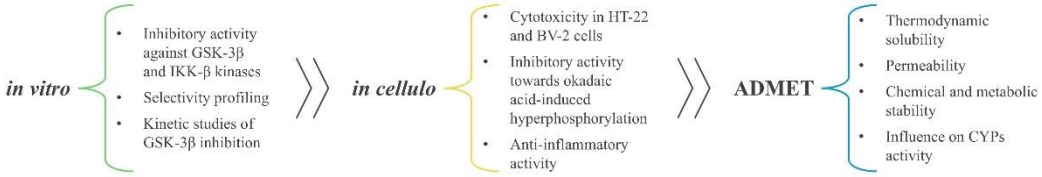

Figure 17. Biological evaluation of compounds covered in the doctoral dissertation.

The primary test *in vitro* aimed at identifying active compounds from the pool of obtained structures was the commercially available ADP-Glo™ bioluminescence assay from Promega. It is based on the spectrophotometric determination of the amount of adenosine diphosphate (ADP) produced from ATP during the kinase reaction. The generated ADP is subsequently converted into ATP and coupled with luciferase. The signal detected from luciferase correlates with the kinase activity. The assay allowed for the high-throughput screening of compounds that were initially evaluated at a concentration of 10 μM. The most active candidates, with inhibition above 50%, were tested at various concentrations to determine the IC_{50} value. As references, we used potent, known selective inhibitors – compound **I** for GSK-3β, the commercially available **TPCA-1** for IKK-β and the non-selective kinase inhibitor **staurosporine**[2]. The selected compounds were evaluated for kinase selectivity in a screening conducted by Eurofins Discovery, using a panel of human kinases within the Kinase Enzymatic Radiometric [Km ATP] Kinase Profiler Lead Hunter Assay[3]. Additionally, for compound **62**, we determined the inhibition type and K_i value against GSK-3β in the kinetic studies by applying varying concentrations of ATP (10–100 μM) and the inhibitor (0–100 nM)[4].

In further studies, the compounds were evaluated in cell-based assays[5]. First, we determined their potential neuro- and immunotoxic concentration on mouse hippocampal neuronal cells HT-22 and mouse microglial cells BV-2 respectively, using PrestoBlue™ Cell Viability assay. The compounds were tested at 5 concentrations – 0.1, 1, 10, 50,

[2] Inhibitory activity against GSK-3β and IKK-β kinases was performed by Justyna Godyń, PhD and Izabella Góral, M.Sc. from the Department of Physicochemical Drug Analysis, JU MC.

[3] Selectivity screening against a panel of human protein kinases was performed at Eurofins Discovery.

[4] Kinetic Studies of GSK-3β Inhibition were performed by Justyna Godyń, PhD from the Department of Physicochemical Drug Analysis, JU MC.

[5] Cell-based assays including cytotoxicity in HT-22 and BV-2 cells, evaluation of inhibitory activity toward okadaic-acid-induced hyperphosphorylation and anti-inflammatory activity were performed by Barbara Mordyl, PhD and Monika Głuch-Lutwin, PhD from the Department of Pharmacobiology, JU MC.

and 100 μM and the results are expressed as IC_{50} values. Subsequently, the most promising nontoxic candidates were examined for their neuroprotective and anti-inflammatory activities. The neuroprotective properties were assessed in the okadaic acid-induced model of neurodegeneration as a potential to restore the viability of HT-22 cells. Okadaic acid (OA) is a phosphatase inhibitor and promotes hyperphosphorylation of, among others, tau protein, mimicking conditions analogous to those observed in AD. In the assay, GSK-3β inhibitor – compound **I**, was used as a reference. The anti-inflammatory effect was examined in LPS-stimulated BV-2 cells that serve as a model of neuroinflammation. The compounds were evaluated for their ability to reduce the levels of key inflammatory markers – NO, IL-6, and TNF-α in comparison to the IKK-β inhibitor **TPCA-1**.

Finally, compounds **40**, **49**, **60**, **62**, **70**, **112**, **119**, **126** and **149** that demonstrated positive performance in previous assays underwent comprehensive studies including *in vitro* ADMET profiling, such as thermodynamic solubility, permeability, chemical and metabolic stability and influence on CYPs activity. Thermodynamic solubility studies were performed in Dulbecco's phosphate-buffered saline (DPBS) using quantitative HPLC analysis after shaking for 24 hours at room temperature[6]. The permeability was assessed in the Parallel Artificial Membrane Permeability Assay (PAMPA), which is a model of passive, intestinal absorption [175]. Caffeine was used as a well-permeable reference[7]. Chemical stability was measured in phosphate buffer at physiological pH 7.4, after 2 hours of incubation at 37 °C[5]. To determine the metabolic stability, the compounds were incubated with human liver microsomes (HLM) or mouse liver microsomes (MLM) in the presence of NADPH, and then analysed with UPLC-MS to detect and identify the mass of potential metabolites. Verapamil, classified as a highly metabolising drug, was used in the studies as a reference[5]. The effects on key CYP isoforms (3A4, 2D6, and 2C9) were assessed using the CYP450 inhibition luminescence assay from Promega. This assay relies on measuring the luminescence intensity from luciferin, generated during incubation of the tested compound (at four concentrations – 0.1, 1, 10 and 25 μM) with the selected CYP isoform. The luminescence signal is proportional to CYP activity, decreasing in case of inhibition and increasing with activation. Isoform-specific substrates were used as reference inhibitors: ketoconazole for 3A4, quinidine for 2D6 and sulfaphenazole for 2C9[8].

[6] Thermodynamic solubility assay and chemical and metabolic stability assays were performed by Natalia Szałaj, PhD and Paula Zaręba, PhD from the Department of Physicochemical Drug Analysis, JU MC.

[7] Permeability PAMPA study was performed by Justyna Godyń, PhD from the Department of Physicochemical Drug Analysis, JU MC.

[8] Influence on CYP P450 isoforms was performed by Gniewomir Latacz, PhD and Ewelina Honkisz-Orzechowska, PhD from the Department of Technology and Biotechnology of Drugs, JU MC.

3.4.1. Series I[9]

Inhibitory activity against GSK-3β and IKK-β kinases

The structure of compounds in **series I** represents a merged inhibitor type. Compound **49**, obtained by directly combining fragments from reference inhibitors **I** (aminopyridine scaffold) and **II** (thiophene with attached urea and amide moiety) displayed potent activity against GSK-3β (IC_{50} = 20 nM) but was inactive against IKK-β (Table 7). Ring closure yielded compound **40** with the tetrahydropyrimidone moiety and this modification not only maintained high activity against GSK-3β (IC_{50} = 10 nM) but also enabled IKK-β inhibition in the micromolar range (IC_{50} = 4.38 μM). With the initial understanding of how to target both kinases simultaneously, the structures of the inhibitors have been extensively modified to ensure in-depth SAR analysis (Tables 7 and 8). Firstly, we focused on the carboxamide moiety attached to the 2-position of pyridine and replaced the cyclopropyl with other alkyl (**38**, **39**, **47** and **48**), cycloalkyl (**41**, **42**, **50** and **51**), and phenyl (**43** and **52**) substituents. According to the IC_{50} values, the highest inhibitory activities against GSK-3β were established for the isopropyl- (**39** and **48**) and cyclobutyl- analogues (**41** and **50**) ranging from 12 nM to 34 nM. The introduction of a small methyl substituent led to the loss of activity against GSK-3β in the urea-based derivative **47** from **series IA**, and the decrease of inhibitory potency (IC_{50} = 1.13 μM) of the cyclic compound **38** from **series IB**. In addition, compound **38** retained the inhibition toward IKK-β (IC_{50} = 6.524 μM), however with reduced potency compared to compound **40**. Larger substituents such as cyclohexyl (**42** and **51**) and phenyl (**43** and **52**) led to reduced activity against GSK-3β and did not result in IKK-β inhibition in both **series IA** and **IB**. Furthermore, the exchange of the amide for a sulfonamide (**44** and **45**) or reduction to an amine (**46**) caused a loss of activity toward both kinases. Subsequently, we focused on the replacement of the pyridine ring with either a 4-fluorobenzene or benzene ring (Table 8). Compound **59** with a 4-fluorobenzene ring in the **series IA**, exhibited moderate, yet balanced activity against both kinases (GSK-3β IC_{50} = 1.847 μM and IKK-β IC_{50} = 7.621 μM). In contrast, the removal of the fluorine atom led to compound **58**, a selective IKK-β inhibitor (IC_{50} = 422 nM), likely due to urea moiety interactions with the hinge region. Among the tetrahydropyrimidone derivatives in the **series IB**, all but one compound **54**, which inhibits GSK-3β (IC_{50} = 453 nM), are inactive against both kinases. The results confirm previous findings that the *N*-(pyridin-2-yl)carboxamide fragment, particularly with a cyclopropyl substituent, ensures the binding and inhibition of GSK-3β,

[9] The research on **series IA** and **IB** was previously described in Publication I: Góral, I.; Wichur, T.; Sługocka, E.; Godyń, J.; Szałaj, N.; Zaręba, P.; Głuch-Lutwin, M.; Mordyl, B.; Panek, D.; Więckowska, A. Connecting GSK-3β Inhibitory Activity with IKK-β or ROCK-1 Inhibition to Target Tau Aggregation and Neuroinflammation in Alzheimer's Disease—Discovery, In Vitro and In Cellulo Activity of Thiazole-Based Inhibitors. *Molecules* 2024, *29*, 2616, doi:10.3390/molecules29112616.

due to the presence of pivotal HBA-HBD groups. Replacing the pyridine nitrogen atom with a fluorine atom retains the ability to form hydrogen bonds but such modification is associated with a decrease in potency. In contrast, removing the HBA group, as in benzene derivatives, results in the expected loss of inhibitory activity. Additionally, the arrangement of the thiophene-based fragment relative to the aminopyridine core is crucial; a shift from the 4- to 5-position of the pyridine ring led to loss of activity against both kinases, as demonstrated for compound **65** (analogue of compound **40**).

As exemplified by the activity of compounds **40** (IC_{50} = 4.38 μM) and **49** (not active) against IKK-β, the tetrahydropyrimidone core is preferred over 3-ureidothiophene-2-carboxamide. To further explore the kinase binding sites, the dimethyl substituent in **40** was replaced by a spirocyclic ring system, retaining the *N*-(pyridin-2-yl)cyclopropanecarboxamide scaffold as a fixed fragment (Table 8). The cyclopentane analogue **60** exhibited comparable activity against both GSK-3β (IC_{50} = 10 nM) and IKK-β (IC_{50} = 7.351 μM) to that of compound **40**. The subsequent introduction of an oxygen atom into the cyclopentane ring (compounds **61** and **62**) did not affect the inhibitory activity for GSK-3β but completely abolished the inhibition of IKK-β, pointing to the dimethyl substituent as a compromise for simultaneous inhibition of both selected kinases.

In the **subseries IC**, we retained the fragment most preferred for IKK-β inhibition – a thiophene-based tetrahydropyrimidone with a dimethyl substituent – and merged it with a heterocyclic 7-azaindole and furo[3,2-*d*]pyrimidine fragments (Table 8). This approach yielded the most potent dual inhibitor, **70**, demonstrating balanced activity against both kinases (GSK-3β IC_{50} = 267 nM and IKK-β IC_{50} = 366 nM) within the entire **series I**. Replacement of the NH group of 7-azaindole with oxygen, as in compound **72**, led to a greater than 8-fold reduction in inhibitory activity for GSK-3β (IC_{50} = 2.217 μM) and loss of activity against IKK-β, emphasizing the necessity of a hydrogen bond donor group in the structure.

Table 7. Inhibitory activity of compounds **47**–**52** from **series IA** and **38**–**46** from **series IB** against GSK-3β and IKK-β kinases.

Cmpd.	GSK-3β	IKK-β	R	Cmpd.	GSK-3β	IKK-β
	IC_{50} [μM][a] or % inh. at 10 μM[b]				IC_{50} [μM][a] or % inh. at 10 μM[b]	
	SERIES IA 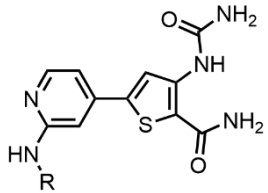				SERIES IB 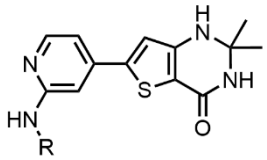	
47	34% ± 9%	17% ± 8%	$-CO-CH_3$	**38**	1.130 ± 0.043	6.524 ± 0.281
48	0.022 ± 0.000	<10%	$-CO-CH(CH_3)_2$	**39**	0.012 ± 0.000	33% ± 6%
49	0.020 ± 0.000	16% ± 3%	$-CO-$ 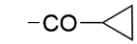	**40**	0.010 ± 0.000	4.380 ± 0.544
50	0.034 ± 0.000	<10%	$-CO-$ 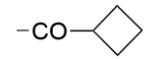	**41**	0.032 ± 0.001	32% ± 4%
51	0.614 ± 0.026	<10%	$-CO-$ 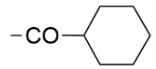	**42**	0.830 ± 0.030	18% ± 3%
52	0.398 ± 0.012	30% ± 2%	$-CO-$ 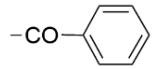	**43**	1.314 ± 0.042	38% ± 5%
			$-SO_2-CH_3$	**44**	32% ± 1%	<10%
			$-SO_2-CH_2CH_3$	**45**	40% ± 9%	<10%
			$-CH_2-$ 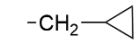	**46**	39% ± 2%	41% ± 2%
	Compound I		0.005 ± 0.000		22% ± 7%	
	TPCA-1[c]		1.316 ± 0.076		0.037 ± 0.001	
	Staurosporine[d]		0.080 ± 0.007		0.894 ± 0.042	

[a] Half maximal inhibitory concentration of the tested compound for selected kinase, mean value ± standard error of the mean (SEM) of triplicates; [b] mean value ± standard deviation (SD) of triplicates; [c] reference, Sigma-Aldrich Chemie GmbH, Steinheim, Germany; [d] reference, Biokom, Janki, Poland.

Table 8. Inhibitory activity of compounds **58**–**59** from **series IA**, **53**–**62** and **65** from **series IB**, **70** and **72** from **series IC** against GSK-3β and IKK-β kinases.

Cmpd.	GSK-3β	IKK-β	R	R_1	Cmpd.	GSK-3β	IKK-β
	IC_{50} [μM][a] or % inh. at 10 μM[b]					IC_{50} [μM][a] or % inh. at 10 μM[b]	
	SERIES IA 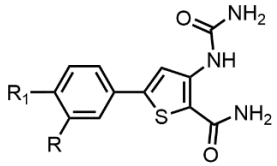					SERIES IB 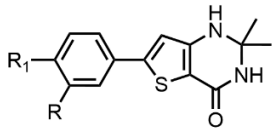	
58	36% ± 8%	0.422 ± 0.012		H	**53**	47% ± 4%	<10%
59	1.847 ± 0.038	7.621 ± 0.695		F	**54**	0.453 ± 13%	10% ± 7%
			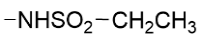	H	**55**	11% ± 3%	16% ± 0%
			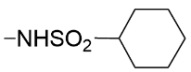	H	**56**	<10%	<10%
			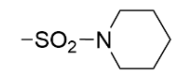	H	**57**	<10%	17% ± 7%

Cmpd.	*	GSK-3β	IKK-β
		IC_{50} [μM][a] or % inh. at 10 μM[b]	
	SERIES IB 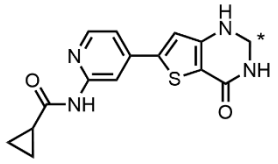		

60		0.010 ± 0.000	7.351 ± 0.196
61		0.012 ± 0.000	<10%
62		0.008 ± 0.000	39% ± 9%
	SERIES IB 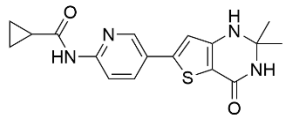		
65		25% ± 2%	<10%
Cmpd.	**Ar**	**GSK-3β**	**IKK-β**
		IC_{50} [μM][a] or % inh. at 10 μM[b]	
	SERIES IC 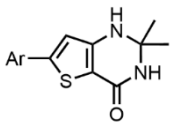		
70	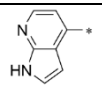	0.267 ± 0.008	0.366 ± 0.007
72		2.217 ± 0.127	<10%
	Compound I	0.005 ± 0.000	22% ± 7%
	TPCA-1[c]	1.316 ± 0.076	0.037 ± 0.001
	Staurosporine[d]	0.080 ± 0.007	0.894 ± 0.042

[a] Half maximal inhibitory concentration of the tested compound for selected kinase, mean value ± standard error of the mean (SEM) of triplicates; [b] mean value ± standard deviation (SD) of triplicates; [c] reference, Sigma-Aldrich Chemie GmbH, Steinheim, Germany; [d] reference, Biokom, Janki, Poland.

The conclusions drawn from the determined IC_{50} values against GSK-3β are consistent with the predicted binding mode within the ATP-binding pocket of the enzyme, exemplified by **49** and **40** (Figure 18)[10]. The *N*-(pyridin-2-yl)cyclopropanecarboxamide fragment interacts with the Val135 residue in the hinge region. Both compounds form bidentate hydrogen bonds with the nitrogen and carbonyl oxygen atoms of Val135 chain via the pyridine nitrogen and amide nitrogen, respectively in an acceptor–donor motif. Another stabilizing interaction is provided by the hydrogen bond between Asp133 and the C(2) hydrogen atom of the pyridine ring. Thiophene derivatives, both with urea and tetrahydropyrimidone moieties, form H-bonds with the catalytic Lys85 by interplay between the side chain amino group and the carbonyl oxygen atom derived from the amide group at the second position of the thiophene ring of **49** or from an incorporated into the cyclic scaffold, as observed for compound **40**. Furthermore, the urea fragment of compound **49** binds to the carbonyl atom of Asn186 via a hydrogen bond, while the dimethyl moiety of compound **40** interacts via London dispersion forces with the Cys199 and Phe67 residues.

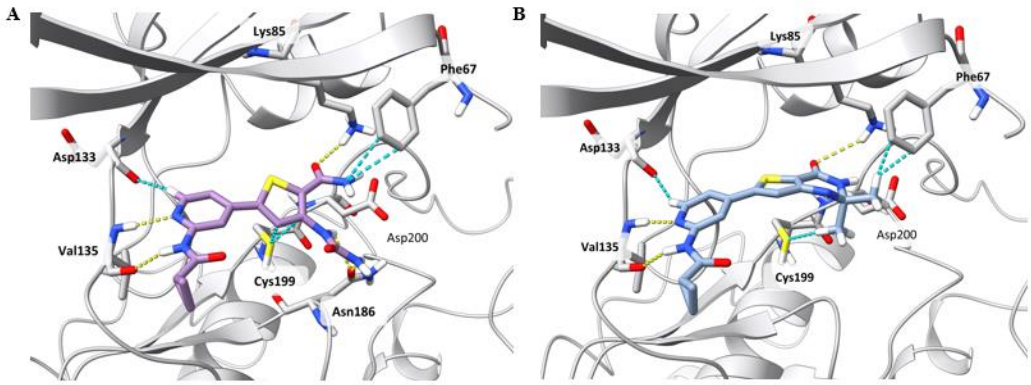

Figure 18. Visualization of the inhibitors docking pose in complex with the refined crystal structure of GSK-3β (PDB ID: 4PTC): (**A**) compound **49**, gscore function value −9.87; (**B**) compound **40**, gscore function value −8.16. All poses were generated using Glide (Schrodinger Suite, 2023). Residues 52–65 are hidden for clarity. Hydrogen bonds are shown as yellow dashed lines. Favorable contacts (van der Waals overlap > −0.3 Å) are shown as cyan-colored dashed lines.

Further docking studies focused on the superiority of the tetrahydropyrimidone fragment in compound **40** over the 3-ureidothiophene-2-carboxamide derivative **49** in binding and activity against IKK-β (Figure 19). Compound **49** is inactive against IKK-β. Therefore, in molecular docking studies, it adopts multiple conformations, suggesting an inability to form a stable anchoring complex with the enzyme. Determining the precise binding pose within the ATP-binding pocket is not feasible. Compound **49** can be oriented in both configurations: with the *N*-(pyridin-2-

[10] Molecular modeling studies were performed by Emilia Sługocka, M.Sc. from the Department of Physicochemical Drug Analysis, JU MC.

yl)cyclopropanecarboxamide fragment facing Cys99 of the hinge and the 3-ureidothiophene-2-carboxamide fragment pointing toward Thr23 and Asn28 (Figure 19A), as well as in a 180-degree reversed configuration to interact with Asp166 (Figure 19B). Based on the high value of calculated conformational entropy, the conformational freedom of the ligand imposes an energetic penalty, making it challenging to fit into the binding pocket. This hinders ligand-protein complex formation. On the contrary, the docking of compound **40**, which exhibits moderate inhibitory activity against IKK-β, resulted in a stable formation of bidentate hydrogen bonds between *N*-(pyridin-2-yl)cyclopropanecarboxamide fragment and Cys99 (Figure 19C). Moreover, the tetrahydropyrimidone moiety interacts via hydrogen bonds with the amide carbonyl group serving as an HBA from Lys44 and the amide nitrogen acting as a HBD to Asp166. The presence of these interactions dictates the activity toward IKK-β.

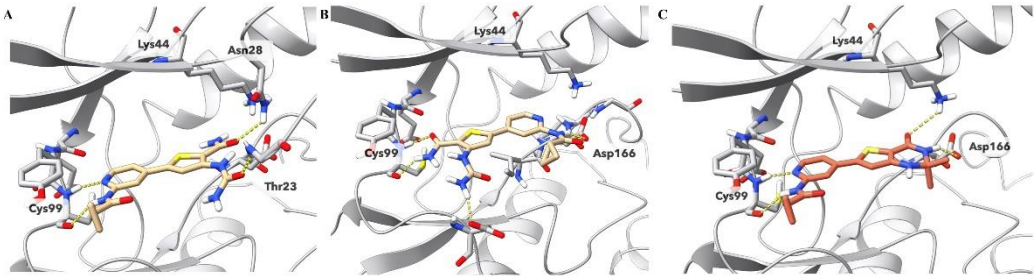

Figure 19. Visualization of the compounds docking pose in complex with the refined crystal structure of IKK-β (PDB ID: 4KIK): (**A**), (**B**) compound **49**; (**C**) compound **40**, gscore function value −9.30. All poses were generated using Glide (Schrodinger Suite, 2023). Residues 18–26 are hidden for clarity. Hydrogen bonds are shown as yellow dashed lines.

Docking studies of **70** revealed stable poses for both GSK-3β and IKK-β kinases (Figure 20). The 7-azaindole fragment, similarly to the aminopyridine core, serves as the hinge binding motif with an acceptor–donor system derived from pyridine and pyrrole nitrogen atoms, respectively. Compound **70** forms a bidentate hydrogen bond with Val135 of GSK-3β and Cys99 of IKK-β. The tetrahydropyrimidone fragment provides additional anchoring interactions via the amide carbonyl oxygen to catalytic Lys85 (in GSK-3β) and Lys44 (in IKK-β), as well as via hydrogen bonds in IKK-β derived from amide and amine to Asp166 and Glu149, respectively. The replacement of the pyrrole nitrogen atom with oxygen in **72** disrupted the interaction with the IKK-β hinge (not shown). The geometry of the molecule and the construction of the binding pocket imply a repulsion at the hinge binding region, whereas the binding of the tetrahydropyrimidone fragment does not provide any compensatory interactions. In GSK-3β, compound **72** is stabilized by the single hydrogen bond between the Val135 of the hinge region and the pyrimidine nitrogen and additionally by a hydrogen bond with the catalytic Lys85 analogously to **70**.

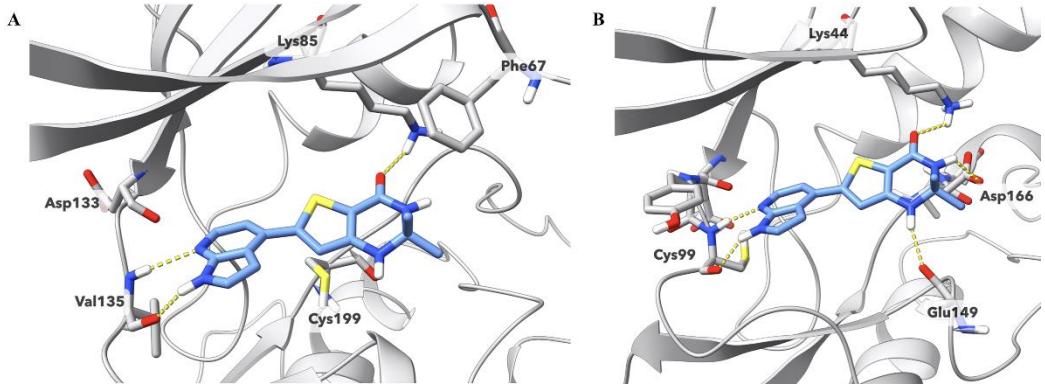

Figure 20. (**A**) Visualization of the docking pose of the **70**/GSK-3β complex in refined crystal structure (PDB ID: 4PTC), gscore function value −8.89. (**B**) Visualization of the docking pose of the **70**/IKK-β complex (PDB ID: 4KIK), gscore function value −8.89. All poses were generated using Glide (Schrodinger Suite, 2023). Residues 52–65 (in GSK-3β) and 18–26 (in IKK-β) are hidden for clarity. Hydrogen bonds are shown as yellow dashed lines.

Cytotoxicity in HT-22 and BV-2 cells

The cytotoxic effects of the most potent GSK-3β/IKK-β inhibitors were examined in HT-22 and BV-2 cell lines (Table 9). Compounds **40**, **41** and **60** decreased the viability of BV-2 cells at 10 μM concentration but did not affect HT-22 cells. Determined IC_{50} values are significantly higher than the effective inhibitory concentrations for GSK-3β by at least 190-fold. However, particular attention should be given when targeting IKK-β by **40** due to the comparable effective and toxic IC_{50} values in BV-2 cells. **70** demonstrated marked toxicity in both cell lines, with a more pronounced toxic effect in BV-2 cells; however, the IC_{50} exceeded the effective inhibitory concentration (for both enzymes) by an order of magnitude. Compounds **38**, **42** and **48** are exhibiting moderate toxicity. None of these compounds affected the viability of BV-2 cells at concentrations up to 10 μM; however, above this, they show significant toxicity, reducing the number of viable cells to below 10%. Compound **48** exhibited greater safety for the HT-22 cells over the BV-2 cell line when comparing IC_{50} values. The other tested compounds (**49**, **50**, **54**, **58**, **59**, **61** and **62**) demonstrated a broad safety margin, showing no effect on cell viability in both cell lines at concentrations up to at least 50 μM.

Table 9. Cytotoxicity of **38**, **40–42**, **48–50**, **54**, **58–62** and **70** in HT-22 and BV-2 cells.

Compound	HT-22 cells	BV-2 cells
	IC_{50} [μM] $\bar{x} \pm$ SEM	
38	n.d.	12.0 ± 0.1
40	19.9 ± 4.1	3.6 ± 0.7
41	>100	6.1 ± 3.1

42	n.d.	17.7 ± 0.1
48	36.6 ± 4.3	21.8 ± 3.8
49	>100	>100
50	>100	>100
54	n.d.	>100
58	67.1 ± 14.5	51.4 ± 0.8
59	n.d.	>100
60	9.7 ± 5.8	3.0 ± 0.0
61	>100	>100
62	58.3 ± 10.0	54.8 ± 1.9
70	6.1 ± 0.2	3.5 ± 0.1
Compound I	>100	15.4 ± 0.6
TPCA-1[a]	73.5 ± 1.5	11.2 ± 0.3
Staurosporine[b]	n.d.	0.001 ± 0.000

Data expressed as the means ± SEM; N ≥ 6; n.d. – not determined.

Evaluation of inhibitory activity toward okadaic acid-induced hyperphosphorylation and anti-inflammatory activity

Of the 10 tested compounds selected based on the dual GSK-3β/IKK-β inhibitory activity (**40**, **60**, **70**), outstanding GSK-3β inhibitory potency (**41**, **48**, **49**, **50**, **61**, **62**) or IKK-β inhibitory activity (**58**), more than half exhibited neuroprotective properties in the okadaic acid-induced hyperphosphorylation assay (Figure 21). The strongest effects were observed for compounds **61** and **70** across all tested concentrations (0.1 μM to 10 μM) and compound **60** at 1 μM. Although compound **70** has a narrow safety margin, with a calculated therapeutic index of 23, it demonstrates neuroprotective properties at a concentration of 10 μM and does not exhibit toxicity toward HT-22 cells. An increase in HT-22 cells' viability was also observed for compounds **40** and **49** at 10 μM, with results comparable to those of reference compound **I**. Statistically significant but less marked neuroprotective effects were also observed for compounds **49** at 1 μM and **62** at 10 μM. Compounds **48**, **50**, **41** and **58** were not active in the assay.

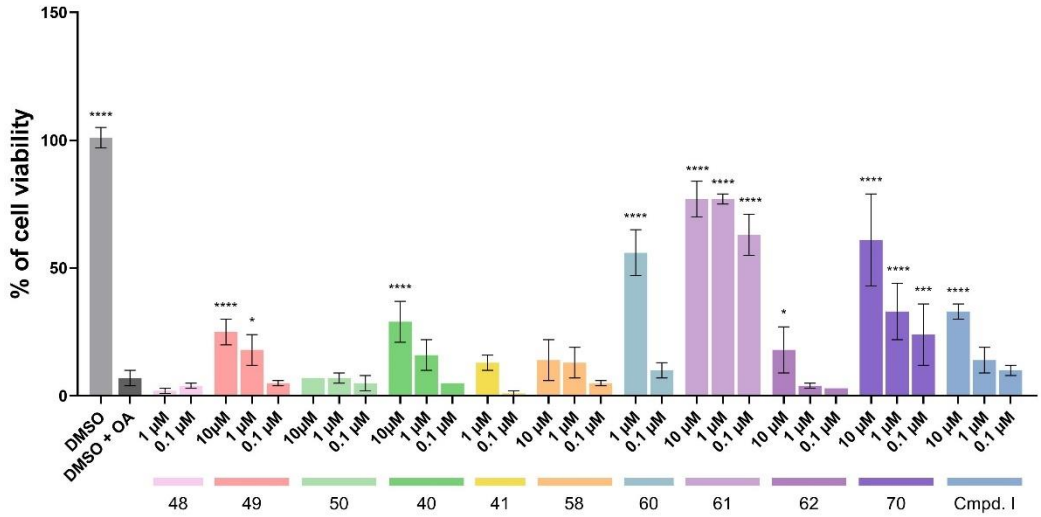

Figure 21. Influence of compounds **48**–**50**, **40**, **41**, **58**, **60**–**62** and **70** on okadaic acid-induced hyperphosphorylation in HT-22 cell line (the cells were pre-treated with 400 nM of okadaic acid for 3 h). Viability was determined using Presto Blue™ cell viability reagent after 24 h. Statistical analysis was performed using GraphPad Prism 9.0.0. All values are expressed as mean with SD. Differences among groups were evaluated by one-way ANOVA followed by post-hoc analysis (Dunnett's multiple comparison tests) *vs*. control group (okadaic acid on HT-22 cells) and were considered statistically significant if $p<0.05$ (*$p<0.05$, **$p<0.01$, ***$p<0.001$, ****$p<0.0001$).

The selected compounds (chosen based on the previously established criteria) displayed significant anti-inflammatory effects reflected in decreasing NO levels in LPS-treated BV-2 cell line (Figure 22A). Nearly all compounds, except **58**, reduced NO production at 10 μM concentration. The effect was also observed for compounds **50**, **41**, **54**, **60** and **62** at 1 μM, and exceeded the reference compound **TPCA-1**, which was not active at this concentration. Compound **54** showed anti-inflammatory properties against NO also at a concentration of 0.1 μM. All but compounds **40** and **70** also decreased IL-6 release in BV-2 cells. The most pronounced effect was determined for **62**, comparable to that observed for **TPCA-1** at 10 μM concentration. A significant reduction in IL-6 levels, although weaker than the reference, was also observed for compounds **49**, **50** and **61** at 10 μM (Figure 22B). Inhibitors **48**, **41** and **60** preserved their anti-inflammatory effect on IL-6 also at 1 μM, while below this concentration, none of the compounds show anti-inflammatory activity toward the following marker. The analysis of TNF-α release revealed that only two compounds, **41** (at 10 μM) and **70** (at 1 μM), exhibited the ability to reduce its levels (Figure 22C). Due to considerable toxicity, compounds **40** and **70** were not tested at a concentration of 10 μM in BV-2 cells.

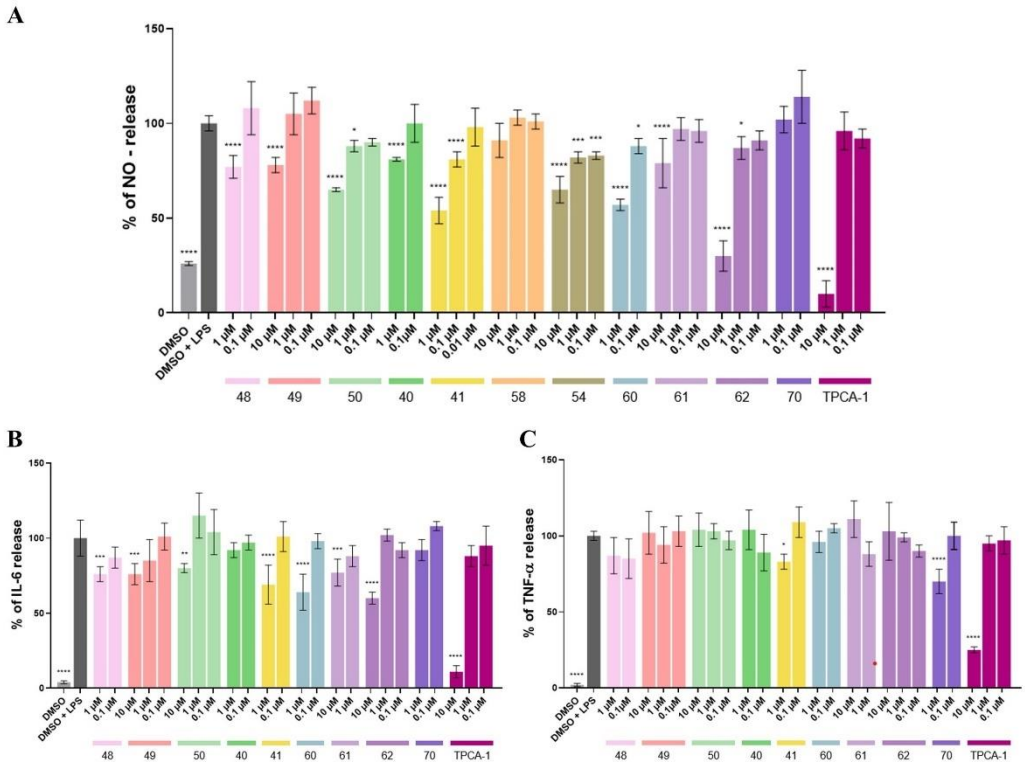

Figure 22. (**A**) Influence of compounds **48**–**50**, **40**, **41**, **58**, **54**, **60**–**62** and **70** on % of NO-release in LPS-treated (100 ng/mL) BV-2 cell line. NO-release was measured using a fluorometric assay with 2,3-diaminonaphthalene (DAN). (**B**), (**C**) Influence of compound **48**–**50**, **40**, **41**, **60**–**62** and **70** on % of IL-6 and TNF-α release in LPS-treated (100 ng/mL) BV-2 cell line. The IL-6 and TNF-α levels were measured using LANCE Ultra TR-FRET Detection Kit (Perkin Elmer). Statistical analysis was performed using GraphPad Prism 9.0.0. All values are expressed as mean with SD. Differences among groups were evaluated by one-way ANOVA followed by post-hoc analysis (Dunnett's multiple comparison tests) *vs*. control group (LPS on BV-2 cells) and were considered statistically significant if $p<0.05$ (*$p<0.05$, **$p<0.01$, ***$p<0.001$, ****$p<0.0001$).

Kinetic Studies of GSK-3β Inhibition

Compound **62** as the most potent GSK-3β inhibitor was selected for kinetic studies to determine its inhibition mode and inhibition constant (K_i) value (Figure 23). Lineweaver−Burk plot analysis proved that compound **62** displays ATP-competitive inhibition type, according to preserved Vmax and increasing K_m with increasing inhibitor concentrations, as shown by the increasing slopes of the converging lines at the same point on the y-axis (1/V) (Figure 23A). This observation was further confirmed by the Cornish–Bowden plot (Figure 23B). The competitive inhibitory nature indicates

the binding of the compound to the free enzyme, thereby preventing ATP from interacting with the active site. The K_i value was read directly from the intersection of the x-axis of the Lineweaver-Burk replot data K_m versus [I] (Figure 23C). The determined K_i (2 nM) is adjacent to IC_{50} (8 nM).

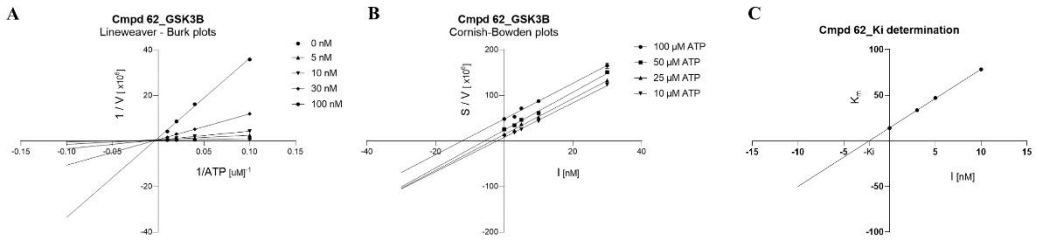

Figure 23. Demonstration of ATP-competitive nature of GSK-3β inhibition by compound **62** on (**A**) Lineweaver−Burk and (**B**) Cornish−Bowden plots. (**C**) Determination of K_i value based on the replot from Lineweaver-Burk plot. Calculated $K_i = 2.22\times10^{-9}$, $pK_i = 8.65$; V = initial velocity rate, S = ATP concentration, I = inhibitor concentration, K_m = Michaelis-Menten constant.

Kinase selectivity

Compounds from **series I** target highly conserved ATP-binding sites, posing questions about affinity for other kinases. Therefore, three selected compounds – **40** and **60** as a dual GSK-3β/IKK-β inhibitors and **62** as the most potent GSK-3β inhibitor were subjected for a selectivity profiling against panel of human protein kinases at Eurofins Discovery (Figure 24 and 25). We considered 19 (for **40** and **60**) or 17 (for **62**) selected kinases from different phylogenetic families:

- The cyclin-dependent kinases (CDK) isoforms 1–9 that activity controls the mammalian cell cycle driving the transitions through the phases [176].
- The casein kinase 1 (CK1) isoforms δ and ε involved in regulation of circadian rhythm [177].
- The dual-specificity tyrosine-regulated (DYRK) kinases 1A and 1B isoforms displaying diverse functions in the neuronal regulation and development [178].
- The GSK family as the major tau phosphorylating enzymes [179].
- All three isoforms from the IKK complex and Tank-binding kinase (TBK) 1 as involved in NF-κB activation [180].
- The superfamily of mitogen-activated protein kinases (MAPK), C-Jun *N*-terminal kinases (JNK) and stress-activated protein kinases (SAPK) activated by pathological stress stimuli and thus regulating the activity of nuclear transcription factors [181].

Compounds **40** and **60** were tested at a concentration of 10 µM, which was a screening concentration against GSK-3β (100% inhibition) and IKK-β (70% inhibition) (Figure 24). Disappointingly, both compounds displayed high affinity for the majority of the tested kinases at this concentration. While targeting CK1 may be particularly

valuable due to its involvement in reducing the amyloid burden in APP-PS1 mice [182], the inhibition of CDK5 might be less desirable. This is due to its variable functions in neuronal development including neurite outgrowth, vesicular transport, and synaptic functions [183], but in terms of AD promotion NFT formation [184]. To enhance therapeutic potential, efforts should focus on improving selectivity against related kinases to minimize off-target effects and reduce potential side effects. Additionally, enhancing the moderate inhibitory activity against IKK-β would be beneficial.

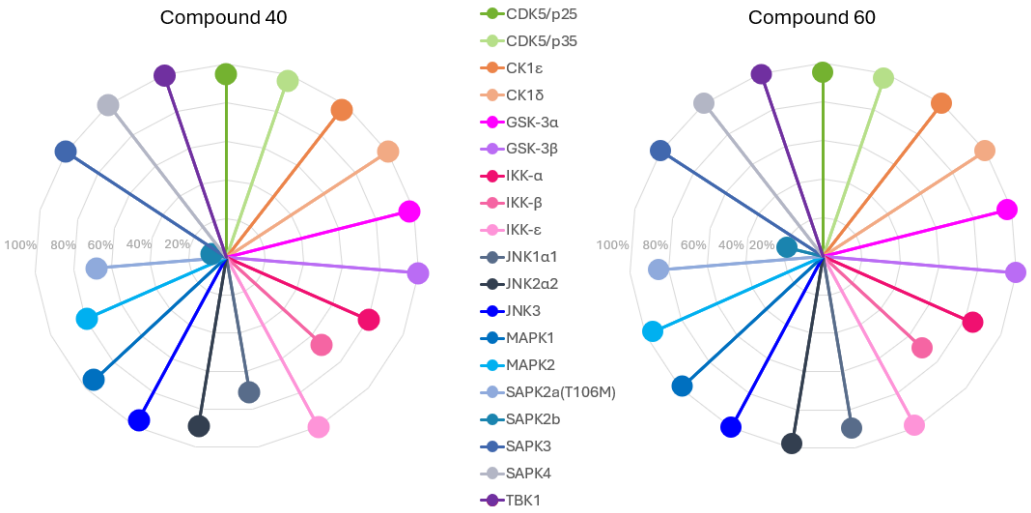

Figure 24. Selectivity of compounds **40** and **60** against 19 selected kinases. The data are presented as the percentage of kinase inhibition at a concentration of 10 μM of both inhibitors.

Regarding its GSK-3β inhibitory potency, compound **62** was evaluated within the CMGC group of kinases, to which GSK-3β belongs (Figure 25). At the concentration of 1 μM compound **62** maintains a high affinity for the GSK family (99% inhibition). In addition, it also displayed similar potency on DYRK 1A and 1B kinases, which may have beneficial effects due to modulation of tau and Aβ formation. The moderate activity was determined for CDK 1,2 and 9, JNK3, MAPK1 and SAPK3 kinases (60% to 80% of inhibition), however at an inhibitory concentration much higher than the effective nanomolar concentration against GSK-3β.

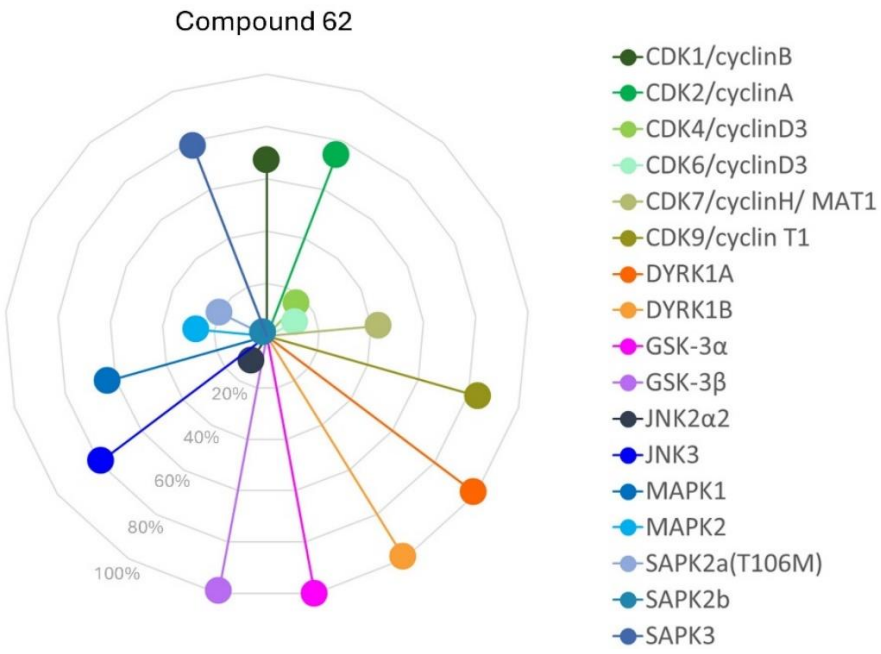

Figure 25. Selectivity of compound **62** against 17 selected kinases. The data are presented as the percentage of kinase inhibition at a concentration of 1 μM of inhibitor **62**.

In addition to the primary research objectives, compounds from **subseries IA** and **IB** were investigated for their affinity toward Rho-associated coiled-coil protein kinase 1 (ROCK1). ROCK1 is considered a potential anti-AD target given its role in regulating amyloidogenic APP processing via BACE1 and tau protein phosphorylation through the interplay with key enzymes such as GSK-3β [185,186]. Among tetrahydropyrimidone derivatives, a few compounds were identified as micromolar ROCK1 inhibitors, with the most potent representatives comprising: **40** (IC_{50} = 1.76 μM), **46** (IC_{50} = 1.73 μM) and **60** (IC_{50} = 1.36 μM).

Preliminary in vitro ADMET profiling

In preliminary ADMET profiling, we first evaluated the permeation ability of compounds **40**, **49**, **60**, **62** and **70**, compound **I** and caffeine as a well-permeable reference (Table 10). The *Pe* values determined for all test compounds were relatively low compared to caffeine. The urea-based derivative **49** was not permeable at all, probably due to 4 hydrogen bond donor groups and a high value of TPSA (140.20 $Å^2$). Compounds **40** and **60** represent higher permeability values, which is consistent with optimized physicochemical parameters in the tetrahydropyrimidone derivatives, due to the reduction of the HBD groups to 3 and the TPSA value (83.12 $Å^2$) in comparison to **49**. However, the determined permeability coefficient values are limiting and do not guarantee that the mentioned compounds will pass through the membranes *in vivo*.

The introduction of an additional hydrogen bond acceptor as an oxygen atom in the spirocyclic ring in compound **62** resulted in an almost 4-fold decrease in *Pe*. Compound **70** can be classified as the highest permeable; however, its penetration coefficient is lower compared to the reference compound **I** despite the preferable values of the physicochemical descriptors (LogP values 2.39 vs. 1.47 and TPSA values 69.81 vs. 107.20 $Å^2$, respectively).

Table 10. Results of permeability evaluation in the PAMPA assay for compounds **40**, **49**, **60**, **62**, **70** and the reference compound **I**.

Cmpd.	**PAMPA**
	Pe **(10^{-6} cm/s)[a] ± SD**
40	2.51 ± 0.63
49	0.00 ± 0.00
60	2.10 ± 0.03
62	0.55 ± 0.22
70	3.33 ± 0.25
Cmpd. I	6.42 ± 3.07
Caffeine	10.44 ± 1.88

[a]PAMPA assay (pre-coated PAMPA Plate System Gentest™, Corning, Tewksbury, MA, USA). Data is expressed as a mean of three replicates (n = 3) ± SD (10^{-6} cm/s).

Despite its low *Pe* value, compound **62** was selected for further evaluation due to its promising potency in the *in vitro* evaluation and cell-based assays. It demonstrates favourable ADME properties compared to compound **I**, including a sixfold increase in solubility (31 μg/mL vs. 5 μg/mL) and high stability in both chemical and metabolic assays. After 2 hours of incubation in phosphate buffer and 15 minutes with mouse liver microsomes, 100% of compound **62** remained intact mirroring the stability of the reference compound **I**.

3.4.2. Series II

Inhibitory activity against GSK-3β and IKK-β kinases

All compounds from **series II** exhibited inhibitory activity against GSK-3β owing to *N*-(pyridin-2-yl)cyclopropanecarboxamide scaffold tailored to the kinase hinge region, however with diversified IC_{50} values ranging from 24 nM to 10.49 μM (Table 11). A starting point for SAR analysis and further structural modifications was the derivative with an unsubstituted phenyl ring **80**, which moderately inhibited GSK-3β (IC_{50} = 623 nM), but not IKK-β. According to the Topliss Tree for aromatic substitution, the phenyl ring was decorated with a chlorine atom in the *para* position to the amide bond, leading to compound **81** with approximately 3-fold decreased potency (IC_{50} = 1.636 μM) compared to compound **80**. Subsequent SAR of the chlorine substitution pattern at the *ortho* and *meta* positions of the phenyl ring revealed the *ortho* compound **82** with the highest inhibitory activity (IC_{50} = 285 nM), and the *meta* **83** with IC_{50} = 956 nM. The identical tendency was observed for compounds bearing trifluoromethyl group (**84–86**), however, with decreased activity compared to the chlorine derivative, while for compounds with fluorine (**87–89**), the *ortho*-substituted compound **88** was less active than *meta*-analogue **89** (IC_{50} = 1.325 μM vs. IC_{50} = 373 nM respectively). The bis substitution with chloride atoms at the 3,4-position in **90** (IC_{50} = 2.135 μM) and 3,5- as in **91** (IC_{50} = 735 nM) did not improve the inhibitory potency, while replacement with 3,5-bis trifluoromethyl group led to the negligibly active compound **92** (IC_{50} = 10.490 μM). Following the Topliss Scheme, the chlorine at the *para* position was exchanged for a methyl ether and then for a methyl group. The compound bearing methyl ether, **93**, was found to be a weak GSK-3β inhibitor, with an IC_{50} of 2.405 μM, whereas the methyl derivative **94** exhibited activity of 927 nM. These promising results led to the synthesis of *ortho*-, and *meta*- methyl-substituted compounds **95** and **96**, which showed similar potencies to **94**, with minor deviations. The *para*-substituted nitro compound **97** and *ortho*-phenol **98** also displayed moderate activity, with a preference for the hydroxyl group at the *ortho* position, as evidenced by IC_{50} values of 873 nM for **97** and 324 nM for **98**. Finally, replacing the phenyl ring with heterocyclic scaffolds yielded the potent GSK-3β inhibitor **99**, an IC_{50} of 24 nM. Changing the thiophene to the HBD-bearing indole (**100**) or pyrrole (**101**) moieties led to decreased activities, with IC_{50} values of 309 nM and 889 nM, respectively.

None of the obtained amide derivatives displayed significant inhibitory activity against IKK-β kinase. Even compound **92**, with the 3,5-bis trifluoromethyl substituent, derived from the reference inhibitor **IMD-0354** (literature IC_{50} = 1 μM), inhibited only 21% of the enzyme in the screening concentration of 10 μM.

Table 11. Inhibitory activity of compounds **80–101** from **series II** against GSK-3β and IKK-β kinases.

Cmpd.	Ar	GSK-3β	IKK-β	Cmpd.	Ar	GSK-3β	IKK-β
		IC_{50} [μM][a] or % inh. at 10 μM[b]				IC_{50} [μM][a] or % inh. at 10 μM[b]	
	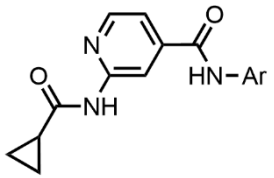						
80	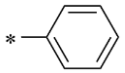	0.623 ± 0.027	<10%	**85**	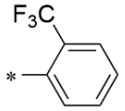	0.847 ± 0.042	21% ± 2%
81	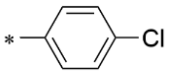	1.636 ± 0.134	17% ± 4%	**86**	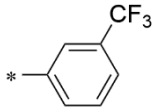	1.514 ± 0.111	<10%
82	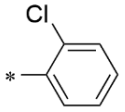	0.285 ± 0.012	11% ± 4%	**87**	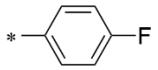	4.690 ±0.116	<10%
83	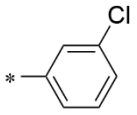	0.956 ± 0.061	<10%	**88**	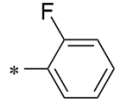	1.325 ± 0.013	<10%
84	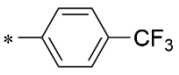	9.308 ± 0.655	<10%	**89**	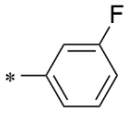	0.373 ± 0.022	<10%

90	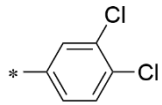	2.135 ± 0.151	<10%	**96**	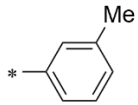	0.870 ±0.067	11% ± 4%
91	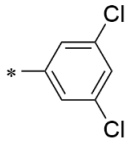	0.732 ± 0.048	<10%	**97**	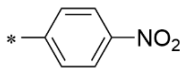	0.873 ± 0.027	<10%
92	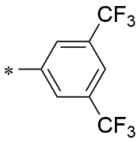	10.490 ± 0.653	21% ± 5%	**98**	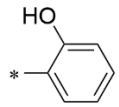	0.324 ± 0.005	18% ± 3%
93	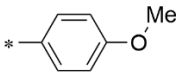	2.405 ± 0.150	17% ± 3%	**99**	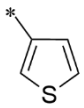	0.024 ± 0.001	<10%
94	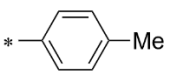	0.927 ± 0.075	<10%	**100**	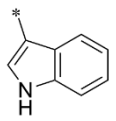	0.309 ± 0.004	19% ± 2%
95	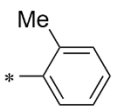	1.088 ±0.045	<10%	**101**	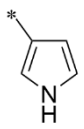	0.889 ± 0.025	21% ± 2%
Compound I		0.005 ± 0.000				22% ± 7%	
TPCA-1[c]		1.316 ± 0.076				0.037 ± 0.001	
Staurosporine[d]		0.080 ± 0.007				0.894 ± 0.042	

[a] Half maximal inhibitory concentration of the tested compound for GSK-3β kinase, mean value ± standard error of the mean (SEM) of triplicates; [b] mean value ± standard deviation (SD) of triplicates; [c] reference, Sigma-Aldrich Chemie GmbH, Steinheim, Germany; [d] reference, Biokom, Janki, Poland.

Cytotoxicity in HT-22 and BV-2 cells

All the compounds from the **series II** can be classified as safe concerning potential neuro- and immunotoxicity in the whole range of tested concentrations. None of the compounds affected cell viability at concentrations up to 100 μM in either the HT-22 or BV-2 lines. The lowest cell viability observed was 62% for compound **98** in HT-22 cells, and 64% for compound **92** in BV-2 cells, both at the highest concentration tested (100 μM).

Permeability

The potential of the most potent inhibitor, **IG100**, to cross biological membranes was evaluated using the PAMPA assay (Table 12). According to the measured permeability coefficient, **IG100** is classified as well permeable, similar to caffeine. This finding aligns with its calculated physicochemical properties, as **99** exhibits the highest CNS MPO score among all compounds in **series II**, with a score of 5.38.

Table 12. Results of permeability evaluation in the PAMPA assay for compound **99**.

Cmpd.	**PAMPA**
	***Pe* (10^{-6} cm/s)[a] ± SD**
99	10.10 ± 2.50
Caffeine	10.44 ± 1.88

[a]PAMPA assay (pre-coated PAMPA Plate System Gentest™, Corning, Tewksbury, MA, USA). Data is expressed as a mean of three replicates (n = 3) ± SD (10^{-6} cm/s).

3.4.3. Series III[11]

Inhibitory activity against GSK-3β and IKK-β kinases

All but one compound (**(*R*)-116**) bearing the 2,5-dihydro-1*H*-pyrrole moiety are active against GSK-3β, with IC_{50} values ranging from 141 nM to 11.27 μM (Table 13). The most potent inhibitors in this series are the urea derivative **112** (IC_{50} = 141 nM) and **111** containing the terminal amide group (IC_{50} = 599 nM). The replacement of the HBA amide carbonyl group or the introduction of additional HBD amine moiety discloses preliminary conclusions regarding SAR. Substitution of the amide with a sulfonamide significantly decreases inhibitory activity, as observed in the compounds **117**–**119**. Similarly, introducing an additional amine, either as a terminal group in the aliphatic chain (**113–114** and **120–121**) or within the 5-membered pyrrolidine ring (**115** and **(*S*)-116**), also reduces inhibition. Among these, compounds with a 2-carbon chain moiety show slightly better activity, such as **113** (IC_{50} = 1.36 μM) and **120** (IC_{50} = 1.374 μM). Removing the carbonyl oxygen, as in **(*R*)-116** and **(*S*)-116**, leads to a decrease (almost 19-fold compared to **111**) or even loss of activity against GSK-3β.

In **series III**, the cyclopentanesulfonamide derivative **119** emerges as a dual GSK-3β/IKK-β inhibitor, displaying balanced activity with IC_{50} values of 3.251 μM and 11.36 μM respectively. Additionally, the results indicate that small substituents like the cyclopentane ring are sterically well-tolerated by IKK-β.

Table 13. Inhibitory activity of compounds **111–121** from **series III** against GSK-3β and IKK-β kinases.

Cmpd.	**R**	**GSK-3β**	**IKK-β**
		IC_{50} [μM][a] or % inh. at 10 μM[b]	
	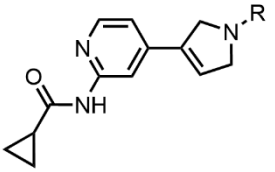		
111		0.599 ± 0.011	<10%

[11] The research on **series III** was described in Publication II: Góral, I.; Wichur, T.; Sługocka, E.; Grygier, P.; Głuch-Lutwin, M.; Mordyl, B.; Honkisz-Orzechowska, E.; Szałaj, N.; Godyń, J.; Panek, D.; Zaręba, P.; Sarka, A.; Żmudzki, P.; Latacz, G.; Pustelny, K.; Bucki, A.; Czarna, A.; Menezes, F.; Więckowska, A. Exploring Novel GSK-3β Inhibitors for Anti-Neuroinflammatory and Neuroprotective Effects: Synthesis, Crystallography, Computational Analysis, and Biological Evaluation. *ACS Chem Neurosci.* 2024, *15*, 3181–3201, doi:10.1021/acschemneuro.4c00365.

112		0.141 ± 0.005	<10%
113	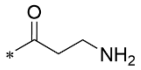	1.360 ± 0.110	<10%
114	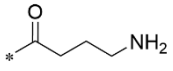	5.489 ± 0.363	<10%
115	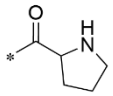	7.723 ± 0.543	<10%
(*R*)-116	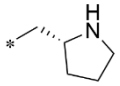	18% ± 2%	<10%
(*S*)-116	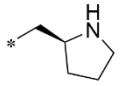	11.270 ± 1.120	<10%
117		6.202 ± 0.163	<10%
118	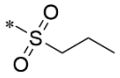	9.266 ± 0.467	10% ± 2%
119	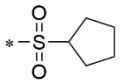	3.251 ± 0.083	11.360 ± 0.829
120	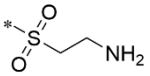	1.374 ± 0.044	22% ± 4%
121	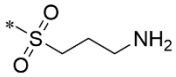	9.988 ± 0.406	11% ± 1%
Compound I		0.005 ± 0.000	22% ± 7%
TPCA-1[c]		1.316 ± 0.076	0.037 ± 0.001
Staurosporine[d]		0.080 ± 0.007	0.894 ± 0.042

[a] Half maximal inhibitory concentration of the tested compound for selected kinase, mean value ± standard error of the mean (SEM) of triplicates; [b] mean value ± standard deviation (SD) of triplicates; [c] reference, Sigma-Aldrich Chemie GmbH, Steinheim, Germany; [d] reference, Biokom, Janki, Poland.

Comparing the arrangement of compounds **112** and **119** within the GSK-3β pocket (Figure 26A and B) and conducting a Quantum Mechanical analysis of selected derivatives provided further insights into their binding pattern. The aminopyridine core is anchored in the hinge binding region through hydrogen bonds with crucial Val135, as previously demonstrated for compounds bearing *N*-(pyridin-2-yl)cyclopropanecarboxamide fragment [187]. Both compounds are additionally stabilized by hydrogen bond between Asp133 and the C(2) hydrogen atom of the pyridine ring. Replacement of the carbonyl oxygen in urea derivative with a sulfonyl moiety

did not disrupt its ability to form a hydrogen bond with the catalytic Lys85; however, it altered the interactions with the Cys199 side chain. In **112**, the 2,5-dihydro-1*H*-pyrrole moiety is stabilized by attractive dispersion forces, whereas in **119** a hydrogen bond is formed with the sulfonyl oxygen. The increased inhibitory activity of **112** is attributed to an additional hydrogen bond between its urea moiety and the side chain carbonyl of Glu97, which further strengthens the hydrogen bond with Lys85, compared to its *N*-acetyl- analogue **111**. The juxtaposition of the short-chain amide derivative **111** and the sulfonamide **117** highlighted the importance of nitrogen hybridization: the sp^3 hybridization of nitrogen in **117** affected the conformation of the 2,5-dihydro-1*H*-pyrrole, thereby disrupting the binding of the aminopyridine core to the hinge region – an effect not observed with the sp^2-hybridized nitrogen in the amide of **111**. Additionally, the increased activity of **120,** featuring ethylaminium chain, over **117** is attributed to a stabilizing hydrogen bond with Asn186 (not shown).

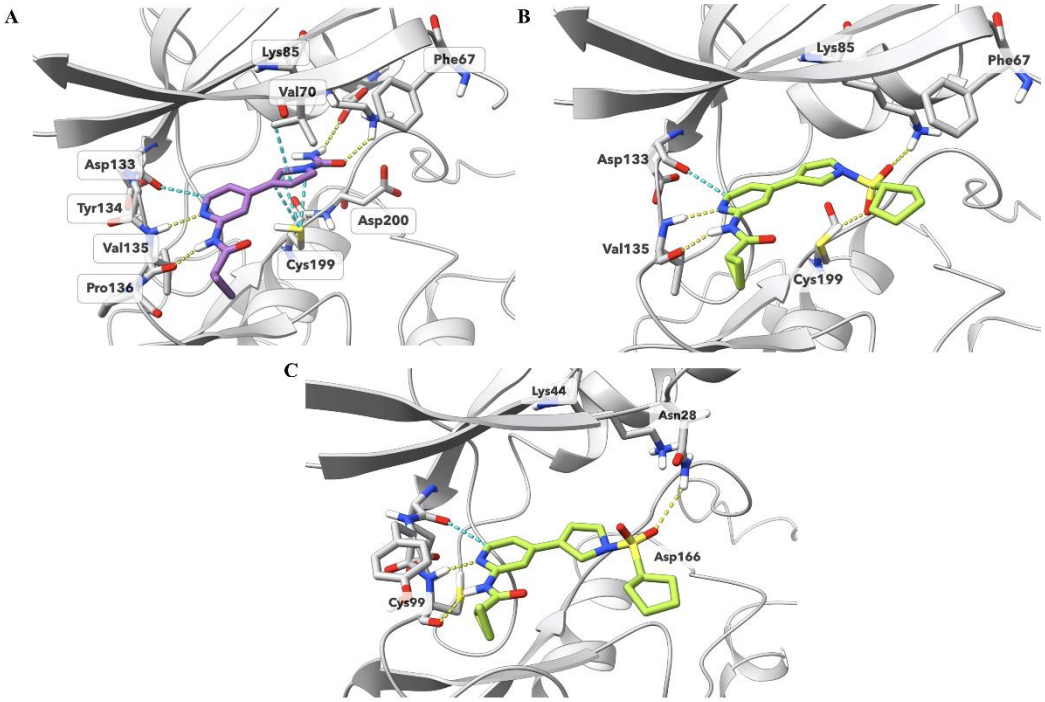

Figure 26. (**A**) Predicted binding mode of compound **112** with the refined crystal structure of GSK-3β (PDB ID: 8QJI), gscore function value −8.79. Hydrogen bonds are shown as yellow dashed lines. Favorable contacts (van der Waals overlap > -0.3 Å) are shown as cyan-colored dashed lines. Residues 58–65 are omitted for clarity. (**B**) Visualization of the docking pose of the **119**/GSK-3β complex of refined crystal structure (PDB ID: 4PTC), gscore function value −10.92. Residues 52–65 are omitted for clarity. (**C**) Visualization of the docking pose of the **119**/IKK-β complex of refined crystal structure (PDB ID: 4KIK), gscore function value −9.55. Residues 18–26 are hidden for clarity. Hydrogen bonds are shown as yellow dashed lines. Favorable contacts (van der Waals overlap > −0.3 Å) are shown as cyan-colored dashed lines.

All poses were generated using Glide (Schrodinger Suite, 2023) for both GSK-3β and IKK-β.

The binding of **119** within the ATP pocket of IKK-β revealed an analogous pattern of interactions in the hinge region, as observed for GSK-3β (Figure 26C). The *N*-(pyridin-2-yl)cyclopropanecarboxamide fragment forms bidentate hydrogen bonds with the nitrogen and carbonyl oxygen atoms of the Cys99 main chain, with the pyridine nitrogen serving as the hydrogen bond acceptor, while the amide nitrogen acts as the donor. The third harbouring motif is provided by the mainchain oxygen of Glu97, which forms an O−CH HB with the C(2) hydrogen atom of the pyridine ring. Furthermore, the compound interacts via sulfonyl oxygen, which serves as the HBA provided by Asn28. The relatively low inhibitory activity may be explained by the absence of the HB shared with the catalytic Lys44.

Cytotoxicity in HT-22 and BV-2 cells

The cytotoxicity was determined for two compounds – **112**, the most potent GSK-3β inhibitor, and **119**, endowed with dual activity against GSK-3β and IKK-β (Table 14). Neither **112** nor **119** significantly affected cell viability up to 50 μM for both HT-22 and BV-2 lines. The determined IC_{50} values exceeded the effective inhibitory concentrations for GSK-3β kinase, especially in the HT-22 cell line. However, a more pronounced cytotoxic effect was observed in the BV-2 cells, notably for compound **119**, with IC_{50} of 17.8 μM, which is near the effective concentration range for IKK-β inhibition.

Table 14. Cytotoxicity of **112** and **119** in HT-22 and BV-2 cells.

Compound	HT-22 cells	BV-2 cells
	IC_{50} [μM] $\bar{x}$ ± SEM	
112	45.8 ± 9.7	23.4 ± 1.7
119	63.5 ± 3.2	17.8 ± 1.0
Compound I	>100	15.4 ± 0.6
TPCA-1[a]	73.5 ± 1.5	11.2 ± 0.3
Staurosporine[b]	n.d.	0.001 ± 0.000

Data expressed as the means ± SEM; N ≥ 6; n.d. – not determined.

Evaluation of inhibitory activity toward okadaic acid-induced hyperphosphorylation and anti-inflammatory activity

Given the GSK-3β inhibitory activity of **112** and **119**, we examined their neuroprotective properties in the okadaic acid-induced neurodegeneration assay (Figure 27A). Only **112** significantly restored HT-22 cell viability, demonstrating this

effect at both 10 μM and 1 μM concentrations, comparable to the reference compound **I**. In contrast, **119** did not improve cell viability in the entire range of tested concentrations.

The anti-inflammatory effects of these inhibitors were subsequently evaluated by measuring the release of NO, IL-6 and TNF-α mediators from LPS-stimulated BV-2 cells (Figure 27B–D). At a concentration of 10 μM, both **112** and **119** significantly reduced NO levels, with **112** showing a more pronounced effect. Additionally, **112** decreased IL-6 release and TNF-α levels at 10 μM, though its efficacy was less than that of the reference compound **TPCA-1**.

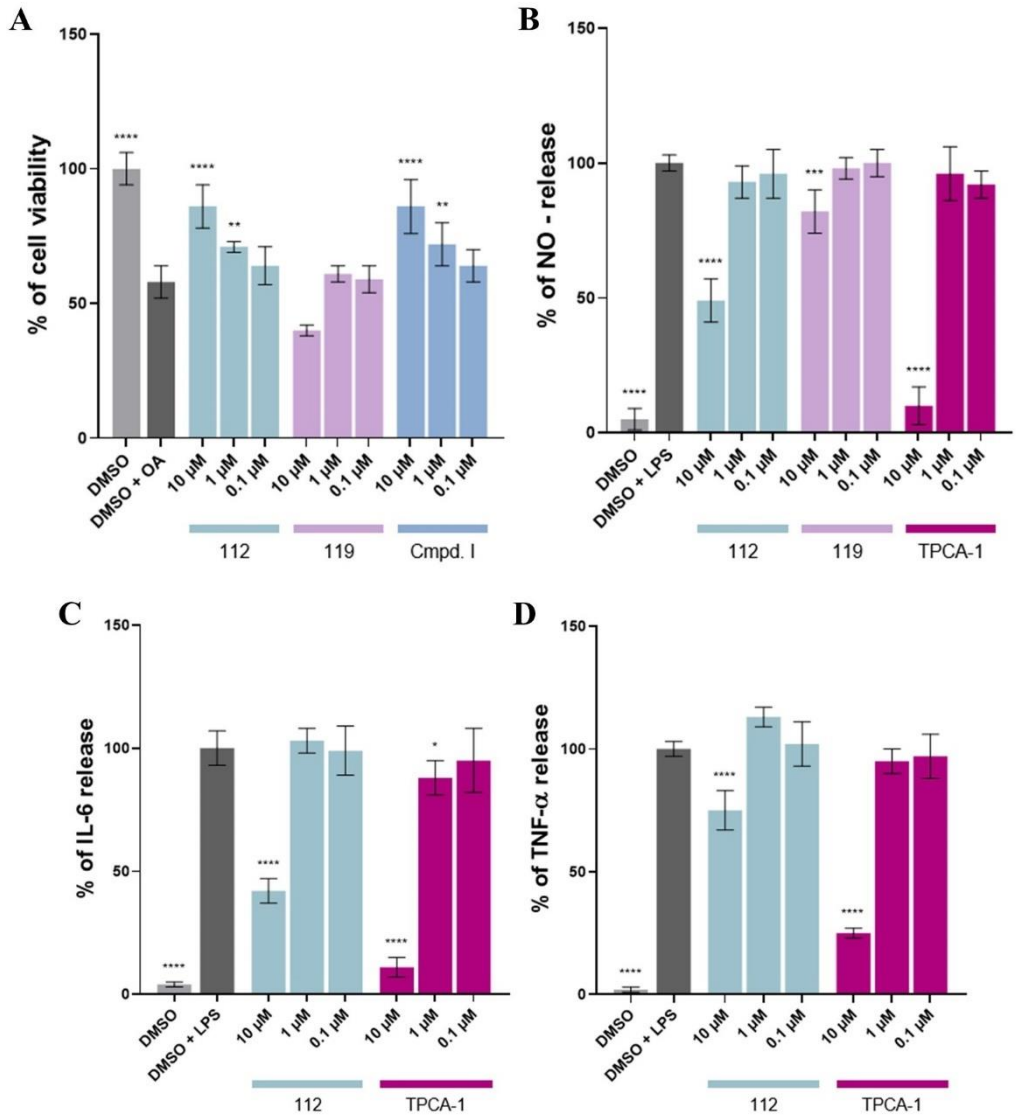

Figure 27. (**A**) Influence of compounds **112** and **119** on okadaic acid-induced hyperphosphorylation in HT-22 cell line (the cells were pre-treated with 400 nM of okadaic acid for 3 h). Viability was determined using Presto Blue™ cell viability

reagent after 24 h. (**B**) Influence of compounds **112** and **119** on % of NO-release in LPS-treated (100 ng/mL) BV-2 cell line. NO-release was measured using a fluorometric assay with 2,3-diaminonaphthalene (DAN). (**C**), (**D**) Influence of compound **112** on % of IL-6 and TNF- a release in LPS-treated (100 ng/mL) BV-2 cell line. The IL-6 and TNF-α levels were measured using LANCE Ultra TR-FRET Detection Kit (Perkin Elmer). Statistical analysis was performed using GraphPad Prism 9.0.0. All values are expressed as mean with SD. Differences among groups were evaluated by one-way ANOVA followed by post-hoc analysis (Dunnett's multiple comparison tests) *vs*. control group (LPS on BV-2 cells and okadaic acid on HT-22 cells) and were considered statistically significant if $p<0.05$ (*$p<0.05$, **$p<0.01$, ***$p<0.001$, ****$p<0.0001$).

Preliminary in vitro ADMET profiling

To assess the ADMET profile, compound **112** was evaluated for permeability in the PAMPA assay, metabolic stability in human liver microsomes (Table 15), and its impact on CYP450 isoform activity *in vitro* (Figure 28). According to the calculated permeability coefficient, **112** is classified as poorly permeable, suggesting limited potential for passive membrane penetration. This low permeability is likely due to the presence of a urea group, which, while enhancing inhibitory activity, significantly reduces the logP and logD values to 0.35, indicating a propensity to accumulate in aqueous environments. Additionally, the TPSA value of 88.32 $Å^2$ approaches the upper limit for compounds targeting CNS, which may further impact its CNS penetration. In contrast, compound **119** has improved physicochemical parameters (please refer to page 72), reflected in a nearly nine-fold higher permeability coefficient (Pe = 4.73 vs. 0.53 for **112**), however, this is accompanied by reduced inhibitory potency.

Incubation with HLM showed that compound **112** is resistant to biotransformation, as no metabolites were detected after 2 hours, compared to highly metabolised control, verapamil (only 27% remaining). Furthermore, **112** exerted a negligible influence on CYP450 isoenzymes, showing inhibitory effects on CYP2C9 and CYP3A4 only at the highest concentration tested (25 μM), and no effect on CYP2D6 activity.

To summarize, these findings support **112**'s favourable profile as a drug candidate, suggesting a low likelihood of rapid metabolism or drug-drug interactions. However, its poor permeability limits the probability of reaching the target site in the CNS, indicating that further optimization of its physicochemical properties is needed to enhance brain-blood barrier penetration.

Table 15. Results of PAMPA for **112** and **119** and metabolic stability of **112**.

Cmpd.	PAMPA	MLM Stability
	Pe **(10^{-6} cm/s)[a] ± SD**	**(%)[b] ± SD**
112	0.53 ± 0.82	100 ± 1
119	4.73 ± 0.26	n.d.
Cmpd. I	6.42 ± 3.07	100 ± 0
Caffeine	10.44 ± 1.88	n.d.

[a] PAMPA assay (pre-coated PAMPA Plate System Gentest™, Corning, Tewksbury, MA, USA). Data is expressed as a mean of three replicates (n = 3) ± SD (10^{-6} cm/s). [b] reference compound: verapamil (23.9%); n.d. – not determined.

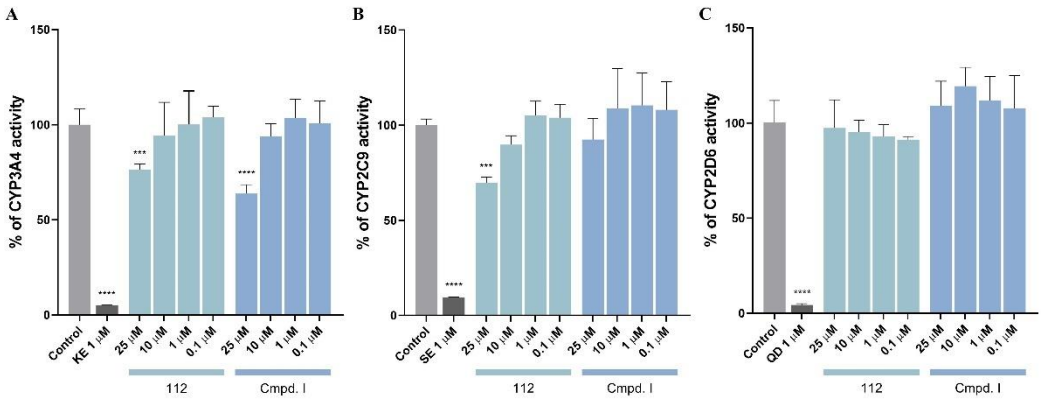

Figure 28. Influence of compound **112** and reference compound **I** on the activity of CYP isoenzymes in comparison to their specific substrates (**A**) CYP3A4 with ketoconazole (KE), (**B**) CYP2C9 with sulfaphenazole (SE) and (**C**) CYP2D6 with quinidine (QD). Statistical analysis was performed using GraphPad Prism 9.0.0. All values are expressed as mean with SD. Differences among groups were evaluated by one-way ANOVA followed by post-hoc analysis (Dunnett's multiple comparison tests) *vs*. control group and were considered statistically significant if $p<0.05$ (*$p<0.05$, **$p<0.01$, ***$p<0.001$, ****$p<0.0001$).

3.4.4. Series IV

Inhibitory activity against GSK-3β and IKK-β kinases

All compounds in **series IV** maintained inhibitory activity toward GSK-3β with similar or slightly reduced potency compared to the parent compound **V** (IC_{50} = 2.3 nM) (Table 16). Introducing a methyl substituent on the nitrogen atom in the amide group, thereby blocking hydrogen bond donation, preserved activity in the nanomolar range as observed for **126** (IC_{50} = 14 nM). Replacing the substituent with a hydroxyethyl, as in compound **133**, led to a slight drop in potency (IC_{50} = 42 nM), whereas the amine derivative **135** showed a 13-fold reduction in activity, with an IC_{50} of 527 nM. Extending the carbon linker by one methylene group further decreased activity to 700 nM, as showed for compound **136**.

In general, cyclic amide derivatives were more potent inhibitors than cyclic sulfonamides. The unsubstituted sulfonamide **149** displayed marginally weaker, yet nanomolar activity compared to compound **V** (IC_{50} = 17 nM vs. IC_{50} = 2.3 nM, respectively). In contrast, the substitution of the nitrogen atom with a methyl group, as in compound **150**, led to a more than 33-fold decrease in inhibitory potency (IC_{50} = 467 nM) compared to its methylated amide analogue **126**. Compound **151** with the hydroxyethyl group is a weaker inhibitor than **133**, with moderate potency (IC_{50} = 271 nM), while the propylamine derivative **152** exhibits slightly stronger GSK-3β inhibition (IC_{50} = 526 nM) compared to the **136**.

The inhibitory activity of compound **153** with a condensed tricyclic system was comparable to the IC_{50} of compound **150** (470 nM vs. 467 nM, respectively). Both compounds lack the HBD derived from the nitrogen of sulfonamide, which is reflected in a 15-fold decrease in the inhibitory potency compared to the compound **149**. This clearly indicates that hydrogen bond donation from the nitrogen of sulfonamide has a fundamental impact on activity, while the presence of the secondary hydroxyl group (as in compound **150**) is insufficient to compensate for reduced inhibitory potency. To summarize, diversification from amide to sulfonamide and the presence of a secondary hydroxyl group, as well as the introduction of different substituents attached to the nitrogen atom, did not lead to the optimization of the activity against GSK-3β.

Table 16. Inhibitory activity of compounds **126**, **133**, **135–136** from **series IVA** and compounds **149–153** from **series IVB** against GSK-3β and IKK-β kinases.

Cmpd.	R	GSK-3β	IKK-β	Cmpd.	R	GSK-3β	IKK-β
		IC_{50} [μM][a] or % inh. at 10 μM[b]				IC_{50} [μM][a] or % inh. at 10 μM[b]	
		SERIES IVA				SERIES IVB	
	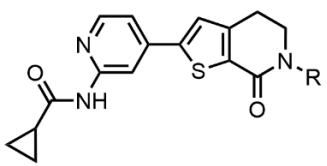				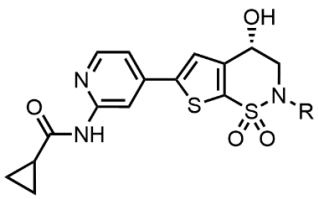		
Cmpd. V	H	0.002 ± 0.000	10.020 ± 1.350	**149**	H	0.017 ± 0.001	<10%
126	*–Me	0.014 ± 0.000	<10%	**150**	*–Me	0.467 ± 0.020	<10%
133	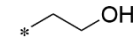	0.042 ± 0.001	<10%	**151**	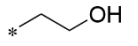	0.271 ± 0.008	<10%
135	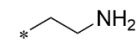	0.527 ± 0.031	<10%	**152**	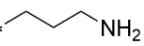	0.526 ± 0.024	<10%
136	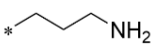	0.700 ± 0.023	<10%	**153**	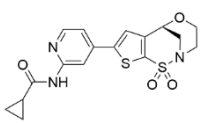	0.470 ± 0.014	14% ± 3%
Compound I		0.005 ± 0.000				22% ± 7%	
TPCA-1[c]		1.316 ± 0.076				0.037 ± 0.001	
Staurosporine[d]		0.080 ± 0.007				0.894 ± 0.042	

[a] Half maximal inhibitory concentration of the tested compound for selected kinase, mean value ± standard error of the mean (SEM) of triplicates; [b] mean value ± standard deviation (SD) of triplicates; [c] reference, Sigma-Aldrich Chemie GmbH, Steinheim, Germany; [d] reference, Biokom, Janki, Poland.

Cytotoxicity in HT-22 and BV-2 cells

For further *in vitro* evaluation, we selected the most potent inhibitor, **126**, and compared it to the parent compound **V**. Cytotoxicity assessment revealed that **126** has more favourable properties than compound **V** (Table 17). It did not significantly reduce HT-22 cell viability across the tested concentration range, and its IC_{50} of 22.7 μM in the BV-2 cells was over 1000-fold times higher than its effective kinase inhibitory concentration. On the contrary, compound **V** showed significant cytotoxicity in both cell lines, with IC_{50} values of 6.6 μM in HT-22 and 3.1 μM in BV-2 cells. Therefore, compound **126** emerged as a safer analogue with high inhibitory activity against GSK-3β.

Table 17. Cytotoxicity of compound **V** and **126** in HT-22 and BV-2 cells.

Compound	HT-22 cells	BV-2 cells
	IC_{50} [μM] $\bar{x}$ ± SEM	
Cmpd. V	6.6 ± 0.7	3.1 ± 0.1
126	> 100	22.7 ± 1.5
Compound I	>100	15.4 ± 0.6
TPCA-1[a]	73.5 ± 1.5	11.2 ± 0.3
Staurosporine[b]	n.d.	0.001 ± 0.000

Data expressed as the means ± SEM; N ≥ 6; n.d. – not determined.

Evaluation of inhibitory activity toward okadaic acid-induced hyperphosphorylation and anti-inflammatory activity

Subsequently, the neuroprotective potential of both compounds was evaluated using the okadaic acid-induced hyperphosphorylation assay in HT-22 cells (Figure 29A). Although **126** exhibits strong inhibitory activity against GSK-3β, it does not confer any neuroprotective benefits, as it fails to enhance cell viability under these conditions. In contrast, the parent compound **V** significantly increased cell viability at 10 μM and 1 μM concentrations. Notably, at 10 μM, compound **V** demonstrates a marked neuroprotective effect, surpassing that of the reference compound **I**.

In the subsequent anti-inflammatory evaluation, **126** demonstrated significant efficacy in reducing levels of key inflammatory mediators: NO, Il-6 and TNF-α, at a concentration of 10 μM (Figure 29B–D). Compound **V**, due to its high toxicity in BV-2 cells at 10 μM, was tested at lower concentrations (1 μM and 0.1 μM). Even at these reduced levels, compound **V** effectively decreased NO production (at 1 μM) and Il-6 (at both concentrations), with a performance that surpassed **126** in these metrics. While **126** also reduced TNF-α levels at 10 μM, its efficacy did not reach the statistical significance observed with the reference compound **TPCA-1**. These findings underscore

compound **V**'s potent anti-inflammatory effects at lower concentrations and suggest that, despite **126**'s broader inhibition profile, compound **V** may offer superior efficacy in specific inflammatory pathways when toxicity constraints are managed.

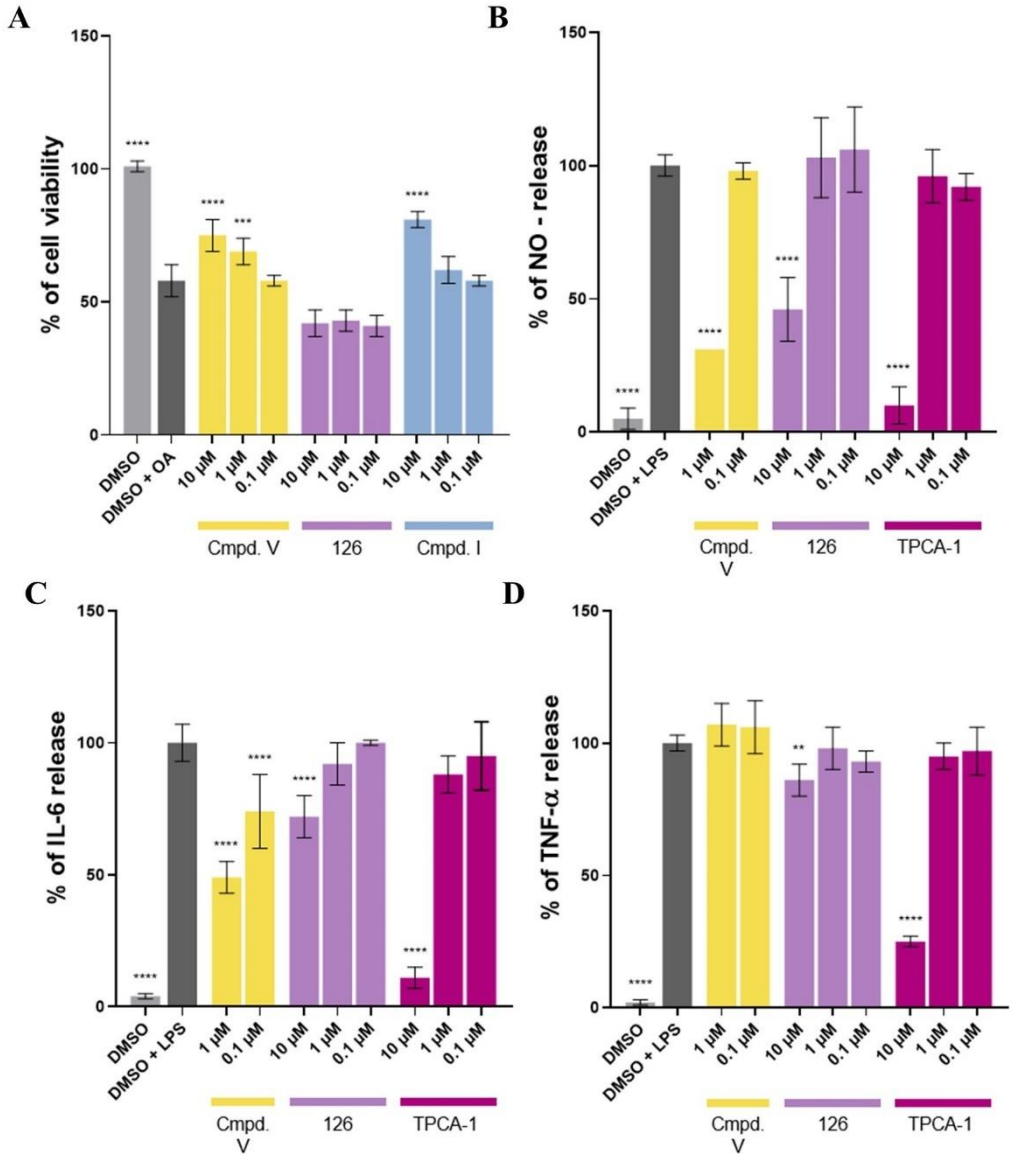

Figure 29. (**A**) Influence of compounds **V** and **126** on okadaic acid-induced hyperphosphorylation in HT-22 cell line (the cells were pre-treated with 400 nM of okadaic acid for 3 h). Viability was determined using Presto Blue™ cell viability reagent after 24 h. (**B**) Influence of compounds **V** and **126** on % of NO-release in LPS-treated (100 ng/mL) BV-2 cell line. NO-release was measured using a fluorometric assay with 2,3-diaminonaphthalene (DAN). (**C**), (**D**) Influence of compounds **V** and **126** on % of IL-6 and TNF-α release in LPS-treated (100 ng/mL) BV-2 cell line. The IL-6 and TNF-α levels were measured using LANCE Ultra TR-FRET

Detection Kit (Perkin Elmer). Statistical analysis was performed using GraphPad Prism 9.0.0. All values are expressed as mean with SD. Differences among groups were evaluated by one-way ANOVA followed by post-hoc analysis (Dunnett's multiple comparison tests) *vs*. control group (LPS on BV-2 cells and okadaic acid on HT-22 cells) and were considered statistically significant if $p<0.05$ (*$p<0.05$, **$p<0.01$, ***$p<0.001$, ****$p<0.0001$).

Permeability

Permeability was evaluated for the most potent inhibitors, including **126** from the cyclic amide series, **149** from the cyclic sulfonamide series, and the parent compound **V** (Table 18). Based on the calculated permeability coefficients, all compounds show a tendency to penetrate biological membranes, with **126** exhibiting the highest permeability potential, consistent with its favourable physicochemical parameters. In contrast, **149** displays the lowest permeability (*Pe*), which might result from a high total polar surface area (108.39 $Å^2$) and an increased number of hydrogen bond donors (3 vs. 1) and acceptors (5 vs. 3) relative to **126**.

Table X. Results of permeability evaluation in the PAMPA assay for compounds **V**, **126** and **149**.

Cmpd.	**PAMPA**
	***Pe* (10^{-6} cm/s)[a] ± SD**
Cmpd. V	4.74 ± 0.33
126	6.63 ± 0.34
149	4.38 ± 0.38
Caffeine	10.44 ± 1.88

[a]PAMPA assay (pre-coated PAMPA Plate System Gentest™, Corning, Tewksbury, MA, USA). Data is expressed as a mean of three replicates (n = 3) ± SD (10^{-6} cm/s).

4. Conclusions

This doctoral dissertation aimed to discover novel compounds with disease-modifying properties by targeting tau protein aggregation and neuroinflammation. The approach focused on the simultaneous inhibition of key regulatory enzymes – GSK-3β and IKK-β kinases – to address the underlying mechanisms of Alzheimer's disease. To achieve the stated objectives:

- Four series of novel compounds were designed and synthetic strategies were developed, resulting in a total of 64 final compounds.
- The structure and purity of each derivative were confirmed using LC-MS, ^{1}H NMR and ^{13}C NMR methods.
- The physicochemical parameters of the novel compounds were calculated using well-established computational methods and experimentally evaluated for selected compounds.
- The inhibitory activity of each compound against GSK-3β and IKK-β kinases was assessed *in vitro*, enabling structure-activity relationship analyses, which were additionally supported by the results of docking studies.
- The most promising candidates from each series underwent comprehensive *in vitro* evaluation, including toxicity assessment, determination of anti-inflammatory activity and neuroprotective properties, and preliminary ADME profiling.

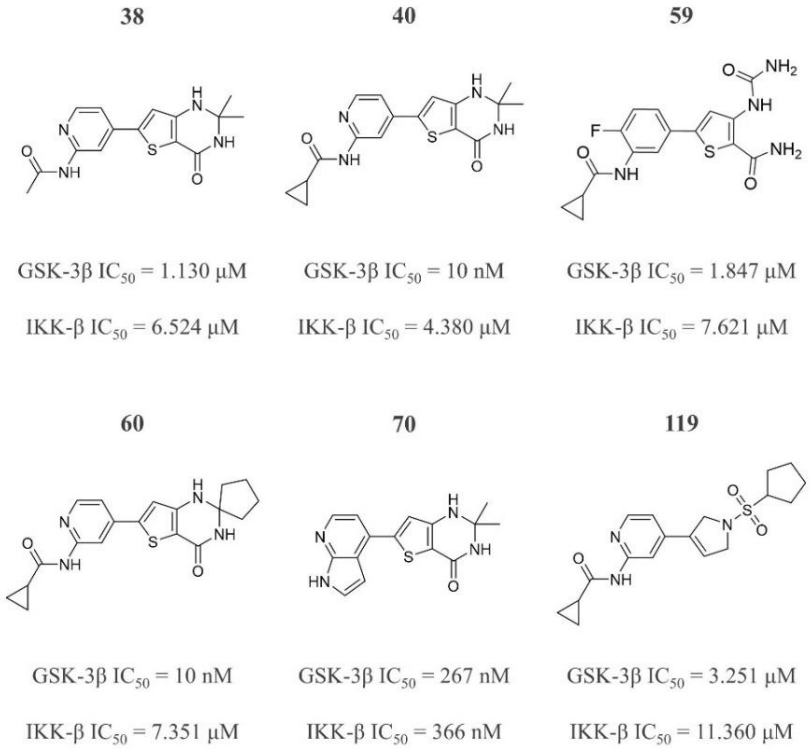

Figure 30. Dual GSK-3β/IKK-β inhibitors presented in the dissertation with their inhibitory activities.

The most significant achievement of this work is the identification and characterization of the biological properties of six compounds with dual GSK-3β and IKK-β inhibitory activity. They represent a significant milestone, as they are the first structures of their kind to exhibit the desired inhibitory activity (Figure 30):

- **38** (GSK-3β IC_{50} = 1.1 μM, IKK-β IC_{50} = 6.5 μM);
- **40** (GSK-3β IC_{50} = 10 nM, IKK-β IC_{50} = 4.4 μM);
- **59** (GSK-3β IC_{50} = 1.8 μM, IKK-β IC_{50} = 7.6 μM);
- **60** (GSK-3β IC_{50} = 10 nM, IKK-β IC_{50} = 7.3 μM);
- **70** (GSK-3β IC_{50} = 267 nM, IKK-β IC_{50} = 366 nM);
- **119** (GSK-3β IC_{50} = 3.2 μM, IKK-β IC_{50} = 11.4 μM).

Among them, the most promising compound that combines balanced activity with nanomolar inhibitory potency is **70**. In cell-based evaluation, **70** exhibited marked neuroprotective properties in the okadaic acid-induced hyperphosphorylation assay across all tested concentrations (from 0.1 μM to 10 μM). However, the compound decreased cell viability with IC_{50} values of 6.1 μM and 3.5 μM for HT-22 and BV-2 cell lines, respectively leaving quite a narrow safety window. Consequently, the anti-inflammatory effect in BV-2 cells was tested at concentrations up to 1 μM, in which **70** did not inhibit the release of NO and IL-6 mediators but effectively reduced TNF-α levels. In *in sillico* evaluation of physicochemical properties **70** was rated with favourable properties and the CNS MPO score of 4.97. This aligns well with the *Pe* = 3.33 ($\cdot 10^{-6}$ cm/s) obtained from *in vitro* PAMPA assay, suggesting that the compound will be absorbed via passive diffusion from the gastrointestinal tract and is likely to reach the CNS *in vivo*. Compounds **40** and **60** also deserve special attention as dual inhibitors. **40** and **60** are potent, nanomolar inhibitors of the GSK-3β enzyme with weaker inhibitory activity against IKK-β. Both compounds are endowed with neuroprotective properties at their safe concentrations. Compound **40** enhanced HT-22 cells' viability at 10 μM, whereas **60** was effective at 1 μM. Interestingly, in terms of anti-inflammatory properties, compound **60** is active in reducing both NO (at 1 μM and 0.1 μM) and IL-6 (at 1 μM) levels, compared to compound **40**, which decreased only NO release (at 1 μM), despite having lower inhibitory potency against IKK-β. The other compounds exhibiting dual activity – **38**, **59**, and **119** are moderate micromolar inhibitors; nevertheless, their inhibitory potency is more balanced concerning both kinases, which is more desirable to enhance therapeutic efficacy and minimize off-target effects when modulating multiple biochemical pathways.

In addition to the primary aim of this thesis, we identified potent, selective GSK-3β inhibitors among each series (Figure 31):

- **62** (IC_{50} = 8 nM);
- **99** (IC_{50} = 24 nM);
- **112** (IC_{50} = 141 nM);
- **126** (IC_{50} = 14 nM).

The most potent and simultaneously displaying favorable *in vitro* profile is compound **62**. Compound **62** confirmed its ATP-competitive nature in the kinetic studies with the determined inhibition constant, K_i = 2 nM, adjacent to IC_{50} = 8 nM. It is a safer structural analogue of compound **60**, with an IC_{50} of 58.3 μM in HT-22 and 54.8 μM BV-2 cells, resulting in a safety window of 5830 and 5480. Moreover, compound **62** exhibited anti-inflammatory properties by reducing NO (at both 10 μM and 1 μM concentrations) and IL-6 (at 10 μM) levels in an LPS-stimulated BV-2 cell line, while also displaying neuroprotective effects by significantly rescuing HT-22 cells' viability at 10 μM. Further comprehensive studies demonstrated that compound **62** is highly selective among other kinases from the CMGC family, with the exception of DYRK kinases, which might be beneficial given their role in modulating tau protein phosphorylation and Aβ formation. Additionally, it was not susceptible to metabolic transformations in both chemical and metabolic stability assays and displayed reasonable solubility. However, the compound exhibited negligible permeability which may limit its activity and negatively impact the development. Nevertheless, compound **62** along with **99**, **112** and **126** represent novel chemotype of GSK-3β inhibitors and expanding knowledge regarding kinase modulation.

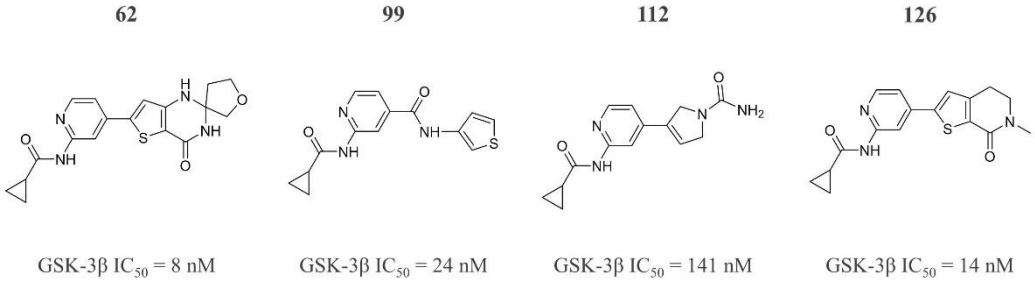

Figure 31. GSK-3β inhibitors described in the dissertation with their inhibitory activity.

In summary, this thesis offers the first insights into the simultaneous inhibition of GSK-3β and IKK-β kinases. Ligands capable of inhibiting both enzymes simultaneously may represent a novel and innovative approach in the development of disease-modifying therapies for Alzheimer's disease.

5. Experimental

5.1. General chemistry information

All reagents were purchased from commercial suppliers and were used without further purification. Tetrahydrofuran (THF) and dichloromethane (DCM) were distilled under argon immediately before use. The drying agent used for THF was sodium/benzophenone ketyl and for DCM, calcium hydride. Reactions were monitored by thin-layer chromatography (TLC) carried out on aluminium sheets precoated with silica gel 60 F254 (Merck) and by high-performance liquid chromatography (HPLC). Compounds were visualized with UV light and by suitable visualization reagents (solution of ninhydrin). HPLC analyses were performed on Waters Alliance e2695 separations module (Waters, Milford, CT, USA), containing 2998 photodiode array (PDA), a detector (Waters, Milford, CT, USA), and a SpeedROD RP-18e 50–4.6 mm column (Merck, KGaA, Darmstadt, Germany). The temperature of the column was preserved at 30 °C. A gradient elution program was conducted by applying a flow rate of 5 mL/min, eluent A (water/0.1% HCOOH), eluent B (MeCN/0.1% HCOOH), and a gradient starting from 0% of B to 100% of B for 3 min. The following solvents were used in TLC and column chromatography: DCM, methanol (MeOH), ethyl acetate (EtOAc), petroleum ether (PE), 25% aqueous ammonia solution ($NH_{3(aq)}$), acetonitrile (MeCN). Compounds were purified with flash chromatography on Isolera™ Spectra (Biotage) with silica gel 60 (63–200 μm; Merck) as a stationary phase or with the reverse-phase HPLC performed on LC-4000 Jasco using a Phenomenex Luna C8 (5 μm, 15 × 21.2 mm) column and water/acetonitrile gradient with 0.1% solution of formic acid (v/v) as a mobile phase. The UPLC-MS analyses were done on the UPLC-MS/MS system comprising Waters ACQUITY UPLC (Waters Corporation, Milford, MA, USA) coupled with Waters TQD mass spectrometer (electrospray ionization mode ESI with tandem quadrupole). Chromatographic separations were carried out using the ACQUITY UPLC BEH (bridged ethyl hybrid) C18 column: 2.1 × 100 mm and 1.7 μm particle size. The column was maintained at 40 °C and eluted under gradient conditions using 95%–0% of eluent A over 10 min, at a flow rate of 0.3 mL/min. Eluent A: 0.1% solution of formic acid in water (v/v); eluent B: 0.1% solution of formic acid in acetonitrile (v/v). A total of 10 μL of each sample was injected and chromatograms were recorded using a Waters eλ PDA detector. The spectra were analysed in the range of 200–700 nm with 1.2 nm resolution and at a sampling rate of 20 points/s. The UPLC/MS purity of all the test compounds was determined to be ≥ 95% and is given for each compound in the following description. ^{1}H NMR and ^{13}C NMR spectra were recorded on Varian Mercury 300 MHz (Varian, Inc., Palo Alto, CA) or Jeol 500 MHz (Jeol Inc., Peabody, MA). The chemical shifts are reported in ppm and were referenced to the residual solvent signals (CHLOROFORM-*d* ^{1}H: 7.26 ppm, ^{13}C: 77.06 ppm; METHANOL-d_4 ^{1}H: 3.31 ppm, ^{13}C: 49.03 ppm; ACETONE-d_6 ^{1}H: 2.05 ppm, ^{13}C: 29.82 ppm, 206.03 ppm; DMSO-d_6 ^{1}H: 2.50 ppm, ^{13}C: 39.52 ppm), coupling constants are reported in hertz (Hz).

Previously reported compounds:

N-(5-Bromopyridin-2-yl)cyclopropanecarboxamide (**63**) [188], *N*-(5-(4,4,5,5-tetramethyl-1,3,2-dioxaborolan-2-yl)pyridin-2-yl)cyclopropanecarboxamide (**64**) [189], *tert*-butyl 4-bromo-1*H*-pyrrolo[2,3-*b*]pyridine-1-carboxylate (**66**), *tert*-butyl 4-(4,4,5,5-tetramethyl-1,3,2-dioxaborolan-2-yl)-1*H*-pyrrolo[2,3-*b*]pyridine-1-carboxylate (**67**) [190], methyl 2-(cyclopropanecarboxamido)isonicotinate (**73**), 2-(cyclopropanecarboxamido)isonicotinic acid (**74**) [191], 3-aminopyrrole (**75**) [192], *tert*-butyl (1*H*-indol-3-yl)carbamate (**76**) [193], 1*H*-indol-3-amine (**77**) [194], *tert*-butyl thiophen-3-ylcarbamate (**78**) [195], 3-aminothiophene (**79**) [196], *tert*-butyl (2-(thiophen-3-yl)ethyl)carbamate (**122**), 5,6-dihydrothieno[2,3-*c*]pyridin-7(4*H*)-one (**123**) [197], 2-bromo-5,6-dihydrothieno[2,3-*c*]pyridin-7(4*H*)-one (**124**) [198], 2-bromo-6-methyl-5,6-dihydrothieno[2,3-*c*]pyridin-7(4*H*)-one (**125**), 2-bromo-6-(2-hydroxyethyl)-5,6-dihydrothieno[2,3-*c*]pyridin-7(4*H*)-one (**130**) [199], 1-(2,5-dibromothiophen-3-yl)ethan-1-one (**137**) [200], 5-bromo-3-(2-bromoacetyl)thiophene-2-sulfonamide (**140**) [201].

5.1.1. General procedure for the synthesis of compounds 63 and 73 (GP1)

An appropriate aromatic amine (1.0 equiv.) was dissolved in DCM, the solution was cooled to 0 °C on an ice bath, and then pyridine (2.0 equiv.) and cyclopropanecarbonyl chloride (1.15 equiv.) were added dropwise. The reaction mixture was then warmed up to room temperature and stirred overnight. After that time, the mixture was extracted with DCM, and the combined organic layer was dried over anhydrous Na_2SO_4, filtered and concentrated under a vacuum. The product did not require further purification.

_N_-(5-Bromopyridin-2-yl)cyclopropanecarboxamide (63)

Following **GP1**, compound **63** was prepared using 2-amino-5-bromopyridine (0.600 g, 3.47 mmol), pyridine (0.559 mL, 6.94 mmol), cyclopropanecarbonyl chloride (0.362 mL, 3.99 mmol) in 12 mL DCM. Yield: 0.670 g (80%). ^{1}H NMR (500 MHz, CHLOROFORM-*d*) δ ppm 0.83 - 0.95 (m, 2H), 1.02 - 1.15 (m, 2H), 1.43 - 1.61 (m, 1H), 7.77 (dd, *J*=8.9, 2.3 Hz, 1H), 8.13 (d, *J*=8.9 Hz, 1H), 8.29 (d, *J*=2.3 Hz, 1H), 8.37 (br s, 1H). Formula: $C_9H_9BrN_2O$.

Methyl 2-(cyclopropanecarboxamido)isonicotinate (73)

Following **GP1**, compound **73** was prepared using methyl 2-aminopyridine-4-carboxylate (1.500 g, 9.86 mmol), pyridine (1.589 mL, 19.72 mmol), cyclopropanecarbonyl chloride (1.029 mL, 11.34 mmol) in 32 mL DCM. Yield: 2.150 g (99%). ^{1}H NMR (500 MHz, ACETONE-d_6) δ ppm 0.81 - 0.86 (m, 3H), 0.91 - 0.95 (m, 2H), 3.90 (s, 3H), 7.50 (dd, *J*=5.0, 1.6 Hz, 1H), 8.40 (dd, *J*=5.2, 0.9 Hz, 1H), 8.73 - 8.75 (m, 1H), 9.95 (br s, 1H). Formula: $C_{11}H_{12}N_2O_3$.

5.1.2. Synthesis of *N*-(5-(4,4,5,5-tetramethyl-1,3,2-dioxaborolan-2-yl)pyridin-2-yl)cyclopropanecarboxamide (64)

The stirred solution of bis(pinacolato)diboron (0.536 g, 2.11 mmol, 1.2 equiv.) in half of the anhydrous DMF (5 mL) was cooled to 0 °C, then potassium acetate (0.518 g, 5.28 mmol, 3.0 equiv.) and Pd(dppf)Cl_2 (39 mg, 0.053 mmol, 0.03 equiv.) were added under Ar. The reaction mixture was heated to 80 °C and a solution of **63** (0.425 g, 1.76 mmol, 1.0 equiv.) in 5 mL DMF was added dropwise. The mixture was heated to 80 °C overnight. After that time, the reaction mixture was cooled to rt, diluted with DCM, filtered through Celite and evaporated under reduced pressure. The residue was dissolved in 15 mL EtOAc, and activated charcoal (5.000 g) was added and stirred under reflux for 1 h. The mixture was then filtered again through Celite and evaporated under reduced pressure. Hexane was added to the residue and filtered. Filtrate was collected and evaporated. Then PE was added to the residue, filtered again, filtrate was collected and evaporated as desired product. Yield: 0.438 g (86%). ^{1}H NMR (500 MHz, CHLOROFORM-*d*) δ ppm 0.97 (br d, *J*=4.3 Hz, 2H), 1.13 (br s, 2H), 1.33 (s, 12H), 1.82 (br s, 1H), 8.17 - 8.26 (m, 1H), 8.37 (br d, *J*=6.0 Hz, 1H), 8.49 (s, 1H), 10.48 (br s, 1H). Formula: $C_{15}H_{21}BN_2O_3$.

5.1.3. Synthesis of *N*-(5-(2,2-dimethyl-4-oxo-1,2,3,4-tetrahydrothieno[3,2-*d*]pyrimidin-6-yl)pyridin-2-yl)-cyclopropanecarboxamide (65)

64 (61 mg, 0.21 mmol, 1.1 equiv.) and **6** (50 mg, 0.19 mmol, 1.0 equiv.) were dissolved in 2 mL of dioxane. Then 1 mL of 2 M Na_2CO_3 solution and Pd(PPh_3)$_4$ (22 mg, 0.02 mmol, 0.1 equiv.) were added. The reaction was stirred under reflux for 3 h. After that time, the reaction mixture was diluted with DCM and filtered. The solid product was washed with MeOH. Yield: 24 mg (37%), yellow solid. Formula: $C_{17}H_{18}N_4O_2S$. MW: 342.42, MS *m/z* 343 ($M+H^+$). Purity 100% (UPLC/MS). ^{1}H NMR (500 MHz, DMSO-d_6) δ ppm 0.81 - 0.85 (m, 4H), 1.41 (s, 6H), 1.99 - 2.06 (m, 1H), 6.92 (s, 1H), 7.09 (s, 1H), 7.52 (s, 1H), 8.03 (dd, *J*=8.9, 2.3 Hz, 1H), 8.13 (d, *J*=8.6 Hz, 1H), 8.61 (d, *J*=2.0 Hz, 1H), 10.98 (s, 1H). ^{13}C NMR (126 MHz, DMSO-d_6) δ ppm 7.87 (2C), 14.27, 28.15 (2C), 68.99, 104.05, 113.21, 113.97, 124.69, 135.20, 144.73, 144.76, 151.94, 152.09, 160.92, 172.77.

5.1.4. Synthesis of t*ert*-butyl 4-bromo-1*H*-pyrrolo[2,3-*b*]pyridine-1-carboxylate (66)

To a stirred solution of 4-bromo-7-azaindole (0.500 g, 2.54 mmol, 1.0 equiv.) in 10 mL anhydrous DCM DMAP (31 mg, 0.25 mmol, 0.1 equiv.) and TEA (1.062 mL, 7.62 mmol, 3.0 equiv.) were added at rt. Then the mixture was cooled to 0 °C on an ice bath and under Ar di-*tert*-butyl dicarbonate (0.666 g, 3.05 mmol, 1.2 equiv.) was added in portions over 20 minutes. The reaction mixture was warmed up to room temperature and stirred for 2 hours. After that time, the mixture was extracted with DCM, and the combined organic layer was dried over anhydrous Na_2SO_4, filtered, and concentrated under a vacuum. The product did not require further purification. Yield: 0.715 g (95%). ^{1}H

NMR (500 MHz, CHLOROFORM-*d*) δ ppm 1.65 (s, 9H), 6.55 (d, *J*=4.0 Hz, 1H), 7.36 (d, *J*=5.2 Hz, 1H), 7.67 (d, *J*=4.0 Hz, 1H), 8.29 (d, *J*=5.2 Hz, 1H). Formula: $C_{12}H_{13}BrN_2O_2$.

5.1.5. General procedure for the synthesis of compounds 67 and 71 (GP2)

An appropriate aryl bromide (1.0 equiv.) and bis(pinacolato)diboron (1.02–2.0 equiv.) were dissolved in anhydrous dioxane. Then potassium acetate (2.1–3.0 equiv.) was added and under Ar Pd(dppf)Cl2 (0.05 equiv.).Tthe reaction was stirred under reflux overnight. After that time, the reaction mixture was cooled to room temperature, diluted with DCM, filtered through Celite, and evaporated under reduced pressure. The crude product was purified by different methods described below.

***Tert*-butyl 4-(4,4,5,5-tetramethyl-1,3,2-dioxaborolan-2-yl)-1*H*-pyrrolo[2,3-*b*]pyridine-1-carboxylate (67)**

Following **GP2**, compound **67** was prepared using **66** (0.755 g, 2.54 mmol), bis(pinacolato)diboron (0.658 g, 2.59 mmol), potassium acetate (0.748 g, 7.62 mmol), Pd(dppf)Cl_2 (95 mg, 0.13 mmol) in 8 mL anhydrous dioxane. Purification: flash chromatography (PE/EtOAc 7:3 then 55:45). Yield: 0.761 g (87%). ^{1}H NMR (500 MHz, CHLOROFORM-*d*) δ ppm 1.24 (s, 12H), 1.39 (s, 9H), 6.93 (d, *J*=4.0 Hz, 1H), 7.55 (d, *J*=4.9 Hz, 1H), 7.65 (d, *J*=4.0 Hz, 1H), 8.51 (d, *J*=4.9 Hz, 1H). Formula: $C_{18}H_{25}BN_2O_4$.

2,2-Dimethyl-6-(4,4,5,5-tetramethyl-1,3,2-dioxaborolan-2-yl)-2,3-dihydrothieno[3,2-*d*]pyrimidin-4(1*H*)-one (71)

Following **GP2**, compound **71** was prepared using **6** (0.100 g, 0.38 mmol), bis(pinacolato)diboron (0.193 g, 0.76 mmol), potassium acetate (79 mg, 0.80 mmol), Pd(dppf)Cl_2 (15 mg, 0.02 mmol) in 2.5 mL anhydrous dioxane. Purification: first, the crude product was dissolved in EtOAc, activated charcoal (0.500 g) was added and the mixture was stirred under reflux for 1 h. The mixture was then filtered through Celite and evaporated under reduced pressure. The solid residue was washed with PE twice. Yield: 98 mg (83%). ^{1}H NMR (500 MHz, DMSO-d_6) δ ppm 1.28 (s, 12H), 1.38 (s, 6H), 6.87 (s, 1H), 6.93 (br s, 1H), 7.64 (br s, 1H). Formula: $C_{14}H_{21}BN_2O_3S$.

5.1.6. General procedure for the synthesis of compounds 68 and 72 (GP3)

The reaction vessel was filled with an appropriate aryl halide (1.0 equiv.), pinacol ester of boronic acid (1.5 equiv.), K_3PO_4 (2.0 equiv.), XPhos (0.06 equiv.) and palladium precatalyst (0.06 equiv.). The vessel was evacuated and backfilled with argon, then anhydrous dioxane and H_2O in 5:1 ratio were added via syringe. The reaction was stirred at 60 °C for 3 hours. After that time, the reaction mixture was cooled to room temperature, diluted with DCM, filtered through Celite, and evaporated under reduced pressure. The crude product was purified by different methods described below.

***Tert*-butyl 4-(4-((*tert*-butoxycarbonyl)amino)-5-carbamoylthiophen-2-yl)-1*H*-pyrrolo[2,3-*b*]pyridine-1-carboxylate (68)**

Following **GP3**, compound **68** was prepared using **3** (60 mg, 0.19 mmol), **67** (0.100 g, 0.29 mmol), K_3PO_4 (81 mg, 0.38 mmol), XPhos (5 mg, 0.0011 mmol) and XPhos Pd G2 (9 mg, 0.0011 mmol) in the mixture of 2 mL anhydrous dioxane and 0.4 mL H_2O. Purification: flash chromatography (0–3% MeOH gradient in DCM). Yield: 73 mg (85%). ^{1}H NMR (500 MHz, DMSO-d_6) δ ppm 1.50 (s, 9H), 1.63 (s, 9H), 6.98 (d, *J*=4.2 Hz, 1H), 7.54 (d, *J*=5.0 Hz, 1H), 7.77 (br s, 2H), 8.00 (d, *J*=4.2 Hz, 1H), 8.31 (br s, 1H), 8.46 (d, *J*=5.0 Hz, 1H), 10.45 (s, 1H). Formula: $C_{22}H_{26}N_4O_5S$.

6-(Furo[2,3-*d*]pyrimidin-4-yl)-2,2-dimethyl-2,3-dihydrothieno[3,2-*d*]pyrimidin-4(1*H*)-one (72)

Following **GP3**, compound **72** was prepared using 4-chlorofuro[3,2-*d*]pyrimidine (22 mg, 0.14 mmol), **71** (65 mg, 0.21 mmol), K_3PO_4 (59 mg, 0.28 mmol), XPhos (4 mg, 0.0084 mmol) and Pd_2dba_3 (8 mg, 0.0084 mmol) in the mixture of 1.5 mL anhydrous dioxane and 0.3 mL H_2O. Purification: preparative HPLC (5–50% MeCN gradient). Yield: 13 mg (30%), yellow solid. Formula: $C_{14}H_{12}N_4O_2S$. MW: 300.34, MS *m/z* 301 ($M+H^+$). Purity 100% (UPLC/MS). ^{1}H NMR (500 MHz, DMSO-d_6) δ ppm 1.45 (s, 6H), 7.04 (s, 1H), 7.45 (d, *J*=2.6 Hz, 1H), 7.51 (s, 1H), 7.81 (s, 1H), 8.36 (d, *J*=2.5 Hz, 1H), 8.93 (s, 1H). ^{13}C NMR (126 MHz, DMSO-d_6) δ ppm 28.30 (2C), 69.25, 104.95, 109.45, 112.14, 119.76, 144.49, 147.43, 151.61, 151.63, 153.08, 160.73, 167.37.

5.1.7. Synthesis of 3-amino-5-(1*H*-pyrrolo[2,3-*b*]pyridin-4-yl)thiophene-2-carboxamide (69)

To a solution of **68** (70 mg, 0.15 mmol) in 2.5 mL DCM TFA (1 mL) was added and the mixture was stirred at room temperature for 1 h. When all starting material was consumed, the pH was adjusted to 8 by the addition of 25% ammonia solution and extracted to EtOAc. The combined organic layer was dried over anhydrous Na_2SO_4, filtered, and concentrated under a vacuum. The product did not require further purification. Yield: 39 mg (100%). ^{1}H NMR (500 MHz, DMSO-d_6) δ ppm 6.50 (br s, 2H), 6.80 (dd, *J*=3.6, 1.9 Hz, 1H), 7.03 (br s, 2H), 7.24 (s, 1H), 7.25 (s, 1H), 7.63 (dd, *J*=3.4, 2.7 Hz, 1H), 8.25 (d, *J*=5.0 Hz, 1H), 11.93 (br s, 1H). Formula: $C_{12}H_{10}N_4OS$.

5.1.8. Synthesis of 2,2-dimethyl-6-(1*H*-pyrrolo[2,3-*b*]pyridin-4-yl)-2,3-dihydrothieno[3,2-*d*]pyrimidin-4(1*H*)-one (70)

To a stirred solution of **69** (39 mg, 0.15 mmol, 1.0 equiv.) in 1 mL acetone, CH_3COOH (0.5 mL) and *p*-TSA (3 mg) were added, then the mixture was heated to 80 °C overnight. After that time, the reaction mixture was cooled to rt, solvents were evaporated under reduced pressure, saturated aqueous $NaHCO_3$ solution was added, and residue was extracted with EtOAc. The combined organic layer was dried over anhydrous Na_2SO_4, filtered, and concentrated under a vacuum. The solid residue was washed with MeCN twice. Yield: 12 mg (27%), yellow solid. Formula: $C_{15}H_{14}N_4OS$. MW: 298.36, MS *m/z* 299 ($M+H^+$). Purity 97% (UPLC/MS). ^{1}H NMR (500 MHz, DMSO-d_6) δ ppm 1.44 (s, 6H), 6.75 (dd, *J*=3.4, 1.7 Hz, 1H), 7.10 (s, 1H), 7.15 (s, 1H), 7.31 (d, *J*=5.0 Hz, 1H), 7.63 (t, *J*=2.6 Hz, 2H), 8.25 (d, *J*=5.0 Hz, 1H), 11.95 (br s, 1H). ^{13}C NMR (126 MHz,

DMSO-d_6) δ ppm 28.28 (2C), 69.08, 99.16, 105.72, 112.74, 115.60, 116.65, 127.60, 132.09, 142.79, 145.56, 149.50, 151.58, 160.91.

5.1.9. Synthesis of 2-(cyclopropanecarboxamido)isonicotinic acid (74)

To a stirred solution of **73** (1.125 g, 9.65 mmol, 1.0 equiv.) in 45 mL MeOH K_2CO_3 (2.67 g, 19.30 mmol, 2.0 equiv.) was added and the mixture was heated under reflux overnight. Then reaction mixture was cooled to room temperature and concentrated under vacuum to remove MeOH. The residue was diluted with water, then pH was adjusted to 2–3 by the addition of an aqueous 6 M HCl solution. Then the precipitated product was collected by filtration. Yield: 1.070 g (54%). ^{1}H NMR (500 MHz, DMSO-d_6) δ ppm 0.77 - 0.81 (m, 4H), 1.94 - 2.01 (m, 1H), 7.45 (dd, *J*=5.2, 1.4 Hz, 1H), 8.43 (dd, *J*=4.9, 0.9 Hz, 1H), 8.53 (dd, *J*=1.4, 0.9 Hz, 1H), 10.99 (s, 1H). Proton of the -COOH group was not detected. Formula: $C_{10}H_{10}N_2O_3$.

5.1.10. Synthesis of 3-aminopyrrole (75)

To a stirred solution of 3-nitro-1*H*-pyrrole (0.500 g, 4.46 mmol, 1.0 equiv.) in 10 mL EtOH 10% Pd/C (0.425 g, 9 mmol%) was added under Ar and the resulting mixture was hydrogenated at room temperature for 2 h. After that time, the reaction mixture was filtered through Celite and evaporated under reduced pressure. The product did not require further purification. Yield: 0.366 g (100%). ^{1}H NMR (500 MHz, DMSO-d_6) δ ppm 5.47 - 5.50 (m, 1H), 6.02 (q, *J*=2.3 Hz, 1H), 6.32 - 6.35 (m, 1H), 9.66 (br s, 1H). Protons of the -NH_2 group were not detected. Formula: $C_4H_6N_2$.

5.1.11. Synthesis of *tert*-butyl (1*H*-indol-3-yl)carbamate (76)

3-Nitro-1*H*-indole (0.500 g, 3.08 mmol, 1.0 equiv.) was dissolved in 25 mL MeOH, then a saturated aqueous solution of NH_4Cl (12.5 mL, 90.86 mmol, 29.5 equiv.) was added. After 15 minutes the solution was cooled to 0 °C on an ice bath, and then Zn (2.013 g, 30.80 mmol, 10.0 equiv.) was added in portions. After 10 minutes di-*tert*-butyl dicarbonate (0.808 g, 3.70 mmol, 1.2 equiv.) dissolved in a small amount of MeOH was added dropwise. The reaction mixture was then warmed up to room temperature and stirred overnight. After that time, solvents were evaporated under reduced pressure. The residue was extracted with DCM, combined organic layer was dried over anhydrous Na_2SO_4, filtered, and concentrated under a vacuum. Purification: preparative HPLC (20–100% MeCN gradient). Yield: 0.320 g (45%). ^{1}H NMR (500 MHz, CHLOROFORM-*d*) δ ppm 1.54 (s, 9H), 6.44 (br s, 1H), 7.10 (t, *J*=7.4 Hz, 1H), 7.19 (t, *J*=7.4 Hz, 1H), 7.31 (d, *J*=8.3 Hz, 1H), 7.47 (br d, *J*=8.0 Hz, 2H), 7.92 (br s, 1H). Formula: $C_{13}H_{16}N_2O_2$.

5.1.12. Synthesis of 1*H*-indol-3-amine (77)

To a stirred solution of **76** (0.220 g, 0.95 mmol, 1.0 equiv.) in 4.5 mL MeOH 37% HCl (0.780 mL, 9.50 mmol, 10.0 equiv.) was added and the mixture was heated under reflux for 1 h. The reaction mixture was cooled to room temperature and concentrated under vacuum to remove MeOH. Then the saturated aqueous $NaHCO_3$ solution was added,

and the residue was extracted with DCM, the combined organic layer was dried over anhydrous Na_2SO_4, filtered and concentrated under vacuum. The solid product was used directly to the next step without further purification. Yield: 0.125 g (100%). ^{1}H NMR (500 MHz, DMSO-d_6) δ ppm 3.93 (br s, 2H), 6.55 (d, *J*=2.3 Hz, 1H), 6.81 (ddd, *J*=7.9, 6.9, 0.9 Hz, 1H), 6.94 (ddd, *J*=8.1, 6.9, 1.3 Hz, 1H), 7.15 (d, *J*=8.0 Hz, 1H), 7.46 (d, *J*=8.0 Hz, 1H), 9.99 (br s, 1H). Formula: $C_8H_8N_2$.

5.1.13. Synthesis of *tert*-butyl thiophen-3-ylcarbamate (78)

To a stirred solution of 3-bromothiophene (0.575 mL, 6.13 mmol, 1.0 equiv.) in 30 mL anhydrous dioxane CuI (0.117 g, 0.61 mmol, 0.1 equiv.), K_2CO_3 (1.695 g, 12.26 mmol, 2.0 equiv.), *tert*-butyl carbamate (0.862 g, 7.36 mmol, 1.2 equiv.) and DMEDA (0.133 mL, 1.23 mmol, 0.2 equiv.) were added under Ar. The reaction was stirred under reflux overnight. After that time, the reaction mixture was diluted with DCM, filtered through Celite and evaporated under reduced pressure. The crude product was then purified by flash chromatography (PE/EtOAc 94:6). Yield: 0.374 g (31%). ^{1}H NMR (500 MHz, DMSO-d_6) δ ppm 1.42 (s, 9H), 6.94 (d, *J*=4.9 Hz, 1H), 7.12 (br s, 1H), 7.34 (dd, *J*=5.2, 3.2 Hz, 1H), 9.59 (br s, 1H). Formula: $C_9H_{13}NO_2S$.

5.1.14. Synthesis of 3-aminothiophene (79)

To a stirred, protected against light solution of **78** (0.160 g, 0.80 mmol) in 4 mL anhydrous EtOH 4 M solution of HCl in dioxane (2 mL) was added and stirred under reflux for 2 h. After that time, the solvents were evaporated under reduced pressure and product was used directly to the next step without further purification. Yield: 79 mg (100%). ^{1}H NMR (500 MHz, DMSO-d_6) δ ppm 7.08 (dd, *J*=5.2, 1.1 Hz, 1H), 7.54 (dd, *J*=3.2, 1.1 Hz, 1H), 7.63 (dd, *J*=5.0, 3.3 Hz, 1H), 10.56 (br s, 2H). Formula: C_4H_5NS.

5.1.15. General procedure for the synthesis of compounds 80–81, 94, 97–98 and 101 (GP4)

74 (1.0 equiv.) was dissolved in anhydrous DMF and then HATU (1.0 equiv.) was added under Ar. After 30 minutes an appropriate aromatic amine (1.0 equiv.) and DIEA (3.0 equiv.) were added. The reaction mixture was stirred overnight at rt. After that time, the solvent was evaporated under reduced pressure and residue was extracted with DCM. The crude product was purified by different methods described below.

2-(Cyclopropanecarboxamido)-*N*-phenylisonicotinamide (80)

Following **GP4**, compound **80** was prepared using compound **74** (0.200 g, 0.97 mmol), aniline (89 µL, 0.97 mmol), HATU (0.369 g, 0.97 mmol), DIEA (0.507 mL, 2.91 mmol) in 8 mL DMF. Purification: flash chromatography (PE/EtOAc 1:1). Yield: 0.234 g (86%), beige solid. Formula: $C_{16}H_{15}N_3O_2$. MW: 281.32, MS *m/z* 282 ($M+H^+$). Purity 100% (UPLC/MS). ^{1}H NMR (500 MHz, DMSO-d_6) δ ppm 0.80 - 0.88 (m, 4H), 2.00 - 2.08 (m, 1H), 7.09 - 7.16 (m, 1H), 7.33 - 7.39 (m, 2H), 7.53 (dd, *J*=5.2, 1.7 Hz, 1H), 7.71 - 7.78 (m, 2H), 8.46 - 8.52 (m, 2H), 10.50 (s, 1H), 11.02 (s, 1H). ^{13}C NMR (126 MHz,

DMSO-d_6) δ ppm 7.83 (2C), 14.26, 111.55, 116.95, 120.48 (2C), 124.17, 128.73 (2C), 138.65, 144.40, 148.53, 152.73, 164.36, 172.90.

***N*-(4-chlorophenyl)-2-(cyclopropanecarboxamido)isonicotinamide (81)**

Following **GP4**, compound **81** was prepared using compound **74** (0.200 g, 0.97 mmol), 4-chloroaniline (0.124 g, 0.97 mmol), HATU (0.369 g, 0.97 mmol), DIEA (0.507 mL, 2.91 mmol) in 8 mL DMF. Purification: flash chromatography (PE/EtOAc 6:4), then the solid residue was washed with MeCN. Yield: 43 mg (14%), white solid. Formula: $C_{16}H_{14}ClN_3O_2$. MW: 315.76, MS *m/z* 316 ($M+H^+$). Purity 97% (UPLC/MS). ^{1}H NMR (500 MHz, DMSO-d_6) δ ppm 0.81 - 0.89 (m, 4H), 1.98 - 2.09 (m, 1H), 7.40 - 7.46 (m, 2H), 7.52 (dd, *J*=5.2, 1.4 Hz, 1H), 7.76 - 7.82 (m, 2H), 8.46 - 8.53 (m, 2H), 10.62 (s, 1H), 11.04 (s, 1H). ^{13}C NMR (126 MHz, DMSO-d_6) δ ppm 7.86 (2C), 14.26, 111.51, 116.94, 122.01 (2C), 127.80, 128.68 (2C), 137.63, 144.10, 148.60, 152.76, 164.46, 172.93.

2-(Cyclopropanecarboxamido)-*N*-(*p*-tolyl)isonicotinamide (94)

Following **GP4**, compound **94** was prepared using compound **74** (0.200 g, 0.97 mmol), *p*-toluidine (0.104 g, 0.97 mmol), HATU (0.369 g, 0.97 mmol), DIEA (0.507 mL, 2.91 mmol) in 8 mL DMF. Purification: flash chromatography (30–70% EtOAc gradient in PE). Yield: 0.115 g (40%), pale yellow solid. Formula: $C_{17}H_{17}N_3O_2$. MW: 295.34, MS *m/z* 296 ($M+H^+$). Purity 100% (UPLC/MS). ^{1}H NMR (500 MHz, DMSO-d_6) δ ppm 0.80 - 0.88 (m, 4H), 1.98 - 2.07 (m, 1H), 2.28 (s, 3H), 7.17 (d, *J*=8.3 Hz, 2H), 7.51 (dd, *J*=5.0, 1.6 Hz, 1H), 7.62 (d, *J*=8.6 Hz, 2H), 8.43 - 8.53 (m, 2H), 10.40 (s, 1H), 11.00 (s, 1H). ^{13}C NMR (126 MHz, DMSO-d_6) δ ppm 7.84 (2C), 14.26, 20.55, 111.55, 116.93, 120.48 (2C), 129.12 (2C), 133.18, 136.13, 144.47, 148.50, 152.72, 164.14, 172.89.

2-(Cyclopropanecarboxamido)-*N*-(4-nitrophenyl)isonicotinamide (97)

Following **GP4**, compound **97** was prepared using compound **74** (0.200 g, 0.97 mmol), 4-nitroaniline (0.134 g, 0.97 mmol), HATU (0.369 g, 0.97 mmol), DIEA (0.507 mL, 2.91 mmol) in 8 mL DMF. Purification: flash chromatography (10–50% EtOAc gradient in PE). Yield: 54 mg (17%), yellow solid. Formula: $C_{16}H_{14}N_4O_4$. MW: 326.31, MS *m/z* 327 ($M+H^+$). Purity 95% (UPLC/MS). ^{1}H NMR (500 MHz, DMSO-d_6) δ ppm 0.82 - 0.87 (m, 4H), 2.01 - 2.08 (m, 1H), 7.56 (dd, *J*=5.0, 1.6 Hz, 1H), 8.01 - 8.07 (m, 2H), 8.26 - 8.31 (m, 2H), 8.51 - 8.54 (m, 2H), 11.06 (d, *J*=11.5 Hz, 2H). ^{13}C NMR (126 MHz, DMSO-d_6) δ ppm 7.88 (2C), 14.26, 111.54, 117.03, 120.15 (2C), 124.88 (2C), 142.87, 143.62, 144.89, 148.73, 152.79, 165.15, 172.99.

2-(Cyclopropanecarboxamido)-*N*-(2-hydroxyphenyl)isonicotinamide (98)

Following **GP4**, compound **98** was prepared using compound **74** (0.200 g, 0.97 mmol), 2-aminophenol (0.106 g, 0.97 mmol), HATU (0.369 g, 0.97 mmol), DIEA (0.507 mL, 2.91 mmol) in 8 mL DMF. Purification: flash chromatography (10–50% EtOAc gradient in PE). Yield: 44 mg (15%), brown solid. Formula: $C_{16}H_{15}N_3O_3$. MW: 297.31, MS *m/z* 298 ($M+H^+$). Purity 100% (UPLC/MS). ^{1}H NMR (500 MHz, DMSO-d_6) δ ppm 0.79 - 0.88 (m, 4H), 1.98 - 2.09 (m, 1H), 6.83 (td, *J*=7.6, 1.1 Hz, 1H), 6.92 (dd, *J*=8.0, 1.1 Hz, 1H), 7.05 (td, *J*=7.7, 1.7 Hz, 1H), 7.55 (d, *J*=4.3 Hz, 1H), 7.65 (br d, *J*=7.7 Hz,

1H), 8.48 (d, *J*=5.2 Hz, 1H), 8.53 (s, 1H), 9.66 (s, 1H), 9.77 (s, 1H), 11.01 (s, 1H). ^{13}C NMR (126 MHz, DMSO-d_6) δ ppm 7.85 (2C), 14.26, 111.47, 115.85, 116.81, 119.00, 124.51, 125.24, 126.16, 143.88, 148.59, 149.69, 152.80, 163.87, 172.88.

2-(Cyclopropanecarboxamido)-*N*-(1*H*-pyrrol-3-yl)isonicotinamide (101)

Following **GP4**, compound **101** was prepared using compound **74** (0.491 g, 2.38 mmol), **75** (0.195 g, 2.38 mmol), HATU (0.905 g, 2.38 mmol), DIEA (1.240 mL, 7.14 mmol) in 20 mL DMF. Purification: flash chromatography (30–70% EtOAc gradient in PE), then preparative HPLC (10–80% MeCN gradient). Yield: 0.111 g (17%), brown solid. Formula: $C_{14}H_{14}N_4O_2$. MW: 270.29, MS *m/z* 271 ($M+H^+$). Purity 100% (UPLC/MS). ^{1}H NMR (500 MHz, DMSO-d_6) δ ppm 0.80 - 0.86 (m, 4H), 1.98 - 2.07 (m, 1H), 6.19 (d, *J*=0.9 Hz, 1H), 6.62 - 6.64 (m, 1H), 7.22 (s, 1H), 7.51 (dd, *J*=5.2, 0.6 Hz, 1H), 8.44 (d, *J*=5.2 Hz, 1H), 8.48 (s, 1H), 10.40 (s, 1H), 10.57 (br s, 1H), 10.95 (s, 1H). ^{13}C NMR (126 MHz, DMSO-d_6) δ ppm 7.80 (2C), 14.26, 100.79, 108.51, 111.50, 115.83, 116.73, 122.84, 144.35, 148.36, 152.73, 161.65, 172.79.

5.1.16. General procedure for the synthesis of compounds 82–93, 95–96 and 99–100 (GP5)

74 (1.0 equiv.) was dissolved in anhydrous DCM and then an appropriate aromatic amine (1.1 equiv.), anhydrous pyridine (2.0 equiv.) and 50% T_3P sol. in ethyl acetate (2.2–3.3 equiv.) were added under Ar. The reaction mixture was stirred for 1–3 h in rt. After that time, the residue was extracted with DCM. The crude product was purified by different methods described below.

***N*-(2-Chlorophenyl)-2-(cyclopropanecarboxamido)isonicotinamide (82)**

Following **GP5**, compound **82** was prepared using compound **74** (0.100 g, 0.48 mmol), 2-chloroaniline (55 µL, 0.53 mmol), pyridine (77 µL, 0.96 mmol), T_3P (0.936 mL, 1.58 mmol) in 5 mL DCM. Purification: flash chromatography (PE/EtOAc 7.5:2.5 then 1:1). Yield: 99 mg (65%), white solid. Formula: $C_{16}H_{14}ClN_3O_2$. MW: 315.76, MS *m/z* 316 ($M+H^+$). Purity 100% (UPLC/MS). ^{1}H NMR (500 MHz, DMSO-d_6) δ ppm 0.79 - 0.90 (m, 4H), 1.99 - 2.08 (m, 1H), 7.29 - 7.36 (m, 1H), 7.40 (td, *J*=7.7, 1.4 Hz, 1H), 7.53 - 7.60 (m, 3H), 8.47 - 8.52 (m, 1H), 8.56 (s, 1H), 10.36 (s, 1H), 11.02 (s, 1H). ^{13}C NMR (126 MHz, DMSO-d_6) δ ppm 7.84 (2C), 14.24, 111.64, 116.84, 127.60, 127.93, 128.57, 129.66, 129.71, 134.55, 143.39, 148.64, 152.84, 164.32, 172.87.

***N*-(3-Chlorophenyl)-2-(cyclopropanecarboxamido)isonicotinamide (83)**

Following **GP5**, compound **83** was prepared using compound **74** (0.100 g, 0.48 mmol), 3-chloroaniline (56 µL, 0.53 mmol), pyridine (77 µL, 0.96 mmol), T_3P (0.936 mL, 1.58 mmol) in 5 mL DCM. Purification: flash chromatography (PE/EtOAc 7.5:2.5 then 1:1). Yield: 66 mg (43%), white solid. Formula: $C_{16}H_{14}ClN_3O_2$. MW: 315.76, MS *m/z* 316 ($M+H^+$). Purity 100% (UPLC/MS). ^{1}H NMR (500 MHz, DMSO-d_6) δ ppm 0.82 - 0.87 (m, 4H), 2.00 - 2.07 (m, 1H), 7.20 (dd, *J*=8.0, 1.4 Hz, 1H), 7.40 (t, *J*=8.0 Hz, 1H), 7.51 - 7.54 (m, 1H), 7.69 (dd, *J*=8.3, 1.1 Hz, 1H), 7.93 (t, *J*=2.0 Hz, 1H), 8.48 - 8.52 (m, 2H), 10.65 (s, 1H), 11.04 (s, 1H). ^{13}C NMR (126 MHz, DMSO-d_6) δ ppm 7.83 (2C),

14.23, 111.48, 116.90, 118.79, 119.86, 123.86, 130.45, 132.99, 140.11, 143.94, 148.61, 152.75, 164.61, 172.91.

2-(Cyclopropanecarboxamido)-*N*-(4-(trifluoromethyl)phenyl)isonicotinamide (84)

Following **GP5**, compound **84** was prepared using compound **74** (0.100 g, 0.48 mmol), 4-(trifluoromethyl)aniline (67 µL, 0.53 mmol), pyridine (77 µL, 0.96 mmol), T_3P (0.625 mL, 1.06 mmol) in 5 mL DCM. Purification: flash chromatography (15–50% EtOAc gradient in PE), then the solid residue was washed with MeCN. Yield: 19 mg (11%), white solid. Formula: $C_{17}H_{14}F_3N_3O_2$. MW: 349.31, MS *m/z* 350 ($M+H^+$). Purity 100% (UPLC/MS). ^{1}H NMR (500 MHz, DMSO-d_6) δ ppm 1.31 - 1.35 (m, 2H), 1.38 - 1.44 (m, 2H), 2.51 - 2.55 (m, 1H), 8.00 (dd, *J*=5.2, 1.4 Hz, 1H), 8.17 (d, *J*=8.9 Hz, 2H), 8.52 (d, *J*=8.6 Hz, 2H), 8.89 (dd, *J*=5.2, 0.6 Hz, 1H), 9.10 (s, 1H), 10.41 (br s, 1H), 10.62 (br s, 1H). ^{13}C NMR (126 MHz, DMSO-d_6) δ ppm 7.85 (2C), 14.26, 111.55, 116.99, 120.35 (2C), 124.34 (q, *J*=271.4 Hz), 124.13 (q, *J*=32.6 Hz), 126.04 (q, *J*=3.02 Hz, 2C), 142.29, 143.89, 148.64, 152.78, 164.89, 172.96.

2-(Cyclopropanecarboxamido)-*N*-(2-(trifluoromethyl)phenyl)isonicotinamide (85)

Following **GP5**, compound **85** was prepared using compound **74** (0.100 g, 0.48 mmol), 3-(trifluoromethyl)aniline (67 µL, 0.53 mmol), pyridine (77 µL, 0.96 mmol), T_3P (0.936 mL, 1.58 mmol) in 5 mL DCM. Purification: flash chromatography (PE/EtOAc 8.5:1.5 then 7:3 and 1:1). Yield: 44 mg (26%), white solid. Formula: $C_{17}H_{14}F_3N_3O_2$. MW: 349.31, MS *m/z* 350 ($M+H^+$). Purity 100% (UPLC/MS). ^{1}H NMR (500 MHz, DMSO-d_6) δ ppm 0.80 - 0.88 (m, 4H), 2.00 - 2.08 (m, 1H), 7.51 (dd, *J*=5.2, 1.1 Hz, 1H), 7.53 - 7.59 (m, 2H), 7.72 - 7.78 (m, 1H), 7.81 (d, *J*=7.7 Hz, 1H), 8.50 (d, *J*=5.2 Hz, 1H), 8.55 (s, 1H), 10.43 (s, 1H), 11.02 (s, 1H). ^{13}C NMR (126 MHz, DMSO-d_6) δ ppm 7.83, 14.25, 111.57, 116.76, 123.57 (q, *J*=272.2 Hz), 126.45 (q, *J*=29.0 Hz), 126.60 (q, *J*=5.4 Hz), 127.84, 131.18, 133.28, 135.18, 143.39, 148.66, 152.86, 165.34, 172.87. ^{19}F NMR (471 MHz, DMSO-d_6) δ ppm -59.29 (s, 3F).

2-(Cyclopropanecarboxamido)-*N*-(3-(trifluoromethyl)phenyl)isonicotinamide (86)

Following **GP5**, compound **86** was prepared using compound **74** (0.100 g, 0.48 mmol), 3-(trifluoromethyl)aniline (66 µL, 0.53 mmol), pyridine (77 µL, 0.96 mmol), T_3P (0.624 mL, 1.06 mmol) in 5 mL DCM. Purification: flash chromatography (PE/EtOAc 7.5:2.5 then 1:1). Yield: 0.111 g (66%), white solid. Formula: $C_{17}H_{14}F_3N_3O_2$. MW: 349.31, MS *m/z* 350 ($M+H^+$). Purity 100% (UPLC/MS). ^{1}H NMR (500 MHz, DMSO-d_6) δ ppm 0.80 - 0.89 (m, 4H), 2.01 - 2.08 (m, 1H), 7.49 (d, *J*=7.7 Hz, 1H), 7.55 (dd, *J*=5.2, 1.4 Hz, 1H), 7.62 (t, *J*=8.0 Hz, 1H), 8.04 (d, *J*=8.6 Hz, 1H), 8.21 (s, 1H), 8.51 (dd, *J*=5.2, 0.6 Hz, 1H), 8.52 - 8.55 (m, 1H), 10.79 (s, 1H), 11.05 (s, 1H). ^{13}C NMR (126 MHz, DMSO-d_6) δ ppm 7.83 (2C), 14.23, 111.49, 116.53 (q, *J*=3.6 Hz), 116.91, 120.47 (q, *J*=3.6 Hz), 124.10 (q, *J*=272.2 Hz), 123.97, 129.41 (q, *J*=32.0 Hz), 130.01, 139.43, 143.81, 148.64, 152.78, 164.73, 172.91.

2-(Cyclopropanecarboxamido)-*N*-(4-fluorophenyl)isonicotinamide (**87**)

Following **GP5**, compound **87** was prepared using compound **74** (0.100 g, 0.48 mmol), 4-fluoroaniline (50 µL, 0.53 mmol), pyridine (77 µL, 0.96 mmol), T_3P (0.936 mL, 1.58 mmol) in 5 mL DCM. Purification: flash chromatography (PE/EtOAc 7.5:2.5). Yield: 82 mg (57%), white solid. Formula: $C_{16}H_{14}FN_3O_2$. MW: 299.31, MS *m/z* 300 ($M+H^+$). Purity 100% (UPLC/MS). ^{1}H NMR (500 MHz, DMSO-d_6) δ ppm 0.82 - 0.87 (m, 4H), 2.00 - 2.07 (m, 1H), 7.18 - 7.25 (m, 2H), 7.52 (dd, *J*=5.2, 1.4 Hz, 1H), 7.73 - 7.81 (m, 2H), 8.49 (d, *J*=5.2 Hz, 1H), 8.50 (s, 1H), 10.54 (s, 1H), 11.02 (s, 1H). ^{13}C NMR (126 MHz, DMSO-d_6) δ ppm 7.82 (2C), 14.23, 111.50, 115.32 (d, *J*=22.3 Hz, 2C), 116.89, 122.34 (d, *J*=7.8 Hz, 2C), 134.99 (d, *J*=2.4 Hz), 144.20, 148.53, 152.74, 158.53 (d, *J*=240.8 Hz), 164.24, 172.88.

2-(Cyclopropanecarboxamido)-*N*-(2-fluorophenyl)isonicotinamide (**88**)

Following **GP5**, compound **88** was prepared using compound **74** (0.100 g, 0.48 mmol), 2-fluoroaniline (51 µL, 0.53 mmol), pyridine (77 µL, 0.96 mmol), T_3P (0.936 mL, 1.58 mmol) in 5 mL DCM. Purification: flash chromatography (PE/EtOAc 7.5:2.5 then 1:1). Yield: 110 mg (76%), white solid. Formula: $C_{16}H_{14}FN_3O_2$. MW: 299.31, MS *m/z* 300 ($M+H^+$). Purity 100% (UPLC/MS). ^{1}H NMR (500 MHz, DMSO-d_6) δ ppm 0.81 - 0.88 (m, 4H), 2.01 - 2.08 (m, 1H), 7.20 - 7.26 (m, 1H), 7.27 - 7.34 (m, 2H), 7.55 (dd, *J*=5.2, 1.4 Hz, 1H), 7.59 (t, *J*=7.4 Hz, 1H), 8.49 (d, *J*=5.2 Hz, 1H), 8.55 (s, 1H), 10.40 (s, 1H), 11.03 (s, 1H). ^{13}C NMR (126 MHz, DMSO-d_6) δ ppm 7.83 (2C), 14.23, 111.68, 115.94 (d, *J*=19.9 Hz), 116.95, 124.40 (d, *J*=3.6 Hz), 125.16 (d, *J*=12.1 Hz), 127.09, 127.38 (d, *J*=7.8 Hz), 143.32, 148.60, 152.78, 155.77 (d, *J*=247.5 Hz), 164.32, 172.87. ^{19}F NMR (471 MHz, DMSO-d_6) δ ppm -120.77 (q, *J*=7.8 Hz, 1F).

2-(Cyclopropanecarboxamido)-*N*-(3-fluorophenyl)isonicotinamide (**89**)

Following **GP5**, compound **89** was prepared using compound **74** (0.100 g, 0.48 mmol), 3-fluoroaniline (51 µL, 0.53 mmol), pyridine (77 µL, 0.96 mmol), T_3P (0.936 mL, 1.58 mmol) in 5 mL DCM. Purification: flash chromatography (PE/EtOAc 7.5:2.5 then 1:1). Yield: 71 mg (49%), pale yellow solid. Formula: $C_{16}H_{14}FN_3O_2$. MW: 299.31, MS *m/z* 300 ($M+H^+$). Purity 100% (UPLC/MS). ^{1}H NMR (500 MHz, DMSO-d_6) δ ppm 0.81 - 0.87 (m, 4H), 2.01 - 2.08 (m, 1H), 6.97 (td, *J*=8.4, 2.1 Hz, 1H), 7.38 - 7.44 (m, 1H), 7.50 - 7.57 (m, 2H), 7.71 (dt, *J*=11.7, 2.2 Hz, 1H), 8.47 - 8.53 (m, 2H), 10.67 (s, 1H), 11.04 (s, 1H). ^{13}C NMR (126 MHz, DMSO-d_6) δ ppm 7.83 (2C), 14.24, 107.14 (d, *J*=26.0 Hz), 110.64 (d, *J*=21.1 Hz), 111.48, 116.14 (d, *J*=2.4 Hz), 116.91, 130.38 (d, *J*=9.7 Hz), 140.38 (d, *J*=10.9 Hz), 144.01 148.59, 152.75, 162.01 (d, *J*=241.4 Hz), 164.62, 172.90.

2-(Cyclopropanecarboxamido)-*N*-(3,4-dichlorophenyl)isonicotinamide (**90**)

Following **GP5**, compound **90** was prepared using compound **74** (0.150 g, 0.73 mmol), 3,4-dichloroaniline (0.130 g, 0.80 mmol), pyridine (0.118 mL, 1.46 mmol), T_3P (0.948 mL, 1.61 mmol) in 7.5 mL DCM. Purification: flash chromatography (15–65% EtOAc gradient in PE), then the solid residue was washed with MeCN. Yield: 70 mg

(28%), white solid. Formula: $C_{16}H_{13}Cl_2N_3O_2$. MW: 350.20, MS *m/z* 350 ($M+H^+$). Purity 98% (UPLC/MS). ^{1}H NMR (500 MHz, DMSO-d_6) δ ppm 0.81 - 0.87 (m, 4H), 2.00 - 2.07 (m, 1H), 7.52 (dd, *J*=5.4, 1.4 Hz, 1H), 7.64 (dd, *J*=8.9, 2.3 Hz, 1H), 7.73 (dd, *J*=8.9, 2.3 Hz, 1H), 8.11 (d, *J*=2.3 Hz, 1H), 8.48 - 8.53 (m, 2H), 10.75 (s, 1H), 11.04 (s, 1H). ^{13}C NMR (126 MHz, DMSO-d_6) δ ppm 7.87 (2C), 14.26, 111.46, 116.92, 120.45, 121.65, 125.69, 130.73, 130.96, 138.78, 143.72, 148.69, 152.79, 164.68, 172.96.

2-(Cyclopropanecarboxamido)-*N*-(3,5-dichlorophenyl)isonicotinamide (91)

Following **GP5**, compound **91** was prepared using compound **74** (0.150 g, 0.73 mmol), 3,5-dichloroaniline (0.130 g, 0.80 mmol), pyridine (0.118 mL, 1.46 mmol), T_3P (0.948 mL, 1.61 mmol) in 7.5 mL DCM. Purification: flash chromatography (20–70% EtOAc gradient in PE), then the solid residue was washed with MeCN. Yield: 138 mg (54%), white solid. Formula: $C_{16}H_{13}Cl_2N_3O_2$. MW: 350.20, MS *m/z* 350 ($M+H^+$). Purity 100% (UPLC/MS). ^{1}H NMR (500 MHz, DMSO-d_6) δ ppm 0.82 - 0.87 (m, 4H), 2.00 - 2.07 (m, 1H), 7.38 (t, *J*=1.9 Hz, 1H), 7.52 (dd, *J*=4.9, 1.8 Hz, 1H), 7.86 (d, *J*=2.0 Hz, 2H), 8.49 - 8.53 (m, 2H), 10.78 (s, 1H), 11.06 (s, 1H). ^{13}C NMR (126 MHz, DMSO-d_6) δ ppm 7.88 (2C), 14.26, 111.45, 116.90, 118.53 (2C), 123.41, 134.07 (2C), 141.01, 143.56, 148.75, 152.81, 164.86, 172.97.

***N*-(3,5-Bis(trifluoromethyl)phenyl)-2-(cyclopropanecarboxamido)isonicotinamide (92)**

Following **GP5**, compound **92** was prepared using compound **74** (0.150 g, 0.73 mmol), 3,5-bis(trifluoromethyl)aniline (0.125 mL, 0.80 mmol), pyridine (0.118 mL, 1.46 mmol), T_3P (0.948 mL, 1.61 mmol) in 7.5 mL DCM. Purification: flash chromatography (10–30% EtOAc gradient in PE), then crystallization from MeCN. Yield: 59 mg (19%), white solid. Formula: $C_{18}H_{13}F_6N_3O_2$. MW: 417.31, MS *m/z* 418 ($M+H^+$). Purity 98% (UPLC/MS). ^{1}H NMR (500 MHz, DMSO-d_6) δ ppm 0.81 - 0.88 (m, 4H), 2.00 - 2.09 (m, 1H), 7.57 (dd, *J*=5.2, 1.4 Hz, 1H), 7.86 (s, 1H), 8.48 (s, 2H), 8.54 (d, *J*=5.2 Hz, 1H), 8.57 (s, 1H), 11.07 (s, 2H). ^{13}C NMR (126 MHz, DMSO-d_6) δ ppm 7.89 (2C), 14.27, 111.47, 116.91, 117.09 (q, *J*=3.0 Hz, 2C), 123.26, (q, *J*=272.8 Hz, 2C), 120.23, 130.73 (q, *J*=32.6 Hz, 2C), 140.60, 143.25, 148.81, 152.88, 165.07, 172.99.

2-(Cyclopropanecarboxamido)-*N*-(4-methoxyphenyl)isonicotinamide (93)

Following **GP5**, compound **93** was prepared using compound **74** (0.100 g, 0.48 mmol), *p*-anisidine (65 mg, 0.53 mmol), pyridine (77 µL, 0.96 mmol), T_3P (0.625 mL, 1.06 mmol) in 5 mL DCM. Purification: flash chromatography (DCM/MeOH 98:2), then the solid residue was washed with MeOH. Yield: 37 mg (25%), white solid. Formula: $C_{17}H_{17}N_3O_3$. MW: 311.34, MS *m/z* 312 ($M+H^+$). Purity 100% (UPLC/MS). ^{1}H NMR (500 MHz, DMSO-d_6) δ ppm 0.80 - 0.88 (m, 4H), 1.99 - 2.07 (m, 1H), 3.74 (s, 3H), 6.94 (d, *J*=8.9 Hz, 2H), 7.52 (d, *J*=5.2 Hz, 1H), 7.65 (d, *J*=8.9 Hz, 2H), 8.43 - 8.53 (m, 2H), 10.37 (s, 1H), 11.00 (s, 1H). ^{13}C NMR (126 MHz, DMSO-d_6) δ ppm 7.84 (2C), 14.27, 55.21, 111.55, 113.85 (2C), 116.90, 122.09 (2C), 131.69, 144.49, 148.48, 152.73, 155.86, 163.87, 172.89.

2-(Cyclopropanecarboxamido)-*N*-(*o*-tolyl)isonicotinamide (95)

Following **GP5**, compound **95** was prepared using compound **74** (0.100 g, 0.48 mmol), *o*-toluidine (57 µL, 0.53 mmol), pyridine (77 µL, 0.96 mmol), T_3P (0.624 mL, 1.06 mmol) in 5 mL DCM. Purification: flash chromatography (PE/EtOAc 7.5:2.5 then 1:1), then preparative HPLC (5–55% MeCN gradient). Yield: 78 mg (55%), white solid. Formula: $C_{17}H_{17}N_3O_2$. MW: 295.34, MS *m/z* 296 ($M+H^+$). Purity 100% (UPLC/MS). ^{1}H NMR (500 MHz, DMSO-d_6) δ ppm 0.79 - 0.90 (m, 4H), 2.04 (td, *J*=4.9, 1.7 Hz, 1H), 2.22 (s, 3H), 7.15 - 7.26 (m, 2H), 7.26 - 7.36 (m, 2H), 7.55 (br d, *J*=4.0 Hz, 1H), 8.48 (br d, *J*=3.7 Hz, 1H), 8.55 (br s, 1H), 10.13 (br s, 1H), 11.00 (br s, 1H). ^{13}C NMR (126 MHz, DMSO-d_6) δ ppm 7.80 (2C), 14.23, 17.84, 111.65, 116.87, 126.09, 126.33, 126.54, 130.40, 133.73, 135.83, 143.99, 148.51, 152.78, 164.18, 172.84.

2-(Cyclopropanecarboxamido)-*N*-(*m*-tolyl)isonicotinamide (96)

Following **GP5**, compound **96** was prepared using compound **74** (0.100 g, 0.48 mmol), *m*-toluidine (57 µL, 0.53 mmol), pyridine (77 µL, 0.96 mmol), T_3P (0.624 mL, 1.06 mmol) in 5 mL DCM. Purification: flash chromatography (PE/EtOAc 7:3 then 1:1), then preparative HPLC (5–55% MeCN gradient). Yield: 86 mg (60%), white solid. Formula: $C_{17}H_{17}N_3O_2$. Molecular Weight: 295.34, MS *m/z* 296 ($M+H^+$). Purity 100% (UPLC/MS). ^{1}H NMR (500 MHz, DMSO-d_6) δ ppm 0.79 - 0.90 (m, 4H), 1.98 - 2.08 (m, 1H), 2.31 (s, 3H), 6.95 (d, *J*=7.7 Hz, 1H), 7.24 (t, *J*=7.9 Hz, 1H), 7.52 (dd, *J*=5.2, 1.7 Hz, 1H), 7.54 (br d, *J*=8.3 Hz, 1H), 7.59 (s, 1H), 8.48 (d, *J*=4.9 Hz, 1H), 8.49 (s, 1H), 10.40 (s, 1H), 11.01 (s, 1H). ^{13}C NMR (126 MHz, DMSO-d_6) δ ppm 7.81 (2C), 14.24, 21.20, 111.54, 116.91, 117.65, 120.98, 124.83, 128.54, 137.89, 138.55, 144.43, 148.48, 152.71, 164.27, 172.86.

2-(Cyclopropanecarboxamido)-*N*-(thiophen-3-yl)isonicotinamide (99)

Following **GP5**, compound **99** was prepared using compound **74** (0.150 g, 0.73 mmol), **79** (79 mg, 0.80 mmol), pyridine (0.118 mL, 1.46 mmol), T_3P (0.948 mL, 1.61 mmol) in 7.5 mL DCM. Purification: flash chromatography (30–70% EtOAc gradient in PE), then the solid residue was washed with MeCN. Yield: 45 mg (22%), white solid. Formula: $C_{14}H_{13}N_3O_2S$. MW: 287.34, MS *m/z* 288 ($M+H^+$). Purity 100% (UPLC/MS). ^{1}H NMR (500 MHz, DMSO-d_6) δ ppm 0.81 - 0.88 (m, 4H), 2.00 - 2.08 (m, 1H), 7.30 (dd, *J*=5.2, 1.1 Hz, 1H), 7.50 (dd, *J*=5.2, 3.2 Hz, 1H), 7.53 (dd, *J*=5.2, 1.7 Hz, 1H), 7.76 (dd, *J*=3.2, 1.1 Hz, 1H), 8.49 (dd, *J*=5.2, 0.6 Hz, 1H), 8.52 (s, 1H), 10.93 (s, 1H), 11.02 (s, 1H). ^{13}C NMR (126 MHz, DMSO-d_6) δ ppm 7.82 (2C), 14.24, 110.37, 111.45, 116.81, 122.02, 124.81, 136.44, 143.76, 148.58, 152.78, 163.19, 172.87.

2-(Cyclopropanecarboxamido)-*N*-(1*H*-indol-3-yl)isonicotinamide (100)

Following **GP5**, compound **100** was prepared using compound **74** (0.100 g, 0.48 mmol), **77** (70 mg, 0.53 mmol), pyridine (77 µL, 0.96 mmol), T_3P (0.625 mL, 1.06 mmol) in 5 mL DCM. Purification: preparative HPLC (10–60% MeCN gradient). Yield: 22 mg (14%), green solid. Formula: $C_{18}H_{16}N_4O_2$. MW: 320.35, MS *m/z* 321 ($M+H^+$). Purity 96% (UPLC/MS). ^{1}H NMR (500 MHz, DMSO-d_6) δ ppm 0.80 - 0.89 (m, 4H), 2.01 - 2.08 (m,

1H), 6.99 - 7.04 (m, 1H), 7.09 - 7.15 (m, 1H), 7.37 (d, *J*=8.3 Hz, 1H), 7.58 (dd, *J*=5.2, 1.4 Hz, 1H), 7.81 (d, *J*=2.6 Hz, 1H), 7.84 (d, *J*=8.0 Hz, 1H), 8.48 (dd, *J*=5.2, 0.6 Hz, 1H), 8.53 (s, 1H), 10.45 (s, 1H), 10.98 (br s, 1H), 10.99 (s, 1H). ^{13}C NMR (126 MHz, DMSO-d_6) δ ppm 7.82 (2C), 14.28, 111.48, 111.80, 114.45, 117.13, 117.14, 118.31, 118.61, 121.04, 121.58, 133.79, 144.33, 148.36, 152.66, 163.49, 172.86.

5.1.17. Synthesis of *tert*-butyl (2-(thiophen-3-yl)ethyl)carbamate (122)

To a mixture of 2-(thiophen-3-yl)ethanamine hydrochloride (0.327 g, 2.00 mmol, 1.0 equiv.) and K_2CO_3 (0.553 g, 4.00 mmol, 2.0 equiv.) in the mixture of 15mL THF and 5 mL H_2O (3:1 ratio) di-*tert*-butyldicarbonate (0.480 g, 2.20 mmol, 1.1 equiv) was added in portions at 0 °C and the reaction was kept at room temperature for 6 h. After that time, the solvent was evaporated under a vacuum, the residue was dissolved in EtOAc and washed with water, and brine, dried over anhydrous Na_2SO_4, and filtrated. The solvent was evaporated under reduced pressure. The resulting product was used without further purification. Yield: 0.405 g (89%). ^{1}H NMR (500 MHz, CHLOROFORM-*d*) δ ppm 7.29 (dd, *J*=4.9, 2.9 Hz, 1H), 6.99 - 7.03 (m, 1H), 6.96 (dd, *J*=4.9, 0.9 Hz, 1H), 4.57 (br s, 1H), 3.32 - 3.43 (m, 2H), 2.84 (t, *J*=6.9 Hz, 2H), 1.45 (s, 9H). Formula: $C_{11}H_{17}NO_2S$.

5.1.18. Synthesis of 5,6-dihydrothieno[2,3-*c*]pyridin-7(4*H*)-one (123)

2-Chloropyridine (0.167 mL, 1.76 mmol, 1.5 equiv.) and 1 M triflic anhydride in DCM (1.290 mL, 1.29 mmol, 1.1 equiv.) were added to a stirred solution of **122** (0.267 g, 1.17 mmol, 1.0 equiv.) in 20 mL of DCM at –78 °C. After 20 min, $BF_3{\cdot}Et_2O$ (0.722 mL, 5.85 mmol, 5.0 equiv.) was added. After 30 min, the reaction mixture was warmed to room temperature and stirred for 2 h. Next, the reaction was quenched at 0 °C with saturated aqueous $NaHCO_3$ solution, diluted with DCM, washed with brine, dried over Na_2SO_4, filtered, and concentrated in vacuo. The residue was purified by flash chromatography (DCM/MeOH 95:5). Yield: 0.118 g (66%). ^{1}H NMR (500 MHz, CHLOROFORM-*d*) δ ppm 7.52 (d, *J*=5.2 Hz, 1H), 6.96 (d, *J*=4.9 Hz, 1H), 5.95 (br s, 1H), 3.63 (td, *J*=6.9, 2.6 Hz, 2H), 2.94 (t, *J*=6.9 Hz, 2H). Formula: C_7H_7NOS.

5.1.19. Synthesis of 2-bromo-5,6-dihydrothieno[2,3-c]pyridin-7(4H)-one (124)

123 (1.223 g, 7.98 mmol, 1.0 equiv.) was dissolved in the mixture of 10.5 mL CH_3COOH and 7.5 mL H_2O, the resulting solution was cooled down to 0 °C and Br_2 (0.450 mL, 8.78 mmol, 1.1 equiv.) was added. After stirring at 0 °C for 1 h, the reaction mixture was diluted with water and extracted with EtOAc. The combined organic extracts were washed with 5% aqueous $Na_2S_2O_3$ solution, then saturated aqueous $NaHCO_3$ solution, dried over Na_2SO_4, filtered, and concentrated in vacuo. The residue was used further without purification. Yield: 1.595 g (86%). ^{1}H NMR (500 MHz, CHLOROFORM-*d*) δ ppm 6.94 (s, 1H), 5.61 (br s, 1H), 3.61 (td, *J*=6.9, 2.6 Hz, 2H), 2.89 (t, *J*=6.9 Hz, 2H). Formula: C_7H_6BrNOS.

5.1.20. Synthesis of ethyl 2-(2-bromo-7-oxo-4,7-dihydrothieno[2,3-*c*]pyridin-6(5*H*)-yl)acetate (129)

The stirred solution of **124** (0.700 g, 3.02 mmol, 1.0 equiv.) in 20 mL anhydrous THF was cooled to 0 °C on an ice bath and then ethyl bromoacetate (0.501 mL, 4.53 mmol, 1.5 equiv.) and *t*-BuOK (0.508 g, 4.53 mmol, 1.5 equiv.) were added. The reaction mixture was warmed up to room temperature and stirred for 1 h. After that time, the reaction mixture was cooled again to 0 °C and quenched with saturated aqueous $NaHCO_3$ solution. The solvent was evaporated under reduced pressure and the residue was extracted with EtOAc, the combined organic layer was dried over anhydrous Na_2SO_4, filtered, and concentrated under a vacuum. The crude product was purified by flash chromatography (10–30% EtOAc gradient in PE). Yield: 0.639 g (67%). ^{1}H NMR (500 MHz, CHLOROFORM-*d*) δ ppm 1.29 (t, *J*=7.2 Hz, 3H), 2.95 (t, *J*=6.9 Hz, 2H), 3.69 (t, *J*=7.0 Hz, 2H), 4.22 (q, *J*=7.2 Hz, 2H), 4.26 (s, 2H), 6.91 (s, 1H). Formula: $C_{11}H_{12}BrNO_3S$.

5.1.21. Synthesis of 2-bromo-6-(2-hydroxyethyl)-5,6-dihydrothieno[2,3-*c*]pyridin-7(4*H*)-one (130)

The stirred solution of **129** (0.639 g, 2.01 mmol, 1.0 equiv.) in 20 mL anhydrous EtOH was cooled to 0 °C on an ice bath and then under Ar $NaBH_4$ (1.140 g, 30.15 mmol, 15.0 equiv.) and Na_2SO_4 (1.430 g, 10.05 mmol, 5.0 equiv.) were added. The reaction mixture was warmed up to room temperature and stirred overnight. When all starting material was consumed pH was adjusted to 6–7 by the addition of an aqueous 6 M HCl solution. The solvent was evaporated under reduced pressure, then the residue was extracted with EtOAc, and the combined organic layer was dried over anhydrous Na_2SO_4, filtered, and concentrated under a vacuum. The product did not require further purification. Yield: 0.526 g (95%). ^{1}H NMR (500 MHz, DMSO-d_6) δ ppm 2.85 (t, *J*=6.9 Hz, 2H), 3.42 - 3.47 (m, 2H), 3.54 (q, *J*=5.6 Hz, 2H), 3.63 (t, *J*=7.0 Hz, 2H), 4.76 (t, *J*=5.6 Hz, 1H), 7.22 (s, 1H). Formula: $C_9H_{10}BrNO_2S$.

5.1.22. Synthesis of 1-(2,5-dibromothiophen-3-yl)ethan-1-one (137)

To the stirred, protected against the light solution of 3-acetylthiophene (5.000 g, 39.63 mmol, 1.0 equiv.) in 80 mL DMF *N*-bromosuccinimide (14.810 g, 83.21 mmol, 2.1 equiv.) was added in portions within 2 hours. The reaction mixture was stirred overnight at 45 °C. When all starting material was consumed, the solvent was evaporated under reduced pressure. The residue was extracted with EtOAc, and the combined organic layer was dried over anhydrous Na_2SO_4, filtered, and concentrated under a vacuum. The crude product was purified by flash chromatography (1–3% EtOAc gradient in PE). Yield: 7.490 g (67%). ^{1}H NMR (500 MHz, CHLOROFORM-*d*) δ ppm 2.59 (s, 3H), 7.33 (s, 1H). Formula: $C_6H_4Br_2OS$.

5.1.23. Synthesis of 1-(2-(benzylthio)-5-bromothiophen-3-yl)ethan-1-one (138)

To the mixture of 57 mL isopropanol and 19 mL water (3:1 ratio), thiourea (2.210 g, 29.01 mmol, 1.1 equiv.) and benzyl chloride (3.040 mL, 26.37 mmol, 1.0 equiv.) were

added and stirred at 90 °C for 2 h. After that time, the reaction mixture was cooled to 60 °C and then **137** (7.490 g, 26.37 mmol, 1.0 equiv.) and 4 M aqueous NaOH solution (15.8 mL) were added, then mixture was warmed up to 90 °C and stirred for 3 h. Finally, the mixture was cooled to rt, 2.25% aqueous sodium hypochlorite solution (4.8 mL) was added and stirred for 0.5 h. Solvents were evaporated under reduced pressure, the residue was suspended in silica gel and purified by flash chromatography (3–5% EtOAc gradient in PE). Yield: 4.740 g (55%). ^{1}H NMR (500 MHz, CHLOROFORM-*d*) δ ppm 2.45 (s, 3H), 4.17 (s, 1H), 7.29 - 7.32 (m, 1H), 7.32 (s, 1H), 7.33 - 7.40 (m, 4H). Formula: $C_{13}H_{11}BrOS_2$.

5.1.24. Synthesis of 3-acetyl-5-bromothiophene-2-sulfonamide (139)

The stirred solution of **138** (2.410 g, 7.35 mmol, 1.0 equiv.) in a 36 mL mixture of EtOAc and water (1:1 ratio) was cooled to 0 °C on an ice bath and *in situ* chlorine gas was bubbled directly to the reaction vessel. When all starting material was consumed 9 mL of 25% ammonia solution was added and stirred for 0.5 h at 0 °C. Solvents were evaporated under reduced pressure, the residue was suspended in silica gel and purified by flash chromatography (PE/EtOAc 8:2 then 7:3). Yield: 0.900 g (43%). ^{1}H NMR (500 MHz, DMSO-d_6) δ ppm 2.57 (s, 3H), 7.70 (s, 2H), 7.81 (s, 1H). Formula: $C_6H_6BrNO_3S_2$.

5.1.25. Synthesis of 5-bromo-3-(2-bromoacetyl)thiophene-2-sulfonamide (140)

To the stirred, protected against the light solution of 1,3-dibromo-5,5-dimethylhydantoin (0.409 g, 1.43 mmol, 0.6 equiv.) in 20 mL EtOAc **139** (0.678 g, 2.39 mmol, 1.0 equiv.) was added and stirred for 1 h at rt. After that time, the reaction mixture was cooled to 0 °C on an ice bath and $H_2SO_{4(conc.)}$ (0.573 mL) was added and stirred for another 1 h. Then the reaction mixture was warmed up to room temperature and stirred overnight. The remaining H_2SO_4 was neutralized by the addition of saturated aqueous $NaHCO_3$ solution and extracted to EtOAc. The combined organic layer was dried over anhydrous Na_2SO_4, filtered, and concentrated under a vacuum. The crude product was purified by flash chromatography (PE/EtOAc 9:1 then 8:2). Yield: 0.430 g (50%). ^{1}H NMR (500 MHz, DMSO-d_6) δ ppm 4.87 (s, 2H), 7.83 (br s, 2H), 7.85 (s, 1H). Formula: $C_6H_5Br_2NO_3S_2$.

5.1.26. Synthesis of (*S*)-6-bromo-4-hydroxy-3,4-dihydro-2*H*-thieno[3,2-*e*][1,2]thiazine 1,1-dioxide (141)

The stirred solution of **140** (0.406 g, 1.12 mmol, 1.0 equiv.) in 7.5 mL MTBE was cooled to -30 °C and then under Ar 58% (+)-β-chlorodiisopinocamphenylborane sol. in hexane (3.519 mL, 5.60 mmol, 5.0 equiv.) was added. Then the temperature was raised to - 20 °C and stirred for 1.5 h. When all starting material was consumed up 4.6 mL of 1 M NaOH was added, and the reaction was stirred for 2 h at rt. After that time, the pH was adjusted to 6–7 by the addition of an aqueous 6 M HCl solution and concentrated under vacuum to remove MTBE. The residue was extracted with EtOAc, combined organic layer was dried over anhydrous Na_2SO_4, filtered, and concentrated under

a vacuum. The crude product was purified by flash chromatography (PE/EtOAc 8:2 then 7:3). Yield: 0.282 g (87%). ^{1}H NMR (500 MHz, DMSO-d_6) δ ppm 3.42 (td, *J*=14.0, 6.9 Hz, 1H), 3.60 (br d, *J*=14.6 Hz, 1H), 4.59 (td, *J*=6.7, 4.6 Hz, 1H), 5.90 (d, *J*=6.6 Hz, 1H), 7.29 (s, 1H), 8.15 (br s, 1H). Formula: $C_6H_6BrNO_3S_2$.

5.1.27. General procedure for the synthesis of compounds 125 and 144 (GP6)

The stirred solution of **124** or **143** (1.0 equiv.) in anhydrous DMF was cooled to 0 °C on an ice bath and then under Ar NaH (60% dispersion in mineral oil) (1.0 equiv.) was added. After 0.5 h methyl iodide (1.2 equiv.) was added, then the reaction mixture was warmed up to room temperature and stirred for 3 h. When all starting material was consumed up reaction was quenched by the addition of water. Solvents were evaporated under reduced pressure. The residue was extracted with EtOAc, combined organic layer was dried over anhydrous Na_2SO_4, filtered, and concentrated under vacuum. The crude product was purified by different methods described below.

2-Bromo-6-methyl-5,6-dihydrothieno[2,3-*c*]pyridin-7(4*H*)-one (125)

Following **GP6**, compound **125** was prepared using compound **124** (60 mg, 0.26 mmol), NaH (10 mg, 0.26 mmol), and methyl iodide (19 µL, 0.31 mmol) in 1.5 mL anhydrous DMF. Purification: flash chromatography (0–5% MeOH gradient in DCM). Yield: 19 mg (30%). ^{1}H NMR (500 MHz, DMSO-d_6) δ ppm 2.87 (t, *J*=7.1 Hz, 2H), 2.93 (s, 3H), 3.56 (t, *J*=7.1 Hz, 2H), 7.22 (s, 1H). Formula: C_8H_8BrNOS.

(*S*)-6-Bromo-4-((*tert*-butyldimethylsilyl)oxy)-2-methyl-3,4-dihydro-2*H*-thieno[3,2-*e*][1,2]thiazine 1,1-dioxide (144)

Following **GP6**, compound **144** was prepared using compound **143** (0.135 g, 0.34 mmol), NaH (14 mg, 0.34 mmol), and methyl iodide (58 µL, 0.41 mmol) in 3 mL anhydrous DMF. The product did not require further purification. Yield: 0.103 g (74%). ^{1}H NMR (500 MHz, DMSO-d_6) δ ppm 0.19 (d, *J*=10.6 Hz, 6H), 0.86 (s, 9H), 2.95 (s, 3H), 3.62 (dd, *J*=15.4, 4.3 Hz, 1H), 3.98 (dd, *J*=15.3, 4.2 Hz, 1H), 4.95 (t, *J*=4.3 Hz, 1H), 7.15 (s, 1H). Formula: $C_{13}H_{22}BrNO_3S_2Si$.

5.1.28. General procedure for the synthesis of compounds 127, 142 and 145–146 (GP7)

The stirred solution of cyclic amide **124** or sulfonamide **141** or **143** (1.0 equiv.) in anhydrous THF was cooled to 0 °C on an ice bath and then NaH (60% dispersion in mineral oil) (1.0 equiv.) was added. The reaction mixture was warmed up to room temperature and stirred for 1 h. After that time, the solvent was evaporated under reduced pressure, the residue was dissolved in DMF and charged with an alkylating agent (1.2 – 8.0 equiv.), K_2CO_3 (2.0 equiv.) and KI (0.2 equiv.). The reaction was stirred overnight at 80 °C. When all starting material was consumed up, the solvent was evaporated under reduced pressure. The residue was extracted with DCM, combined organic layer was dried over anhydrous Na_2SO_4, filtered, and concentrated under a vacuum. The crude product was purified by flash chromatography.

2-(3-(2-Bromo-7-oxo-4,7-dihydrothieno[2,3-*c*]pyridin-6(5*H*)-yl)propyl)isoindoline-1,3-dione (**127**)

Following **GP7**, compound **127** was prepared using **124** (79 mg, 0.34 mmol), NaH (13 mg, 0.34 mmol), *N*-(3-bromopropyl)phthalimide (0.110 g, 0.41 mmol), K_2CO_3 (94 mg, 0.68 mmol), KI (12 mg, 0.07 mmol) in 3 mL DMF. Purification: flash chromatography (DCM/MeOH 95:5). Yield: 30 mg (21%). ^{1}H NMR (500 MHz, DMSO-d_6) δ ppm 1.65 - 1.73 (m, 1H), 1.79 - 1.88 (m, 2H), 2.83 (t, *J*=6.9 Hz, 1H), 3.36 - 3.43 (m, 2H), 3.51 - 3.63 (m, 4H), 7.76 - 7.85 (m, 5H). Formula: $C_{18}H_{15}BrN_2O_3S$.

(*S*)-6-Bromo-2-(2-bromoethyl)-4-hydroxy-3,4-dihydro-2*H*-thieno[3,2-*e*][1,2]thiazine 1,1-dioxide (**142**)

Following **GP7**, compound **142** was prepared using **141** (0.102 g, 0.36 mmol), NaH (14 mg, 0.36 mmol), 1,2-dibromoethane (0.248 mL, 2.88 mmol), K_2CO_3 (0.100 g, 0.72 mmol), KI (12 mg, 0.07 mmol) in 3 mL DMF. Purification: flash chromatography (PE 100% then DCM 100% subsequently DCM/MeOH 99:1). Yield: 61 mg (43%). ^{1}H NMR (500 MHz, DMSO-d_6) δ ppm 3.64 - 3.72 (m, 4H), 3.78 (dd, *J*=15.5, 5.3 Hz, 1H), 3.97 (dd, *J*=15.4, 4.4 Hz, 1H), 4.76 (q, *J*=5.3 Hz, 1H), 6.08 (d, *J*=6.0 Hz, 1H), 7.34 (s, 1H). Formula: $C_8H_9Br_2NO_3S_2$.

(*S*)-6-Bromo-4-((*tert*-butyldimethylsilyl)oxy)-2-(2-((*tert*-butyldimethylsilyl)oxy)ethyl)-3,4-dihydro-2*H*-thieno[3,2-*e*][1,2]thiazine 1,1-dioxide (**145**)

Following **GP7**, compound **145** was prepared using **143** (0.102 g, 0.36 mmol), NaH (14 mg, 0.26 mmol), (2-bromoethoxy)(*tert*-butyl)dimethylsilane (0.232 mL, 1.08 mmol), K_2CO_3 (0.100 g, 0.72 mmol), KI (12 mg, 0.07 mmol) in 5 mL DMF. Purification: flash chromatography (PE 100%). Yield: 0.118 g (59%). ^{1}H NMR (500 MHz, DMSO-d_6) δ ppm 0.05 (d, *J*=1.6 Hz, 6H), 0.19 (d, *J*=9.2 Hz, 6H), 0.86 (s, 18H), 3.41 - 3.50 (m, 2H), 3.73 (dd, *J*=5.7, 3.4 Hz, 2H), 3.76 (d, *J*=4.5 Hz, 1H), 4.01 (dd, *J*=15.4, 4.1 Hz, 1H), 4.95 (t, *J*=4.3 Hz, 1H), 7.14 (s, 1H). Formula: $C_{20}H_{38}BrNO_4S_2Si_2$.

(*S*)-2-(3-(6-Bromo-4-((*tert*-butyldimethylsilyl)oxy)-1,1-dioxido-3,4-dihydro-2*H*-thieno[3,2-*e*][1,2]thiazin-2-yl)propyl)isoindoline-1,3-dione (**146**)

Following **GP7**, compound **146** was prepared using **143** (0.104 g, 0.26 mmol), NaH (12 mg, 0.26 mmol), *N*-(3-bromopropyl)phthalimide (83 mg, 0.31 mmol), K_2CO_3 (72 mg, 0.52 mmol), KI (9 mg, 0.05 mmol) in 3 mL DMF. Purification: flash chromatography (PE/EtOAc 85:15). Yield: 0.123 g (79%). ^{1}H NMR (500 MHz, DMSO-d_6) δ ppm 0.16 (d, *J*=19.6 Hz, 6H), 0.78 (s, 9H), 1.92 - 2.00 (m, 2H), 3.23 - 3.33 (m, 2H), 3.59 - 3.67 (m, 2H), 3.70 (dd, *J*=15.6, 4.2 Hz, 1H), 3.99 (dd, *J*=15.6, 4.1 Hz, 1H), 4.91 (t, *J*=4.2 Hz, 1H), 7.12 (s, 1H), 7.82 - 7.88 (m, 4H). Formula: $C_{23}H_{29}BrN_2O_5S_2Si$.

5.1.29. General procedure for the synthesis of compounds 126, 128, 132, 147–150 and 153 (GP8)

26 (1.0 equiv.) and 6-bromothiophene with a cyclic amide or sulfonamide moiety (1.0 equiv.) were dissolved in anhydrous DMF. Then K_2CO_3 (3.0 equiv.) was added and under Ar Pd(dppf)Cl_2 (0.2 equiv.). The reaction was stirred overnight at 80 °C. After that time, the reaction mixture was diluted with DCM, filtered through Celite and evaporated under reduced pressure. The crude product was purified by different methods described below.

***N*-(4-(6-Methyl-7-oxo-4,5,6,7-tetrahydrothieno[2,3-*c*]pyridin-2-yl)pyridin-2-yl) cyclopropanecarboxamide (126)**

Following **GP8**, compound **126** was prepared using **26** (49 mg, 0.17 mmol), **125** (43 mg, 0.17 mmol), K_2CO_3 (70 mg, 0.51 mmol), Pd(dppf)Cl_2 (25 mg, 0.0034 mmol) in 2.5 mL DMF. Purification: flash chromatography (PE/EtOAc 35:65), then the solid residue was washed with MeCN. Yield: 13 mg (23%), beige solid. Formula: $C_{17}H_{17}N_3O_2S$. MW: 327.40, MS *m/z* 328 ($M+H^+$). Purity 100% (UPLC/MS). ^{1}H NMR (500 MHz, DMSO-d_6) δ ppm 0.79 - 0.88 (m, 4H), 1.98 - 2.07 (m, 1H), 2.94 (t, *J*=7.1 Hz, 2H), 2.98 (s, 3H), 3.62 (t, *J*=7.0 Hz, 2H), 7.41 (dd, *J*=5.3, 1.7 Hz, 1H), 7.63 (s, 1H), 8.35 (d, *J*=5.3 Hz, 1H), 8.40 (d, *J*=1.0 Hz, 1H), 10.94 (s, 1H). ^{13}C NMR (126 MHz, DMSO-d_6) δ ppm 7.82 (2C), 14.24, 23.83, 33.80, 48.53, 108.87, 115.26, 126.04, 132.24, 141.74, 144.69, 145.38, 148.98, 153.06, 160.34, 173.00.

***N*-(4-(6-(3-(1,3-Dioxoisoindolin-2-yl)propyl)-7-oxo-4,5,6,7-tetrahydrothieno[2,3-*c*]pyridin-2-yl)pyridin-2-yl)cyclopropanecarboxamide (128)**

Following **GP8**, compound **128** was prepared using **26** (18 mg, 0.062 mmol), **127** (26 mg, 0.06 mmol), K_2CO_3 (26 mg, 0.19 mmol), Pd(dppf)Cl_2 (9 mg, 0.0124 mmol) in 1 mL DMF. Purification: flash chromatography (0–3% MeOH gradient in DCM). Yield: 20 mg (65%). ^{1}H NMR (500 MHz, CHLOROFORM-*d*) δ ppm 0.82 - 0.88 (m, 2H), 1.02 - 1.09 (m, 2H), 1.52 - 1.58 (m, 1H), 1.96 (quin, *J*=7.2 Hz, 2H), 2.89 (t, *J*=7.0 Hz, 2H), 3.53 - 3.60 (m, 4H), 3.70 (t, *J*=7.3 Hz, 2H), 7.12 (dd, *J*=5.2, 1.7 Hz, 1H), 7.62 - 7.67 (m, 3H), 7.75 - 7.78 (m, 2H), 8.18 (d, *J*=5.2 Hz, 1H), 8.45 (s, 1H), 8.74 (s, 1H). Formula: $C_{27}H_{24}N_4O_4S$.

***N*-(4-(6-(2-((*Tert*-butyldimethylsilyl)oxy)ethyl)-7-oxo-4,5,6,7-tetrahydrothieno[2,3-*c*]pyridin-2-yl)pyridin-2-yl)cyclopropanecarboxamide (132)**

Following **GP8**, compound **132** was prepared using **26** (37 mg, 0.13 mmol), **131** (50 mg, 0.13 mmol), K_2CO_3 (54 mg, 0.39 mmol), Pd(dppf)Cl_2 (19 mg, 0.026 mmol) in 2 mL DMF. Purification: flash chromatography (DCM/EtOAc 9:1 then 8:2). Yield: 43 mg (71%). ^{1}H NMR (500 MHz, CHLOROFORM-*d*) δ ppm 0.06 (s, 6H), 0.90 (s, 9H), 0.91 - 0.95 (m, 2H), 1.11 - 1.17 (m, 2H), 1.56 - 1.62 (m, 1H), 2.91 (t, *J*=7.0 Hz, 2H), 3.65 (t, *J*=5.3 Hz, 2H), 3.78 (t, *J*=7.0 Hz, 2H), 3.85 (t, *J*=5.3 Hz, 2H), 7.21 (dd, *J*=5.3, 1.6 Hz, 1H), 7.35 (s, 1H), 8.27 (d, *J*=5.2 Hz, 1H), 8.48 (s, 1H), 8.53 (s, 1H). Formula: $C_{24}H_{33}N_3O_3SSi$.

(*S*)-*N*-(4-(4-((*Tert*-butyldimethylsilyl)oxy)-2-(2-((*tert*-butyldimethylsilyl)oxy)ethyl)-1,1-dioxido-3,4-dihydro-2*H*-thieno[3,2-*e*][1,2]thiazin-6-yl)pyridin-2-yl)cyclopropanecarboxamide (**147**)

Following **GP8**, compound **147** was prepared using **26** (60 mg, 0.21 mmol), **145** (0.118 g, 0.21 mmol), K_2CO_3 (87 mg, 0.63 mmol), $Pd(dppf)Cl_2$ (31 mg, 0.042 mmol) in 4 mL DMF. Purification: flash chromatography (DCM/MeOH 100:0 then 97:3). Yield: 0.113 g (84%). ^{1}H NMR (500 MHz, DMSO-d_6) δ ppm 0.06 (d, *J*=2.1 Hz, 6H), 0.23 (d, *J*=14.1 Hz, 6H), 0.82 - 0.85 (m, 4H), 0.87 (d, *J*=2.1 Hz, 18H), 2.00 - 2.06 (m, 1H), 3.46 - 3.52 (m, 2H), 3.71 - 3.77 (m, 2H), 3.79 (dd, *J*=15.5, 4.3 Hz, 1H), 4.06 (dd, *J*=15.7, 3.9 Hz, 1H), 5.04 (t, *J*=4.1 Hz, 1H), 7.45 (dd, *J*=5.2, 1.7 Hz, 1H), 7.48 (s, 1H), 8.38 (s, 1H), 8.40 (dd, *J*=5.2, 0.4 Hz, 1H), 11.00 (s, 1H). Formula: $C_{29}H_{47}N_3O_5S_2Si_2$.

(*S*)-*N*-(4-(2-(3-(1,3-Dioxoisoindolin-2-yl)propyl)-4-hydroxy-1,1-dioxido-3,4-dihydro-2*H*-thieno[3,2-*e*][1,2]thiazin-6-yl)pyridin-2-yl)cyclopropanecarboxamide (**148**)

Following **GP8**, compound **148** was prepared using **26** (55 mg, 0.19 mmol), **146** (0.114 g, 0.19 mmol), K_2CO_3 (79 mg, 0.57 mmol), $Pd(dppf)Cl_2$ (28 mg, 0.038 mmol) in 4 mL DMF. Purification: flash chromatography (PE/EtOAc 4:6 then 2:8). Yield: 59 mg (55%). ^{1}H NMR (500 MHz, CHLOROFORM-*d*) δ ppm 0.90 - 0.95 (m, 2H), 1.10 (quin, *J*=3.8 Hz, 2H), 1.62 - 1.66 (m, 1H), 2.01 - 2.11 (m, 2H), 3.30 - 3.39 (m, 1H), 3.50 - 3.59 (m, 1H), 3.81 (tt, *J*=13.5, 6.9 Hz, 2H), 3.89 (dd, *J*=15.3, 3.7 Hz, 1H), 4.14 (dd, *J*=15.4, 3.9 Hz, 1H), 4.77 (t, *J*=3.6 Hz, 1H), 7.13 (dd, *J*=5.2, 1.3 Hz, 1H), 7.51 (s, 1H), 7.69 (dd, *J*=5.5, 3.0 Hz, 2H), 7.80 (dd, *J*=5.4, 3.1 Hz, 2H), 8.22 (d, *J*=5.2 Hz, 1H), 8.50 (d, *J*=1.1 Hz, 1H) 8.94 (br s, 1H). Proton of the -OH group was not detected. Formula: $C_{26}H_{24}N_4O_6S_2$.

(*S*)-*N*-(4-(4-Hydroxy-1,1-dioxido-3,4-dihydro-2*H*-thieno[3,2-*e*][1,2]thiazin-6-yl)pyridin-2-yl)cyclopropanecarboxamide (**149**)

Following **GP8**, compound **149** was prepared using **26** (52 mg, 0.18 mmol), **143** (72 mg, 0.18 mmol), K_2CO_3 (75 mg, 0.54 mmol), $Pd(dppf)Cl_2$ (26 mg, 0.036 mmol) in 4 mL DMF. Purification: flash chromatography (DCM/MeOH 96:4 then 94:6), then the solid residue was washed with MeCN. Yield: 15 mg (23%), brown solid. Formula: $C_{15}H_{15}N_3O_4S_2$. MW: 365.42, MS *m/z* 366 ($M+H^+$). Purity 100% (UPLC/MS). ^{1}H NMR (500 MHz, DMSO-d_6) δ ppm 0.81 - 0.88 (m, 4H), 1.99 - 2.07 (m, 1H), 3.46 (dt, *J*=14.7, 7.6 Hz, 1H), 3.65 (dt, *J*=14.6, 5.0 Hz, 1H), 4.69 (td, *J*=6.7, 4.7 Hz, 1H), 5.96 (d, *J*=6.6 Hz, 1H), 7.44 (dd, *J*=5.3, 1.7 Hz, 1H), 7.46 - 7.46 (m, 1H), 7.71 (s, 1H), 8.16 (br t, *J*=7.1 Hz, 1H), 8.38 (d, *J*=5.2 Hz, 1H), 8.42 (d, *J*=1.0 Hz, 1H), 11.00 (s, 1H). ^{13}C NMR (126 MHz, DMSO-d_6) δ ppm 7.89 (2C), 14.27, 24.97, 62.21, 109.04, 115.58, 125.74, 134.49, 140.68, 143.39, 147.83, 149.22, 153.09, 173.13.

(*S*)-*N*-(4-(4-Hydroxy-2-methyl-1,1-dioxido-3,4-dihydro-2*H*-thieno[3,2-*e*][1,2]thiazin-6-yl)pyridin-2-yl)cyclopropanecarboxamide (150)

Following **GP8**, compound **150** was prepared using **26** (69 mg, 0.24 mmol), **144** (97 mg, 0.24 mmol), K_2CO_3 (0.100 g, 0.72 mmol), $Pd(dppf)Cl_2$ (35 mg, 0.048 mmol) in 4 mL DMF. Purification: flash chromatography (DCM/EtOAc 4:6 then 2:8), then preparative HPLC (10–60% MeCN gradient). Yield: 8 mg (9%), white solid. Formula: $C_{16}H_{17}N_3O_4S_2$. MW: 379.45, MS *m/z* 380 ($M+H^+$). Purity 100% (UPLC/MS). ^{1}H NMR (500 MHz, DMSO-d_6) δ ppm 0.81 - 0.88 (m, 4H), 2.00 - 2.08 (m, 1H), 2.94 (s, 3H), 3.71 (dd, *J*=14.9, 6.2 Hz, 1H), 3.92 (dd, *J*=14.9, 4.8 Hz, 1H), 4.89 (q, *J*=5.7 Hz, 1H), 6.11 (d, *J*=6.1 Hz, 1H), 7.44 (dd, *J*=5.3, 1.6 Hz, 1H), 7.76 (s, 1H), 8.39 (d, *J*=5.2 Hz, 1H), 8.44 (d, *J*=1.5 Hz, 1H), 11.01 (s, 1H). ^{13}C NMR (126 MHz, DMSO-d_6) δ ppm 7.92 (2C), 14.29, 37.39, 55.19, 59.90, 109.09, 115.63, 126.20, 131.51, 140.61, 144.15, 147.23, 149.29, 153.12, 173.17.

***N*-(4-((6*S*)-1,1-Dioxido-3,4-dihydro-6*H*-2,6-methanothieno[2,3-*f*][1,5,4]oxathiazocin-8-yl)pyridin-2-yl)cyclopropanecarboxamide (153)**

Following **GP8**, compound **153** was prepared using **26** (95 mg, 0.33 mmol), **142** (0.129 g, 0.33 mmol), K_2CO_3 (0.137 g, 0.99 mmol), $Pd(dppf)Cl_2$ (48 mg, 0.066 mmol) in 5 mL DMF. Purification: flash chromatography (DCM/EtOAc 8:2), then the solid residue was washed with MeCN. Yield: 41 mg (43%), white solid. Formula: $C_{17}H_{17}N_3O_4S_2$. MW: 391.46, MS *m/z* 392 ($M+H^+$). Purity 100% (UPLC/MS). ^{1}H NMR (500 MHz, DMSO-d_6) δ ppm 0.79 - 0.89 (m, 4H), 2.00 - 2.07 (m, 1H), 3.44 - 3.58 (m, 2H), 3.58 - 3.68 (m, 2H), 3.96 - 4.05 (m, 2H), 4.83 (t, *J*=1.6 Hz, 1H), 7.48 (dd, *J*=5.2, 1.7 Hz, 1H), 7.85 (s, 1H), 8.41 (d, *J*=5.2 Hz, 1H), 8.43 (d, *J*=1.0 Hz, 1H), 11.02 (s, 1H). ^{13}C NMR (126 MHz, DMSO-d_6) δ ppm 7.88 (2C), 14.25, 48.75, 51.97, 56.59, 62.20, 109.30, 115.65, 126.13, 137.90, 140.47, 140.95, 144.78, 149.22, 153.11, 173.10.

5.1.30. General procedure for the synthesis of compounds 135–136 and 152 (GP9)

To a solution of phthalimide-protected aliphatic amine derivative – **128, 134** or **148** (1.0 equiv.) dissolved in anhydrous EtOH, NH_2NH_2 H_2O (7.0–10.0 equiv.) was added, and the mixture was stirred under reflux for 2 h. When all starting material was consumed up, the solvent was evaporated under reduced pressure and crude product was purified by flash chromatography. After purification the compounds were dissolved in MeOH and transformed into solid hydrochloride salt by adding concentrated $HCl_{(aq)}$ and removing the solvent in vacuo.

***N*-(4-(6-(2-Aminoethyl)-7-oxo-4,5,6,7-tetrahydrothieno[2,3-*c*]pyridin-2-yl)pyridin-2-yl)cyclopropanecarboxamide hydrochloride (135)**

Following **GP9**, compound **135** was prepared using **134** (0.102 g, 0.21 mmol), $NH_2NH_2 \cdot H_2O$ (71 µL, 1.47 mmol) in 2 mL EtOH. Purification: flash chromatography (DCM/MeOH/$NH_{3(aq)}$ 9:1:0.1 *v/v*). Yield: 49 mg (60%), pale yellow solid. Formula: $C_{18}H_{21}ClN_4O_2S$. MW of free base: 356.44, MS *m/z* 357 ($M+H^+$). Purity 100% (UPLC/MS). ^{1}H NMR (500 MHz, DMSO-d_6) δ ppm 0.87 (d, *J*=6.3 Hz, 4H), 2.06 (quin,

J=6.2 Hz, 1H), 2.99 (t, *J*=7.0 Hz, 2H), 3.03 (q, *J*=6.0 Hz, 2H), 3.68 (q, *J*=6.9 Hz, 4H), 7.50 (dd, *J*=5.4, 1.7 Hz, 1H), 7.70 (s, 1H), 8.03 (br s, 3H), 8.36 (d, *J*=5.4 Hz, 1H), 8.38 (d, *J*=1.1 Hz, 1H), 11.35 (br s, 1H). ^{13}C NMR (126 MHz, DMSO-d_6) δ ppm 8.40 (2C), 14.47, 23.98, 37.02, 44.04, 47.15, 109.35, 115.41, 127.17, 133.14, 143.57, 143.95, 146.08, 146.13, 151.61, 160.81, 173.83.

_N_-(4-(6-(3-Aminopropyl)-7-oxo-4,5,6,7-tetrahydrothieno[2,3-_c_]pyridin-2-yl)pyridin-2-yl)cyclopropanecarboxamide hydrochloride (136)

Following **GP9**, compound **136** was prepared using **128** (20 mg, 0.04 mmol), NH_2NH_2 H_2O (19 µL, 0.40 mmol) in 1 mL EtOH. Purification: flash chromatography (DCM/MeOH/$NH_{3(aq)}$ 95:5:0.5 then 9:1:0.1 *v/v*), then the solid residue was washed with MeCN. Yield: 7 mg (44%), yellow solid. Formula: $C_{19}H_{23}ClN_4O_2S$. MW of free base: 370.47, MS *m/z* 371 ($M+H^+$). Purity 95% (UPLC/MS). ^{1}H NMR (500 MHz, DMSO-d_6) δ ppm 0.87 (d, *J*=6.0 Hz, 4H), 1.86 (quin, *J*=7.3 Hz, 2H), 2.02 - 2.09 (m, 1H), 2.76 - 2.83 (m, 2H), 2.97 (t, *J*=6.9 Hz, 2H), 3.51 (t, *J*=6.7 Hz, 2H), 3.65 (t, *J*=7.0 Hz, 2H), 7.48 (dd, *J*=5.3, 1.6 Hz, 1H), 7.69 (s, 1H), 7.95 (br s, 3H), 8.32 - 8.39 (m, 2H), 11.32 (br s, 1H). ^{13}C NMR (126 MHz, DMSO-d_6) δ ppm 8.63 (2C), 14.87, 24.54, 25.99, 37.19, 43.71, 47.18, 109.66, 115.87, 127.13, 133.08, 143.15, 145.01, 146.33, 148.06, 152.85, 160.82, 173.93.

(_S_)-_N_-(4-(2-(3-Aminopropyl)-4-hydroxy-1,1-dioxido-3,4-dihydro-2_H_-thieno[3,2-_e_][1,2]thiazin-6-yl)pyridin-2-yl)cyclopropanecarboxamide hydrochloride (152)

Following **GP9**, compound **152** was prepared using **148** (44 mg, 0.08 mmol), NH_2NH_2 H_2O (27 µL, 0.56 mmol) in 1.5 mL EtOH. Purification: flash chromatography (DCM/MeOH/ $NH_{3(aq)}$ 9.5:0.5:0.05 then 9:1:0.1 *v/v*). Yield: 20 mg (55%), yellow solid. Formula: $C_{18}H_{23}ClN_4O_4S_2$. MW of free base: 422.52, MS *m/z* 423 ($M+H^+$). Purity 95% (UPLC/MS). ^{1}H NMR (500 MHz, DMSO-d_6) δ ppm 0.86 (br d, *J*=5.9 Hz, 4H), 1.88 - 1.96 (m, 2H), 2.02 - 2.08 (m, 1H), 2.78 - 2.89 (m, 2H), 3.35 - 3.42 (m, 2H), 3.78 (br dd, *J*=15.4, 6.0 Hz, 1H), 3.94 (dd, *J*=14.9, 4.5 Hz, 1H), 4.88 (t, *J*=5.1 Hz, 1H), 7.46 (dd, *J*=5.4, 1.3 Hz, 1H), 7.80 (s, 1H), 7.92 (br t, *J*=5.4 Hz, 3H), 8.40 (d, *J*=5.4 Hz, 1H), 8.41 (s, 1H), 11.16 (s, 1H).The proton of the -OH group was not detected. ^{13}C NMR (126 MHz, METHANOL-d_4) δ ppm 10.76 (2C), 16.30, 28.29, 38.44, 48.54, 54.87, 62.43, 112.11, 117.83, 131.29, 138.98, 140.23, 142.52, 148.22, 150.06, 150.39, 178.01.

5.1.31. General procedure for the synthesis of compounds 131 and 143 (GP10)

To a solution of compound with primary **130** or secondary **141** hydroxyl group (1.0 equiv.) in DCM imidazole (2.9 equiv.) and *tert*-butyl(chloro)dimethylsilane (2.0–2.5 equiv.) were added and the mixture was stirred at room temperature overnight. After that time, water was added, the mixture was transferred to a separatory funnel and extracted with DCM. The combined organic layer was dried over anhydrous Na_2SO_4, filtered, and concentrated under a vacuum. The product did not require further purification.

2-Bromo-6-(2-((*tert*-butyldimethylsilyl)oxy)ethyl)-5,6-dihydrothieno[2,3-*c*]pyridin-7(4*H*)-one (131)

Following **GP10**, compound **131** was prepared using **130** (0.100 g, 0.36 mmol), imidazole (71 mg, 1.04 mmol) and *tert*-butyl(chloro)dimethylsilane (0.109 g, 0.72 mmol) in 3 mL DCM. Yield: 0.122 g (87%). ^{1}H NMR (500 MHz, CHLOROFORM-*d*) δ ppm 0.05 (d, *J*=0.6 Hz, 6H), 0.89 (d, *J*=0.6 Hz, 9H), 2.86 (t, *J*=6.9 Hz, 2H), 3.60 (t, *J*=5.3 Hz, 2H), 3.73 (t, *J*=7.0 Hz, 2H), 3.82 (t, *J*=5.3 Hz, 2H), 6.89 (s, 1H). Formula: $C_{15}H_{24}BrNO_2SSi$.

(*S*)-6-Bromo-4-((*tert*-butyldimethylsilyl)oxy)-3,4-dihydro-2*H*-thieno[3,2-*e*][1,2]thiazine 1,1-dioxide (143)

Following **GP10**, compound **143** was prepared using **141** (0.363 g, 1.28 mmol), imidazole (0.253 g, 3.71 mmol) and *tert*-butyl(chloro)dimethylsilane (0.482 g, 3.20 mmol) in 10 mL DCM. Yield: 456 mg (90%). ^{1}H NMR (500 MHz, DMSO-d_6) δ ppm 0.17 (d, *J*=12.4 Hz, 6H), 0.89 (s, 9H), 3.37 - 3.42 (m, 1H), 3.62 (ddd, *J*=14.6, 6.0, 4.5 Hz, 1H), 4.81 (dd, *J*=6.9, 4.4 Hz, 1H), 7.10 (s, 1H), 8.29 (dd, *J*=8.5, 6.2 Hz, 1H). Formula: $C_{12}H_{20}BrNO_3S_2Si$.

5.1.32. General procedure for the synthesis of compounds 133 and 151 (GP11)

To a solution of TBDMS-protected hydroxyl derivative – **132** or **147** (1.0 equiv.) dissolved in anhydrous THF was cooled to 0 °C on an ice bath and then 1 M TBAF solution in THF (1.5–3.0 equiv.) was added and stirred on ice for 2 h. After that time, the solvent was evaporated under reduced pressure and the residue was extracted with DCM. The combined organic layer was dried over anhydrous Na_2SO_4, filtered, and concentrated under a vacuum. The crude product was purified by flash chromatography.

***N*-(4-(6-(2-Hydroxyethyl)-7-oxo-4,5,6,7-tetrahydrothieno[2,3-*c*]pyridin-2-yl)pyridin-2-yl)cyclopropanecarboxamide (133)**

Following **GP11**, compound **133** was prepared using **132** (0.111 g, 0.24 mmol) and 1 M TBAF solution in THF (0.360 mL, 0.36 mmol) in 5 mL anhydrous THF. Purification: flash chromatography (2–6% MeOH gradient in DCM). Yield: 61 mg (73%), white solid. Formula: $C_{18}H_{19}N_3O_3S$. MW: 357.43, MS *m/z* 358 ($M+H^+$). Purity 100% (UPLC/MS). ^{1}H NMR (500 MHz, DMSO-d_6) δ ppm 0.80 - 0.87 (m, 4H), 1.99 - 2.06 (m, 1H), 2.92 (t, *J*=6.9 Hz, 2H), 3.46 - 3.52 (m, 2H), 3.54 - 3.59 (m, 2H), 3.69 (t, *J*=7.0 Hz, 2H), 4.78 (t, *J*=5.4 Hz, 1H), 7.41 (dd, *J*=5.2, 1.7 Hz, 1H), 7.63 (s, 1H), 8.35 (dd, *J*=5.2, 0.6 Hz, 1H), 8.41 (d, *J*=0.9 Hz, 1H), 10.94 (s, 1H). ^{13}C NMR (126 MHz, DMSO-d_6) δ ppm 7.82 (2C), 14.25, 24.10, 47.81, 48.79, 58.89, 108.88, 115.27, 125.95, 132.56, 141.76, 144.68, 145.53, 148.98, 153.07, 159.95, 173.01.

(*S*)-*N*-(4-(4-Hydroxy-2-(2-hydroxyethyl)-1,1-dioxido-3,4-dihydro-2*H*-thieno[3,2-*e*][1,2]thiazin-6-yl)pyridin-2-yl)cyclopropanecarboxamide (151)

Following **GP11**, compound **151** was prepared using **147** (0.112 g, 0.18 mmol) and 1 M TBAF solution in THF (0.540 mL, 0.54 mmol) in 5 mL anhydrous THF. Purification: flash chromatography (DCM/MeOH 96:4 then 94:6). Yield: 46 mg (64%), beige oil. Formula: $C_{17}H_{19}N_3O_5S_2$. MW: 409.48, MS *m/z* 410 ($M+H^+$). Purity 100% (UPLC/MS). ^{1}H NMR (500 MHz, DMSO-d_6) δ ppm 0.82 - 0.87 (m, 4H), 2.00 - 2.07 (m, 1H), 3.36 - 3.44 (m, 2H), 3.60 (q, *J*=5.8 Hz, 2H), 3.80 (dd, *J*=15.1, 6.2 Hz, 1H), 3.94 - 4.01 (m, 1H), 4.85 - 4.92 (m, 2H), 6.08 (d, *J*=6.1 Hz, 1H), 7.43 (dd, *J*=5.3, 1.6 Hz, 1H), 7.74 (s, 1H), 8.39 (d, *J*=5.2 Hz, 1H), 8.43 (d, *J*=0.9 Hz, 1H), 11.01 (s, 1H). ^{13}C NMR (126 MHz, METHANOL-d_4) δ ppm 8.88 (2C), 15.80, 53.21, 55.38, 62.01, 62.62, 111.41, 117.27, 126.94, 135.79, 143.08, 146.16, 147.67, 150.35, 154.33, 175.81.

5.1.33. Synthesis of *N*-(4-(6-(2-(1,3-dioxoisoindolin-2-yl)ethyl)-7-oxo-4,5,6,7-tetrahydrothieno[2,3-*c*]pyridin-2-yl)pyridin-2-yl)cyclopropanecarboxamide (134)

The stirred solution of **133** (48 mg, 0.13 mmol, 1.0 equiv.) in 1.5 mL mixture of anhydrous THF and toluene (1:1 ratio) was cooled to 0 °C on an ice bath and then under Ar phthalimide (25 mg, 0.17 mmol, 1.3 equiv.), PPh_3 (45 mg, 0.17 mmol, 1.3 equiv.) and DIAD (33 μL, 0.17 mmol, 1.3 equiv.) were added. Then, the reaction mixture was warmed up to room temperature and stirred for 1 h. After that time, solvents were evaporated under reduced pressure and the residue was extracted with DCM. The combined organic layer was dried over anhydrous Na_2SO_4, filtered, and concentrated under a vacuum. The crude product was purified by flash chromatography (DCM/EtOAc 8.5:1.5 then DCM/MeOH 98:2). Yield: 0.102 g (100%). ^{1}H NMR (500 MHz, DMSO-d_6) δ ppm 0.79 - 0.87 (m, 4H), 1.98 - 2.06 (m, 1H), 2.91 (t, *J*=7.0 Hz, 2H), 3.68 - 3.74 (m, 4H), 3.78 - 3.85 (m, 2H), 7.36 (dd, *J*=5.4, 1.7 Hz, 1H), 7.60 (s, 1H), 7.78 - 7.88 (m, 4H), 8.31 - 8.34 (m, 1H), 8.35 (d, *J*=1.1 Hz, 1H), 10.93 (s, 1H). Formula: $C_{26}H_{22}N_4O_4S$.

5.2. Other methodologies

A detailed description of the computational studies and biological evaluation methodology presented in this doctoral dissertation is provided in Publications I and II:

1. *In vitro* studies (inhibitory activity against GSK-3β and IKK-β, kinetics studies of GSK-3β inhibition).
2. *In cellulo* studies (cell preparation, preparation of test compound solutions, cell viability assay, okadaic acid-treated HT-22 cells, LPS-treated BV-2 cells, NO release measurement, measurement of cytokine levels).
3. *In vitro* ADME-Tox studies (thermodynamic solubility assay, permeability in the PAMPA, chemical and metabolic stability assay, influence on CYPs activity).

6. References:

1. Alzheimer's Association. 2024 Alzheimer's Disease Facts and Figures. *Alzheimers Dement.* **2024**, *20*, 3708-3821, doi:10.1002/alz.13809.
2. Bessey, L.J.; Walaszek, A. Management of Behavioral and Psychological Symptoms of Dementia. *Curr. Psychiatry Rep.* **2019**, *21*, 66, doi:10.1007/s11920-019-1049-5.
3. Tiwari, S.; Atluri, V.; Kaushik, A.; Yndart, A.; Nair, M. Alzheimer's Disease: Pathogenesis, Diagnostics, and Therapeutics. *Int. J. Nanomedicine.* **2019**, *14*, 5541–5554, doi:10.2147/IJN.S200490.
4. Song, L.; Oseid, D.E.; Wells, E.A.; Robinson, A.S. The Interplay between GSK3β and Tau Ser262 Phosphorylation during the Progression of Tau Pathology. *Int. J. Mol. Sci.* **2022**, *23*, doi:10.3390/ijms231911610.
5. Martin, L.; Latypova, X.; Wilson, C.M.; Magnaudeix, A.; Perrin, M.L.; Terro, F. Tau Protein Phosphatases in Alzheimer's Disease: The Leading Role of PP2A. *Ageing Res. Rev.* **2013**, *12*, 39–49, doi:10.1016/j.arr.2012.06.008.
6. Kametani, F.; Hasegawa, M. Reconsideration of Amyloid Hypothesis and Tau Hypothesis in Alzheimer's Disease. *Front. Neurosci.* **2018**, *12*, 3286–3300, doi:10.3389/fnins.2018.00025.
7. Chen, G.F.; Xu, T.H.; Yan, Y.; Zhou, Y.R.; Jiang, Y.; Melcher, K.; Xu, H.E. Amyloid Beta: Structure, Biology and Structure-Based Therapeutic Development. *Acta Pharmacol. Sin.* **2017**, *38*, 1205–1235, doi:10.1038/aps.2017.28.
8. Canevari, L.; Abramov, A.Y.; Duchen, M.R. Toxicity of Amyloid β Peptide: Tales of Calcium, Mitochondria, and Oxidative Stress. *Neurochem. Res.* **2004**, *29*, 637–650, doi:10.1023/B:NERE.0000014834.06405.af.
9. Chiarini, A.; Armato, U.; Hu, P.; Dal Prà, I. Danger-Sensing/Patten Recognition Receptors and Neuroinflammation in Alzheimer's Disease. *Int. J. Mol. Sci.* **2020**, *21*, 9036, doi: 10.3390/ijms21239036.
10. Leng, F.; Edison, P. Neuroinflammation and Microglial Activation in Alzheimer Disease: Where Do We Go from Here? *Nat. Rev. Neurol.* **2021**, *17*, 157–172, doi:10.1038/s41582-020-00435-y.
11. Al-Ghraiybah, N.F.; Wang, J.; Alkhalifa, A.E.; Roberts, A.B.; Raj, R.; Yang, E.; Kaddoumi, A. Glial Cell-Mediated Neuroinflammation in Alzheimer's Disease. *Int. J. Mol. Sci.* **2022**, *23*, 10572, doi: 10.3390/ijms231810572.
12. Li, Y.; Liu, L.; Barger, S.W.; Griffin, W.S.T. Interleukin-1 Mediates Pathological Effects of Microglia on Tau Phosphorylation and on Synaptophysin Synthesis in Cortical Neurons through a P38-MAPK Pathway. *J. Neurosci.* **2003**, *23*, 1605–1611, doi: 10.1523/JNEUROSCI.23-05-01605.2003.
13. Lyman, M. Lloyd, D.G. Ji, X. Vizcaychipi, M.P. Ma, D. Neuroinflammation: The

Role and Consequences. *Neurosci. Res.* **2014**, *79*, 1–12, doi:10.1016/j.neures.2013.10.004.

14. Matsunaga, S.; Fujishiro, H.; Takechi, H. Efficacy and Safety of Cholinesterase Inhibitors for Mild Cognitive Impairment:A Systematic Review and Meta-Analysis. *J. Alzheimer's Dis.* **2019**, *71*, 513–523, doi:10.3233/JAD-190546.
15. Blanco-Silvente, L.; Capellà, D.; Garre-Olmo, J.; Vilalta-Franch, J.; Castells, X. Predictors of Discontinuation, Efficacy, and Safety of Memantine Treatment for Alzheimer's Disease: Meta-Analysis and Meta-Regression of 18 Randomized Clinical Trials Involving 5004 Patients. *BMC Geriatr.* **2018**, *18*, 168, doi:10.1186/s12877-018-0857-5.
16. Joszt, L. Biogen Abandons Aducanumab, Pivots Focus to Lecanemab for Alzheimer Disease. Available online: https://www.ajmc.com/view/biogen-abandons-aducanumab-pivots-focus-to-lecanemab-for-alzheimer-disease (accessed on 10 November 2024)
17. Salloway, S.; Chalkias, S.; Barkhof, F.; Burkett, P.; Barakos, J.; Purcell, D.; Suhy, J.; Forrestal, F.; Tian, Y.; Umans, K.; Wang, G.; Singhal, P.; Budd Haeberlein, S.; Smirnakis, K. Amyloid-Related Imaging Abnormalities in 2 Phase 3 Studies Evaluating Aducanumab in Patients with Early Alzheimer Disease. *JAMA Neurol.* **2022**, *79*, 13–21, doi:10.1001/jamaneurol.2021.4161.
18. Whittington, M.D.; Campbell, J.D.; Rind, D.; Fluetsch, N.; Lin, G.A.; Pearson, S.D. Cost-Effectiveness and Value-Based Pricing of Aducanumab for Patients with Early Alzheimer Disease. *Neurology* **2022**, *98*, 968–977, doi:10.1212/WNL.0000000000013314.
19. van Dyck, C.H.; Swanson, C.J.; Aisen, P.; Bateman, R.J.; Chen, C.; Gee, M.; Kanekiyo, M.; Li, D.; Reyderman, L.; Cohen, S.; Froelich, L.; Katayama, S.; Sabbagh, M.; Vellas, B.; Watson, D.; Dhadda, S.;, Irizarry, M.; Kramer, L.D.; Iwatsubo, T. Lecanemab in Early Alzheimer's Disease. *N. Engl. J. Med.* **2023**, *388*, 9–21, doi:10.1056/NEJMoa2212948.
20. Gueorguieva, I.; Willis, B.A.; Chua, L.; Chow, K.; Ernest, C.S.; Shcherbinin, S.; Ardayfio, P.; Mullins, G.R.; Sims, J.R. Donanemab Population Pharmacokinetics, Amyloid Plaque Reduction, and Safety in Participants with Alzheimer's Disease. *Clin. Pharmacol. Ther.* **2023**, *113*, 1258–1267, doi:10.1002/cpt.2875.
21. Cummings, J.; Zhou, Y.; Lee, G.; Zhong, K.; Fonseca, J.; Cheng, F. Alzheimer's Disease Drug Development Pipeline: 2024. *Alzheimer's Dement. Transl. Res. Clin. Interv.* **2024**, *10*, e12465, doi:10.1002/trc2.12465.
22. Beurel, E.; Grieco, S.F.; Jope, R.S.; Glycogen Synthase Kinase-3 (GSK3): Regulation, Actions, and Diseases. *Pharmacol Ther.* **2015**, *148*, 114–131. doi: 10.1016/j.pharmthera.2014.11.016.
23. Hoeflich, K.P.; Luo, J.; Rubie, E.A.; Tsao, M.S.; Jin, O.; Woodgett, J.R.

Requirement for Glycogen Synthase Kinase-3β in Cell Survival and NF-KB Activation. *Nature* **2000**, *406*, 86–90, doi:10.1038/35017574.

24. Mccubrey, J.A.; Steelman, L.S.; Bertrand, F.E.; Davis, N.M.; Sokolosky, M.; Abrams, S.L.; Montalto, G.; D'Assoro, A.B.; Libra, M.; Nicoletti, F.; Maestro, R.; Basecke, J.; Rakus, D.; Gizak, A.; Demidenko, Z.N.; Cocco, L.; Martelli, A.M.; Cervello, M. GSK-3 as Potential Target for Therapeutic Irvention in Cancer. *Oncotarget* **2014**, *5*, 2881–2911, doi:10.18632/oncotarget.2037.
25. Lee, S.J.; Chung, Y.H.; Joo, K.M.; Lim, H.C.; Jeon, G.S.; Kim, D.; Lee, W.B.; Kim, Y.S.; Cha, C.I. Age-Related Changes in Glycogen Synthase Kinase 3β (GSK3β) Immunoreactivity in the Central Nervous System of Rats. *Neurosci. Lett.* **2006**, *409*, 134–139, doi:10.1016/j.neulet.2006.09.026.
26. Ly, P.T.T.; Wu, Y.; Zou, H.; Wang, R.; Zhou, W.; Kinoshita, A.; Zhang, M.; Yang, Y.; Cai, F.; Woodgett, J.; Song, W. Inhibition of GSK3β-Mediated BACE1 Expression Reduces Alzheimer-Associated Phenotypes. *J. Clin. Invest.* **2013**, *123*, 224–235, doi:10.1172/JCI64516.
27. Avrahami, L.; Farfara, D.; Shaham-Kol, M.; Vassar, R.; Frenkel, D.; Eldar-Finkelman, H. Inhibition of Glycogen Synthase Kinase-3 Ameliorates β-Amyloid Pathology and Restores Lysosomal Acidification and Mammalian Target of Rapamycin Activity in the Alzheimer Disease Mouse Model: In Vivo and in Vitro Studies. *J. Biol. Chem.* **2013**, *288*, 1295–1306, doi:10.1074/jbc.M112.409250.
28. Ding, Y.; Qiao, A.; Fan, G.H. Indirubin-3'-Monoxime Rescues Spatial Memory Deficits and Attenuates β-Amyloid-Associated Neuropathology in a Mouse Model of Alzheimer's Disease. *Neurobiol. Dis.* **2010**, *39*, 156–168, doi:10.1016/j.nbd.2010.03.022.
29. Ferrao Santos, S.; Tasiaux, B.; Sindic, C.; Octave, J.N. Inhibition of Neuronal Calcium Oscillations by Cell Surface APP Phosphorylated on T668. *Neurobiol. Aging* **2011**, *32*, 2308–2313, doi:10.1016/j.neurobiolaging.2010.01.006.
30. Onishi, T.; Iwashita, H.; Uno, Y.; Kunitomo, J.; Saitoh, M.; Kimura, E.; Fujita, H.; Uchiyama, N.; Kori, M.; Takizawa, M. A Novel Glycogen Synthase Kinase-3 Inhibitor 2-methyl-5-(3-{4-[(*S*)-methylsulfinyl]phenyl}-1-benzofuran-5-yl)-1,3,4-oxadiazole Decreases Tau Phosphorylation and Ameliorates Cognitive Deficits in a Transgenic Model of Alzheimer's Disease. *J. Neurochem.* **2011**, *119*, 1330–1340, doi:10.1111/j.1471-4159.2011.07532.x.
31. Bao, X.Q.; Li, N.; Wang, T.; Kong, X.C.; Tai, W.J.; Sun, H.; Zhang, D. FLZ Alleviates the Memory Deficits in Transgenic Mouse Model of Alzheimer's Disease via Decreasing Beta-Amyloid Production and Tau Hyperphosphorylation. *PLoS One* **2013**, *8*, 1–11, doi:10.1371/journal.pone.0078033.
32. Koistinaho, J.; Malm, T.; Goldsteins, G. Glycogen Synthase Kinase-3β: A Mediator of Inflammation in Alzheimer's Disease? *Int. J. Alzheimers. Dis.* **2011**, *2011*,

129753, doi:10.4061/2011/129753.

33. Steinbrecher, K.A.; Wilson, W. 3rd; Cogswell, P.C.; Baldwin, A.S. Glycogen Synthase Kinase 3β Functions To Specify Gene-Specific, NF-κB-Dependent Transcription. *Mol. Cell. Biol.* **2005**, *25*, 8444–8455, doi:10.1128/mcb.25.19.8444-8455.2005.

34. Wang, M.J.; Huang, H.Y.; Chen, W.F.; Chang, H.F.; Kuo, J.S. Glycogen Synthase Kinase-3β Inactivation Inhibits Tumor Necrosis Factor-α Production in Microglia by Modulating Nuclear Factor κB and MLK3/JNK Signaling Cascades. *J. Neuroinflammation*. **2010**, *7*, 99, doi:10.1186/1742-2094-7-99.

35. Medunjanin, S.; Schleithoff, L.; Fiegehenn, C.; Weinert, S.; Zuschratter, W.; Braun-Dullaeus, R.C. GSK-3β Controls NF-KappaB Activity via IKKγ/NEMO. *Sci. Rep.* **2016**, *6*, 38553, doi:10.1038/srep38553.

36. Martin, M.; Rehani, K.; Jope, R.S.; Michalek, S.M. Toll-like Receptor – Mediated Cytokine Production Is Differentially Regulated by Glycogen Synthase Kinase 3. **2005**, *6*, 777–784, doi:10.1038/ni1221.

37. Yuskaitis, C.J.; Jope, R.S. Glycogen Synthase Kinase-3 Regulates Microglial Migration, Inflammation, and Inflammation-Induced Neurotoxicity. *Cell. Signal.* **2009**, *21*, 264–273, doi:10.1016/j.cellsig.2008.10.014.

38. Green, H.F.; Nolan, Y.M. GSK-3 Mediates the Release of IL-1β, TNF-α and IL-10 from Cortical Glia. *Neurochem. Int.* **2012**, *61*, 666–671, doi:10.1016/j.neuint.2012.07.003.

39. Manceur, A.P.; Tseng, M.; Holowacz, T.; Witterick, I.; Weksberg, R.; McCurdy, R.D.; Warsh, J.J.; Audet, J. Inhibition of Glycogen Synthase Kinase-3 Enhances the Differentiation and Reduces the Proliferation of Adult Human Olfactory Epithelium Neural Precursors. *Exp. Cell Res.* **2011**, *317*, 2086–2098, doi:10.1016/j.yexcr.2011.06.004.

40. Morales-Garcia, J.A.; Luna-Medina, R.; Alonso-Gil, S.; Sanz-Sancristobal, M.; Palomo, V.; Gil, C.; Santos, A.; Martinez, A.; Perez-Castillo, A. Glycogen Synthase Kinase 3 Inhibition Promotes Adult Hippocampal Neurogenesis In Vitro and In Vivo. *ACS Chem. Neurosci.* **2012**, *3*, 963–971, doi:10.1021/cn300110c.

41. Zhu, L.Q.; Wang, S.H.; Liu, D.; Yin, Y.Y.; Tian, Q.; Wang, X.C.; Wang, Q.; Chen, J.G.; Wang, J.Z. Activation of Glycogen Synthase Kinase-3 Inhibits Long-Term Potentiation with Synapse-Associated Impairments. *J. Neurosci.* **2007**, *27*, 12211–12220, doi:10.1523/JNEUROSCI.3321-07.2007.

42. Hooper, C.; Markevich, V.; Plattner, F.; Killick, R.; Schofield, E.; Engel, T.; Hernandez, F.; Anderton, B.; Rosenblum, K.; Bliss, T.; Cooke, S.F.; Avila, J.; Lucas, J.J.; Giese, K.P.; Stephenson, J.; Lovestone, S. Glycogen Synthase Kinase-3 Inhibition Is Integral to Long-Term Potentiation. *Eur. J. Neurosci.* **2007**, *25*, 81–86, doi:10.1111/j.1460-9568.2006.05245.x.

43. Hernández, F.; Borrell, J.; Guaza, C.; Avila, J.; Lucas, J.J. Spatial Learning Deficit in Transgenic Mice That Conditionally Over-Express GSK-3β in the Brain but Do Not Form Tau Filaments. *J. Neurochem.* **2002**, *83*, 1529–1533, doi:10.1046/j.1471-4159.2002.01269.x.

44. MacAulay, K.; Woodgett, J.R. Targeting Glycogen Synthase Kinase-3 (GSK-3) in the Treatment of Type 2 Diabetes. *Expert Opin. Ther. Targets* **2008**, *12*, 1265–1274, doi:10.1517/14728222.12.10.1265.

45. Domoto, T.; Uehara, M.; Bolidong, D.; Minamoto, T. Glycogen Synthase Kinase 3β in Cancer Biology and Treatment. *Cells* **2020**, *9*, 1388, doi:10.3390/cells9061388.

46. Cortés-Vieyra, R.; Silva-García, O.; Gómez-García, A.; Gutiérrez-Castellanos, S.; Álvarez-Aguilar, C.; Baizabal-Aguirre, V.M. Glycogen Synthase Kinase 3β Modulates the Inflammatory Response Activated by Bacteria, Viruses, and Parasites. *Front. Immunol.* **2021**, *12*, 675751, doi:10.3389/fimmu.2021.675751.

47. Wang, Y.; Meng, C.; Zhang, J.; Wu, J.; Zhao, J. Inhibition of GSK-3β Alleviates Cerebral Ischemia/Reperfusion Injury in Rats by Suppressing NLRP3 Inflammasome Activation through Autophagy. *Int. Immunopharmacol.* **2019**, *68*, 234–241, doi:10.1016/j.intimp.2018.12.042.

48. Yu, H.; Xiong, M.; Zhang, Z. The Role of Glycogen Synthase Kinase 3 Beta in Neurodegenerative Diseases. *Front. Mol. Neurosci.* **2023**, *16*, 1209703, doi:10.3389/fnmol.2023.1209703.

49. Pandey, M.K.; Degrado, T.R. Glycogen Synthase Kinase-3 (GSK-3)–Targeted Therapy and Imaging. **2016**, *6*, 571–593, doi:10.7150/thno.14334.

50. Arciniegas Ruiz, S.M.; Eldar-Finkelman, H. Glycogen Synthase Kinase-3 Inhibitors: Preclinical and Clinical Focus on CNS–A Decade Onward. *Front. Mol. Neurosci.* **2022**, *14*, 792364, doi:10.3389/fnmol.2021.792364.

51. Cheng, Z.; Han, T.; Yao, J.; Wang, K.; Dong, X.; Yu, F.; Huang, H.; Han, M.; Liao, Q.; He, S.; Lyu, W.; Li, Q. Targeting Glycogen Synthase Kinase-3β for Alzheimer's Disease: Recent Advances and Future Prospects. *Eur. J. Med. Chem.* **2024**, *265*, 116065, doi:10.1016/j.ejmech.2023.116065.

52. Gianferrara, T.; Cescon, E.; Grieco, I.; Spalluto, G.; Federico, S. Glycogen Synthase Kinase 3β Involvement in Neuroinflammation and Neurodegenerative Diseases. *Curr. Med. Chem.* **2022**, *29*, 4631–4697, doi:10.2174/0929867329666220216113517.

53. Coghlan, M.P.; Culbert, A.A.; Cross, D.A.E.; Corcoran, S.L.; Yates, J.W.; Pearce, N.J.; Rausch, O.L.; Murphy, G.J.; Carter, P.S.; Roxbee Cox, L.; Mills, D.; Brown, M.J.; Haigh, D.; Ward, R.W.; Smith, D.G.; Murray, K.J.; Reith, A.D.; Holder, J.C. Selective Small Molecule Inhibitors of Glycogen Synthase Kinase-3 Modulate Glycogen Metabolism and Gene Transcription. *Chem. Biol.* **2000**, *7*, 793–803, doi:10.1016/S1074-5521(00)00025-9.

54. Cross, D.A.; Culbert, A.A.; Chalmers, K.A.; Facci, L.; Skaper, S.D.; Reith, A.D. Selective Small-Molecule Inhibitors of Glycogen Synthase Kinase-3 Activity Protect Primary Neurones from Death. *J. Neurochem.* **2001**, *77*, 94–102, doi: 10.1046/j.1471-4159.2001.t01-1-00251.x.

55. Selenica, M.L.; Jensen, H.S.; Larsen, A.K.; Pedersen, M.L.; Helboe, L.; Leist, M.; Lotharius, J. Efficacy of Small-Molecule Glycogen Synthase Kinase-3 Inhibitors in the Postnatal Rat Model of Tau Hyperphosphorylation. *Br. J. Pharmacol.* **2007**, *152*, 959–979, doi:10.1038/sj.bjp.0707471.

56. Saraswati, A.P.; Ali Hussaini, S.M.; Krishna, N.H.; Babu, B.N.; Kamal, A. Glycogen Synthase Kinase-3 and Its Inhibitors: Potential Target for Various Therapeutic Conditions. *Eur. J. Med. Chem.* **2018**, *144*, 843–858, doi:10.1016/j.ejmech.2017.11.103.

57. Engler, T.A.; Malhotra, S.; Burkholder, T.P.; Henry, J.R.; Mendel, D.; Porter, W.J.; Furness, K.; Diefenbacher, C.; Marquart, A.; Reel, J.K.; Li, Y.; Clayton, J.; Cunningham, B.; McLean, J.; O'toole, J.C.; Brozinick, J.; Hawkins, E.; Misener, E.; Briere, D.; Brier, R.A.; Wagner, J.R.; Campbell, R.M.; Anderson, B.D.; Vaughn, R.; Bennett, D.B.; Meier, T.I.; Cook, J.A. The Development of Potent and Selective Bisarylmaleimide GSK3 Inhibitors. *Bioorganic Med. Chem. Lett.* **2005**, *15*, 899–903, doi:10.1016/j.bmcl.2004.12.063.

58. Zhang, H.C.; Boñaga, L.V.R.; Ye, H.; Derian, C.K.; Damiano, B.P.; Maryanoff, B.E. Novel Bis(Indolyl)Maleimide Pyridinophanes That Are Potent, Selective Inhibitors of Glycogen Synthase Kinase-3. *Bioorganic Med. Chem. Lett.* **2007**, *17*, 2863–2868, doi:10.1016/j.bmcl.2007.02.059.

59. Kramer, T.; Schmidt, B.; Lo Monte, F. Small-Molecule Inhibitors of GSK-3: Structural Insights and Their Application to Alzheimer's Disease Models. *Int. J. Alzheimers. Dis.* **2012**, *2012*, 381029, doi:10.1155/2012/381029.

60. Ōmura, S.; Asami, Y.; Crump, A. Staurosporine: New Lease of Life for Parent Compound of Today's Novel and Highly Successful Anti-Cancer Drugs. *J. Antibiot. (Tokyo).* **2018**, *71*, 688–701, doi:10.1038/s41429-018-0029-z.

61. Sivaprakasam, P.; Han, X.; Civiello, R.L.; Jacutin-Porte, S.; Kish, K.; Pokross, M.; Lewis, H.A.; Ahmed, N.; Szapiel, N.; Newitt, J.A.; Baldwin, E.T.; Xiao, H.; Krause, C.M.; Park, H.; Nophsker, M.; Lippy, J.S.; Burton, C.R.; Langley, D.R.; Macor, J.E.; Dubowchik, G.M. Discovery of New Acylaminopyridines as GSK-3 Inhibitors by a Structure Guided in-Depth Exploration of Chemical Space around a Pyrrolopyridinone Core. *Bioorganic Med. Chem. Lett.* **2015**, *25*, 1856–1863, doi:10.1016/j.bmcl.2015.03.046.

62. Luo, G.; Chen, L.; Burton, C.R.; Xiao, H.; Sivaprakasam, P.; Krause, C.M.; Cao, Y.; Liu, N.; Lippy, J.; Clarke, W.J.; Snow, K.; Raybon, J.; Arora, V.; Pokross, M.; Kish, K.; Lewis, H.A.; Langley, D.R.; Macor, J.E.; Dubowchik, G.M. Discovery of Isonicotinamides as Highly Selective, Brain Penetrable, and Orally Active Glycogen

Synthase Kinase-3 Inhibitors. *J. Med. Chem.* **2016**, *59*, 1041–1051, doi:10.1021/acs.jmedchem.5b01550.

63. Luo, G.; Chen, L.; Jacutin-Porte, S.; Han, Y.; Burton, C.R.; Xiao, H.; Krause, C.M.; Cao, Y.; Liu, N.; Kish, K.; Lewis, H.A.; Macor, J.E.; Dubowchik, G.M. Structure-Activity Relationship (SAR) Studies on Substituted *N*-(Pyridin-3-yl)-2-Amino-Isonicotinamides as Highly Potent and Selective Glycogen Synthase Kinase-3 (GSK-3) Inhibitors. *Bioorg. Med. Chem. Lett.* **2023**, *81*, 129143, doi:10.1016/j.bmcl.2023.129143.
64. Shi, X.L.; Wu, J.D.; Liu, P.; Liu, Z.P. Synthesis and Evaluation of Novel GSK-3β Inhibitors as Multifunctional Agents against Alzheimer's Disease. *Eur. J. Med. Chem.* **2019**, *167*, 211–225, doi:10.1016/j.ejmech.2019.02.001.
65. Kepp, K.P. Alzheimer's Disease: How Metal Ions Define β-Amyloid Function. *Coord. Chem. Rev.* **2017**, *351*, 127–159, doi:10.1016/j.ccr.2017.05.007.
66. Greenough, M.A.; Camakaris, J.; Bush, A.I. Neurochemistry International Metal Dyshomeostasis and Oxidative Stress in Alzheimer's Disease. *Neurochem. Int.* **2013**, *62*, 540–555, doi:10.1016/j.neuint.2012.08.014.
67. Hartz, R.A.; Ahuja, V.T.; Luo, G.; Chen, L.; Sivaprakasam, P.; Xiao, H.; Krause, C.M.; Clarke, W.J.; Xu, S.; Tokarski, J.S.; Kish, K.; Lewis, H.; Szapiel, N.; Ravirala, R.; Mutalik, S.; Nakmode, D.; Shah, D.; Burton, C.R.; Macor, J.E.; Dubowchik, G.M. Discovery of 2-(Anilino)Pyrimidine-4-Carboxamides as Highly Potent, Selective, and Orally Active Glycogen Synthase Kinase-3 (GSK-3) Inhibitors. *J. Med. Chem.* **2023**, *66*, 7534–7552, doi:10.1021/acs.jmedchem.3c00364.
68. Domínguez, J.M.; Fuertes, A.; Orozco, L.; Monte-Millán, M. Del; Delgado, E.; Medina, M. Evidence for Irreversible Inhibition of Glycogen Synthase Kinase-3β by Tideglusib. *J. Biol. Chem.* **2012**, *287*, 893–904, doi:10.1074/jbc.M111.306472.
69. Serenó, L.; Coma, M.; Rodríguez, M.; Sánchez-Ferrer, P.; Sánchez, M.B.; Gich, I.; Agulló, J.M.; Pérez, M.; Avila, J.; Guardia-Laguarta, C.; Clarimón, J.; Lleó, A.; Gómez-Isla, T. A Novel GSK-3β Inhibitor Reduces Alzheimer's Pathology and Rescues Neuronal Loss In Vivo. *Neurobiol. Dis.* **2009**, *35*, 359–367, doi:10.1016/j.nbd.2009.05.025.
70. DaRocha-Souto, B.; Coma, M.; Pérez-Nievas, B.G.; Scotton, T.C.; Siao, M.; Sánchez-Ferrer, P.; Hashimoto, T.; Fan, Z.; Hudry, E.; Barroeta, I.; Serenó, L.; Rodríguez, M.; Sánchez, M.B.; Hyman, B.T.; Gómez-Isla, T. Activation of Glycogen Synthase Kinase-3 Beta Mediates β-Amyloid Induced Neuritic Damage in Alzheimer's Disease. *Neurobiol. Dis.* **2012**, *45*, 425–437, doi: 10.1016/j.nbd.2011.09.002.
71. Luna-Medina, R.; Cortes-Canteli, M.; Sanchez-Galiano, S.; Morales-Garcia, J.A.; Martinez, A.; Santos, A.; Perez-Castillo, A. NP031112, a Thiadiazolidinone Compound, Prevents Inflammation and Neurodegeneration under Excitotoxic

Conditions: Potential Therapeutic Role in Brain Disorders. *J. Neurosci.* **2007**, *27*, 5766–5776, doi:10.1523/JNEUROSCI.1004-07.2007.

72. del Ser, T.; Steinwachs, K.C.; Gertz, H.J.; Andrés, M.V.; Gómez-Carrillo, B.; Medina, M.; Vericat, J.A.; Redondo, P.; Fleet, D.; León, T. Treatment of Alzheimer's Disease with the GSK-3 Inhibitor Tideglusib: A Pilot Study. *J. Alzheimer's Dis.* **2013**, *33,* 205–215, doi:10.3233/JAD-2012-120805.
73. Lovestone, S.; Boada, M.; Dubois, B.; Hüll, M.; Rinne, J.O.; Huppertz, H.J.; Calero, M.; Andrés, M.V.; Gómez-Carrillo, B.; León, T.; del Ser, T.; ARGO investigators. A Phase II Trial of Tideglusib in Alzheimer's Disease. *J. Alzheimer's Dis.* **2015**, *45*, 75–88, doi:10.3233/JAD-141959.
74. U.S. National Library of Medicine. NP-031112 in Clinical Trials. Available online: https://clinicaltrials.gov/expert-search?term=NP-031112 (accessed on 15 November 2024).
75. Georgievska, B.; Sandin, J.; Doherty, J.; Mörtberg, A.; Neelissen, J.; Andersson, A.; Gruber, S.; Nilsson, Y.; Schött, P.; Arvidsson, P.I.; Hellberg, S.; Osswald, G.; Berg, S.; Fälting, J.; Bhat, R.V. AZD1080, a Novel GSK3 Inhibitor, Rescues Synaptic Plasticity Deficits in Rodent Brain and Exhibits Peripheral Target Engagement in Humans. *J. Neurochem.* **2013**, *125*, 446–456, doi:10.1111/jnc.12203.
76. Bhat, R. V.; Andersson, U.; Andersson, S.; Knerr, L.; Bauer, U.; Sundgren-Andersson, A.K. The Conundrum of GSK3 Inhibitors: Is It the Dawn of a New Beginning? *J. Alzheimer's Dis.* **2018**, *64*, S547–S554, doi:10.3233/JAD-179934.
77. Chen, Y.Q.; Zheng, L.; Aldarouish, M.; Zhou, Z.H.; Pan, N.; Liu, J.Q.; Chen, F.X.; Wang, L.X. Wnt Pathway Activator TWS119 Enhances the Proliferation and Cytolytic Activity of Human γδT Cells against Colon Cancer. *Exp. Cell Res.* **2018**, *362*, 63–71, doi:10.1016/j.yexcr.2017.11.003.
78. Gray, J.E.; Infante, J.R.; Brail, L.H.; Simon, G.R.; Cooksey, J.F.; Jones, S.F.; Farrington, D.L.; Yeo, A.; Jackson, K.A.; Chow, K.H.; Zamek-Gliszczynski, M.J.; Burris, H.A. 3rd. A First-in-Human Phase I Dose-Escalation, Pharmacokinetic, and Pharmacodynamic Evaluation of Intravenous LY2090314, a Glycogen Synthase Kinase 3 Inhibitor, Administered in Combination with Pemetrexed and Carboplatin. *Invest. New Drugs* **2015**, *33*, 1187–1196, doi:10.1007/s10637-015-0278-7.
79. Ugolkov, A. V.; Bondarenko, G.I.; Dubrovskyi, O.; Berbegall, A.P.; Navarro, S.; Noguera, R.; O'Halloran, T. V.; Hendrix, M.J.; Giles, F.J.; Mazar, A.P. 9-ING-41, a Small-Molecule Glycogen Synthase Kinase-3 Inhibitor, Is Active in Neuroblastoma. *Anticancer. Drugs* **2018**, *29*, 717–724, doi:10.1097/CAD.0000000000000652.
80. Kuroki, H.; Anraku, T.; Kazama, A.; Bilim, V.; Tasaki, M.; Schmitt, D.; Mazar, A.P.; Giles, F.J.; Ugolkov, A.; Tomita, Y. 9-ING-41, a Small Molecule Inhibitor of GSK-3beta, Potentiates the Effects of Anticancer Therapeutics in Bladder Cancer.

Sci. Rep. **2019**, *9*, 19977, doi:10.1038/s41598-019-56461-4.

81. Jeffers, A.; Qin, W.; Owens, S.; Koenig, K.B.; Komatsu, S.; Giles, F.J.; Schmitt, D.M.; Idell, S.; Tucker, T.A. Glycogen Synthase Kinase-3β Inhibition with 9-ING-41 Attenuates the Progression of Pulmonary Fibrosis. *Sci. Rep.* **2019**, *9*, 18925, doi:10.1038/s41598-019-55176-w.
82. Wang, W.; Li, M.; Wang, Y.; Li, Q.; Deng, G.; Wan, J.; Yang, Q.; Chen, Q.; Wang, J. GSK-3β Inhibitor TWS119 Attenuates rtPA-Induced Hemorrhagic Transformation and Activates the Wnt/β-Catenin Signaling Pathway after Acute Ischemic Stroke in Rats. *Mol. Neurobiol.* **2016**, *53*, 7028–7036, doi:10.1007/s12035-015-9607-2.
83. Actuate Receives FDA Orphan Drug Designation for Elraglusib for Treatment of Soft Tissue Sarcomas. News Release. Actuate Therapeutics, Inc. Available online: https://www.globenewswire.com/news-release/2024/09/11/2944428/0/en/Actuate-Receives-FDA-Orphan-Drug-Designation-for-Elraglusib-for-Treatment-of-Soft-Tissue-Sarcomas.html (accessed on 16 November 2024).
84. Sun, E.; Motolani, A.; Campos, L.; Lu, T. The Pivotal Role of NF-κB in the Pathogenesis and Therapeutics of Alzheimer's Disease. *Int. J. Mol. Sci.* **2022**, *23*, 8972, doi:10.3390/ijms23168972.
85. Gutierrez, H.; Davies, A.M. Regulation of Neural Process Growth, Elaboration and Structural Plasticity by NF-κB. *Trends Neurosci.* **2011**, *34*, 316–325, doi:10.1016/j.tins.2011.03.001.
86. Gamble, C.; McIntosh, K.; Scott, R.; Ho, K.H.; Plevin, R.; Paul, A. Inhibitory Kappa B Kinases as Targets for Pharmacological Regulation. *Br. J. Pharmacol.* **2012**, *165*, 802–819, doi:10.1111/j.1476-5381.2011.01608.x.
87. Sil, A.K.; Maeda, S.; Sono, Y.; Roop, D.B.; Karin, M. IκB Kinase-α Acts in the Epidermis to Control Skeletal and Craniofacial Morphogenesis. *Nature* **2004**, *428*, 660–664, doi:10.1038/nature02421.
88. Maqbool, A.; Lattke, M.; Wirth, T.; Baumann, B. Sustained, Neuron-Specific IKK/NF-κB Activation Generates a Selective Neuroinflammatory Response Promoting Local Neurodegeneration with Aging. *Mol. Neurodegener.* **2013**, *8*, 40, doi:10.1186/1750-1326-8-40.
89. Schnöder, L.; Quan, W.; Yu, Y.; Tomic, I.; Luo, Q.; Hao, W.; Peng, G.; Li, D.; Fassbender, K.; Liu, Y. Deficiency of IKKβ in Neurons Ameliorates Alzheimer's Disease Pathology in APP- and Tau-Transgenic Mice. *FASEB J.* **2023**, *37*, e22778, doi:10.1096/fj.202201512R.
90. Liu, Y.; Liu, X.; Hao, W.; Decker, Y.; Schomburg, R.; Fülöp, L.; Pasparakis, M.; Menger, M.D.; Fassbender, K. IKKβ Deficiency in Myeloid Cells Ameliorates Alzheimer's Disease-Related Symptoms and Pathology. *J. Neurosci.* **2014**, *34*, 12982–12999, doi:10.1523/JNEUROSCI.1348-14.2014.

91. Albensi, B.C.; Mattson, M.P. Evidence for the Involvement of TNF and NF-κB in Hippocampal Synaptic Plasticity. *Synapse*. **2000**, *35*, 151–159, doi:10.1002/(SICI)1098-2396(200002)35:2<151::AID-SYN8>3.0.CO;2-P.

92. Zhang, F.; Qian, L.; Flood, P.M.; Shi, J.S.; Hong, J.S.; Gao, H.M. Inhibition of IκB Kinase-β Protects Dopamine Neurons against Lipopolysaccharide-Induced Neurotoxicity. *J. Pharmacol. Exp. Ther.* **2010**, *333*, 822–833, doi:10.1124/jpet.110.165829.

93. Chen, C.H.; Zhou, W.; Liu, S.; Deng, Y.; Cai, F.; Tone, M.; Tone, Y.; Tong, Y.; Song, W. Increased NF-κB Signalling Up-Regulates BACE1 Expression and Its Therapeutic Potential in Alzheimer's Disease. *Int. J. Neuropsychopharmacol.* **2012**, *15*, 77–90, doi:10.1017/S1461145711000149.

94. Hideshima, T.; Chauhan, D.; Richardson, P.; Mitsiades, C.; Mitsiades, N.; Hayashi, T.; Munshi, N.; Dang, L.; Castro, A.; Palombella, V.; Adams, J.; Anderson, K.C. NF-κB as a Therapeutic Target in Multiple Myeloma. *J. Biol. Chem.* **2002**, *277*, 16639–16647, doi:10.1074/jbc.M200360200.

95. Sanda, T.; Iida, S.; Ogura, H.; Asamitsu, K.; Murata, T.; Bacon, K.B.; Ueda, R.; Okamoto, T. Growth Inhibition of Multiple Myeloma Cells by a Novel IκB Kinase Inhibitor. *Clin. Cancer Res.* **2005**, *11*, 1974–1982, doi:10.1158/1078-0432.CCR-04-1936.

96. Sanda, T.; Asamitsu, K.; Ogura, H.; Iida, S.; Utsunomiya, A.; Ueda, R.; Okamoto, T. Induction of Cell Death in Adult T-Cell Leukemia Cells by a Novel IκB Kinase Inhibitor. *Leukemia* **2006**, *20*, 590–598, doi:10.1038/sj.leu.2404129.

97. Jani, T.S.; DeVecchio, J.; Mazumdar, T.; Agyeman, A.; Houghton, J.A. Inhibition of NF-κB Signaling by Quinacrine Is Cytotoxic to Human Colon Carcinoma Cell Lines and Is Synergistic in Combination with Tumor Necrosis Factor-Related Apoptosis-Inducing Ligand (TRAIL) or Oxaliplatin. *J. Biol. Chem.* **2010**, *285*, 19162–19172, doi:10.1074/jbc.M109.091645.

98. Hideshima, H.; Yoshida, Y.; Ikeda, H.; Hide, M.; Iwasaki, A.; Anderson, K.C.; Hideshima, T. IKKβ Inhibitor in Combination with Bortezomib Induces Cytotoxicity in Breast Cancer Cells. *Int. J. Oncol.* **2014**, *44*, 1171–1176, doi:10.3892/ijo.2014.2273.

99. Goyal, G.; Kalonia, H.; Lather, V. Therapeutic Potential of Catechin as an IKK-β Inhibitor for the Management of Arthritis: In Vitro and In Vivo Approach. *J. Pharm. Bioallied Sci.* **2023**, *15*, 172–179, doi:10.4103/jpbs.jpbs_280_23.

100. Han, X.; Li, Q.; Zhang, S.; Sun, L.; Liu, W.; Wang, J. Inhibition of NEMO Alleviates Arthritis by Blocking the M1 Macrophage Polarization. *Int. Immunopharmacol.* **2023**, *117*, 109983, doi:10.1016/j.intimp.2023.109983.

101. Sunami, Y.; Leithäuser, F.; Gul, S.; Fiedler, K.; Güldiken, N.; Espenlaub, S.; Holzmann, K.H.; Hipp, N.; Sindrilaru, A.; Luedde, T.; Baumann, B.; Wissel, S.;

Kreppel, F.; Schneider, M.; Scharffetter-Kochanek, K.; Kochanek, S.; Strnad, P.; Wirth, T. Hepatic Activation of IKK/NFκB Signaling Induces Liver Fibrosis via Macrophage-Mediated Chronic Inflammation. *Hepatology.* **2012**, *56*, 1117–1128, doi:10.1002/hep.25711.

102. Inayama, M.; Nishioka, Y.; Azuma, M.; Muto, S.; Aono, Y.; Makino, H.; Tani, K.; Uehara, H.; Izumi, K.; Itai, A.; Sone, S. A Novel IκB Kinase-β Inhibitor Ameliorates Bleomycin-Induced Pulmonary Fibrosis in Mice. *Am. J. Respir. Crit. Care Med.* **2006**, *173*, 1016–1022, doi:10.1164/rccm.200506-947OC.

103. Kedzierska, K.; Crowe, S.M. Cytokines and HIV-1: Interactions and Clinical Implications. *Antivir. Chem. Chemother.* **2001**, *12*, 133–150, doi:10.1177/095632020101200301.

104. Jiménez, V.C.; Booiman, T.; De Taeye, S.W.; Van Dort, K.A.; Rits, M.A.N.; Hamann, J.; Kootstra, N.A. Differential Expression of HIV-1 Interfering Factors in Monocyte-Derived Macrophages Stimulated with Polarizing Cytokines or Interferons. *Sci. Rep.* **2012**, *2*, 763, doi:10.1038/srep00763.

105. Victoriano, A.F.B.; Asamitsu, K.; Hibi, Y.; Imai, K.; Barzaga, N.G.; Okamoto, T. Inhibition of Human Immunodeficiency Virus Type 1 Replication in Latently Infected Cells by a Novel IκB Kinase Inhibitor. *Antimicrob. Agents Chemother.* **2006**, *50*, 547–555, doi:10.1128/AAC.50.2.547-555.2006.

106. Kang, J.; Jiang, M.H.; Min, H.J.; Jo, E.K.; Lee, S.; Karin, M.; Yune, T.Y.; Lee, S.J. IKK-β-Mediated Myeloid Cell Activation Exacerbates Inflammation and Inhibits Recovery after Spinal Cord Injury. *Eur. J. Immunol.* **2011**, *41*, 1266–1277, doi:10.1002/eji.201040582.

107. Han, X.; Lu, M.; Wang, S.; Lv, D.; Liu, H. Targeting IKK/NF-κB Pathway Reduces Infiltration of Inflammatory Cells and Apoptosis after Spinal Cord Injury in Rats. *Neurosci. Lett.* **2012**, *511*, 28–32, doi:10.1016/j.neulet.2012.01.030.

108. Yao, Z.; Li, Y.; Yin, X.; Dong, Y.; Xing, L.; Boyce, B.F. NF-κB RelB Negatively Regulates Osteoblast Differentiation and Bone Formation. *J. Bone Miner. Res.* **2014**, *29*, 866–877, doi:10.1002/jbmr.2108.

109. Swarnkar, G.; Zhang, K.; Mbalaviele, G.; Long, F.; Abu-Amer, Y. Constitutive Activation of IKK2/NF-κB Impairs Osteogenesis and Skeletal Development. *PLoS One* **2014**, *9*, e91421, doi:10.1371/journal.pone.0091421.

110. Kamon, J.; Yamauchi, T.; Muto, S.; Takekawa, S.; Ito, Y.; Hada, Y.; Ogawa, W.; Itai, A.; Kasuga, M.; Tobe, K.; Kadowaki, T. A Novel IKKβ Inhibitor Stimulates Adiponectin Levels and Ameliorates Obesity-Linked Insulin Resistance. *Biochem. Biophys. Res. Commun.* **2004**, *323*, 242–248, doi:10.1016/j.bbrc.2004.08.083.

111. Hernandez, R.; Zhou, C. Recent Advances in Understanding the Role of IKKβ in Cardiometabolic Diseases. *Front. Cardiovasc. Med.* **2021**, *8*, 752337, doi:10.3389/fcvm.2021.752337.

112. Llona-Minguez, S.; Baiget, J.; Mackay, S.P. Small-Molecule Inhibitors of IκB Kinase (IKK) and IKK-Related Kinases. *Pharm. Pat. Anal.* **2013**, *2*, 481–498, doi:10.4155/ppa.13.31.

113. Prescott, J.A.; Cook, S.J. Targeting IKKβ in Cancer: Challenges and Opportunities for the Therapeutic Utilisation of IKKβ Inhibitors. *Cells*. **2018**, *7*, 115, doi:10.3390/cells7090115.

114. Awasthee, N.; Rai, V.; Chava, S.; Nallasamy, P.; Kunnumakkara, A.B.; Bishayee, A.; Chauhan, S.C.; Challagundla, K.B.; Gupta, S.C. Targeting IκappaB Kinases for Cancer Therapy. *Semin. Cancer Biol.* **2019**, *56*, 12–24, doi:10.1016/j.semcancer.2018.02.007.

115. Zhang, J.; Zhang, R.; Li, W.; Ma, X.C.; Qiu, F.; Sun, C.P. IκB Kinase β (IKKβ): Structure, Transduction Mechanism, Biological Function, and Discovery of Its Inhibitors. *Int. J. Biol. Sci.* **2023**, *19*, 4181–4203, doi:10.7150/ijbs.85158.

116. Palanki, M.S.S.; Gayo-Fung, L.M.; Shevlin, G.I.; Erdman, P.; Sato, M.; Goldman, M.; Ransone, L.J.; Spooner, C. Structure-Activity Relationship Studies of Ethyl 2-[(3-methyl-2,5-dioxo(3-pyrrolinyl))amino]-4-(trifluoromethyl)pyrimidine- 5-carboxylate: An Inhibitor of AP-1 and NF-κB Mediated Gene Expression. *Bioorganic Med. Chem. Lett.* **2002**, *12*, 2573–2577, doi:10.1016/S0960-894X(02)00517-6.

117. Griessinger, E.; Imbert, V.; Lagadec, P.; Gonthier, N.; Dubreuil, P.; Romanelli, A.; Dreano, M.; Peyron, J.F. AS602868, a Dual Inhibitor of IKK2 and FLT3 to Target AML Cells. *Leukemia*. **2007**, *21*, 877–885, doi:10.1038/sj.leu.2404614.

118. Bingham, A.H.; Davenport, R.J.; Gowers, L.; Knight, R.L.; Lowe, C.; Owen, D.A.; Parry, D.M.; Pitt, W.R. A Novel Series of Potent and Selective IKK2 Inhibitors. *Bioorganic Med. Chem. Lett.* **2004**, *14*, 409–412, doi:10.1016/j.bmcl.2003.10.047.

119. Bingham, A.H.; Davenport, R.J.; Fosbeary, R.; Gowers, L.; Knight, R.L.; Lowe, C.; Owen, D.A.; Parry, D.M.; Pitt, W.R. Synthesis and Structure-Activity Relationship of Aminopyrimidine IKK2 Inhibitors. *Bioorganic Med. Chem. Lett.* **2008**, *18*, 3622–3627, doi:10.1016/j.bmcl.2008.04.062.

120. Shin, Y.; Lim, S.M.; Yan, H.H.; Jung, S.; Fang, Z.; Jung, K.H.; Hong, S.S.; Hong, S. Optimization and Biological Evaluation of Aminopyrimidine-Based IκB Kinase β Inhibitors with Potent Anti-Inflammatory Effects. *Eur. J. Med. Chem.* **2016**, *123*, 544–556, doi:10.1016/j.ejmech.2016.07.075.

121. Waelchli, R.; Bollbuck, B.; Bruns, C.; Buhl, T.; Eder, J.; Feifel, R.; Hersperger, R.; Janser, P.; Revesz, L.; Zerwes, H.G.; Schlapbach, A. Design and Preparation of 2-Benzamido-Pyrimidines as Inhibitors of IKK. *Bioorganic Med. Chem. Lett.* **2006**, *16*, 108–112, doi:10.1016/j.bmcl.2005.09.035.

122. Sordi, R.; Chiazza, F.; Johnson, F.L.; Patel, N.S.A.; Brohi, K.; Collino, M.; Thiemermann, C. Inhibition of IκB Kinase Attenuates the Organ Injury and

Dysfunction Associated with Hemorrhagic Shock. *Mol. Med.* **2015**, *21*, 563–575, doi:10.2119/molmed.2015.00049.

123. Coldewey, S.M.; Rogazzo, M.; Collino, M.; Patel, N.S.A.; Thiemermann, C. Inhibition of IκB Kinase Reduces the Multiple Organ Dysfunction Caused by Sepsis in the Mouse. *DMM Dis. Model. Mech.* **2013**, *6*, 1031–1042, doi:10.1242/dmm.012435.

124. Shu, Y.S.; Tao, W.; Miao, Q.B.; Zhu, Y.B.; Yang, Y.F. Improvement of Ventilation-Induced Lung Injury in a Rodent Model by Inhibition of Inhibitory κB Kinase. *J. Trauma Acute Care Surg.* **2014**, *76*, 1417–1424, doi:10.1097/TA.0000000000000229.

125. Johnson, F.L.; Patel, N.S.A.; Purvis, G.S.D.; Chiazza, F.; Chen, J.; Sordi, R.; Hache, G.; Merezhko, V. V.; Collino, M.; Yaqoob, M.M.; Thiemermann, C. Inhibition of κB Kinase at 24 Hours after Acute Kidney Injury Improves Recovery of Renal Function and Attenuates Fibrosis. *J. Am. Heart Assoc.* **2017**, *6*, e005092, doi:10.1161/JAHA.116.005092.

126. Deng, C.; Lipstein, M.; Rodriguez, R.; Serrano, X.O.J.; McIntosh, C.; Tsai, W.Y.; Wasmuth, A.S.; Jaken, S.; O'Connor, O.A. The Novel IKK2 Inhibitor LY2409881 Potently Synergizes with Histone Deacetylase Inhibitors in Preclinical Models of Lymphoma through the Downregulation of NF-κB. *Clin. Cancer Res.* **2015**, *21*, 134–145, doi:10.1158/1078-0432.CCR-14-0384.

127. Murata, T.; Shimada, M.; Sakakibara, S.; Yoshino, T.; Kadono, H.; Masuda, T.; Shimazaki, M.; Shintani, T.; Fuchikami, K.; Sakai, K.; Inbe, H.; Takeshita, K.; Niki, T.; Umeda, M.; Bacon, K.B.; Ziegelbauer, K.B.; Lowinger, T.B. Discovery of Novel and Selective IKK-β Serine-Threonine Protein Kinase Inhibitors. Part 1. *Bioorganic Med. Chem. Lett.* **2003**, *13*, 913–918, doi:10.1016/S0960-894X(02)01046-6.

128. Murata, T.; Shimada, M.; Kadono, H.; Sakakibara, S.; Yoshino, T.; Masuda, T.; Shimazaki, M.; Shintani, T.; Fuchikami, K.; Bacon, K.B.; Ziegelbauer, K.B.; Lowinger, T.B. Synthesis and Structure-Activity Relationships of Novel IKK-β Inhibitors. Part 2: Improvement of In Vitro Activity. *Bioorganic Med. Chem. Lett.* **2004**, *14*, 4013–4017, doi:10.1016/j.bmcl.2004.05.040.

129. Murata, T.; Shimada, M.; Sakakibara, S.; Yoshino, T.; Masuda, T.; Shintani, T.; Sato, H.; Koriyama, Y.; Fukushima, K.; Nunami, N.; Yamauchi, M.; Fuchikami, K.; Komura, H.; Watanabe, A.; Ziegelbauer, K.B.; Bacon, K.B.; Lowinger, T.B. Synthesis and Structure-Activity Relationships of Novel IKK-β Inhibitors. Part 3: Orally Active Anti-Inflammatory Agents. *Bioorganic Med. Chem. Lett.* **2004**, *14*, 4019–4022, doi:10.1016/j.bmcl.2004.05.041.

130. Xiao, K.; He, W.; Guan, W.; Hou, F.; Yan, P.; Xu, J.; Zhou, T.; Liu, Y.; Xie, L. Mesenchymal Stem Cells Reverse EMT Process through Blocking the Activation of NF-κB and Hedgehog Pathways in LPS-Induced Acute Lung Injury. *Cell Death Dis.*

2020, *11*, 863, doi:10.1038/s41419-020-03034-3.

131. Mia, M.M.; Bank, R.A. The IκB Kinase Inhibitor ACHP Strongly Attenuates TGFβ1-Induced Myofibroblast Formation and Collagen Synthesis. *J. Cell. Mol. Med.* **2015**, *19*, 2780–2792, doi:10.1111/jcmm.12661.

132. Kishore, N.; Sommers, C.; Mathialagan, S.; Guzova, J.; Yao, M.; Hauser, S.; Huynh, K.; Bonar, S.; Mielke, C.; Albee, L.; Weier, R.; Graneto, M.; Hanau, C.; Perry, T.; Tripp, C.S. A Selective IKK-2 Inhibitor Blocks NF-κB-Dependent Gene Expression in Interleukin-1β-Stimulated Synovial Fibroblasts. *J. Biol. Chem.* **2003**, *278*, 32861–32871, doi:10.1074/jbc.M211439200.

133. Baxter, A.; Brough, S.; Cooper, A.; Floettmann, E.; Foster, S.; Harding, C.; Kettle, J.; McInally, T.; Martin, C.; Mobbs, M.; Needham, M.; Newham, P.; Paine, S.; St-Gallay, S.; Salter, S.; Unitt, J.; Xue, Y. Hit-to-Lead Studies: The Discovery of Potent, Orally Active, Thiophenecarboxamide IKK-2 Inhibitors. *Bioorganic Med. Chem. Lett.* **2004**, *14*, 2817–2822, doi:10.1016/j.bmcl.2004.03.058.

134. Birrell, M.A.; Hardaker, E.; Wong, S.; McCluskie, K.; Catley, M.; De Alba, J.; Newton, R.; Haj-Yahia, S.; Pun, K.T.; Watts, C.J.; Shaw, R.J.; Savage, T.J.; Belvisi, M.G. Iκ-B Kinase-2 Inhibitor Blocks Inflammation in Human Airway Smooth Muscle and a Rat Model of Asthma. *Am. J. Respir. Crit. Care Med.* **2005**, *172*, 962–971, doi:10.1164/rccm.200412-1647OC.

135. Podolin, P.L.; Callahan, J.F.; Bolognese, B.J.; Li, Y.H.; Carlson, K.; Davis, T.G.; Mellor, G.W.; Evans, C.; Roshak, A.K. Attenuation of Murine Collagen-Induced Arthritis by a Novel, Potent, Selective Small Molecule Inhibitor of IκB Kinase 2, TPCA-1 (2-[(aminocarbonyl)amino]-5-(4-fluorophenyl)-3-thiophenecarboxamide), Occurs via Reduction of Proinflammatory Cytokines and Antigen-Induced T Cell Proliferation. *J. Pharmacol. Exp. Ther.* **2005**, *312*, 373–381, doi:10.1124/jpet.104.074484.

136. Nan, J.; Du, Y.; Chen, X.; Bai, Q.; Wang, Y.; Zhang, X.; Zhu, N.; Zhang, J.; Hou, J.; Wang, Q.; Yang, J. TPCA-1 Is a Direct Dual Inhibitor of STAT3 and NF-κB and Regresses Mutant EGFR-Associated Human Non-Small Cell Lung Cancers. *Mol. Cancer Ther.* **2014**, *13*, 617–629, doi:10.1158/1535-7163.MCT-13-0464.

137. Liddle, J.; Bamborough, P.; Barker, M.D.; Campos, S.; Cousins, R.P.C.; Cutler, G.J.; Hobbs, H.; Holmes, D.S.; Ioannou, C.; Mellor, G.W.; Morse, M.A.; Payne, J.J.; Pritchard, J.M.; Smith, K.J.; Tape, D.T.; Whitworth, C.; Williamson, R.A. 4-Phenyl-7-azaindoles as Potent and Selective IKK2 Inhibitors. *Bioorg. Med. Chem. Lett.* **2009**, *19*, 2504–2508, doi:10.1016/j.bmcl.2009.03.034.

138. Miller, D.D.; Bamborough, P.; Christopher, J.A.; Baldwin, I.R.; Champigny, A.C.; Cutler, G.J.; Kerns, J.K.; Longstaff, T.; Mellor, G.W.; Morey, J. V.; Morse, M.A.; Nie, H.; Rumsey, W.L.; Taggart, J.J. 3,5-Disubstituted-indole-7-carboxamides: The Discovery of a Novel Series of Potent, Selective Inhibitors of IKK-β. *Bioorg. Med. Chem. Lett.* **2011**, *21*, 2255–2258, doi:10.1016/j.bmcl.2011.02.107.

139. Verstrepen, L.; Beyaert, R. Receptor Proximal Kinases in NF-κB Signaling as Potential Therapeutic Targets in Cancer and Inflammation. *Biochem. Pharmacol.* **2014**, *92*, 519–529, doi:10.1016/j.bcp.2014.10.017.

140. Okazaki, Y.; Sawada, T.; Nagatani, K.; Komagata, Y.; Inoue, T.; Muto, S.; Itai, A.; Yamamoto, K. Effect of Nuclear Factor-KB Inhibition on Rheumatoid Fibroblast-Like Synoviocytes and Collagen Induced Arthritis. *J. Rheumatol.* **2005**, *32*, 1440–1447.

141. U.S. National Library of Medicine. IMD-1041 Chronic Obstructive Pulmonary Disease: Proof of Concept (POC) Study (COPD) Available online: https://clinicaltrials.gov/study/NCT00883584?intr=IMD-1041&rank=1. (accessed on 20 November 2024).

142. Olsen, L.S.; Hjarnaa, P.J.V.; Latini, S.; Holm, P.K.; Larsson, R.; Bramm, E.; Binderup, L.; Madsen, M.W. Anticancer Agent CHS 828 Suppresses Nuclear Factor-κB Activity in Cancer Cells through Downregulation of IKK Activity. *Int. J. Cancer* **2004**, *111*, 198–205, doi:10.1002/ijc.20255.

143. Hovstadius, P.; Larsson, R.; Jonsson, E.; Skov, T.; Kissmeyer, A.M.; Krasilnikoff, K.; Bergh, J.; Karlsson, M.O.; LÖnnebo, A.; Ahlgren, J. A Phase I Study of CHS 828 in Patients with Solid Tumor Malignancy. *Clin. Cancer Res.* **2002**, *8*, 2843–2850.

144. Grothe, K.; Flechsenhar, K.; Paehler, T.; Ritzeler, O.; Beninga, J.; Saas, J.; Herrmann, M.; Rudolphi, K. IκB Kinase Inhibition as a Potential Treatment of Osteoarthritis – Results of a Clinical Proof-of-Concept Study. *Osteoarthr. Cartil.* **2017**, *25*, 46–52, doi:10.1016/j.joca.2016.08.010.

145. Tanvir Kabir, M.; Sahab Uddin, M.; Al Mamun, A.; Jeandet, P.; Aleya, L.; Mansouri, R.A.; Md Ashraf, G.; Mathew, B.; Bin-Jumah, M.N.; Abdel-Daim, M.M. Combination Drug Therapy for the Management of Alzheimer's Disease. *Int. J. Mol. Sci.* **2020**, *21*, 3272, doi:10.3390/ijms21093272.

146. Trstenjak, U.; Kikelj, D. Multitarget Cardiovascular Drugs. *Curr. Med. Chem.* **2011**, *18*, 2531–2542, doi:10.2174/092986711795933768.

147. Doostmohammadi, A.; Jooya, H.; Ghorbanian, K.; Gohari, S.; Dadashpour, M. Potentials and Future Perspectives of Multi-Target Drugs in Cancer Treatment: The next Generation Anti-Cancer Agents. *Cell Commun. Signal.* **2024**, *22*, 228, doi:10.1186/s12964-024-01607-9.

148. Cavalli, A.; Bolognesi, M.L.; Minarini, A.; Rosini, M.; Tumiatti, V.; Recanatini, M.; Melchiorre, C. Multi-Target-Directed Ligands to Combat Neurodegenerative Diseases. *J. Med. Chem.* **2008**, *51*, 347–372, doi:10.1021/jm7009364.

149. Zhou, J.; Jiang, X.; He, S.; Jiang, H.; Feng, F.; Liu, W.; Qu, W.; Sun, H. Rational Design of Multi-Target-Directed Ligands: Strategies and Emerging Paradigms. *J. Med. Chem.* **2019**, *62*, 8881–8914, doi:10.1021/acs.jmedchem.9b00017.

150. Pathak, C.; Kabra, U.D. A Comprehensive Review of Multi-Target Directed Ligands in the Treatment of Alzheimer's Disease. *Bioorg. Chem.* **2024**, *144*, 107152, doi:10.1016/j.bioorg.2024.107152.

151. Kumar, N.; Kumar, V.; Anand, P.; Kumar, V.; Ranjan, A.; Kumar, V. Advancements in the Development of Multi-Target Directed Ligands for the Treatment of Alzheimer's Disease. *Bioorg. Med. Chem.* **2022**, *61*, 116742, doi:10.1016/j.bmc.2022.116742.

152. Sang, Z.; Wang, K.; Dong, J.; Tang, L. Alzheimer's Disease: Updated Multi-Targets Therapeutics Are in Clinical and in Progress. *Eur. J. Med. Chem.* **2022**, *238*, 114464, doi:10.1016/j.ejmech.2022.114464.

153. Jankowska, A.; Satała, G.; Bojarski, A.J.; Pawłowski, M.; Chłoń-Rzepa, G. Multifunctional Ligands with Glycogen Synthase Kinase 3 Inhibitory Activity as a New Direction in Drug Research for Alzheimer's Disease. *Curr. Med. Chem.* **2021**, *28*, 1731–1745, doi:10.2174/0929867327666200427100453.

154. De Simone, A.; Tumiatti, V.; Andrisano, V.; Milelli, A. Glycogen Synthase Kinase 3β: A New Gold Rush in Anti-Alzheimer's Disease Multitarget Drug Discovery? *J. Med. Chem.* **2021**, *64*, 26–41, doi:10.1021/acs.jmedchem.0c00931.

155. Joshi, N.J.; Raja, A.; Reddy, S. Navigating the GSK-3β Inhibitors as Versatile Multi-Target Drug Ligands in Alzheimer's Disease Intervention – A Comprehensive Review. *Results Chem.* **2024**, *7*, 101500, doi:10.1016/j.rechem.2024.101500.

156. Cohen, P.; Cross, D.; Jänne, P.A. Kinase Drug Discovery 20 Years after Imatinib: Progress and Future Directions. *Nat. Rev. Drug Discov.* **2021**, *20*, 551–569, doi:10.1038/s41573-021-00195-4.

157. Attwood, M.M.; Fabbro, D.; Sokolov, A. V.; Knapp, S.; Schiöth, H.B. Trends in Kinase Drug Discovery: Targets, Indications and Inhibitor Design. *Nat. Rev. Drug Discov.* **2021**, *20*, 839–861, doi:10.1038/s41573-021-00252-y.

158. Fabbro, D.; Cowan-Jacob, S.W.; Moebitz, H. Ten Things You Should Know about Protein Kinases: IUPHAR Review 14. *Br. J. Pharmacol.* **2015**, *172*, 2675–2700, doi:10.1111/bph.13096.

159. Kornev, A.P.; Taylor, S.S. Defining the Conserved Internal Architecture of a Protein Kinase. *Biochim. Biophys. Acta.* **2010**, *1804*, 440–444, doi:10.1016/j.bbapap.2009.10.017.

160. Zuccotto, F.; Ardini, E.; Casale, E.; Angiolini, M. Through the "Gatekeeper Door": Exploiting the Active Kinase Conformation. *J. Med. Chem.* **2010**, *53*, 2681–2694, doi:10.1021/jm901443h.

161. Pan, Y.; Mader, M.M. Principles of Kinase Allosteric Inhibition and Pocket Validation. *J. Med. Chem.* **2022**, *65*, 5288–5299, doi:10.1021/acs.jmedchem.2c00073.

162. Zhao, Z.; Liu, Q.; Bliven, S.; Xie, L.; Bourne, P.E. Determining Cysteines Available

for Covalent Inhibition Across the Human Kinome. *J. Med. Chem.* **2017**, *60*, 2879–2889, doi:10.1021/acs.jmedchem.6b01815.

163. Serafimova, I.M.; Pufall, M.A.; Krishnan, S.; Duda, K.; Cohen, M.S.; Maglathlin, R.L.; McFarland, J.M.; Miller, R.M.; Frödin, M.; Taunton, J. Reversible Targeting of Noncatalytic Cysteines with Chemically Tuned Electrophiles. *Nat. Chem. Biol.* **2012**, *8*, 471–476, doi:10.1038/nchembio.925.

164. Li, Y.R.; Lin, C.C.; Huang, C.Y.; Wong, Y.H.; Hsieh, C.H.; Wu, H.W.; Chen, J.J.W.; Wu, Y.S. Study of the Inhibitory Effects on TNF-α-Induced NF-κB Activation of IMD0354 Analogs. *Chem. Biol. Drug Des.* **2017**, *90*, 1307–1311, doi:10.1111/cbdd.13032.

165. Champagne, P.A.; Desroches, J.; Paquin, J.F. Organic Fluorine as a Hydrogen-Bond Acceptor: Recent Examples and Applications. *Synthesis.* **2015**, *47*, 306–322, doi:10.1055/s-0034-1379537.

166. Düfert, M.A.; Billingsley, K.L.; Buchwald, S.L. Suzuki-Miyaura Cross-Coupling of Unprotected, Nitrogen- Rich Heterocycles: Substrate Scope and Mechanistic Investigation. *J. Am. Chem. Soc.* **2013**, *135*, 12877–12885, doi:10.1021/ja4064469.

167. Lipinski, C.A.; Lombardo, F.; Dominy, B.W.; Feeney, P.J. Experimental and Computational Approaches to Estimate Solubility and Permeability in Drug Discovery and Development Settings. *Adv. Drug Deliv. Rev.* **2001**, *46*, 3–26. doi:10.1016/s0169-409x(00)00129-0.

168. Tinworth, C.P.; Young, R.J. Facts, Patterns, and Principles in Drug Discovery: Appraising the Rule of 5 with Measured Physicochemical Data. *J. Med. Chem.* **2020**, *63*, 10091–10108, doi:10.1021/acs.jmedchem.9b01596.

169. Veber, D.F.; Johnson, S.R.; Cheng, H.Y.; Smith, B.R.; Ward, K.W.; Kopple, K.D. Molecular Properties That Influence the Oral Bioavailability of Drug Candidates. *J. Med. Chem.* **2002**, *45*, 2615–2623, doi:10.1021/jm020017n.

170. Didziapetris, R.; Japertas, P.; Avdeef, A.; Petrauskas, A. Classification Analysis of P-Glycoprotein Substrate Specificity. *J. Drug Target.* **2003**, *11*, 391–406, doi:10.1080/10611860310001648248.

171. Lovering, F.; Bikker, J.; Humblet, C. Escape from Flatland: Increasing Saturation as an Approach to Improving Clinical Success. *J. Med. Chem.* **2009**, *52*, 6752–6756, doi:10.1021/jm901241e.

172. Wager, T.T.; Hou, X.; Verhoest, P.R.; Villalobos, A. Moving beyond Rules: The Development of a Central Nervous System Multiparameter Optimization (CNS MPO) Approach to Enable Alignment of Druglike Properties. *ACS Chem. Neurosci.* **2010**, *1*, 435–449, doi:10.1021/cn100008c.

173. ChemAxon Chemicalize - Instant Cheminformatics Solutions Available online: https://chemicalize.com/welcome (accessed on 15 September 2024).

174. Fong, C.W. Permeability of the Blood–Brain Barrier: Molecular Mechanism of

Transport of Drugs and Physiologically Important Compounds. *J. Membr. Biol.* **2015**, *248*, 651–669, doi:10.1007/s00232-015-9778-9.

175. Chen, X.; Murawski, A.; Patel, K.; Crespi, C.L.; Balimane, P. V A Novel Design of Artificial Membrane for Improving the PAMPA Model. **2008**, *25*, 1511–1520, doi:10.1007/s11095-007-9517-8.
176. Łukasik, P.; Załuski, M.; Gutowska, I. Cyclin-Dependent Kinases (Cdk) and Their Role in Diseases Development–Review. *Int. J. Mol. Sci.* **2021**, *22*, 2935, doi:10.3390/ijms22062935.
177. Philpott, J.M.; Narasimamurthy, R.; Ricci, C.G.; Freeberg, A.M.; Hunt, S.R.; Yee, L.E.; Pelofsky, R.S.; Tripathi, S.; Virshup, D.M.; Partch, C.L. Casein Kinase 1 Dynamics Underlie Substrate Selectivity and the PER2 Circadian Phosphoswitch. *Elife.* **2020**, *9*, e52343, doi:10.7554/eLife.52343.
178. Arbones, M.L.; Thomazeau, A.; Nakano-Kobayashi, A.; Hagiwara, M.; Delabar, J.M. DYRK1A and Cognition: A Lifelong Relationship. *Pharmacol. Ther.* **2019**, *194*, 199–221, doi:10.1016/j.pharmthera.2018.09.010.
179. Martin, L.; Latypova, X.; Wilson, C.M.; Magnaudeix, A.; Perrin, M.L.; Yardin, C.; Terro, F. Tau Protein Kinases: Involvement in Alzheimer's Disease. *Ageing Res. Rev.* **2013**, *12*, 289–309, doi:10.1016/j.arr.2012.06.003.
180. Guo, Q.; Jin, Y.; Chen, X.; Ye, X.; Shen, X.; Lin, M.; Zeng, C.; Zhou, T.; Zhang, J. NF-κB in Biology and Targeted Therapy: New Insights and Translational Implications. *Signal Transduct. Target. Ther.* **2024**, *9*, 53, doi:10.1038/s41392-024-01757-9.
181. Cargnello, M.; Roux, P.P. Activation and Function of the MAPKs and Their Substrates, the MAPK-Activated Protein Kinases. *Microbiol. Mol. Biol. Rev.* **2011**, *75*, 50–83, doi:10.1128/mmbr.00031-10.
182. Sundaram, S.; Nagaraj, S.; Mahoney, H.; Portugues, A.; Li, W.; Millsaps, K.; Faulkner, J.; Yunus, A.; Burns, C.; Bloom, C.; Said, M.; Pinto, L.; Azam, S.; Flores, M.; Henriksen, A.; Gamsby, J.; Gulick, D. Inhibition of Casein Kinase 1δ/ε Improves Cognitive-Affective Behavior and Reduces Amyloid Load in the APP-PS1 Mouse Model of Alzheimer's Disease. *Sci. Rep.* **2019**, *9*, 13743, doi:10.1038/s41598-019-50197-x.
183. Fang, W.Q.; Ip, J.P.K.; Li, R.; Ng, Y.P.; Lin, S.C.; Chen, Y.; Fu, A.K.Y.; Ip, N.Y. Cdk5-Mediated Phosphorylation of Axin Directs Axon Formation during Cerebral Cortex Development. *J. Neurosci.* **2011**, *31*, 13613–13624, doi:10.1523/JNEUROSCI.3120-11.2011.
184. Cruz, J.C.; Tseng, H.C.; Goldman, J.A.; Shih, H.; Tsai, L.H. Aberrant Cdk5 Activation by p25 Triggers Pathological Events Leading to Neurodegeneration and Neurofibrillary Tangles. *Neuron.* **2003**, *40*, 471–483, doi:10.1016/S0896-6273(03)00627-5.

185. Hu, Y.B.; Ren, R.J.; Zhang, Y.F.; Huang, Y.; Cui, H.L.; Ma, C.; Qiu, W.Y.; Wang, H.; Cui, P.J.; Chen, H.Z.; Wang, G. Rho-Associated Coiled-Coil Kinase 1 Activation Mediates Amyloid Precursor Protein Site-Specific Ser655 Phosphorylation and Triggers Amyloid Pathology. *Aging Cell.* **2019**, *18*, e13001, doi:10.1111/acel.13001.

186. Hamano, T.; Shirafuji, N.; Yen, S.H.; Yoshida, H.; Kanaan, N.M.; Hayashi, K.; Ikawa, M.; Yamamura, O.; Fujita, Y.; Kuriyama, M.; Nakamoto, Y. Rho-Kinase ROCK Inhibitors Reduce Oligomeric Tau Protein. *Neurobiol. Aging.* **2020**, *89*, 41–54, doi:10.1016/j.neurobiolaging.2019.12.009.

187. Góral, I.; Wichur, T.; Sługocka, E.; Godyń, J.; Szałaj, N.; Zaręba, P.; Głuch-Lutwin, M.; Mordyl, B.; Panek, D.; Więckowska, A. Connecting GSK-3β Inhibitory Activity with IKK-β or ROCK-1 Inhibition to Target Tau Aggregation and Neuroinflammation in Alzheimer's Disease—Discovery, In Vitro and In Cellulo Activity of Thiazole-Based Inhibitors. *Molecules.* **2024**, *29*, 2616, doi:10.3390/molecules29112616.

188. Wang, J.; Zhang, L.; Pan, X.; Dai, B.; Sun, Y.; Li, C.; Zhang, J. Discovery of Multi-Target Receptor Tyrosine Kinase Inhibitors as Novel Anti-Angiogenesis Agents. *Sci. Rep.* **2017**, *7*, 45145, doi:10.1038/srep45145.

189. Cherian, J.; Nacro, K.; Poh, Z. Y.; Guo, S.; Jeyaraj, D. A.; Wong, Y. X.; Ho, M.; Yang, H. Y.; Joy, J. K.; Kwek, Z. P.; Liu, B.; Wee, J. L. K.; Ong, E. HQ.; Choong, M. L.; Poulsen, A.; Lee, M. A.; Pendharkar, V.; Ding, L. J.; Manoharan, V.; Chew, Y. S.; Sangthongpitag, K.; Lim, S.; Ong, S.T.; Hill, J.; Keller, T.H. Structure-Activity Relationship Studies of Mitogen Activated Protein Kinase Interacting Kinase (MNK) 1 and 2 and BCR-ABL1 Inhibitors Targeting Chronic Myeloid Leukemic Cells. *J. Med. Chem.* **2016**, *59*, 3063–3078, doi:10.1021/acs.jmedchem.5b01712.

190. McCarver, S.; Hanna, L.; Samant, A.; Thompson, A. A.; Seierstad, M.; Saha, A.; Wu, D.; Lord, B.; Sutton, S. W.; Shah, V.; Milligan, C. M.; Wennerholm, M.; Shelton, J.; Lebold, T. P.; Shireman, B.T. Structure-Based Optimization of Selective and Brain Penetrant CK1δ Inhibitors for the Treatment of Circadian Disruptions. *ACS Med. Chem. Lett.* **2024**, *15*, 486–492, doi:10.1021/acsmedchemlett.3c00523.

191. Gao, M.; Wang, M.; Zheng, Q.H. Synthesis of Carbon-11-Labeled Isonicotinamides as New Potential PET Agents for Imaging of GSK-3 Enzyme in Alzheimer's Disease. *Bioorganic Med. Chem. Lett.* **2017**, *27*, 740–743, doi:10.1016/j.bmcl.2017.01.041.

192. De Rosa, M.; Arnold, D. Aromaticity and Aminopyrroles: Desmotropy and Solution Tautomerism of 1*H*-pyrrol-3-aminium and 1*H*-pyrrol-3(2*H*)-iminium Cation: A Stable σ-Complex. *J. Org. Chem.* **2013**, *78*, 1107–1112, doi:10.1021/jo302457y.

193. Sharma, S.K.; Mandadapu, A.K.; Saifuddin, M.; Gupta, S.; Agarwal, P.K.; Mandwal, A.K.; Gauniyal, H.M.; Kundu, B. Three-Component Reaction Involving

Metal-Free Heteroannulation of *N*-Boc-3-amido Indole, Aryl Aldehydes, and Aromatic Alkynes under Microwave Conditions: Synthesis of Highly Diversified δ-Carbolines. *Tetrahedron Lett.* **2010**, *51*, 6022–6024, doi:10.1016/j.tetlet.2010.09.054.

194. Bahekar, R.H.; Jain, M.R.; Goel, A.; Patel, D.N.; Prajapati, V.M.; Gupta, A.A.; Jadav, P.A.; Patel, P.R. Design, Synthesis, and Biological Evaluation of Substituted-*N*-(Thieno[2,3-*b*]pyridin-3-yl)-guanidines, *N*-(1*H*-Pyrrolo[2,3-*b*]pyridin-3-yl)-guanidines, and *N*-(1*H*-Indol-3-yl)-guanidines. *Bioorganic Med. Chem.* **2007**, *15*, 3248–3265, doi:10.1016/j.bmc.2007.02.029.

195. Ma, F.; Xie, X.; Zhang, L.; Peng, Z.; Ding, L.; Fu, L.; Zhang, Z. Palladium-Catalyzed Amidation of Aryl Halides Using 2-Dialkylphosphino-2′-alkoxyl-1,1′-binaphthyl as Ligands. *J. Org. Chem.* **2012**, *77*, 5279–5285, doi:10.1021/jo3005827.

196. Xie, H.; Ng, D.; Savinov, S.N.; Dey, B.; Kwong, P.D.; Wyatt, R.; Smith, A.B. 3rd; Hendrickson, W.A. Structure-Activity Relationships in the Binding of Chemically Derivatized CD4 to gp120 from Human Immunodeficiency Virus. *J. Med. Chem.* **2007**, *50*, 4898–4908, doi:10.1021/jm070564e.

197. In, J.; Hwang, S.; Kim, C.; Seo, J.H.; Kim, S. Synthesis of 3,4-Dihydroisoquinolin-1-ones from *N*-Boc-(β-Arylethyl)carbamates via Isocyanate Intermediates. *Eur. J. Org. Chem.* **2013**, *2013*, 965–971, doi:10.1002/ejoc.201201408.

198. Gadhachanda, V. R.; Wiles, J. A.; Onyango, E. Pharmaceutical Compounds for the Treatment of Complement Mediated Disorders. WO 2023/183405, **2023**.

199. Seitsu, F.; Shiokawa, M.; Kawano, Y.; Kano, Y.; Sato, S.; Sato, E.; Kouchi, T.; Ishikawa, M.; Ishikawa, M.; Kaneda, K.; Sakamaki, N.; Baba, S.; Koresawa, T. 2-Thienylcarbapenem Derivative. JP2008273924A, **2008**.

200. Hu, X.; Fu, W.; Zuo, L.; Shi, H.; Chen, M.; Liu, S.; Pan, J.; Fu, L.; Shi, M.; Chen, H. New -(D-A1-D-A2)$_n$- Type Conjugated Polymers for Photovoltaic Applications: Consensus between Low Band-Gap and Low HOMO Energy Level. *Tetrahedron.* **2013**, *69*, 3419–3424, doi:10.1016/j.tet.2013.02.074.

201. May, J. K.; Chen, H.-H.; Dupre, B.; Dean, T.R. Thienothiazine Sulfonamide Derivatives Process and Intermediates for Their Preparation and Their Use as Carbonic Anhydrase Inhibitors. WO1995019981A1, **1995**.